



**HAL**  
open science

# Flexural strengthening of RC continuous beams with FRP reinforcements according to the NSM and EB techniques: experimental, analytical and numerical (FE) study

Mohammad Abdallah

## ► To cite this version:

Mohammad Abdallah. Flexural strengthening of RC continuous beams with FRP reinforcements according to the NSM and EB techniques: experimental, analytical and numerical (FE) study. Engineering Sciences [physics]. Université de Lorraine, 2021. English. NNT: 2021LORR0156. tel-03423289

**HAL Id: tel-03423289**

**<https://hal.univ-lorraine.fr/tel-03423289>**

Submitted on 10 Nov 2021

**HAL** is a multi-disciplinary open access archive for the deposit and dissemination of scientific research documents, whether they are published or not. The documents may come from teaching and research institutions in France or abroad, or from public or private research centers.

L'archive ouverte pluridisciplinaire **HAL**, est destinée au dépôt et à la diffusion de documents scientifiques de niveau recherche, publiés ou non, émanant des établissements d'enseignement et de recherche français ou étrangers, des laboratoires publics ou privés.



## AVERTISSEMENT

Ce document est le fruit d'un long travail approuvé par le jury de soutenance et mis à disposition de l'ensemble de la communauté universitaire élargie.

Il est soumis à la propriété intellectuelle de l'auteur. Ceci implique une obligation de citation et de référencement lors de l'utilisation de ce document.

D'autre part, toute contrefaçon, plagiat, reproduction illicite encourt une poursuite pénale.

Contact : [ddoc-theses-contact@univ-lorraine.fr](mailto:ddoc-theses-contact@univ-lorraine.fr)

## LIENS

Code de la Propriété Intellectuelle. articles L 122. 4

Code de la Propriété Intellectuelle. articles L 335.2- L 335.10

[http://www.cfcopies.com/V2/leg/leg\\_droi.php](http://www.cfcopies.com/V2/leg/leg_droi.php)

<http://www.culture.gouv.fr/culture/infos-pratiques/droits/protection.htm>



UNIVERSITÉ  
DE LORRAINE



INSTITUT  
JEAN LAMOUR

G2MP



École doctorale Chimie – Mécanique – Matériaux – Physique

Thèse

Docteur de l'Université de Lorraine

Mention : « sciences des matériaux »

Par : Mohammad ABDALLAH

---

Flexural strengthening of RC continuous beams with FRP reinforcements  
according to the NSM and EB techniques: experimental, analytical and  
numerical (FE) study

---

Thèse soutenue publiquement le 08 octobre 2021 à Nancy devant le jury suivant :

**Rapporteurs**

Danièle WALDMANN  
Jules ASSIH

Professeur des universités – Université du Luxembourg  
Maître de Conférences (HDR) – Université de Reims Champagne-Ardenne

**Examineurs**

Marion MARTINY  
Hugues SOMJA  
Firas AL MAHMOUD  
Abdelouahab KHELIL

Professeur des universités – Université de Lorraine  
Professeur des universités – INSA de Rennes (**Président de jury**)  
Maître de Conférences (HDR) – Université de Lorraine (**directeur de thèse**)  
Professeur des universités – Université de Lorraine (**co-directeur de thèse**)

**Invité**

Julien MERCIER

R&D Project Manager – Freyssinet International & Cie





*'The difference between ordinary and extraordinary is that little extra'*

*– Jimmy Johnson*



## ACKNOWLEDGMENTS

The present work was developed at the laboratories of the Institute Jean Lamour (IJL), the University of Lorraine, France.

This research was carried out under the supervision of Prof. Firas Al Mahmoud and Prof. Abdelouahab Khelil. I would like to express my deepest gratitude and appreciation for their encouragement; endless support; and their helpful guidance, advice, and suggestions. Their continuous guidance throughout my studies in France helped me to stay motivated and productive.

Besides my supervisors, I would like to thank the rest of my thesis committee, Prof. Jean-François Bocquet and Prof. Jurkiewicz Bruno, for their insightful comments and suggestions.

Many thanks go to my fellow lab mates, the academic staff, and the technicians at the IUT (Institut Universitaire de Technologie), in particular Dr. Damien Descieux, Mr. Laurent Rouge, Mr. Jonathan Martens and Mr. Pierre Dupont for their assistance and support in running the experiments. In addition, I thank my friends, including all those who have directly or indirectly supported me throughout my stay in France.

I wish to acknowledge the financial support provided by the Campus France and CNRS, and the logistic support provided by Fressyniet Company.

I would like to express my deepest gratitude to my family in Palestine (my father, mother, sisters, nephews and nieces) and to my wife and daughter in Germany for their love, prayers, and encouragement.

Mohammad Abdallah

Nancy, France, June 2021



## ABSTRACT

---

This thesis is composed of four parts. Each part contains several research items according to the structural topic planned to be studied. Although the logical sequence was preserved in the thesis, each part was structured to discuss and address a specific flexural issue regarding strengthening reinforced concrete (RC) beams with fiber-reinforced polymers (FRPs). In general, the thesis experimentally, analytically, and numerically studies the possibility of using near surface mounted (NSM) and externally bonded (EB) techniques for strengthening and repairing continuous two-span beams. In summary, the experimental scheme of this thesis comprised 21 beams: 6 beams were simply supported with a 3-m length each, and 15 beams were continuous over two spans with a 6-m total beam length and 2.85-m span length each. The analytical analysis and design approaches as well as the finite element (FE) numerical models were developed or/and utilized in some parts according to their importance and necessity.

The first part studies the possibility of strengthening RC beams on their side surfaces instead of their soffits. Therefore, the side near surface mounted (SNSM or side-NSM) technique was proposed and investigated on six simply supported beams: one control beam and five others initially strengthened with 2 $\emptyset$ 6 carbon-FRP (CFRP) bars. Overall, the influence of CFRP length (as a ratio of the beam length), CFRP position (on the same level or above the steel rebar), and the filling material type (resin or mortar) were investigated. The results of the side-NSM CFRP beams tested in this part were compared with the results of the NSM-CFRP beam tested in the literature to assess and approve the use of the proposed side-NSM technique. An analytical model based on the conventional approaches was developed and evaluated for predicting the load deflection curves of tested beams. The test results showed that using the SNSM-CFRP rods technique allowed for significantly improving the load carrying capacity of RC beams but decreased their ductility and deflection at maximum load. The results obtained indicated that the failure mode was influenced by the length of CFRP rods and the filling material characteristics, while the strengthening position did not have a significant impact. The SNSM strengthening technique can be used as an alternative method to the NSM method, and in some cases, it may be used to prevent the nonconventional failure modes, due to degradation of the NSM strengthening system, such as the pull-out of CFRP-rods or premature debonding failure. The conventional analytical model accurately predicted the strength capacity and midspan deflection of the SNSM strengthened beams.

The second part presents an experimental and analytical study regarding the assessment of using the NSM technique for flexural strengthening of continuous RC beams. The experimental program of this part consists of six full-scale two-span beams: one control beam and five others strengthened with FRP bars in both hogging and sagging regions. The strengthening scenarios adopted in this part aimed to study and discuss important influential factors such as FRP type (carbon or glass), ratio ( $A_f/A_s= 18\%$  or  $26\%$ ), and length (according to the inflection point location) as well as the effects of the filling material characteristics (resin or mortar) on the global performance of continuous RC beams. Furthermore, an analytical model was proposed to predict the moment-curvature curves and the ultimate carrying load of NSM-FRP bar beams by taking advantage of the nonlinear analysis approach. The test results showed that

implementing the NSM technique in an appropriate way could significantly improve the yielding and load-carrying capacity of beams without a large decrease in their ductility or moment redistribution degree despite the nonconventional failure mode. The beams' failure was primarily affected by the strengthening length; terminating the FRP bars before the zero moment point caused the failure mode to change from a pulling-out of the FRP bars to a premature peeling-off of the concrete cover. On the other hand, the moment redistribution and ductility of the NSM-FRP beams were negatively affected by (i) increasing the FRP reinforcement, (ii) decreasing the FRP length, or (iii) using mortar as a filling material instead of using epoxy-resin. Finally, it was found that adopting the nonlinear analysis approach of the cross-sections could accurately quantify the moment-curvature and the ultimate load of the NSM-FRP continuous beams.

The third part presents a comparison between the NSM and side-NSM techniques for strengthening continuous two-span RC beams with CFRP rods. The study comprises two main sections: an experimental section and a FE section. First, results obtained from testing four beams (two of these four from the previous part; one control beam, two NSM beams, and one side-NSM beam) were analyzed and discussed. Several comparisons were made between the tested beams on the basis of their load-carrying capacity, failure mode, moment redistribution and CFRP bond strength. The ductility and energy absorption capacity of the beams as well as the strengthening effectiveness of the CFRP bars were also studied. Second, a numerical model based on the FE analysis using ABAQUS software was developed. The numerical model was assessed and validated through detailed comparisons between the results obtained from the FE simulations and the above mentioned experimental tests. The FE simulations were three dimensional (3D) and used the cohesive zone model (CZM) to describe the bond between the CFRP bars and concrete. Finally, the proposed numerical model was used for a parameter study to investigate and compare the potential of NSM and side-NSM systems for strengthening continuous beams. The parametric study focused on the influence of steel and CFRP arrangements on the moment redistribution and load-carrying capacity. The results obtained indicated that both the NSM and side-NSM techniques could be used to significantly improve the load-carrying capacity of continuous beams. For some strengthening configurations, the side-NSM technique proved to be more efficient than the NSM technique, particularly when the CFRP bars were applied solely in the hogging region or the sagging regions. In addition, the moment redistribution was negatively affected when the steel reinforcement ratio in the hogging region was increased, regardless of the CFRP position used.

The fourth part presents an experimental study that was primarily conducted to fill in the gaps in the literature regarding strengthening continuous RC beams with EB-CFRP. Generally, this part consists of three main sections. In the first section, seven large-scale two-span beams are statically investigated: one control beam (from part two) and six beams initially strengthened in terms of bending with CFRP sheets or plates. The principle aim of the first section is to investigate the effects of several factors, such as (i) the CFRP reinforcement position (side or top/bottom), (ii) the CFRP form (sheet or plate), (iii) the CFRP layer number (one or multilayer), and (iv) the weight of the carbon fibers (350 g/m<sup>2</sup>, 700 g/m<sup>2</sup>, or 1100 g/m<sup>2</sup>), on the load-carrying capacity, failure modes, cracking patterns, moment redistribution, and strain

analysis of continuous beams. The results showed that the side bonding system is a convenient alternative to the conventional system for strengthening beams. Moreover, increasing the carbon fiber weight per unit area was found to be effective for improving the strength capacity of beams, and it may be used as an alternative to multiple sheet layers. Furthermore, the moment redistribution that was found to occur in the region between the concrete cracking and the first steel yielding cannot be neglected and should be used when calculating the redistribution degree of EB-CFRP members. The second section evaluates the effectiveness of the current design codes in determining the flexural strength of continuous beams strengthened externally with CFRP sheets or plates. The experimental flexural strength capacities of the above tested beams are compared with those obtained from the design formulas provided in the American ACI 440.2R-08, the Italian CNR-DT 200 R1/2013, and the technical report of *fib* Bulletin 14. The assessments showed that the American and Italian guidelines are (relatively) more appropriate than the *fib* Bulletin 14 guideline. However, the current design codes accurately predicted the ultimate strength of beams strengthened with one CFRP layer but not with multiple layers. Finally, the third section assesses and compares the efficiencies of the EB and NSM techniques. For this purpose, another two beams (from part three) strengthened by means of the NSM and side-NSM-CFRP bars technique are tested and presented. Comparisons regarding the global flexural performance, including failure modes and load-carrying capacities, allow for confirming the higher efficiency of the NSM system in comparison to the EB system.

**Keywords:** RC beam, continuous, simply supported, flexural behavior, strengthening, NSM, Side-NSM, EB, side-EB, FRP rods, CFRP sheet, CFRP plate, moment redistribution, analytical model, finite element, ABAQUS.

---





## RÉSUMÉ EN FRANÇAIS

---

Cette thèse est composée de quatre parties, chacune présente plusieurs éléments de recherche en fonction du sujet abordé. Chaque partie a été structurée de sorte à aborder et analyser un problème de flexion spécifique concernant le renforcement des poutres en béton armé avec des matériaux composites (Fibre Reinforced Polymer (FRP)). L'objectif de cette thèse est d'étudier expérimentalement, analytiquement et numériquement par Eléments Finis (EF) les techniques de renforcement et de réparation par l'insertion des joncs composites (Near Surface Mounted reinforcement (NSM)) ou par le collage des tissus ou des lamelles composites (Externally Bonded (EB)) des poutres continues à deux travées. Le programme expérimental dans cette thèse comprend vingt et une poutres: six poutres de trois mètres de longueur chacune simplement appuyées, et quinze poutres continues de 6 mètres de longueur avec deux travées de 2,8 mètres. Les approches analytiques et de dimensionnement ainsi que la modélisation par EF ont été développées et utilisées dans certaines parties en fonction de leur importance et de leur nécessité.

La première partie concerne la possibilité de renforcer les poutres en Béton Armé (BA) par l'insertion de joncs de carbone (CFRP) dans les faces latérales des poutres (technique de SNSM) au lieu de leur faces inférieure ou supérieure tendues. Par conséquent, la technique de SNSM a été proposée et étudiée sur six poutres simplement appuyées: une poutre témoins sans renforcement et cinq autres renforcées avec deux joncs CFRP de 6mm de diamètre. L'influence de la longueur du jonc par rapport à la longueur totale de la poutre, sa position (au même niveau ou au-dessus des armatures longitudinales), ainsi que le type de matériau de scellement (résine ou mortier), ont été étudiés. Les résultats expérimentaux des poutres renforcées avec la technique SNSM testées dans cette partie ont été comparés à ceux des poutres renforcées avec la technique NSM testées dans la littérature afin d'évaluer et approuver l'utilisation de la technique SNSM proposée. Un modèle analytique basé sur les approches conventionnelles a été développé et évalué afin de prédire les courbes charge-flèche des poutres testées. Les résultats des essais expérimentaux ont montré que l'utilisation de la technique de SNSM permet d'améliorer de manière significative la capacité portante des poutres en BA mais elle diminue leur ductilité et leur flèche à la charge maximale. Les résultats obtenus montrent que le mode de ruine est influencé principalement par la longueur des joncs CFRP et les caractéristiques du matériau de scellement, tandis que la position des joncs n'a pas d'impact significatif. La technique de renforcement SNSM peut être utilisée comme technique alternative à la technique NSM, et dans certains cas, elle peut être utilisée pour éviter les modes de ruine non conventionnels causés par la rupture du système de renforcement par la technique NSM, tel que l'arrachement (pull-out) des joncs ou encore la rupture par le décollement prématuré. Le modèle analytique conventionnel prédit avec précision la charge ultime et la flèche à mi-portée des poutres renforcées par la technique SNSM.

La deuxième partie présente des études expérimentale et analytique concernant l'évaluation de l'utilisation de la technique NSM pour le renforcement en flexion des poutres continues en BA. Le programme expérimental de cette partie comporte six poutres de 6 m de longueur à deux travées de 2,8m : une poutre témoin et cinq autres poutres renforcées avec des joncs composites dans la région du moment positif (sagging) ainsi que celle du moment négatif (hogging). Les

configurations de renforcement adoptées dans cette partie visent à étudier et discuter des facteurs importants influençant la performance globale des poutres continues en BA tels que le type du matériaux composite (carbone ou verre), le rapport section de joncs composites( $A_f$ )/section d'armature ( $A_s$ ) ( $A_f / A_s = 18\%$  ou  $26\%$ ) et la longueur de ces joncs (en fonction de l'emplacement du point d'inflexion) ainsi que les effets des caractéristiques du matériau de scellement (résine ou mortier). De plus, un modèle analytique pour prédire les courbes moment-courbure et la charge ultime des poutres renforcées avec la technique NSM en considérant l'avantage de l'approche d'analyse non linéaire a été élaboré. Les résultats des essais ont montré que l'application de la technique NSM de manière appropriée peut améliorer considérablement la charge de plastification (limite élastique) des aciers et la charge ultime des poutres sans diminution significative de leur ductilité ou de leur degré de redistribution des moments malgré le mode de ruine non conventionnel. La rupture des poutres est principalement affectée par la longueur des joncs FRP; l'arrêt de ces joncs avant le point où l'inflexion entraîne le changement du mode de ruine par pull-out à la délamination prématurée du béton d'enrobage (peeling-off). D'autre part, la redistribution du moment et la ductilité des poutres renforcées par la technique NSM ont été affectées de manière négative par: (i) l'augmentation de la section des joncs, (ii) la diminution de leur longueur d'application ou (iii) l'utilisation du mortier comme matériau de scellement au lieu de la résine époxy. Enfin, il a été constaté que l'adoption de l'approche d'analyse non linéaire des sections transversales peut reproduire avec précision la relation moment-courbure ainsi que la charge ultime des poutres continues renforcées avec la technique NSM.

La troisième partie présente une étude comparative entre les techniques de renforcement NSM et SNSM des poutres continues en BA à deux travées. L'étude comprend deux sections principales; une section expérimentale et une section modélisation par EF. Premièrement, les résultats obtenus par les essais effectués sur quatre poutres continues (dont deux de la partie précédente); une poutre témoin, deux poutres renforcées avec la technique NSM et une poutre renforcée avec la technique SNSM ont été analysées et discutés. Plusieurs comparaisons ont été faites entre les poutres testées en termes, du mode de ruine, de la redistribution des moments et de la contrainte d'adhérence des joncs CFRP. La ductilité et la capacité d'absorption d'énergie des poutres ainsi que l'efficacité des renforcements ont également été évaluées. Ensuite, un modèle numérique basé sur l'analyse par EF a été développé à l'aide du logiciel ABAQUS. Le modèle numérique a été examiné et validé par des comparaisons détaillées entre les résultats obtenus à partir des simulations EF et les essais expérimentaux mentionnés ci-dessus. Les modélisations par EF sont tridimensionnelles (3D) et utilisent le modèle de zone cohésive (CZM) pour décrire la liaison entre joncs FRP et le béton. Enfin, le modèle numérique proposé a été utilisé pour une étude paramétrique afin d'analyser et comparer le potentiel des systèmes NSM et SNSM pour renforcer les poutres en BA continues. L'étude paramétrique s'est concentrée sur l'influence des dispositions constructives de l'acier et des joncs FRP sur la redistribution des moments et la charge ultime. Les résultats obtenus indiquent que les techniques NSM et SNSM pourraient être utilisées pour améliorer considérablement la capacité portante des poutres continues. Pour certaines configurations de renforcement, la technique SNSM s'est avérée plus efficace que la technique NSM, en particulier lorsque les joncs composites ont été appliqués uniquement dans la région hogging ou les régions sagging. De

plus, la redistribution des moments est affectée de manière négative lorsque le pourcentage d'aciers dans la région hogging augmente, quelle que soit la position des joncs FRP utilisés.

La quatrième partie présente une étude expérimentale menée principalement afin d'essayer de combler les lacunes dans la littérature concernant le renforcement des poutres continues en BA avec la technique EB. Cette partie est composée de trois sections principales. Dans la première section, sept poutres continues de 6 m de longueur à deux travées de 2,8 m sont étudiées statiquement: une poutre témoin (de la deuxième partie) et six poutres renforcées avec des tissus ou des lamelles CFRP. L'objectif principal de la première section est d'étudier les effets de plusieurs facteurs, tels que (i) la position de renforcement (zones hogging et sagging); (ii) le type du matériaux composite utilisé (tissu ou lamelle); (iii) le nombre de couches de tissus CFRP (une ou multicouche); et (iv) le poids des fibres de carbone (350 g / m<sup>2</sup>, 700 g / m<sup>2</sup> ou 1100 g / m<sup>2</sup>), sur la capacité portante, les modes de ruine, le comportement de fissuration, la redistribution des moments et l'analyse des déformations des poutres continues en BA renforcées. Les résultats montrent que le collage des tissus ou lamelles FRP sur la face latérale des poutres est une alternative pratique au système conventionnel pour le renforcement des poutres. De plus, l'augmentation du poids de la fibre de carbone par unité de surface s'avère efficace pour améliorer la capacité portante des poutres et elle peut être utilisée pour éviter de multiplier les couches de tissus CFRP. De plus, la redistribution des moments qui s'est produite dans la phase entre la fissuration du béton et la limite élastique des aciers ne peut pas être négligée et doit être utilisée pour calculer le degré de redistribution des membres renforcées avec des tissus ou des lamelles. La deuxième section de cette partie évalue l'efficacité des règlements de conception actuels pour déterminer la résistance à la flexion des poutres continues en BA renforcées à l'extérieur avec des tissus ou des lamelles. Les capacités portantes des poutres testées sont comparées à celles obtenues à partir des formules de conception fournies dans l'ACI américain 440.2R-08, l'italien CNR-DT 200 R1 / 2013 et le rapport technique du Bulletin 14 du fib. Les comparaisons ont montré que les codes américains et italiens sont relativement plus appropriés que les codes du Bulletin 14 du fib. Cependant, ils ont prédit avec précision la charge ultime des poutres renforcées avec une couche de tissus CFRP, mais pas avec plusieurs couches. Enfin, la troisième section évalue et compare les efficacités des techniques EB et NSM. A cet effet, deux autres poutres (de la troisième partie) renforcées par les techniques NSM et SNSM sont testées et présentées. Les comparaisons concernant les performances globales de flexion, en termes des modes de ruine et des capacités portantes, permettent de confirmer l'efficacité supérieure du système NSM par rapport à celui de EB.

**Mots clés:** Poutre en Béton Armé, Continue, Simplement Appuyée, Comportement en Flexion, Renforcement, Insertion de Joncs, Insertion de Joncs dans la Surface latérale, tissus en fibre de carbone, lamelle en fibre de carbone, redistribution de moment, modèle analytique, méthode des éléments finis, ABAQUS.

---



## NOMENCLATURE

### Acronyms

ABAQUS	Computer program
BL	Beam length
CFRP	Carbon fiber reinforced polymer
CZM	Cohesive zone model
CDP	Concrete damage plasticity
CCD	Concrete cover delamination
EB	Externally bonding
Epx	Epoxy-resin
FE	Finite element
FEA	Finite element analysis
FRPs	Fiber reinforced polymers
GFRP	Glass fiber reinforced polymer
H/Hogging	Negative bending moment region
ICs	Intermediate cracks
IP	Inflection point
LVDTs	Linear variable differential transducers
MPBM	Modified perfect bond model
NSM	Near surface mounted
PBM	Perfect bond model
RC	Reinforced concrete
Rebar	Reinforcement bars
S/Sagging	Positive bending moment region
S-EB	Side externally bonding
SL	Strengthening length
S-NSM/SNSM	Side near surface mounted
SSBs	Simply supported beams
3D	Three dimensions

### Notations

$A_s$	<i>Area of tension steel.</i>
$A'_s$	<i>Area of compression steel.</i>
$A_f$	<i>Area of FRP reinforcement.</i>
$A_f^H$	<i>Area of CFRP bars in the hogging region.</i>
$A_f^S$	<i>Area of CFRP bars in the sagging region.</i>
$A_{s1}$	<i>Area of the tensile steel reinforcement in the hogging region,</i>
$A_{s2}$	<i>Area of the tensile steel reinforcement in the sagging region, or the area of compression steel.</i>
$A_v$	<i>Area of the shear reinforcement of one stirrup</i>

$a$	<i>Distance between the applied point load and support.</i>
$B$	<i>Bottom.</i>
$b$	<i>Width of the cross section.</i>
$b_f$	<i>Width of the FRP sheet or plate.</i>
$C$	<i>Concrete compressive force.</i>
$C_E$	<i>Environmental reduction factor.</i>
$d_b, d_{FRP}$	<i>Diameter of FRP bar.</i>
$d$ or $d_s$	<i>Effective depth of tension steel bars.</i>
$d_1$ or $d_f$	<i>Effective depth of the FRP reinforcement.</i>
$d_2$	<i>Effective depth of compression steel bars.</i>
$d_c$	<i>Degradation of concrete under compression.</i>
$d_t$	<i>Degradation of concrete under tension.</i>
$E_{ab}$	<i>Energy absorption capacity.</i>
$E_c$	<i>Elastic modulus of concrete.</i>
$E_{FRP}$	<i>Modulus of elasticity of FRP.</i>
$E_{sp}$	<i>Plastic modulus of steel.</i>
$F$	<i>Filling material.</i>
$F_s$	<i>Steel tensile force.</i>
$F_f$	<i>FRP tensile force.</i>
$FC$	<i>A calibrated factor</i>
$f_t$	<i>Concrete tensile strength.</i>
$f_{ct}$	<i>Maximum tensile strength of concrete.</i>
$f_a$	<i>Maximum tensile strength of resin.</i>
$f_y$	<i>Elastic limit stress of the tensile steel.</i>
$f'_c$	<i>Concrete compressive strength.</i>
$f_{cm}$	<i>The concrete mean compressive strength.</i>
$f_{ctm}$	<i>The concrete mean tensile strength.</i>
$f_{fk}$	<i>The characteristic value of the FRP tensile strength.</i>
$G_1, G_2$	<i>Coefficients function determined according to the ratio of adhesive to the diameter of FRP bar.</i>
$G_{cr}$	<i>Fracture energy.</i>
$h''$	<i>Width of the confined concrete zone measured to the outside periphery of the steel stirrups.</i>
$I_{eff}$	<i>Effective moment of inertia of the entire beam.</i>
$I_g$	<i>Gross moment of inertia.</i>
$I_{cr}$	<i>Cracked moment of inertia.</i>
$I_{tr}$	<i>Un-cracked moment of inertia of the transformed section.</i>
$K$	<i>The strength coefficients of the Kent-Scott-Park model.</i>
$k_{G2}$	<i>A corrective factor calibrated on the experimental results.</i>
$k_q$	<i>A coefficient that considers load distribution</i>
$k_b$	<i>Geometrical corrective factor</i>
$L$	<i>Length of the FRP or span.</i>
$L_d$	<i>Embedment length of FRP bar.</i>
$l_b$	<i>Bond length.</i>
$l_{ed}$	<i>The design optimal bond length</i>

$M_n$	Nominal moment.
$m$	Coefficient of friction between adhesive and FRP bar.
$M_h^{Exp}$ or $M_2^{Exp}$	Experimental flexural moment in the hogging region.
$M_s^{Exp}$ or $M_1^{Exp}$	Experimental flexural moment in the sagging region.
$M_h^{Th}$ or $M_2^{Th}$	Theoretical flexural moment in the hogging region.
$M_s^{Th}$ or $M_1^{Th}$	Theoretical flexural moment in the hogging region.
$M_{cr}$	Cracking moment.
$M_y$	Yielding moment.
$M_u$	Ultimate moment.
$M$	Bending moment.
$M_{Rd}$	The flexural strength of the strengthened section
$N_s^{cr(max)}$	Maximum number of cracks in the sagging regions.
$N_h^{cr}$	Total number of cracks in the hogging region.
$n_s$	Ratio of $N_s^{cr(max)}$ of NSM beam to $N_s^{cr(max)}$ of CB
$n_h$	Ratio of $N_h^{cr}$ of NSM beam to $N_h^{cr}$ of CB.
$P$	Applied load.
$P_t$	Total applied load.
$P_{cr}$	Cracking load.
$P_y$	Yielding load.
$P_u$	Ultimate load.
$P_u^{Th}$	Theoretical ultimate load capacity of a beam.
$P_u^{Exp}$	Experimental ultimate load capacity of a beam.
$P_e$	External reaction.
$R$	Ratio of the FRP.
$R_c$ or $P_c$	Central reaction.
$s$	Center to center spacing of the steel stirrups.
$s_m$	The ultimate slip
$S_s^{avg}$	Average crack spacing in the sagging regions.
$S_h^{avg}$	Average crack spacing in the hogging region.
$S_u$	The FRP-concrete interfacial debonding slip
$T$	Top or Temperature.
$X, X_i$ or $X_e$	Depth of the neutral axis.
$\chi$	Efficiency ratio of the CFRP rods.
$x_s$	Values (load, displacement...etc) of a strengthened beam.
$x_r$	Values (load, displacement...etc) of a control beam.
$x_s$	Ratio of $S_s^{avg}$ of NSM beam to $S_s^{avg}$ of CB.
$x_h$	Ratio of $S_h^{avg}$ of NSM beam to $S_h^{avg}$ of CB.
$y_b$	Distance between the most tensile concrete fiber and the neutral axis before cracking.
$y_{nc}$	Neutral axis depth of the transformed section.
$Z$	The strain coefficients of the Kent-Scott-Park model.
$\delta$	Deflection.
$\delta_u$	Deflection at the ultimate load.

$\delta_{cr}$	<i>Deflection at the cracking load.</i>
$\delta_y$	<i>Deflection at the yielding load.</i>
$\delta_f$	<i>Deflection at the end of the test</i>
$\delta_G$	<i>The coefficient of the rectangular stress centroid for concrete in compression.</i>
$\varepsilon_{y(exp)}$	<i>Experimental steel yielding strain.</i>
$\varepsilon_{fu}$ or $\varepsilon_{fud}$	<i>Ultimate tensile strain of FRP rod.</i>
$\varepsilon_{fk}$	<i>Characteristic failure strain in FRP.</i>
$\varepsilon_{ef}$	<i>The effective level of strain in FRP.</i>
$\varepsilon_{fd}$	<i>Debonding strain in FRP.</i>
$\varepsilon_{fdd}$	<i>The FRP IC-induced debonding strain.</i>
$\varepsilon_{cu}$	<i>Ultimate compressive strain of concrete.</i>
$\varepsilon_f$ or $\varepsilon_{CFRP}$	<i>Strain in FRP.</i>
$\varepsilon_s$	<i>Strain in steel.</i>
$\varepsilon_{s1}$	<i>Strain in the tension steel.</i>
$\varepsilon_{s2}$	<i>Strain in the compression steel.</i>
$\varepsilon_{sy}$	<i>The design yield strain of the steel reinforcement</i>
$\varepsilon_0$	<i>The maximum tensile strains present before the FRP is applied</i>
$\varepsilon_h$	<i>The strain of steel at the beginning of strain hardening zone.</i>
$\varepsilon_f$	<i>Strain in FRP.</i>
$\varepsilon_c$	<i>Strain in concrete.</i>
$\varepsilon_{FRP}^{max}$	<i>Maximum recorded tensile strain of FRP.</i>
$\varepsilon_{FRP}^{ult}$	<i>Ultimate tensile strain of FRP.</i>
$\mu$	<i>Ductility index.</i>
$\sigma$	<i>Tensile stress.</i>
$\sigma_c$	<i>Compressive strength of concrete.</i>
$\sigma_s$ or $\sigma_{s1}$	<i>Stress of steel in tension.</i>
$\sigma'_s$ or $\sigma_{s2}$	<i>Stress of steel in compression.</i>
$\sigma_f$	<i>Stress of FRP bars.</i>
$\sigma_{FRP}^{max}$	<i>Maximum tensile stress in FRP.</i>
$\sigma_{FRP}^{ult}$	<i>Ultimate tensile stress in FRP.</i>
$\sigma_{bo}$	<i>The biaxial compressive yield stress.</i>
$\sigma_{co}$	<i>The uniaxial compressive yield stress.</i>
$\sigma_n$	<i>Normal stress.</i>
$\rho_s$	<i>Reinforcement ratio of tensile steel.</i>
$\rho'_s$	<i>Reinforcement ratio of compression steel.</i>
$\rho_s^S$	<i>The steel reinforcement ratio in the sagging region.</i>
$\rho_s^H$	<i>The steel reinforcement ratio in the hogging region.</i>
$\beta$	<i>Moment redistribution.</i>
$\beta_1$	<i>The concrete stress block factor.</i>
$\beta_H$	<i>The moment redistribution degree in the hogging region.</i>
$\beta_S$	<i>The moment redistribution degree in the sagging region.</i>
$\alpha$	<i>Ratio between hogging and sagging moment redistribution.</i>
$\emptyset$	<i>Diameter, curvature or strength reduction factor.</i>
$v$	<i>Shear force.</i>
$\alpha$	<i>Debonding factor.</i>



$\alpha_1$	<i>The concrete stress block factor.</i>
$\tau$	<i>The experimental average bond stress.</i>
$\tau_m$ or $\tau_{max}$	<i>The maximum bond stress.</i>
$\tau_s$ and $\tau_t$	<i>The shear stresses of the interface.</i>
$\Psi$	<i>The dilatation angle.</i>
$\psi_f$	<i>Reduction factor.</i>
$\psi$	<i>A coefficients representing the intensity of the compressive concrete resultant</i>
$\epsilon$	<i>Flow potential eccentricity.</i>
$K_c$	<i>The ratio of the second stress invariant on the tensile meridian.</i>
$\varphi$	<i>The aspect ratio of the interface failure plane.</i>
$\lambda$	<i>The load-carrying capacity index.</i>
$\gamma_f$	<i>The material safety factor.</i>
$\gamma_{f,d}$	<i>A safety factor that depends on the probability associated with debonding failure.</i>
$\gamma_{Rd}$	<i>The partial factor for resistance models.</i>
$\eta$	<i>The FRP stress limitation coefficient.</i>



# TABLE OF CONTENTS

Table of contents .....	1
List of figures .....	5
List of tables .....	9
I. Résumé long en français .....	11
II. Introduction.....	35
Chapter 1: Experimental study on strengthening of RC beams with Side Near Surface Mounted technique-CFRP bars.....	39
1.1 Introduction .....	40
1.2 Experimental program .....	43
1.2.1 Test beams and materials. ....	43
1.2.2 Beam strengthening.....	44
1.2.3 Instruments and test procedure.....	45
1.3 Results and discussion .....	46
1.3.1 Load-deflection response .....	46
1.3.2 Failure mods and cracking pattern .....	47
1.3.3 Enhancement of load carrying capacity of SNSM strengthened beams. ....	50
1.3.4 Ductility.....	54
1.3.5 Energy absorption .....	55
1.4 SNSM and NSM techniques: comparison and discussion.....	55
1.5 Analytical model- Application of conventional prediction techniques .....	62
1.5.1 Prediction of deflection response ( $\delta_{mid}$ ).....	62
1.5.2 Prediction of cracking moment( $M_{cr}$ ).....	63
1.5.3 Prediction of yielding moment ( $M_y$ ) .....	63
1.5.4 Prediction of ultimate moment( $M_u$ ) .....	63
1.5.5 Performance of the analytical model.....	64
1.6 Conclusion: .....	64
1.7 Appendix (A): Calculation of the transformed moment of inertia. ....	65
1.8 Appendix (B): Calculation of the failure moment. ....	65
1.9 References .....	69
Chapter 2: Assessment of the flexural behavior of continuous RC beams strengthened with NSM-FRP bars, experimental and analytical study .....	73
2.1 Introduction .....	74

2.2	Materials .....	77
2.2.1	Concrete and filling material .....	77
2.2.2	Steel and FRP reinforcement.....	77
2.3	Experimental program .....	78
2.3.1	Beam details .....	78
2.3.2	Test description .....	79
2.3.3	Groove preparation and strengthening procedure .....	83
2.3.4	Test setup and instrumentation.....	83
2.4	Results and discussion .....	84
2.4.1	Load-deflection response .....	84
2.4.2	Energy absorption capacity .....	87
2.4.3	Failure mode and overall capacity .....	87
2.4.4	Cracking maps and cracking behavior .....	90
2.4.5	Beam ductility .....	91
2.4.6	Moment redistribution.....	94
2.4.7	Strain analysis .....	96
2.5	Nonlinear analysis of strengthened sections.....	102
2.6	Conclusion.....	111
2.7	References .....	112

Chapter 3 : Experimental and numerical investigation on the effectiveness of NSM and side-NSM CFRP bars for strengthening continuous two-span RC beams..... 117

3.1	Introduction .....	118
3.2	Experimental work .....	121
3.2.1	Experimental program.....	121
3.2.2	Main test results and discussion.....	124
3.3	Numerical investigation.....	131
3.3.1	Material properties .....	132
3.3.2	Interaction and contact conditions.....	134
3.3.3	Finite element modelling of tested beams.....	137
3.3.4	Finite element results and discussion .....	138
3.3.5	Parametric study-Arrangement of the reinforcement.....	142
3.4	Conclusion .....	146
3.5	Appendix .....	148
3.6	References .....	148

Chapter 4 : Efficiency of EB CFRP composites for flexural strengthening of continuous RC beams: A comparative study with NSM CFRP rods..... 151

4.1	Introduction .....	152
4.2	Experimental Program .....	155
4.2.1	Tested beams and material properties .....	155
4.2.2	Surface preparation and strengthening technique .....	160

4.2.3	Instrumentation and test setup .....	160
4.3	Results and Discussion .....	161
4.3.1	Load-deflection response .....	161
4.3.2	Failure modes .....	164
4.3.3	Crack maps and crack width .....	167
4.3.4	Strain of steel and CFRP reinforcement.....	170
4.3.5	Moment redistribution.....	173
4.4	Evaluation of the effectiveness of the current guidelines in determining the flexural strength of EB-CFRP continuous beams .....	178
4.4.1	ACI 440.2R-08 .....	179
4.4.2	CNR-DT 200 R1/2013 .....	180
4.4.3	<i>fib</i> Bulletin 14.....	182
4.4.4	Comparison of the ultimate moment obtained from tests and current design codes	
	183	
4.5	Comparison between the EB and NSM for strengthening continuous RC beams. .	183
4.5.1	Overall performance.....	185
4.5.2	Failure mode and cracks maps .....	186
4.5.3	Yield and ultimate strength capacity .....	186
4.5.4	Moment redistribution.....	187
4.6	Conclusion .....	188
4.7	References .....	192
III. General conclusion & future work.....		195
IV. Scientific Production.....		201
V. References.....		203



## LIST OF FIGURES

Figure I-1 : Procédure de la technique NSM.....	12
Figure I-2 : Procédure de la technique EB (tissus ou lamelles) .....	12
Figure I-3 : Schémas des poutres testées et leurs ferrillages. (toutes les dimensions sont en mm) .....	14
Figure I-4 : Comparaison entre les techniques NSM et SNSM pour le renforcement des poutres testées en chapitre I par des courbes moment de flexion-flèche en fonction de plusieurs configurations.....	15
Figure I-5 : Schémas des poutres testées et leurs ferrillages. (toutes les dimensions sont en mm) .....	15
Figure I-6 : Schémas des renforcements des poutres testées. (toutes les dimensions sont en mm) .....	17
Figure I-7 : Modes de ruine principaux observés pour les poutres continues renforcées par la technique NSM.....	18
Figure I-8 : Courbes charge-flèche des poutres continues renforcées avec la technique testées en Chapitre 2 .....	19
Figure I-9 : Moments de flexion expérimental et élastique des poutres testées à la charge ultime, ( $\rho_s^h/\rho_s^s=1$ ). .....	20
Figure I-10 : Courbes charge-flèche des poutres testées .....	21
Figure I-11 : Variation longitudinale des déformations des joncs CFRP en fonction de la charge appliquée. ....	22
Figure I-12 : Modèle d'une liaison parfaite.....	23
Figure I-13 : Modèle avec une zone adhésive (CZM) .....	23
Figure I-14 : Comparaison de courbes charge-déformation expérimentales et numériques des poutres testées .....	24
Figure I-15 : Schémas de fissuration et modes de ruines des poutres renforcées .....	25
Figure I-16 : Coubes charge-flèche des poutres simulées par EF .....	26
Figure I-17 : Tissus CFRP avec différentes masses par unité de surface. ....	27
Figure I-18 : Courbes charge-flèche des poutres testées.....	28
Figure I-19 : pourcentage des moments de flexion des poutres renforcées testées.....	29
Figure I-20 : Comparaison des performances des poutres renforcées . ....	30
Figure 1-1:Minimum dimensions of grooves .....	44
Figure 1-2 : Test beams details and reinforcement configuration. (All dimensions are in mm) .....	44
Figure 1-3 : (a) Test setup, (b) Instrumentation and (c) Strain gauges of steel and CFRP bars (top view). (All dimension are in mm).....	46
Figure 1-4 : Load vs. mid-span deflection curves .....	47
Figure 1-5 : Failure mode of beams; (a) BC1(270-SR) and (b) BC5(270-UR) .....	48
Figure 1-6 : Failure mode of beams: (a) BC3(270-SM) and (b) BC4(210-SM) .....	49
Figure 1-7 : Failure mode of beam: BC2(210-SR) .....	50
Figure 1-8 : Total applied load vs. strains of the CFRP rods .....	51
Figure 1-9 : Total applied load vs. steel strain .....	51
Figure 1-10 : Energy absorption of beam specimens .....	56
Figure 1-11 : Comparisons between NSM and SNSM beams tested in chapter 1 based on the load deflection curves.....	58

Figure 1-12 : Failure mechanism of a) S-C6(270-R) beam and b) BC1(270-SR) and BC5(270-UR) beams.....	60
Figure 1-13 : Debonding failure mechanism of : a) BC3(270-SM) beam and b) S-C6(270-M) beam .....	60
Figure 1-14 : Peeling off failure mechanism of: a) BC2(210-SR) beam and b) S-C6(210-R) beam .....	61
Figure 1-15 : Ductility comparison between the SNSM and NSM specimens.....	61
Figure 1-16 : Deflection calculation methodology.....	63
Figure 1-17 : Cracked section .....	63
Figure 1-18 : Compression between the experimental and computed deflection. ....	67
Figure 1-19 : Comparison between experimental and theoretical moment-deflection curves. ....	68
Figure 2-1 : Filling materials for bonding the NSM-FRP bars to concrete.....	77
Figure 2-2 : FRP reinforcements .....	78
Figure 2-3 : Dimensions, steel reinforcement layout as well as support and load arrangement of tested beams. ....	80
Figure 2-4 : Beam specimens strengthened with FRP rods by using the NSM technique.....	81
Figure 2-5 : Strengthening procedure of NSM-FRP bars.....	82
Figure 2-6 : Test setup and the instrumentations used for testing beams .....	84
Figure 2-7 : Locations of strain gages on steel bars, FRP bars and concrete.....	85
Figure 2-8 : Load-deflection response of tested beams.....	86
Figure 2-9 : Conventional flexural failure of control beam, CB. ....	87
Figure 2-10 : Failure mode of beam BC1 .....	88
Figure 2-11 : Failure mode of beam BG1 .....	88
Figure 2-12 : Failure mode of beam BC2-R .....	89
Figure 2-13 : Failure mode of beam BC3-L.....	90
Figure 2-14 : Failure mode of beam BC4-F .....	90
Figure 2-15 : Cracks maps of tested beam specimens .....	93
Figure 2-16 : Total applied load vs. crack width at hogging region of tested beams.....	94
Figure 2-17 : Total applied load versus central support reaction of tested beams. ....	96
Figure 2-18 : Experimental and elastic bending moment of tested beams at the ultimate load. ....	98
Figure 2-19 : Strains of tension steel bars, FRP bars and compressive concrete at central support. ....	99
Figure 2-20 : Strains of tension steel bars, FRP bars and compressive concrete at right mid-span.....	100
Figure 2-21 : Variation in longitudinal strain of FRP bars at different loads. ....	103
Figure 2-22 : Beam cross-section, strains and stresses. ....	107
Figure 2-23 : Stress strain of steel .....	108
Figure 2-24 : Stress strain of FRP. ....	108
Figure 2-25 : External and internal loads. ....	108
Figure 2-26 : Experimental and prediction of moment curvature diagrams of strengthened beam .....	111
Figure 3-1 : Dimensions, steel layout as well as support and load arrangement of tested beams. (All dimensions are in mm).....	121
Figure 3-2 : Beam specimens strengthened with CFRP rods. (All dimensions are in mm)...	123
Figure 3-3 : Test setup and the instrumentations used for testing beams. ....	123
Figure 3-4 : Load deflection curve of tested beams .....	125



Figure 3-5 : Failure mode of control beam, CB-E .....	127
Figure 3-6 : Failure mode of beam BC1-E-NSM.....	127
Figure 3-7 : Failure mode of beam BC2-E-SNSM .....	127
Figure 3-8 : Total applied load versus (a) bending moment; (b) central support reaction.....	129
Figure 3-9 : Variation in longitudinal strain of FRP bars at different loads. ....	130
Figure 3-10 : Experimental average shear stress.....	130
Figure 3-11 : Response of concrete to uniaxial loading in (a) compression and (b) tension .	132
Figure 3-12 : Constitutive model of steel reinforcement .....	133
Figure 3-13 : Constitutive model of CFRP reinforcement .....	134
Figure 3-14 : Perfect bond model.....	135
Figure 3-15 : Cohesive zone model.....	135
Figure 3-16 : Bond slip law .....	135
Figure 3-17 : Comparison between the experimental results and FEA results with different value of maximum shear stress for beam BC1-E/N-NSM.....	137
Figure 3-18 : Detail and boundary condition of the FE beam (all dimension are in mm) .....	138
Figure 3-19 : Effect of the mesh size .....	139
Figure 3-20 : The experimental and numerical load deflection curves of tested beams. ....	140
Figure 3-21 : Cracks maps and failure of strengthened beams .....	141
Figure 3-22 : The experimental and FEA results of central support reaction of tested beams	142
Figure 3-23 : The FEA (CZM) tensile stress of CFRP bars in the strengthened beams at the ultimate load level .....	143
Figure 3-24 : Load-deflection curves of FE beams.....	147
Figure 4-1 : Dimensions, steel reinforcement layout and support arrangement of the tested beams.....	158
Figure 4-2 : (a) Elevation view and cross-sections of the beam specimens and (b) Length of CFRP sheets/plates in beams. (All dimensions are in mm) .....	159
Figure 4-3 : CFRP sheets used for strengthening beams.....	160
Figure 4-4 : Epoxy resin material for bonding the CFRP (a) sheets and (b) plates .....	160
Figure 4-5 : Strengthening procedure of EB-CFRP beam specimens.....	161
Figure 4-6 : Instrumentation and test setup .....	162
Figure 4-7 : Load deflection curves of tested beams .....	163
Figure 4-8 : Failure mode of control beam, CB. ....	165
Figure 4-9 : Failure mode of beam BC2-EB1P.....	165
Figure 4-10 : Failure mode of beam BC6-EB1S-weight (1100).....	166
Figure 4-11 : Failure mode of beam BC1-EB1S.....	166
Figure 4-12 : Failure mode of beam BC4-EB2S.....	167
Figure 4-13 : Failure mode of beam BC5-EB1S-weight(700).....	167
Figure 4-14 : Failure mode of beam BC3-SEB1S-side.....	167
Figure 4-15 : Crack maps of tested beams .....	169
Figure 4-16 : Total applied load vs. the cracks width of control an strengthened beams. ....	170
Figure 4-17 : Total applied load versus tensile strain of the steel bars. ....	171
Figure 4-18 : Axial stiffness ratio vs. increasing the yielding load.....	172
Figure 4-19 : Total applied load versus tensile strain of CFRP reinforcement.....	173
Figure 4-20 : CFRP sheet area vs. debonding strain. ....	173
Figure 4-21 : Moment redistribution of tested strengthened beams.....	177
Figure 4-22 : Moment ratio of tested strengthened beams.....	178

Figure 4-23 : Cross-section and groove dimensions details of NSM beams (All dimensions are in mm). .....	185
Figure 4-24 : Variation in longitudinal strain of NSM-CFRP bars at different loads.....	187
Figure 4-25 : Variation in longitudinal strain of EB-CFRP bars at different loads. ....	188
Figure 4-26 : Load deflection curves of NSM beams and EB beams. ....	190

## LIST OF TABLES

Table II-1: Outline and objectives of the present research.....	36
Table 1-1: Characteristics of the filling material.....	45
Table 1-2 : Strengthening details of the test beams. ....	45
Table 1-3 : Experimental results of the test beams .....	52
Table 1-4 : Mid-span deflection and ductility of the tested beams .....	55
Table 1-5 : Comparison between experimental results of the SNSM and NSM techniques ...	59
Table 2-1 : Characteristics of the filling material.....	77
Table 2-2 : Characteristics of the FRP bars.....	78
Table 2-3 : Test matrix and details of the control and strengthened beams .....	82
Table 2-4 : Cracks number and average crack spacing of strengthened and unstrengthened beams. .....	92
Table 2-5 : Ductility index of tested beams. ....	94
Table 2-6 : Total applied load, central support reaction, bending moments and moment redistribution of tested beams at level of peak applied load .....	97
Table 2-7 : Compression between experimental and analytical maximum strain of FRP bars .....	107
Table 2-8 : Experimental and theoretical ultimate load of strengthened beams. ....	111
Table 3-1 : Test matrix and details of the control and strengthened beams.....	122
Table 3-2 : Main experimental results of control, NSM and SNSM beam.....	125
Table 3-3 : Crack width of tested beams at different load levels. ....	128
Table 3-4 : Tensile strains of CFRP bars at different load levels.....	131
Table 3-5a : Resume of the strengthening arrangements, $\rho_s H = 0.5\%$ . (2D10).....	144
Table 3-6a : FEA results of the strengthening arrangements, $\rho_s H = 0.5\%$ . (2D10).....	145
Table 4-1 : Beams details .....	157
Table 4-2 : Characteristics of the CFRP composites.....	157
Table 4-3 : Characteristics of the epoxy-resin .....	157
Table 4-4 : Moment redistribution, as reported from literature, for continuous beams strengthened with EB-FRP at the ultimate state level.....	176
Table 4-5 : Comparison of the ultimate bending moment obtained from the tests and current design codes. ....	184
Table 4-6 : Details of the NSM-CFRP bar beams.....	184
Table 4-7 : Comparison between the test results of the NSM/SNSM beams and EB beams.	190
Table 4-8 : Crack maps and failure mode of the NSM beams . ....	191



## I. RÉSUMÉ LONG EN FRANÇAIS

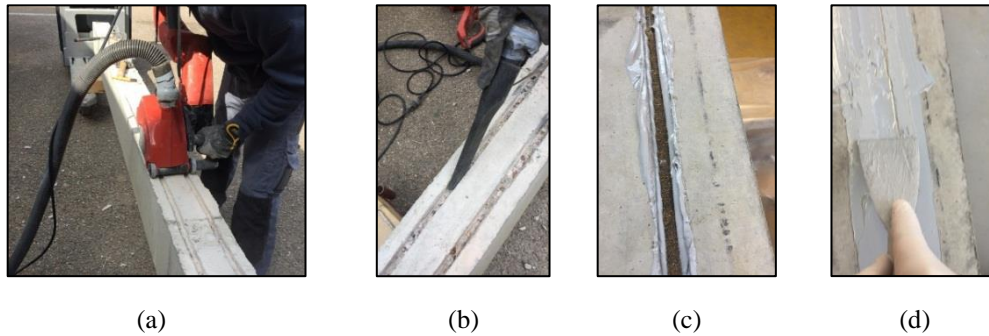
---

La poutre en Béton Armé (BA) est un élément structurel horizontal généralement utilisé pour supporter le poids des planchers et des toits d'une structure et pour transférer la charge à un élément porteur vertical tel qu'un poteau ou un mur. Elle peut être simplement appuyée, continue ou en porte-à-faux. Les poutres continues sont la forme la plus utilisée dans les structures. Elles sont préférées pour les ponts à poutres uniformes et les bâtiments situés dans des environnements sévères ou dans des zones exposées à des risques sismiques élevés. Les poutres continues ont le potentiel d'améliorer l'intégrité et la rigidité de la structure et peuvent offrir une redistribution des moments en raison de la redondance de la structure. Cela permet d'exploiter la réserve de résistance disponible et d'optimiser les sections sans congestion de renforcement aux sections critiques (en travées et sur appuis). De plus, les poutres continues sont généralement utilisées comme parties d'un portique. Ce mode d'emploi réduit les moments en travée et les déformées et offre une meilleure résistance aux charges latérales comparé aux poutres simplement appuyées.

Les poutres en BA, comme les autres éléments structurels, peuvent nécessiter des réparations ou des renforcements, soit pour augmenter leur durée de vie, soit pour améliorer leurs capacités de chargement et de déformation. Plusieurs raisons justifient la nécessité d'un processus de renforcement ou de réparation, par exemple : placement ou longueur insuffisante des armatures principales, utilisation d'un béton à faible résistance ou sa détérioration, amélioration des conceptions initiales et restauration de la résistance des éléments structurels à la suite d'accidents ou de risques naturels tels que les tremblements de terre. Dans les années 1980, le renforcement des ponts [1] et des poteaux [2] avec des plaques ou des manchons en acier était couramment pratiqué, en particulier aux États-Unis et en Europe. Depuis le début des années 1990, la tendance était d'étudier la faisabilité d'utiliser les matériaux composites (Fiber Reinforced Polymer (FRP)) dans l'industrie de la construction [3]. Quelques années plus tard, et plus particulièrement depuis le début des années 2000, les FRP ont presque entièrement remplacé les plaques et les manchons en acier comme matériaux de renforcement pour les structures en BA [4-6]. En effet, les FRP ont montré d'excellentes propriétés comparés aux armatures en acier conventionnelles, telles qu'une résistance à la traction plus élevée, une meilleure résistance à la corrosion et au feu et un poids plus faible. Au cours des dix dernières années, la technologie de renforcement par l'insertion des joncs composites dans la surface de béton (Near Surface Mounted reinforcement (NSM)) est considérée comme une alternative prometteuse à la technique de renforcement par le collage externe des tissus ou lamelles (Externally Bonded (EB)) [7]. En général, les FRP sous forme de tissus ou lamelles peuvent être appliqués aux éléments structurels endommagés en tant que renforcement externe via la technique EB, tandis que ceux sous forme de joncs sont utilisés en tant que renforcement interne via la technique NSM. Les [Figure I-1](#) et [Figure I-2](#) montrent les principales étapes qui sont généralement suivies pour mettre en œuvre ces techniques. La technique NSM s'avère plus intéressante en raison des avantages suivants :

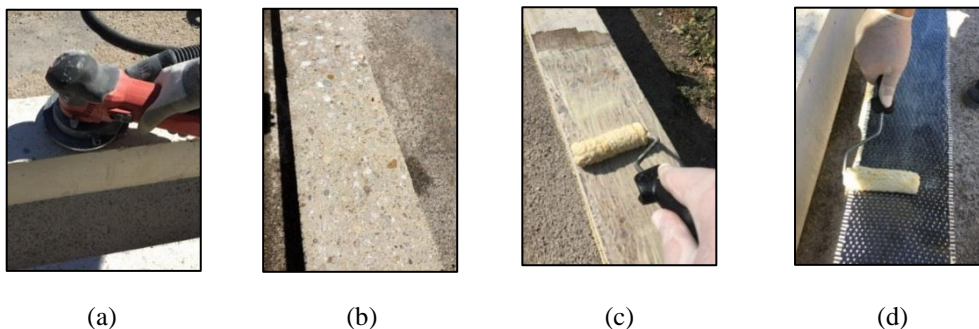
1. Elle est assez simple et ne nécessite pas de travaux de préparation de surface importants. Les joncs ou les bandes de FRP sont insérés à côté des barres d'acier longitudinales et scellés dans des engravures prédécoupées dans la structure. Elles sont liées au béton avec des résines Époxy ou des mortiers [8];

2. Les éléments en BA renforcés par la technique NSM sont plus ductiles et subissent des ruptures à un niveau plus élevé comparés éléments renforcés avec la technique EB [9, 10] ;
3. Le renforcement des éléments en BA par la technique NSM offre une meilleure liaison avec le béton et une meilleure protection pour le renforcement en FRP par rapport à la technique de renforcement EB [11].



(a) Réalisation des engravures à l'aide d'une scie à béton spéciale; (b) Nettoyage des engravures par aspiration d'air; (c) Mise en place des joncs de FRP sur une couche de matériau de scellement préalablement coulée (d) Arasement de la surface à l'aide d'une spatule à main après le remplissage total des engravures.

Figure I-1 : Procédure de la technique NSM



(a) Préparation de la surface de béton par une meuleuse, (b) Nettoyage de la surface de béton par aspirateur d'air, (c) application d'une couche de résine époxy; et (d) collage des tissus de FRP.

Figure I-2 : Procédure de la technique EB (tissus ou lamelles)

Des études approfondies ont été menées sur l'utilisation des FRP pour renforcer et réparer les poutres simplement appuyées (Simply Supported Beams (SSB)) [12-18], les jonctions poutres-poteaux [19-21] et les colonnes [22-24]. Malgré les modes de ruine non conventionnels, il a été constaté que l'amélioration de la résistance à la flexion des poutres SSB grâce aux FRP est significative et peut atteindre, dans certaines configurations de renforcement, plus de 90 % avec la technique EB [12] et plus de 130 % avec la technique NSM [25]. Les systèmes de renforcement EB ou NSM peuvent ne pas être réalisables dans leur forme initiale pour certains cas pratiques. Ces systèmes peuvent présenter des lacunes ou des limitations dues aux contraintes architecturales imposées, aux dimensions insuffisantes de la poutre elle-même et à la possibilité d'endommager d'autres éléments, tels que les poteaux, pendant la préparation et l'installation. Il est donc essentiel de trouver d'autres méthodes de renforcement pour surmonter ces limites. Salama et al. [12], ont étudié expérimentalement la possibilité de coller

extérieurement des tissus de CFRP sur les surfaces latérales des poutres SSB. Les résultats ont montré une réduction d'environ 16,1% de la résistance ultime des poutres renforcées sur leurs surfaces latérales par rapport à celles renforcées sur la face inférieure (face tendue).

Dans le premier chapitre de cette thèse, l'approche de renforcement latéral est adoptée et étudiée expérimentalement sur les poutres SSB. Un total de six poutres rectangulaires en BA, y compris une poutre témoin, ont été testées jusqu'à la ruine. La charge de flexion à quatre points est appliquée de façon monotone. Les poutres en BA ont été conçues pour subir une ruine par flexion conformément au code ACI [26]. Elles ont été armées par deux barres d'acier HA ordinaires de 12 mm de diamètre dans la zone tendue et deux barres de 6 mm de diamètre dans la zone de compression, comme le montre la [Figure I-3](#).

Le plan de ferrailage concernant le premier chapitre a été conçu afin d'étudier l'efficacité de la technique NSM pour des joncs insérés dans les surfaces latérales des poutres (Side NSM (SNSM)) dans l'amélioration de la capacité de flexion des poutres en BA. La performance globale en flexion des poutres de série BC1(270-SR), BC2(210-SR), BC3(270-SM) et BC4(210-SM), a été étudiée en fonction de la longueur des joncs de carbone et du type de matériau de scellement. Les joncs de carbone utilisés pour renforcer les quatre poutres ci-dessus ont été placés au même niveau que l'acier de traction (à environ 42 mm de la surface inférieure de la poutre). Les poutres BC1(270-SR) et BC3(270-SM) ont été renforcées avec des joncs de carbone (CFRP) de 270 cm de long, tandis que des joncs CFRP de 210 cm de long ont été utilisés dans les poutres BC4(210-SM) et BC2(210-SR). Les joncs CFRP ont été scellés dans la résine dans le cas des poutres BC1(270-SR) et BC2(210-SR); alors que pour les poutres BC3(270-SM) et BC4(210-SM), les joncs ont été scellés dans le mortier. En outre, une autre poutre, à savoir la BC5(270-UR), a été renforcée par deux joncs CFRP de 6 mm de diamètre scellés dans la résine et placés 20 mm plus haut que le niveau des barres d'acier longitudinales (à environ 62 mm de la surface inférieure de la poutre). L'objectif de l'étude de la poutre BC5(270-UR) était d'évaluer les effets de la position des joncs CFRP sur la réponse en flexion de la poutre. En effet, l'efficacité de la technique SNSM est fortement influencée par la qualité de la couverture en béton. Ainsi, la nécessité de modifier la position des aciers dans certaines conditions pourrait s'avérer essentielle pour assurer une couverture suffisante du béton pour la préparation des rainures et l'installation des joncs CFRP.

Dans l'ensemble, les résultats ont été suffisamment convaincants pour recommander la technique SNSM comme une alternative pratique à la technique NSM. La [Figure I-4](#) présente une comparaison entre les courbes charge-flèche des poutres renforcées par la technique SNSM testées ci-dessus et celles des poutres renforcées par la technique NSM testées dans [8]. Dans le scénario où la résine époxy est utilisée comme matériau de scellement, l'insertion des joncs CFRP dans les côtés latéraux de la poutre, au même niveau que les barres d'armature en acier au lieu du côté inférieur, diminue la charge de ruine d'environ 12,9%. Néanmoins, le mode de ruine passe de l'arrachement des joncs CFRP pour la poutre renforcée par la technique NSM à l'écrasement du béton pour la poutre renforcée par la technique SNSM. D'autre part, dans le scénario où le mortier était utilisé comme matériau de scellement ou si le rapport entre la longueur de renforcement (SL) et la longueur de la poutre (BL) était inférieur à 0,6, aucun

changement significatif n'est observé entre les poutres SNSM et NSM en termes de charge de ruine et de mode de ruine.

La charge de ruine des poutres BC1(270-SR), BC2(210-SR), BC3(270-SM), BC4(210-SM) et BC5(270-UR) est supérieure à celle de la poutre témoin de 59,3%, 46,2%, 45,6%, 29,3% et 41,1%, respectivement. Cependant, en ce qui concerne le mode de ruine des poutres SNSM testées, les résultats suivants ont été observés :

- La longueur des joncs CFRP s'avère avoir un effet considérable sur le mode de ruine de la poutre. Deux poutres, à savoir BC2(210-SR) et BC4(210-SM), sur cinq poutres ont montré une ruine prématurée due à la longueur insuffisante des joncs d CFRP ( $SL/BL = 0.56$ ),
- L'utilisation de mortier comme matériau de scellement a entraîné un changement du mode de ruine, passant d'une rupture par la délimitation du béton d'enrobage dans le cas de la poutre BC2(210-SR) à une ruine par la perte d'adhérence précoce l'interface béton-mortier dans le cas de la poutre BC4(210-SM),
- La position des joncs CFRP n'a pas eu d'impact significatif sur le mode de ruine. La ruine des poutres BC1(270-SR) et BC5(270-UR) s'est produite par écrasement du béton comprimé,
- Le mode de ruine de la poutre BC3(270-SM) était par perte d'adhérence à l'interface béton-mortier à cause de la nature de ce matériau de remplissage.

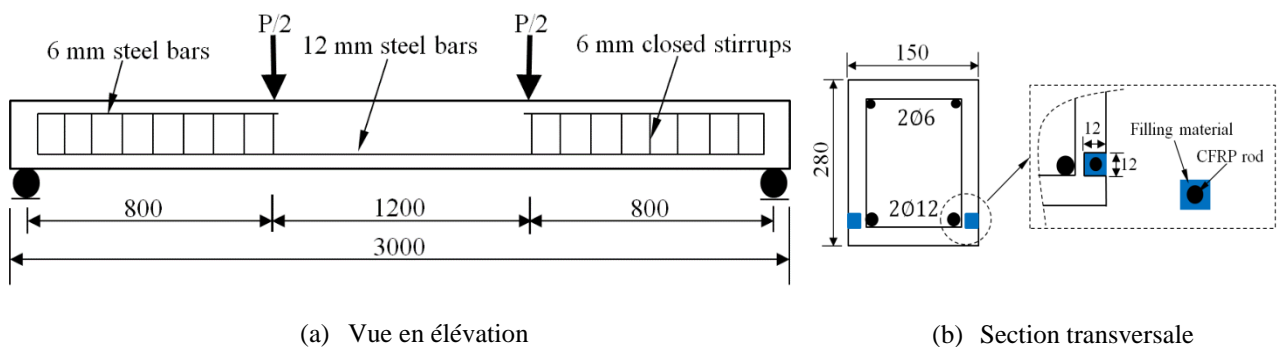
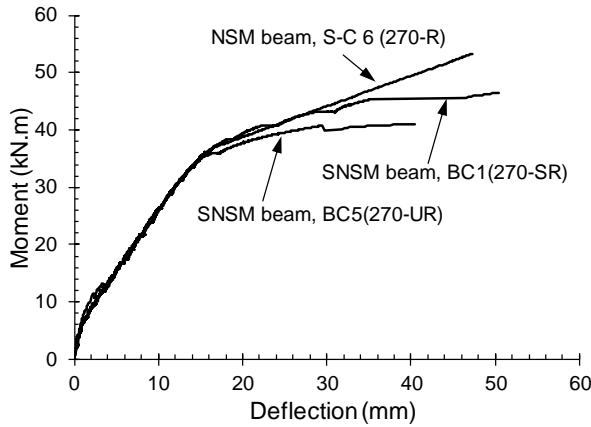


Figure I-3 : Schémas des poutres testées et leurs ferrailages. (toutes les dimensions sont en mm)

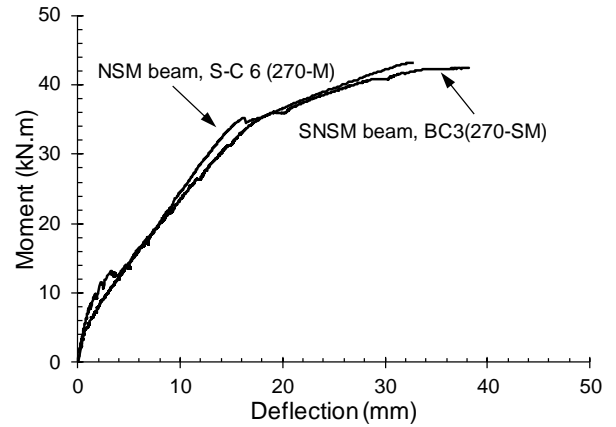
Dans les structures en BA, le comportement en flexion et les modes de ruine des poutres continues sont différents de ceux des poutres SSB. Ceci est essentiel car les poutres continues ont des régions de moment de flexion positif (sagging) et négatif (hogging). L'implication des renforts en FRP dans le renforcement ou la réparation de ces éléments indéterminés complique la prédiction de leur performance en flexion. En fait, les avantages comportementaux, le mécanisme de ruine et le taux de gain de résistance de l'utilisation des FRP dans les poutres continues ont à peine été explorés, et à ce jour, les concepts utilisés pour la plupart des chercheurs et des ingénieurs restent vagues. En effet, très peu d'études se sont concentrées sur le renforcement de poutres continues en BA avec la technique EB [27-29] alors qu'aucune étude n'a été trouvée dans la littérature sur le renforcement de poutres continues avec des joncs par la technique NSM. Par conséquent, d'autres études de recherche sur l'utilisation de la technique NSM pour renforcer les poutres en BA continues sont un besoin primordial dans le but de : (i) étudier la possibilité d'utiliser cette technique pour améliorer la résistance à la flexion des



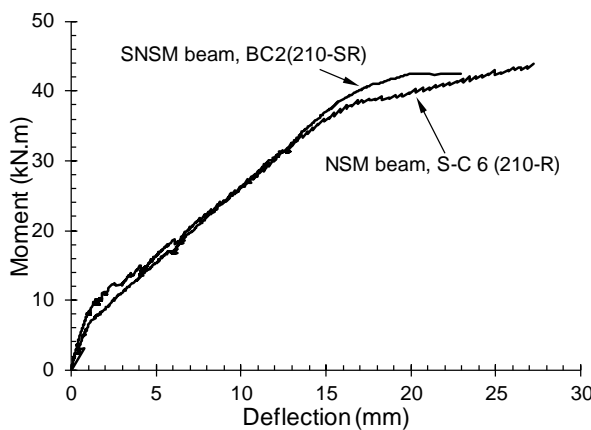
poutres, en particulier pour traiter le moment de flexion négatif ; (ii) explorer les différences dans le mécanisme de renforcement, en particulier en ce qui concerne la défaillance du système NSM ; et (iii) vérifier l'éventualité de la redistribution du moment et le niveau de ductilité dans de telles structures renforcées.



(a) Selon la position des joncs CFRP



(b) Selon le matériau de remplissage



(c) Selon la longueur des joncs CFRP

- **BC1 (270-SR)** : Poutre renforcée avec 2 joncs CFRP de 6mm (de longueur de 270 cm) insérés dans les faces latérales, au même niveau que les aciers et en utilisant de la résine Époxy.
- **BC2 (210-SR)** : Poutre renforcée avec 2 joncs CFRP de 6mm (de longueur de 210 cm) insérés dans les faces latérales, au même niveau que les aciers et en utilisant de la résine Époxy.
- **BC3(270-SM)** : Poutre renforcée avec 2 joncs CFRP de 6mm (de longueur de 270 cm) insérés dans les faces latérales, au même niveau que les aciers et en utilisant du mortier.
- **BC5 (270-UR)** : Poutre renforcée avec 2 joncs CFRP de 6mm (de longueur de 270 cm) insérés dans les faces inférieures, en utilisant de la résine Époxy.

Figure I-4 : Comparaison entre les techniques NSM et SNSM pour le renforcement des poutres testées en chapitre I par des courbes moment de flexion-flèche en fonction de plusieurs configurations

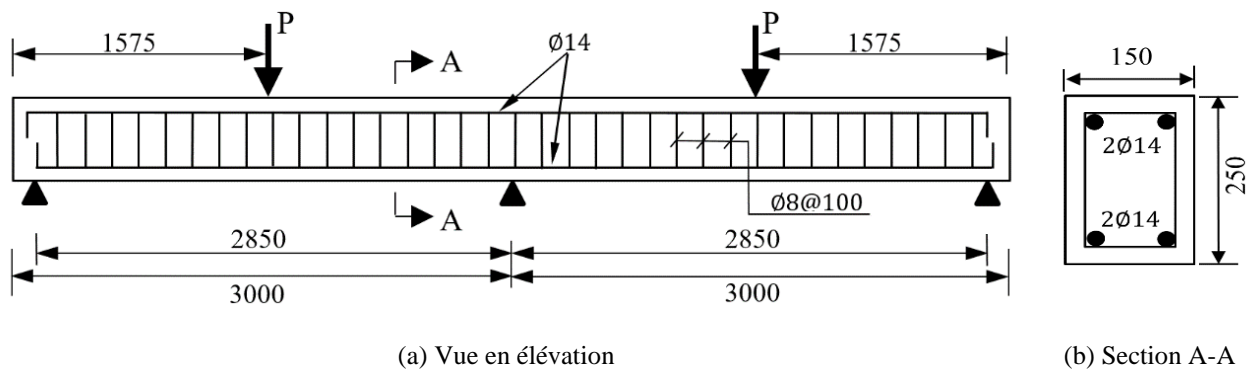


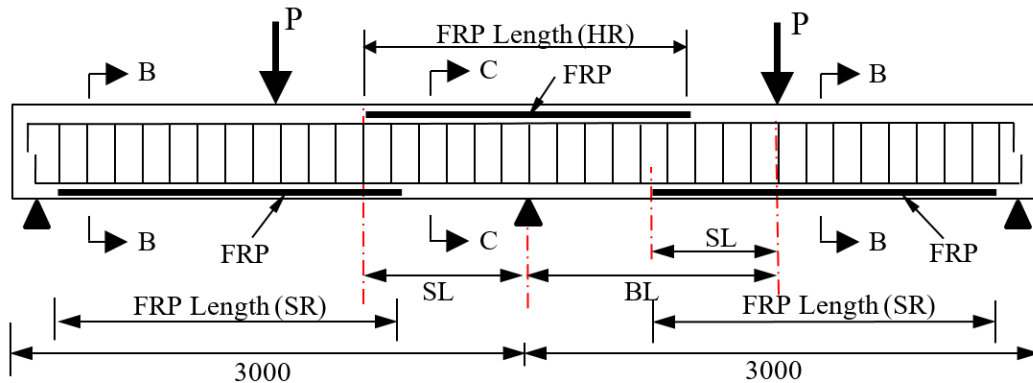
Figure I-5 : Schémas des poutres testées et leurs ferrailages. (toutes les dimensions sont en mm)

Dans le second chapitre de cette thèse, une étude expérimentale et analytique est présentée afin d'évaluer le comportement en flexion des poutres en BA continues renforcées avec des joncs FRP par la technique NSM. Pour la partie expérimentale, six poutres de grande envergure à deux travées (une poutre témoin et cinq poutres renforcées avec des joncs FRP (BC1, BG1, BC2-R, BC3-L, BC4-F)) ont été chargées jusqu'à la ruine. Chaque poutre testée a été armée par deux barres d'acier HA de 14 mm de diamètre et en cisaillement par des étriers de 8 mm de diamètre. Les étriers de cisaillement étaient uniformément espacés de 100 mm sur la longueur de la poutre afin d'éviter une rupture prématurée par l'effort tranchant. Les poutres avaient toutes les mêmes dimensions : 150 mm de largeur, 250 mm de hauteur, 2800 mm de portée effective et 6000 mm de longueur totale, comme le montre la [Figure I-5](#). Les poutres NSM ont été renforcées à la fois dans les régions sagging et hogging ([Figure I-6](#)). Les scénarios de renforcement appliqués dans le chapitre 2 sont les suivants :

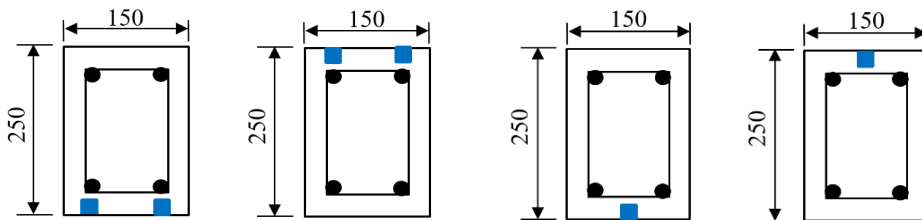
- Le scénario de renforcement appliqué pour la poutre BC1 a pris en compte les recommandations génériques tant du point de vue opérationnel que théorique [30]. Dans cette poutre, deux joncs CFRP de 6mm de diamètre ont été insérés dans la surface du béton et scellés dans la résine, ils ont été placés dans les travées sagging et hogging de la poutre. Les joncs CFRP dans les deux régions ont été arrêtés au-delà du point d'inflexion théorique (c'est-à-dire qu'une longueur d'ancrage a été appliquée).
- La seule différence entre les poutres BC1 et BG1 est le type de joncs FRP. Des joncs de verre (GFRP) ont été utilisés pour renforcer la poutre BG1. L'objectif de la poutre BG1 était d'étudier la réponse en flexion d'une poutre continue en fonction du type de matériau de renforcement par la technique NSM.
- La poutre BC2-R a été renforcée par un jonc de carbone de 10mm de diamètre. Elle a été testée afin d'étudier les influences de l'augmentation de la section/ratio de joncs de carbone sur l'amélioration de la capacité portante de la poutre. La longueur des joncs FRP et le matériau de scellement utilisés dans la poutre BC2-R étaient identiques à ceux utilisés dans la poutre BC1.
- Les poutres BC3-L et BC4-F ont été testées afin d'étudier l'impact de la longueur des joncs FRP et des caractéristiques du matériau de scellement, respectivement, sur la réponse des poutres continues renforcées, en particulier pour étudier les changements de mode de ruine dans le système NSM. Les deux poutres ci-dessus ont été renforcées par deux joncs CFRP de 6 mm de diamètre dans chaque région de flexion. Ces joncs ont été arrêtés juste avant les points d'inflexion théoriques dans la poutre BC3-L (c'est-à-dire qu'aucune longueur d'ancrage n'a été appliquée). La poutre BC4-F, est caractérisée par l'insertion des joncs de carbone dans le mortier au lieu de la résine époxy.

Les principaux résultats des essais menés ont révélé que la contribution de la technique NSM à l'amélioration de la capacité portante des poutres en BA à deux travées était limitée par le décollement des joncs de FRP (pull-out) au niveau de l'appui intermédiaire ([Figure I-7a](#)) ou par la délamination du béton d'enrobage (Concrete Cover Delamination (CCD)) ([Figure I-7b](#)). La ruine par délamination du béton d'enrobage s'est produite principalement en raison de la concentration de contraintes à l'extrémité des joncs FRP. Cette concentration de contraintes a été produite en raison de l'arrêt des joncs FRP avant le point d'inflexion. Cependant,

l'amélioration de la capacité portante des poutres testées était comprise entre 25,7 % et 36,3 % selon le scénario de renforcement appliqué, comme le montre la Figure I-8. D'autre part, les résultats expérimentaux montrent également que l'augmentation de la section des joncs CFRP, l'arrêt des joncs CFRP avant le point d'inflexion ou l'utilisation de mortier comme matériau de scellement ont considérablement réduit la ductilité de la poutre. L'indice de ductilité le plus élevé parmi les spécimens renforcés testés a été trouvé pour la poutre renforcée avec des joncs GFRP, et ceci peut être expliqué par le fait que le module élastique et la déformation à la traction des joncs GFRP sont, respectivement, plus faibles et plus élevés que ceux des joncs CFRP.



(a) Vue en élévation



(b) Sections B-B et C-C pour les poutres BC1, BG1, BC3-L, et BC4-F

(c) Section B-B et C-C pour la poutre BC2-R

Figure I-6 : Schémas des renforcements des poutres testées. (toutes les dimensions sont en mm)

La redistribution des moments est une caractéristique clé des poutres en BA continues. La redistribution des moments dans une poutre peut être attribuée à la redondance structurelle et au comportement non linéaire du béton armé. La quantification de la redistribution des moments dans les poutres ordinaires indéterminées est complexe car elle dépend de plusieurs facteurs tels que la quantité, la disposition et les caractéristiques mécaniques des aciers internes, la disposition des charges, la géométrie de l'élément ainsi que la largeur des supports. En ce qui concerne la quantité de l'acier de traction ( $\rho_s$ ) dans les sections critiques (hogging (h) et sagging (s)), le transfert du moment se produit de la région hogging à la région sagging lorsque  $\rho_s^h / \rho_s^s$  n'est pas supérieur à 1,0, tandis que lorsque ce rapport est supérieur à 1,5, le transfert du moment se produit de la région sagging à la région hogging. Lorsque  $\rho_s^h / \rho_s^s$  se situe entre 1,0 et 1,5, le transfert de moment est indistinct [31]. Cependant, la quantification de la redistribution du moment devient plus compliquée pour les poutres renforcées avec des joncs FRP. Les codes de construction existants tels que l'ACI 318-14 [26], l'Eurocode 2 [32] et l'AS 3600 [33] permettent

de tirer profit de l'analyse élastique linéaire avec redistribution du moment (15-30%) pour les conceptions structurelles conventionnelles; cela signifie que le moment dans les sections critiques est réduit tout en augmentant celui dans les autres sections afin de satisfaire l'équilibre statique. Ces codes ont souvent tendance à être conservateurs et ne permettent pas la redistribution du moment pour les poutres renforcées avec des matériaux FRP en raison de : (1) le comportement fragile des matériaux FRP, (2) les conditions de liaison entre ces matériaux et le substrat en béton, et (3) le niveau de ductilité requis pour la redistribution des moments dans ces éléments n'est toujours pas clair. Par contre, les résultats expérimentaux obtenus lors des essais réalisés dans le deuxième chapitre de cette thèse (Figure I-9) ont montré que les poutres renforcées par la technique NSM pouvaient atteindre une redistribution des moments similaire à celle d'une poutre non renforcée, tant que le mode de ruine n'est pas par le CCD ou par pull-out des joncs FRP. La poutre renforcée avec des joncs GFRP de 6mm de diamètre ( $A_f/A_s=18\%$ ) a montré une redistribution du moment similaire à sa contrepartie avec des joncs CFRP de 6mm ( $A_f/A_s=18\%$ ), et les deux poutres ont atteint un degré de redistribution du moment ( $\beta$ ) presque similaire à celui de la poutre non renforcée ( $\beta_h=20,53\%$ ,  $\beta_s=-12,43\%$ ). En général, le degré de redistribution du moment d'une poutre à deux travées symétrique en termes de renforcement ( $\rho_s^h/\rho_s^s=1$ ) et de chargement est affecté négativement par l'augmentation de la section de jonc de FRP ( $A_f/A_s > 18\%$ ), la diminution de la longueur de jonc FRP ( $SL/BL < 0.6$ ) ou l'utilisation de mortier comme matériau de scellement au lieu de la résine époxy.



(a) Mode de rupture par arrachement (pull-out) des joncs CFRP.



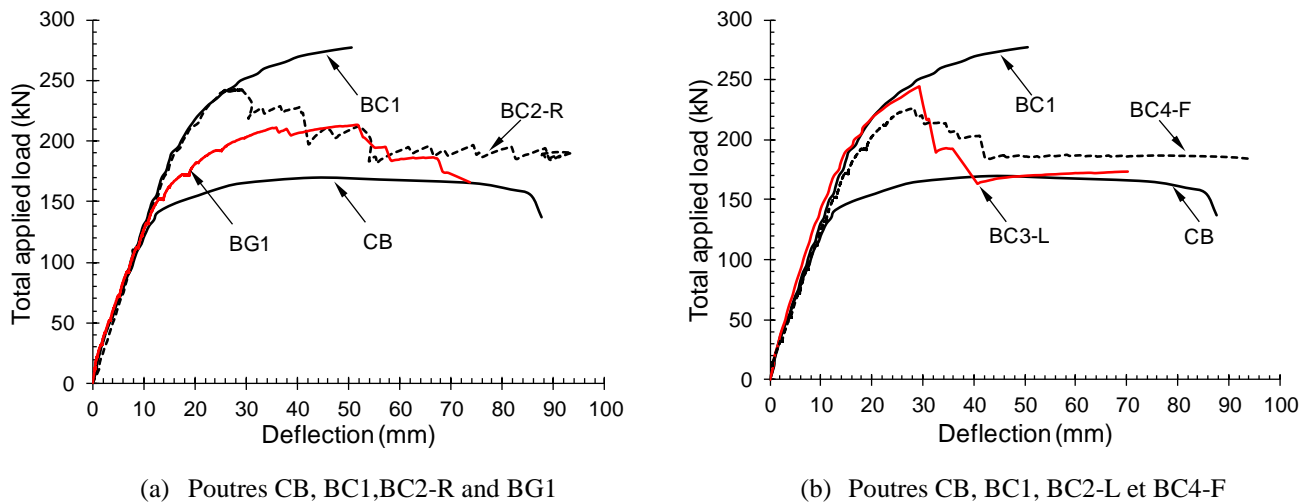
(b) Mode de rupture par délamination du béton d'enrobage.

Figure I-7 : Modes de ruine principaux observés pour les poutres continues renforcées par la technique NSM.

Dans la partie analytique du deuxième chapitre, l'analyse non linéaire de la section transversale a été adoptée pour produire un modèle analytique précis permettant de prédire les courbes moment-flèche et la charge ultime des poutres renforcées par la technique NSM. Ce modèle dépend de l'augmentation progressive de la courbure et de l'intégration numérique pas à pas. Globalement, il utilise les hypothèses suivantes :

- Les comportements non-linéaires du béton et de l'acier tels que décrits par [34-36];
- Le comportement linéaire du matériau de renforcement tel que décrit par [37];
- La résistance à la traction du béton a été négligée;
- Les différences entre les propriétés mécaniques du béton et du matériau de scellement au niveau des engravures ont été négligées, du fait que la résine ou le mortier occupent une petite fraction de la section transversale de la poutre;

- La rupture de la section transversale a eu lieu lorsque l'une des déformations ultimes du béton ou du jonc FRP a été atteinte;
- Les courbes moment-courbure ont été dérivées des principes fondamentaux d'équilibre pour les forces et les moments agissant sur la section transversale de la poutre ainsi que des conditions de compatibilité des déformations pour les matériaux utilisés. Le rapport entre la charge ultime théorique ( $P_u^{Th}$ ), obtenue par l'approche analytique proposée, et la charge expérimentale ( $P_u^{Exp}$ ) pour les poutres testées était compris entre 0,90 et 1,01.



- **CB** : Poutre témoin; **BC1** : Poutre renforcée avec 2 joncs CFRP de 6mm dans les régions “hogging” (SL/BL=0,7) et “sagging” (SL/BL=0,65) scellés dans la résine; **BG1** : Poutre renforcée avec 2 joncs GFRP de 6mm dans les régions “hogging” (SL/BL=0,65) et “sagging” (SL/BL=0,7) scellés dans la résine; **BC2-R** : Poutre renforcée avec un jonc CFRP de 10mm dans les régions “hogging” (SL/BL=0,7) et “sagging” (SL/BL=0,65) scellé dans la résine; **BC3-L**: Poutre renforcée avec 2 joncs CFRP de 6mm dans les régions “hogging” (SL/BL=0,53) et “sagging” (SL/BL=0,44) scellés dans la résine; et **BC4-F** : Poutre renforcée avec 2 joncs CFRP de 6mm dans les régions “hogging” (SL/BL=0,7) et “sagging” (SL/BL=0,44) scellés dans le mortier..

Figure I-8 : Courbes charge-flèche des poutres continues renforcées avec la technique testées en Chapitre 2

Le comportement en flexion d'une poutre BA continue renforcée par la technique NSM ne dépend pas seulement des facteurs décrits ci-avant. Il peut également dépendre de la position et de la disposition des joncs FRP. Par conséquent, le troisième chapitre de cette thèse a été consacré à l'étude expérimentale et numérique de l'efficacité des joncs CFRP en utilisant les techniques de NSM ou SNSM pour renforcer les poutres en BA continues à deux travées. Ce chapitre comprend deux parties: une partie expérimentale et une partie numérique par éléments finis (EF). Tout d'abord, trois poutres de grande envergure à deux travées ont été étudiées du point de vue statique; une poutre témoin et deux autres poutres (BC1-E-NSM et BC2-E-SNSM) initialement renforcées en flexion avec 2 joncs CFRP de 6 mm de diamètre dans les régions hogging et sagging. La seule différence entre les poutres renforcées ci-dessus est la position des joncs CFRP. La technique NSM a été utilisée pour renforcer la poutre BC1-E-NSM tandis que la technique SNSM a été utilisée pour renforcer la poutre BC2-E-SNSM.

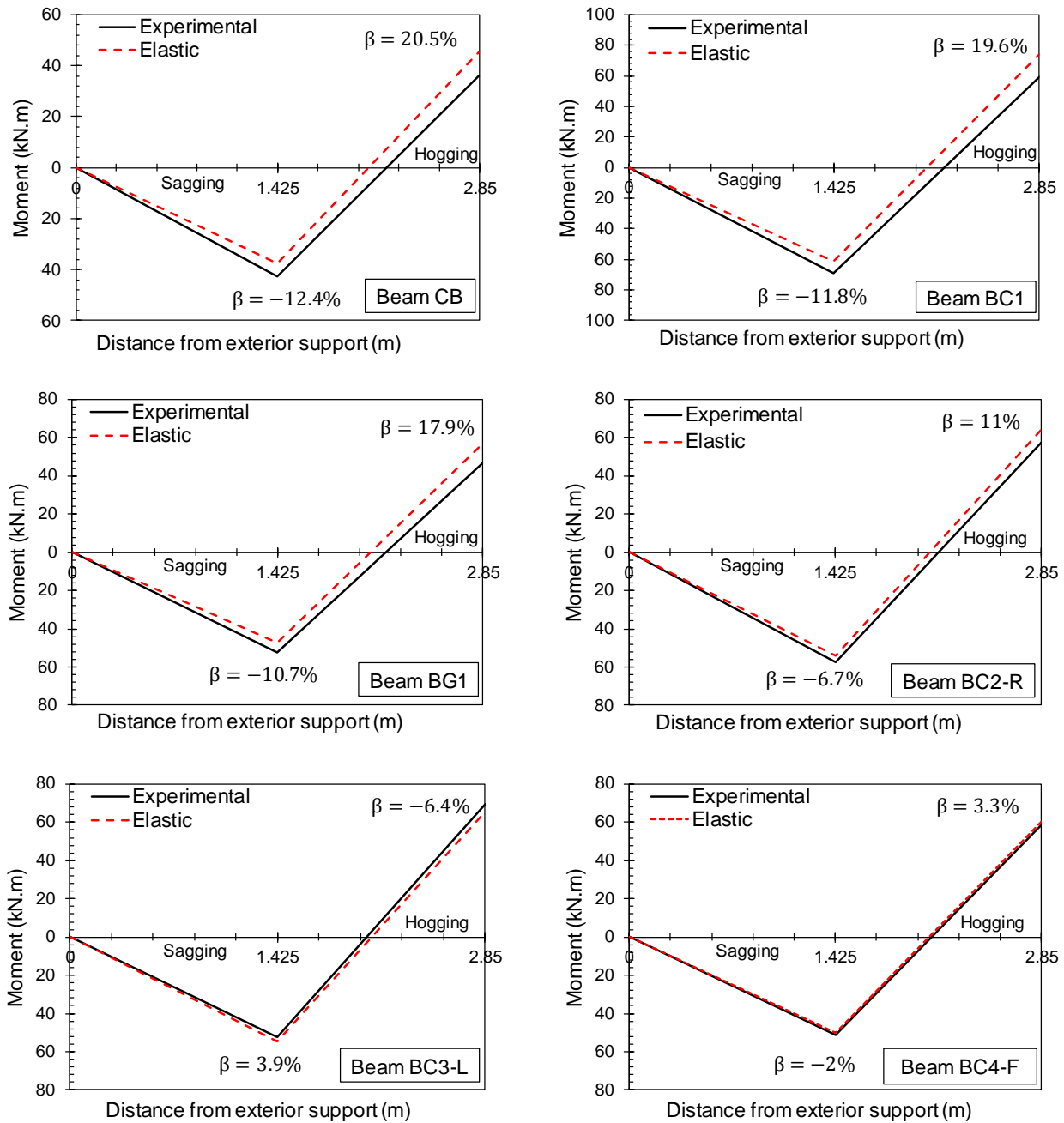
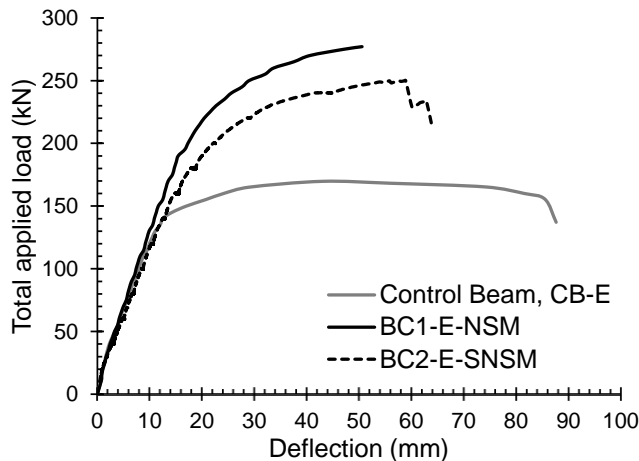


Figure I-9 : Moments de flexion expérimental et élastique des poutres testées à la charge ultime, ( $\rho_s^h/\rho_s^s=1$ ).

Les études expérimentales comparatives réalisées entre les poutres testées ont confirmé que le système SNSM est une alternative pratique au système conventionnel NSM pour renforcer les poutres continues, bien qu'il se soit avéré légèrement moins efficace (<10%) que le système NSM pour améliorer la résistance à la flexion des poutres en BA (Figure I-10). La déformation maximale en traction mesurée des joncs CFRP dans les sections critiques des poutres NSM et SNSM s'est avérée presque identique (déformation à la ruine  $\varepsilon_{deb}^{FRP} = \sim 0,7 \varepsilon_{max}^{FRP}$ ), comme le montre la Figure I-11, et la ruine des deux poutres s'est produite principalement en raison de la rupture des systèmes de renforcement, quelle que soit la position des joncs CFRP appliqués. Les résultats



expérimentaux indiquent également que l'insertion des joncs CFRP dans les côtés latéraux adjacents aux barres d'acier par de la technique du SNSM a augmenté considérablement le nombre de fissures dans les régions hogging et sagging. Cependant, avec les deux techniques de renforcement, l'ouverture des fissures des poutres était presque identique sous la même charge appliquée. En outre, la technique SNSM a permis d'augmenter la flèche moyenne à mi-portée de la poutre, améliorant ainsi son indice de ductilité de déplacement et sa capacité d'absorption d'énergie par rapport à la technique NSM.



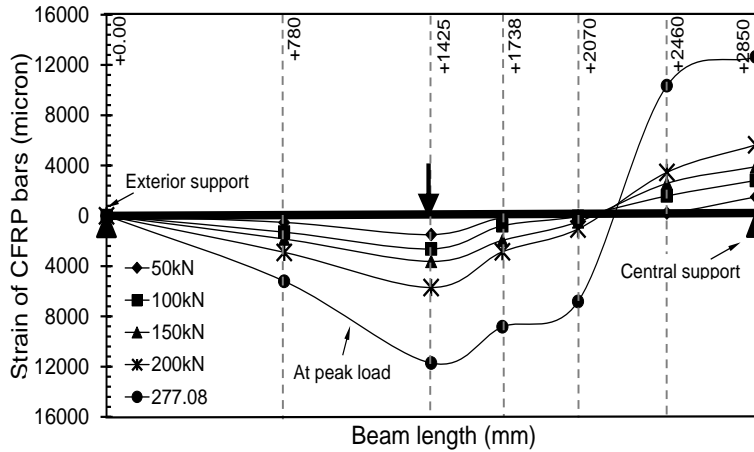
- **BC1-E-NSM** : Poutre renforcée avec 2 joncs CFRP de 6 mm dans les régions “hogging” et “sagging” sur les parties inférieure et supérieure.
- **BC2-E-SNSM** : Poutre renforcée avec 2 joncs CFRP de 6 mm dans les régions “hogging” et “sagging” sur la partie latérale.

Figure I-10 : Courbes charge-flèche des poutres testées

Ensuite, un modèle numérique tridimensionnel (3D) a été développé à l'aide du logiciel ABAQUS [38] afin d'étudier l'effet de l'utilisation de différents modèles d'interface jonc FRP-résine-béton sur la prédiction de la capacité portante des poutres renforcées et pour étendre l'étude expérimentale en mettant en œuvre une étude paramétrique par éléments finis (EF). La majorité des études EF disponibles dans la littérature [39-41] s'est concentrée sur l'utilisation du modèle de liaison parfaite (Perfect Bond Model (PBM)) pour simuler le contact d'interface entre les joncs FRP et le matériau de scellement, ainsi qu'entre ce dernier et le béton. En fait, ce modèle PBM ignore le développement des contraintes de cisaillement aux interfaces et suppose qu'aucun glissement ne se produit entre les éléments de renforcement (jonc FRP-résine-béton). En outre, le modèle PBM ne tient pas compte de la rupture de la liaison. Le concept général du modèle PBM peut être décrit comme suit : (i) Le contact entre la résine et le béton est considéré comme une liaison parfaite ; et (ii) Les joncs FRP sont encastrés dans la résine époxy en utilisant l'option de contact encastré (Figure I-12).

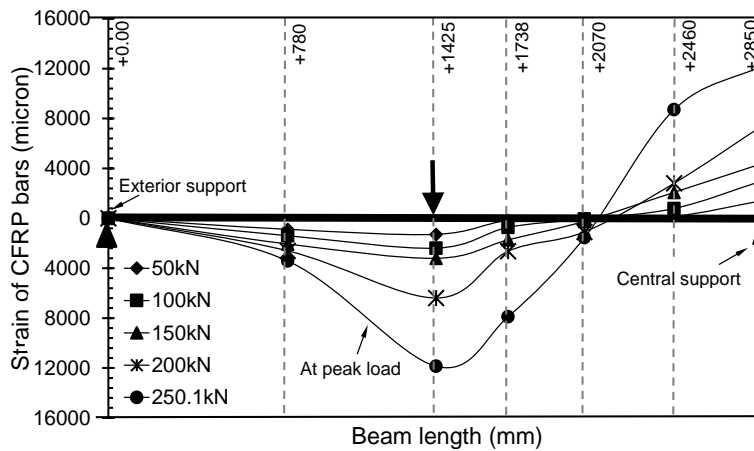
D'autre part, le modèle de zone cohésive (Cohesive Zone Model (CZM)) est proposé dans cette étude EF afin de simuler la perte d'adhérence qui peut se produire dans les poutres renforcées. La réponse globale du système NSM ou SNSM a été modélisée en utilisant une couche adhésive très fine de 1 mm d'épaisseur. Cette couche a été créée à l'aide de l'option de décalage disponible dans ABAQUS ; elle est située entre les joncs CFRP et le béton, comme le montre la Figure I-13. L'analyse 3D-FE développée avec le modèle CZM a montré sa capacité à reproduire les principaux aspects observés lors des expériences, pour les poutres NSM et SNSM, en ce qui concerne la capacité portante (Figure I-14), la configuration des fissures (Figure I-15), la performance des joncs CFRP et la redistribution du moment de la poutre. Par conséquent, le

modèle CZM proposé est utilisé pour l'étude paramétrique afin d'étudier et de comparer le potentiel des systèmes NSM et SNSM pour le renforcement des poutres en BA continues. L'étude paramétrique s'est concentrée sur l'influence des dispositions de l'acier et des joncs CFRP sur la redistribution du moment et la capacité portante. Au total, 21 poutres renforcées ont été étudiées numériquement. Les poutres EF présentaient différents ratios d'acier dans la région hogging, c'est-à-dire  $\rho_s^H = 0,5\%$ ,  $1\%$  et  $1,25\%$ . Pour chaque ratio d'acier, les dispositions de renforcement appliquées ont été classées en trois groupes : a) la région hogging ( $x-0$ ), b) la région sagging ( $0-x$ ) et c) les régions hogging et sagging ( $x-x$ ), où  $x$  désigne le nombre de joncs CFRP.



(a) BC1-E-NSM

Les déformations sont présentées pour la moitié de la longueur de la poutre, de l'appui extérieur de la travée droite à l'appui intérieur.



(b) BC2-E-SNSM

Les déformations sont présentées pour la moitié de la longueur de la poutre, de l'appui extérieur de la travée droite à l'appui intérieur.

Figure I-11 : Variation longitudinale des déformations des joncs CFRP en fonction de la charge appliquée.

Les principaux résultats obtenus à partir de l'étude paramétrique EF peuvent être conclus comme suit:

- La disposition des joncs CFRP et la quantité de l'armature en acier ont des effets significatifs sur la redistribution du moment des poutres en BA continues, et elles peuvent même changer la direction de cette redistribution. Cependant, l'augmentation du ratio d'aciers dans la région hogging ( $\rho_s^H$ ) a provoqué une diminution de la



redistribution positive du moment des poutres en BA continues, quelle que soit la technique de renforcement utilisée.

- En ce qui concerne la capacité de redistribution du moment à l'état ultime pour les poutres renforcées uniquement dans la région hogging, il a été constaté qu'avec la technique SNSM une diminution légère de la rigidité dans la région hogging par rapport à la technique NSM.
- L'application de joncs CFRP dans les régions hogging et sagging de la poutre s'est avérée être la plus efficace pour améliorer la capacité portante de la poutre, comme le montre la Figure I-16.
- La technique de SNSM s'est avérée relativement plus efficace que la technique de NSM lorsque les joncs CFRP ont été appliqués uniquement dans la zone hogging ou dans la zone sagging, comme le montre la Figure I-16.
- La contribution des joncs CFRP à augmenter la charge ultime des poutres était limitée par la ruine par écrasement du béton ou par la rupture du système de renforcement. Il a été également observé que le taux d'utilisation des joncs CFRP ( $\sigma_{CFRP}^{max}/\sigma_{CFRP}^{ult}$ ) à la charge ultime variait de 64% à 77%, ce qui a confirmé l'influence relativement faible du ratio d'acier ( $\rho_s^H$ ), de la disposition et de la position du renforcement sur l'efficacité des joncs CFRP.

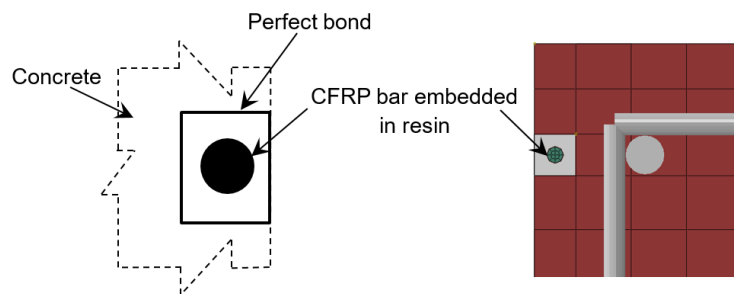


Figure I-12 : Modèle d'une liaison parfaite

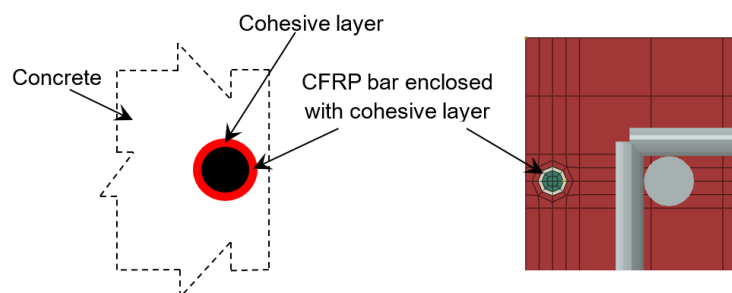


Figure I-13 : Modèle avec une zone adhésive (CZM)

Comme il a déjà été mentionné, peu d'études ont été réalisées sur des poutres en BA continues renforcées avec la technique EB, et aucune étude n'a été trouvée sur le renforcement des poutres en BA continues par les techniques NSM ou SNSM. La plupart des études sur la technique EB se sont concentrées sur l'impact de la disposition [27], du nombre de couches [29] et de la longueur des tissus ou lamelles [42] sur les modes de ruine et la capacité de flexion des poutres. Il convient de mentionner que l'augmentation du poids des fibres de carbone par unité de surface

(Figure I-17) a récemment été utilisée dans l'industrie de la construction et de la réhabilitation comme une alternative aux couches multiples de tissus. Néanmoins, il n'y a pas d'études disponibles dans la littérature explorant l'efficacité de cette alternative en termes d'amélioration de la performance des poutres en BA continues. Par conséquent, l'objectif principal du quatrième chapitre de cette thèse est d'essayer de combler les lacunes de la littérature concernant le renforcement des poutres en BA continues avec la technique EB.

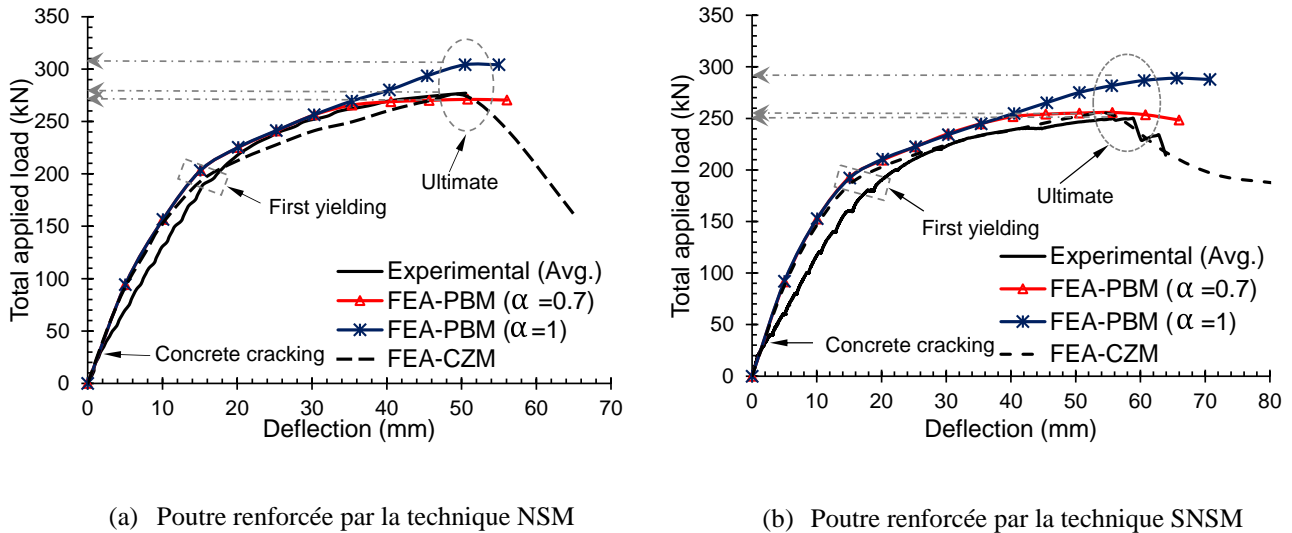


Figure I-14 : Comparaison de courbes charge-déformation expérimentales et numériques des poutres testées

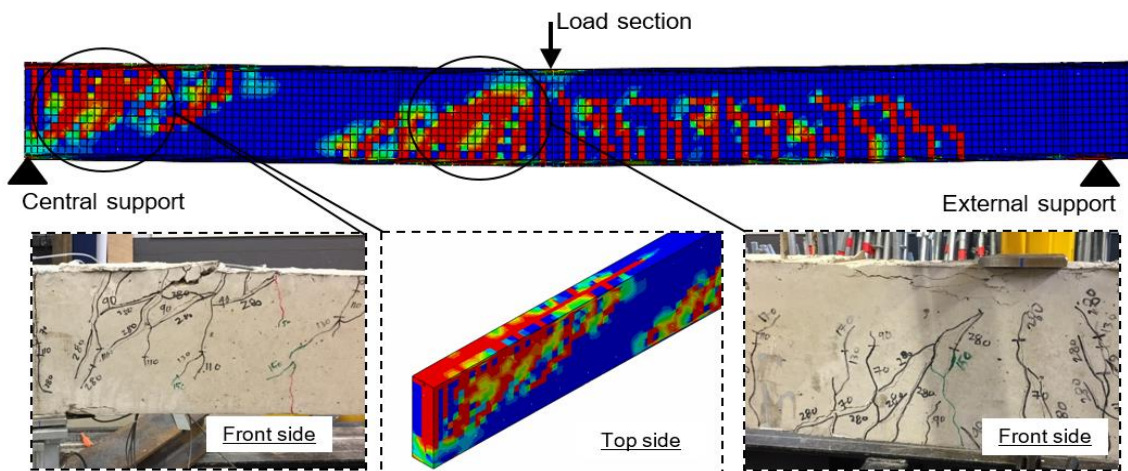
De manière générale, le quatrième chapitre se compose de trois sections principales. Dans la première section, sept poutres de portée importante à deux travées sont étudiées du point de vue statique : une poutre témoin et six poutres initialement renforcées en flexion avec des tissus ou des lamelles CFRP. Les détails des poutres et les armatures en acier sont présentés sur la Figure I-5. L'objectif principal de la première section est d'étudier les effets des paramètres importants, tels que :

1. La position du renforcement;
2. Le type de renforcement, soit des tissus ou des lamelles;
3. Le nombre de couches de tissus en fibre de carbone;
4. Le poids des fibres de carbone,

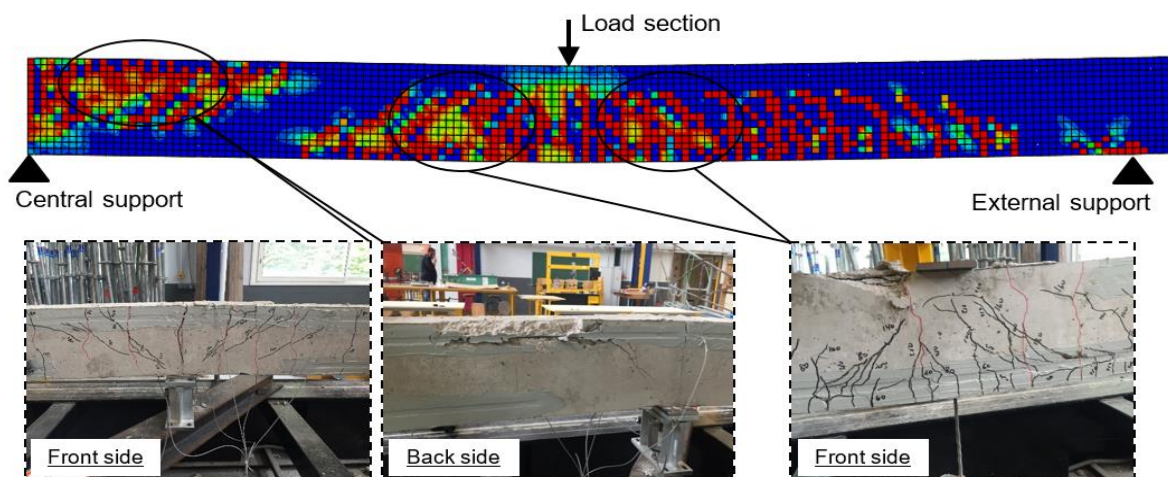
Sur la capacité portante, les modes de ruine, la fissuration, la redistribution des moments et l'analyse des déformations des poutres continues.

Les poutres BC1-EB1S et BC2-EB1P ont été testées afin d'étudier l'efficacité de la technique EB à travers le type du matériau de renforcement. Deux types ont été utilisés : des tissus (S) et des lamelles (P). Bien que les tissus et les lamelles CFRP aient des propriétés différentes, les ratios de rigidité axiale du renforcement total  $(1 + \frac{E_f \times A_f}{E_s \times A_s})$  des poutres BC1-EB1S et BC2-EB1P ont été conçus pour être proches les uns des autres. La poutre BC3-EB1S-side a été testée pour évaluer l'effet de la position des tissus CFRP sur la performance en flexion des poutres continues. La quantité de renforcement utilisée dans cette poutre était similaire à celle utilisée

dans la poutre BC1-EB1S. Cependant, dans la poutre (BC3-EB1S-side), les tissus de CFRP ont été coupés au préalable dans la direction longitudinale des fibres en deux moitiés égales, et chaque moitié a été collée sur l'une des faces latérales de la poutre. Les poutres BC4-EB2S, BC5-EB1S-weight (700), et BC6-EB1S-weight (1100) ont été testées afin de mesurer l'effet de l'augmentation du ratio de renforcement par tissus CFRP par le nombre de couches ou le poids des fibres de carbone sur le comportement en flexion de la poutre. La poutre BC4-EB2S a été renforcée par deux couches de tissus CFRP similaires à celles utilisées dans la poutre BC1-EB1S, tandis que les poutres BC5-EB1S-weight (700) et BC6-EB1S-weight (1100) ont été renforcées par une couche de tissus CFRP pesant 700 g/m<sup>2</sup> et 1100 g/m<sup>2</sup>, respectivement. Le poids des fibres de carbone longitudinales des tissus CFRP appliqués aux poutres BC1-EB1S, BC3-EB1S-side, et BC4-EB2S était d'environ 350 g/m<sup>2</sup>.



(a) Poutre renforcée par NSM



(b) Poutre renforcée par SNSM

Figure I-15 : Schémas de fissuration et modes de ruines des poutres renforcées

Étant donné que les directives de conception actuelles ont été élaborées pour renforcer les poutres SSB renforcées avec la technique EB, la deuxième section du quatrième chapitre évalue l'efficacité des codes de conception actuels pour déterminer la résistance à la flexion des poutres continues renforcées avec des tissus ou des lamelles CFRP. Les capacités portantes des poutres testées sont comparées à celles obtenues à partir des formules de conception fournies dans la norme américaine ACI 440.2R-08 [30], la norme italienne CNR-DT 200 R1/2013 [43], et le rapport technique du Bulletin 14 du FIB [44].

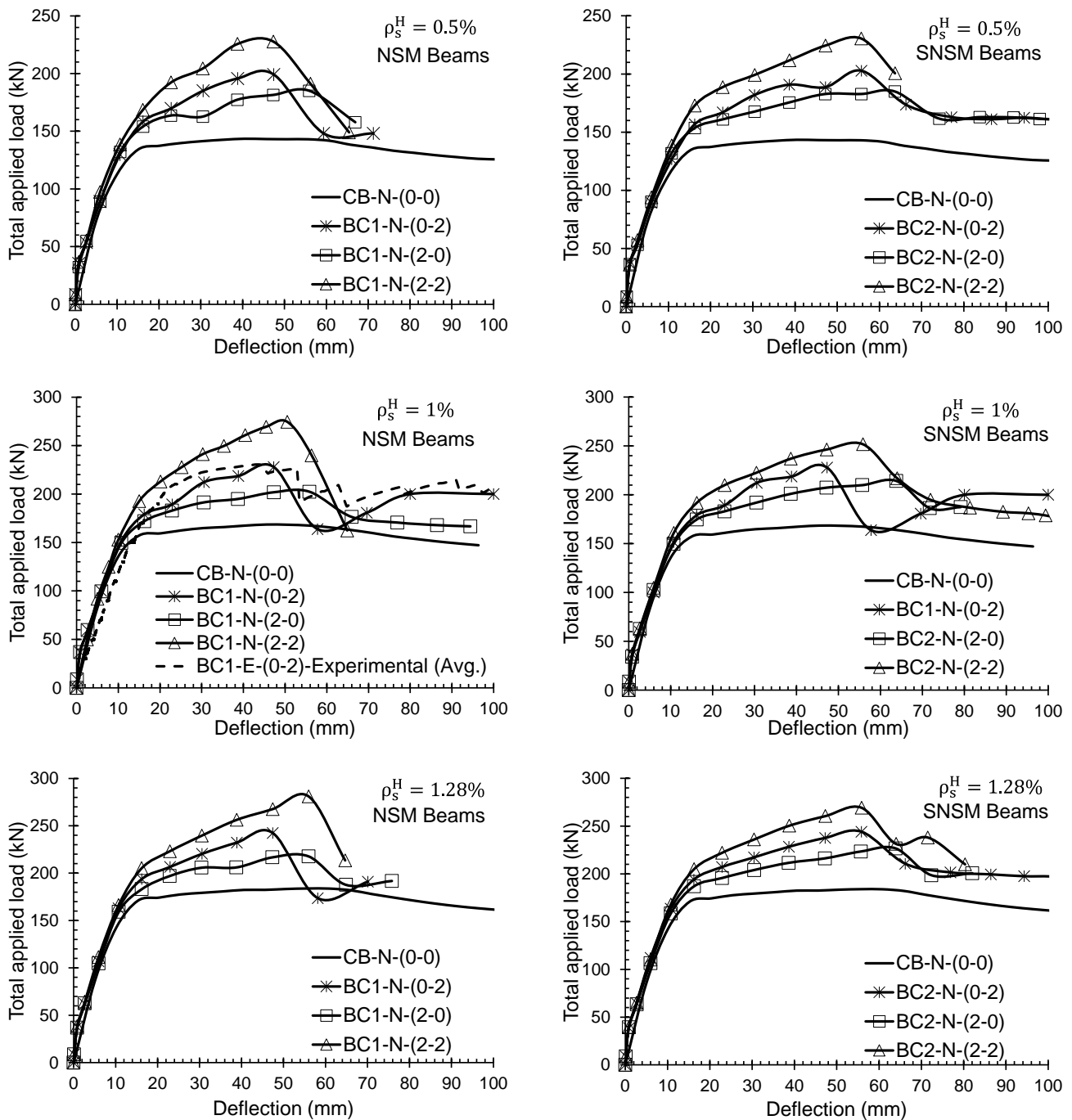
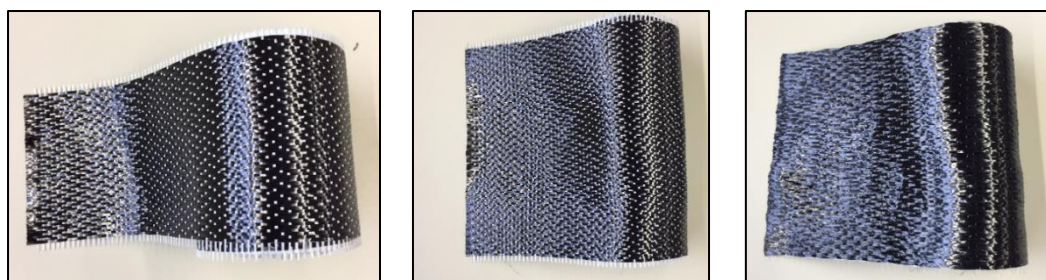


Figure I-16 : Coubes charge-flèche des poutres simulées par EF



Enfin, la troisième section évalue et compare les efficacités des techniques EB, NSM et SNSM. À cette fin, deux autres poutres renforcées par les techniques NSM et SNSM sont testées et présentées.

En ce qui concerne l'efficacité de la technique EB dans l'amélioration des performances de flexion des poutres en BA continues, les résultats des essais ont montré que, quel que soit le scénario de renforcement appliqué, toutes les poutres renforcées ont montré une amélioration de leur résistance à la flexion par rapport à la poutre témoin non renforcée. Le pourcentage d'augmentation de la charge limite d'élasticité et de la charge ultime de ces poutres allait de 25,5 % à 59,1 % et de 7,6 % à 49,8 %, respectivement, comme le montre la [Figure I-18](#). De plus, une densité des fibres de carbone plus élevée s'est avérée efficace pour améliorer la charge ultime de la poutre et elle peut être utilisée comme alternative aux couches de tissus multiples, mais cette efficacité était conditionnée par le rapport de rigidité axiale totale de la poutre et la résine utilisée. L'analyse de la répartition du moment de flexion a montré que la majorité de la redistribution du moment s'est produite dans la phase entre la fissuration du béton et la limite d'élasticité de l'acier pour toutes les poutres testées, tandis qu'une légère redistribution du moment s'est produite après cette limite, comme le montre la [Figure I-19](#). D'autre part, le décollement des tissus et des lamelles CFRP en raison de la fissuration intermédiaire (Intermediate Cracking (IC)) aux sections critiques (mi-travée et au-dessus de l'appui central) était le mode de ruine dominant observé dans les poutres renforcées. Le décollement des tissus CFRP semble être le seul mode de ruine dans les poutres BC2-EB1P et BC6-EB1S-weight (1100), alors qu'il a été suivi par d'autres types de ruine, comme le CCD, dans les poutres BC1-EB1S, BC4-EB2S et BC5-EB1S-weight (700), ainsi que par la rupture par traction des tissus CFRP dans la poutre BC3-SEB1S-side. Ce décollement des tissus CFRP résultant des IC a d'abord commencé au milieu des travées ou au-dessus du support central, puis s'est développé vers les extrémités des tissus avec l'augmentation de la charge appliquée. Par contre, dans les régions où la ruine s'est produite à la suite de CCD, la séparation de la couverture de béton a commencé aux extrémités des tissus de CFRP en raison de la formation de fissures de cisaillement diagonale, puis cette fissure s'est propagée vers la section critique intérieure.

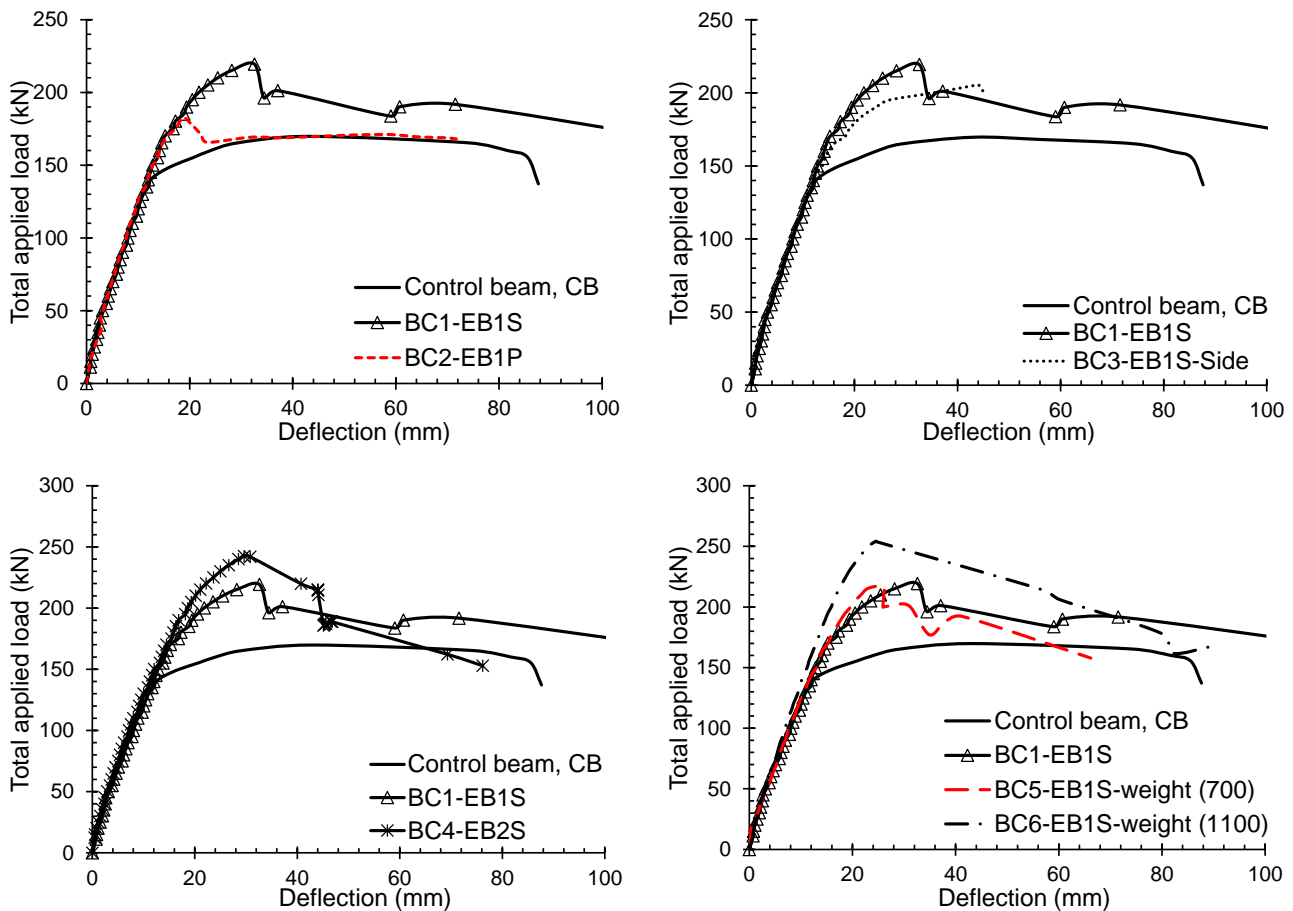


- (a) Tissus CFRP ordinaire (350g/m<sup>2</sup>).  
(b) Tissus CFRP dense (700g/m<sup>2</sup>).  
(c) Tissus CFRP dense (1100g/m<sup>2</sup>).

Figure I-17 : Tissus CFRP avec différentes masses par unité de surface.

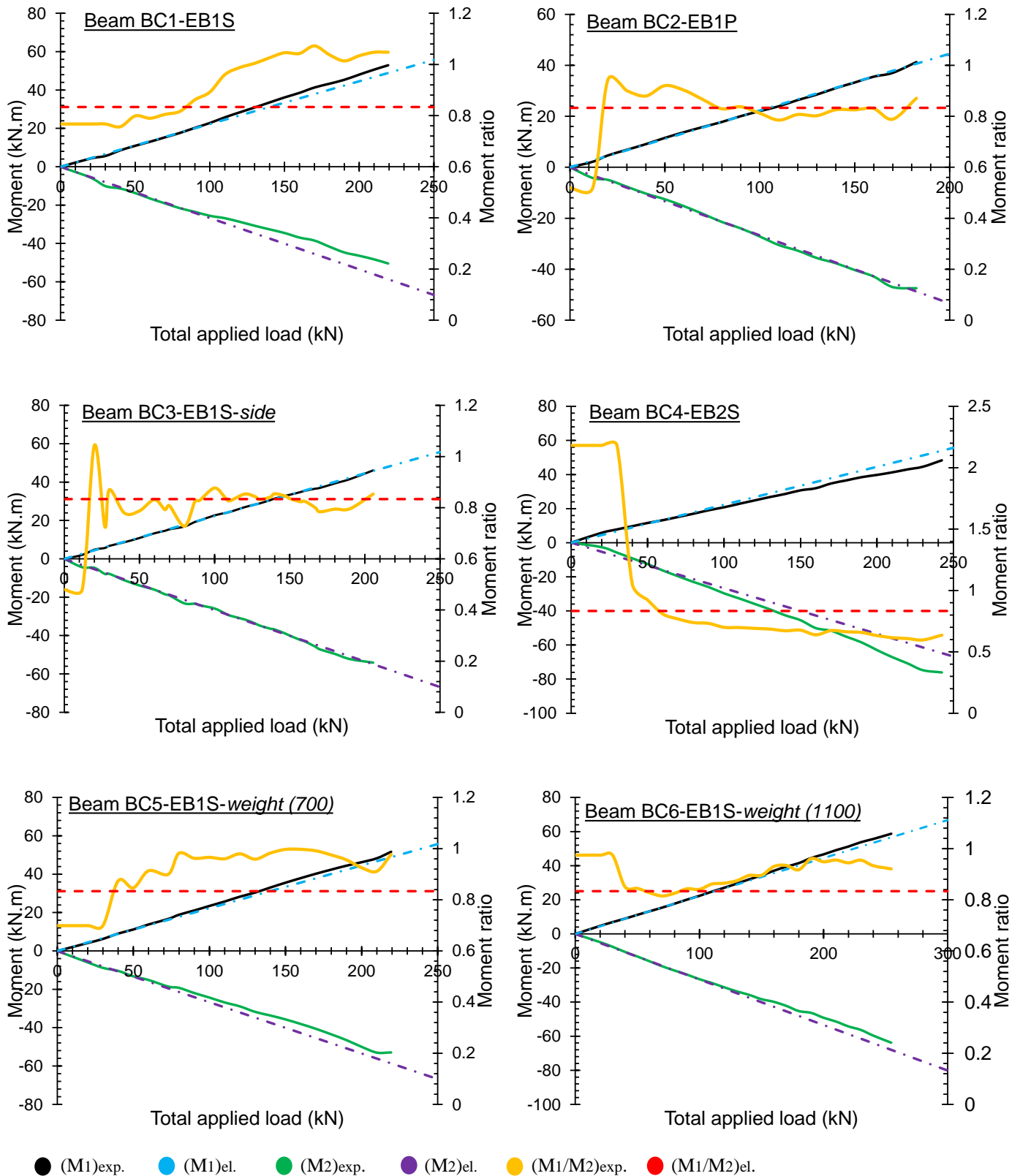
En ce qui concerne l'évaluation de l'efficacité des directives actuelles pour déterminer la résistance à la flexion des poutres continues BA renforcées avec des tissus CFRP, les directives

de conception actuelles fournissent une prédiction acceptable pour la résistance ultime des poutres renforcées avec une couche de CFRP, alors qu'elles montrent une faible précision dans la prédiction de la résistance ultime des poutres renforcées avec des couches multiples de CFRP.



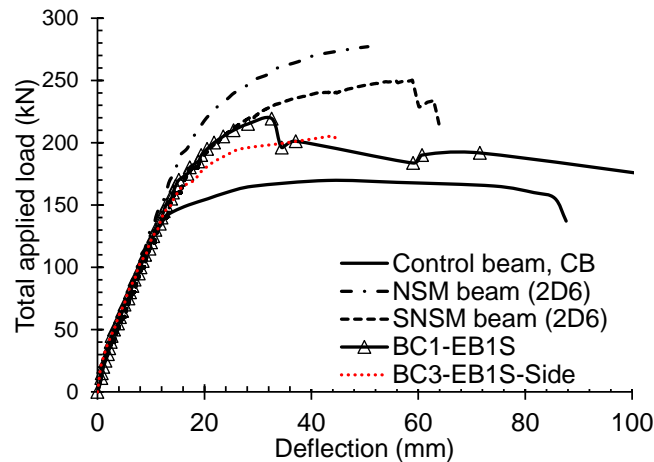
**CB** : Poutre témoin ; **BC1-EB1S** : Poutre renforcées avec une couche de tissus CFRP (350 g/m<sup>2</sup>) dans les régions “hogging” (SL/BL=0.7) et “sagging” (SL/BL=0.65) avec l’utilisation de la résine TFC-350; **BC2-EB1P** : Poutre renforcées avec lamelles CFRP (50\*1.2 mm) dans les régions “hogging” (SL/BL=0.7) et “sagging” (SL/BL=0.65) avec l’utilisation de la résine SC980; **BC3-EB1S-Side** : Poutre renforcées avec une couche de tissus CFRP (350 g/m<sup>2</sup>) dans les régions “hogging” (SL/BL=0.7) et “sagging” (SL/BL=0.65) dans les faces latérales avec l’utilisation de la résine TFC-350; **BC4-EB2S**: Poutre renforcées avec deux couches de tissus CFRP (350 g/m<sup>2</sup>) dans les régions “hogging” (SL/BL=0.7) et “sagging” (SL/BL=0.65) avec l’utilisation de la résine TFC-350; **BC5-EB1S weight (700)**: Poutre renforcées avec une couche de tissus CFRP (700 g/m<sup>2</sup>) dans les régions “hogging” (SL/BL=0.7) et “sagging” (SL/BL=0.65) avec l’utilisation de la résine TFC-350; and **BC6-EB1S weight (1100)**: Poutre renforcées avec une couche de tissus CFRP (1100 g/m<sup>2</sup>) dans les régions “hogging” (SL/BL=0.7) et “sagging” (SL/BL=0.65) avec l’utilisation de la résine TFC-1000.

Figure I-18 : Courbes charge-flèche des poutres testées.



M1: Moment dans les régions sagging; and M2: Moment dans les régions hogging

Figure I-19 : pourcentage des moments de flexion des poutres renforcées testées



- **CB** : Poutre témoin; **NSM beam**: Poutre renforcée avec 2 joncs CFRP de 6mm dans les deux régions “hogging” et “sagging” sur les surfaces inférieure et supérieure avec l’utilisation d’une résine SC980 ; **SNSM beam**: Poutre renforcée avec 2 joncs CFRP dans les deux régions “hogging” et “sagging” sur les surfaces latérales avec l’utilisation d’une résine SC980; **BC1-EB1S**: Poutre renforcées avec une couche de tissus CFRP (350 g/m<sup>2</sup>) dans les régions “hogging” et “sagging” avec l’utilisation de la résine TFC-350; and **BC3-EB1S-side**: Poutre renforcées avec une couche de tissus CFRP (350 g/m<sup>2</sup>) dans les régions “hogging” et “sagging” dans les faces latérales avec l’utilisation de la résine TFC-350.

Figure I-20 : Comparaison des performances des poutres renforcées .

Enfin, en ce qui concerne la comparaison entre les deux techniques de renforcement, NSM et EB, les principaux résultats suivants ont été obtenus :

- La technique NSM permet de mieux exploiter la résistance à la traction du jonc CFRP que la technique EB. La déformation de décollement dans la poutre BC1-NSM est 51,5 % plus importante que celle de la poutre BC1-EBIS et était également 17,6 % plus importante dans la poutre BC2-SNSM que celle de la poutre BC3-EBIS.
- La rigidité à la flexion, la charge de la limite élastique d’acier, la charge ultime, l’état de ductilité et la capacité d’absorption d’énergie des poutres NSM se sont avérées considérablement plus élevées que celles des poutres EB, confirmant l’efficacité supérieure de la technique NSM par rapport à la technique EB (Figure I-20)
- Les joncs CFRP dans les poutres en BA continues se sont avérées moins sensibles aux phénomènes de décollement causés par le CI, ce qui n'est pas le cas pour les poutres renforcées par la technique EB. La ruine des poutres EB a été caractérisée par le décollement des composites CFRP aux sections critiques en raison de l’IC, suivi par la rupture par CCD ou du CFRP.
- La technique NSM permet une valeur de redistribution du moment à l’état ultime plus élevée que celle obtenue avec la technique EB. Les poutres BC1-NSM et BC2-SNSM présentent un degré de redistribution du moment de +19,59% et +11,49% dans la région hogging et de -11,83% et -6,92% dans la région sagging, respectivement, alors que les poutres renforcées par la technique EB présentent des valeurs de +13,87% et +1,48% dans la région hogging et de -8,32% et -0,89% dans la région sagging.



## Bibliographie

1. Eberline DK, Klaiber FW, Dunker K (1988), Bridge Strengthening with Epoxy-Bonded Steel Plates, Transportation Research Record 1180, pp.7–11.
2. Chai, Y. H., Priestley, M. J. N., and Seible, F. (1991), Seismic retrofit of circular bridge columns for enhanced flexural performance, ACI Structural Journal, Vol. 88, No. 5, pp. 572–584.
3. Meier U. Strengthening of structures using carbon fibre/epoxycomposities. Construct Build Mater 1995;9(6):341 – 51.
4. Lam L, Teng JG. Strength models for fiber-reinforced plastic-confined concrete. J Struct Eng 2002;128(5).
5. Ninoslav Pešić, Kypros Pilakoutas. Concrete beams with externally bonded flexural FRP-reinforcement: analytical investigation of debonding failure. Composites: Part B 34 (2003) 327–338.
6. Li LJ, Guo YC, Liu F, Bungey JH. An experimental and numerical study of the effects of thickness and length of CFRP on performance of repaired reinforced concrete beams. Constr Build Mater 2006;20(10):901–9.
7. Zhang SS, Yu T, Chen GM. Reinforced concrete beams strengthened in flexure with near-surface mounted (NSM) CFRP strips: current status and research needs. Compos B 2017;131:30–42.
8. Al-Mahmoud F, Caste A I, François R, Tourneur C. Strengthening of RC members with near surface mounted CFRP rods. Composite Structures 2009; 91:138-147
9. Hassan T, Rizkalla S. Investigation of bond in concrete structures strengthened with near surface mounted carbon fiber reinforced polymer strips. J Compos Constr., 2003; 7(3):248–57
10. Barros JA, Ferreira D R, Fortes AS, Dias SJ. Assessing the effectiveness of embedding CFRP laminates in the near surface for structural strengthening. Constr. Build Mater 2006; 20(7):478–91.
11. De Lorenzis L, Teng JG. Near-surface mounted FRP reinforcement: an emerging technique for strengthening structures. Composites Part B-Engineering 2007; 38(2):119-143.
12. Salama ASD, Hawileh RA, Abdalla JA. Performance of externally strengthened RC beams with side-bonded CFRP sheets. Composite Structures 212 (2019) 281–290
13. Abdallah M, Al Mahmoud F, Boissière R, Khelil A, Mercier J. Experimental study on strengthening of RC beams with Side Near Surface Mounted technique-CFRP bars. Composite Structures 234 (2020) 111716. <https://doi.org/10.1016/j.compstruct.2019.111716>.
14. Capozucca R, Nilde Cerri M. Static and dynamic behaviour of RC beam model strengthened by CFRP-sheets. Construction and Building Materials 16 2002 91 Ž . 99.
15. Zhou CY, Yu YN, Xie EL. Strengthening RC beams using externally bonded CFRP sheets with end selflocking. Composite Structures 241 (2020) 112070

16. Song L, Yu Zh. Fatigue performance of corroded reinforced concrete beams strengthened with CFRP sheets. *Construction and Building Materials* 90 (2015) 99–109
17. Sharaky IA, Baena M, Barris C, Sallam HEM, Torres L. Effect of axial stiffness of NSM FRP reinforcement and concrete cover confinement on flexural behaviour of strengthened RC beams: Experimental and numerical study. *Engineering Structures* 173 (2018), 987–1001.
18. Le-Trung K, Lee K, Lee J, Lee DH, Woo S. Experimental study of RC beam–column joints strengthened using CFRP composites. *Composites: Part B* 41 (2010) 76–85
19. Jawdhari A, Peiris A, Harika I. Experimental study on RC beams strengthened with CFRP rod panels. *Engineering Structures* 173 (2018) 693–705
20. Obaidat YT, Abu-Farsakh GAFR, Ashteyat AM. Retrofitting of partially damaged reinforced concrete beam-column joints using various plate-configurations of CFRP under cyclic loading. *Construction and Building Materials* 198 (2019) 313–322
21. Mahmoud MH, Afefy HM, Kassem NM, Fawzy TM. Strengthening of defected beam–column joints using CFRP. *Journal of Advanced Research* (2014) 5,67-77
22. Lignola GP, Prota A, Manfredi G, Cosenza E. Experimental performance of RC hollow columns confined with CFRP. *J Compos Construct* 2007;11(1). 1090-0268.
23. Shaikh FUA, Alishahi R. Behaviour of CFRP wrapped RC square columns under eccentric compressive loading. *Structures* 20 (2019) 309–323
24. Saljoughian A, Mostofinejad D. Axial-flexural interaction in square RC columns confined by intermittent CFRP wraps. *Composites Part B* 89 (2016) 85-95.
25. Akter Hosen Md, Jumaat MZ, Saiful Islam ABM. Side Near Surface Mounted (SNSM) technique for flexural enhancement of RC beams. *Materials & Design* 2015; 83 : 587–597.
26. ACI. Building code requirements for structural concrete and commentary. American Concrete Institute, ACI 318-14, Farmington Hills, MI., September 2014.
27. Ashour AF, El-Refaie SA, Garrity SW. Flexural strengthening of RC continuous beams using CFRP laminates. *Cem Concr Compos* 2004;26:765–75.
28. Aiello MA, Valente L, Rizzo A. Moment Redistribution In Continuous Reinforced Concrete Beams Strengthened With Carbon-Fiber-Reinforced Polymer Laminates. *Mechanics of Composite Materials*, Vol. 43, No. 5, 2007.
29. Akbarzadeh H, Maghsoudi AA. Experimental and analytical investigation of reinforced high strength concrete continuous beams strengthened with fiber reinforced polymer. *Mater Des* 2010;31:1130–47.
30. ACI Committee 440. Guide For The Design And Construction Of Externally Bonded FRP Systems For Strengthening Concrete Structures. American Concrete Institute, 2017, Farmington Hills, MI., USA.
31. Li L, Zheng W, Wang Y. Review of moment redistribution in statically indeterminate RC members. *Engineering Structures* 196 (2019) 109306.
32. BS EN 1992-1-1:2004. Eurocode 2: Design of concrete structures - Part 1–1: General rules and rules for buildings. London, UK: British Standards Institution; 2004.

33. AS 3600-2009. Concrete structures. Sydney, Australia: Australia Standards; 2009.
34. Goldberg JE, Richard RM. Analysis of nonlinear structures. ASCE J Struct Div – Proc Am Soc Civ Eng 1963;89:333–51.
35. Richard RM, Abbott BJ. Versatile elastic-plastic stress-strain formula. ASCE J Eng Mech Div – Proc Am Soc Civ Eng 1975;101:511–5.
36. Scott BD, Park R, Priestley MJN. Stress-strain behavior of concrete confined by overlapping hoops at low and high strain rates. J Am Concr Inst 1982;79:13–27.
37. Al-Mahmoud F, Castel A, François R, Tourneur C. Effect of surface preconditioning on bond of carbon fiber reinforced polymer rods to concrete. Cem Concr Compos 2007;29(9):677–89.
38. ABAQUS version 6.13, 2013. Computer software, Assault Systems, Waltham. MA.
39. Almassri B, Al Mahmoud F, Francois R. Behaviour of corroded reinforced concrete beams repaired with NSM CFRP rods, experimental and finite element study. Composites Part B, 92
40. Sharaky IA, Baena M, Barris C, Sallam HEM, Torres L. Effect of axial stiffness of NSM FRP reinforcement and concrete cover confinement on flexural behaviour of strengthened RC beams: Experimental and numerical study. Engineering Structures 173 (2018), 987–1001.
41. Abouali S, Shahverdia M, Ghassemieh M, Motavallia M. Nonlinear simulation of reinforced concrete beams retrofitted by nearsurface mounted iron-based shape memory alloys, Engineering Structures, 187(2019), 133–148.
42. Ali H, Assih J, Li A. Flexural capacity of continuous reinforced concrete beams strengthened or repaired by CFRP/GFRP sheets. International Journal of Adhesion and Adhesives 104 (2021) 102759.
43. CNR-DT 200 R1/2013, Guide for the design and construction of externally bonded FRP systems for strengthening existing structures, Rome, Italy: National Research Council; 2013.
44. FIB Bulletin 14. Externally Bonded FRP Reinforcement for RC Structures. International Federation for Structural Concrete, Zürich, Switzerland, 2001.



## II. INTRODUCTION

---

The reinforced concrete (RC) beam is a horizontal structural element usually used to support the weight of the floors and roofs of a structure and to transfer the load to a vertical load-bearing element such as a column and wall. The RC beam can be simply supported, continuous, or cantilevered. Continuous beams are the most widely used form. They are preferred for uniform girder bridges and buildings located in severe environments or in areas exposed to high levels of seismic. Continuous beams have the potential to enhance structural integrity and rigidity, and they can offer redistribution of moments due to their structural redundancy, which permits exploiting the available reserve strength and achieving optimal design sections without the congestion of reinforcement at the critical sections (midspan and over supports). Furthermore, continuous beams are usually used as a part of a frame, which in turn provide less span moment and deflection as well as provide better resistance to lateral forces when compared to that of simply supported beams (SSBs).

RC beams as the other structural members may require repair or strengthening either to increase their service life or to enhance their loading and deformation capacities. There are several reasons that point out the need for strengthening or repairing processes: for instance, insufficient placement or length of the main reinforcement, using low-strength concrete, deteriorating the RC material, upgrading the initial designs, and restoring the strength of structural members as a result of accidents or natural hazards such as earthquakes. The first strengthening or retrofitting operation carried out on RC structures is not exactly known. However, in the 1980s, retrofitting RC bridges [1] and columns [2] with steel plates or steel jackets was acceptable and commonly done, particularly in the United State and Europe. Since the early 1990s, the trend began of studying the possibility of involving fiber-reinforced polymers (FRPs) in the construction industry [3]. A few years later, particularly since the early 2000s, FRPs have almost completely replaced steel as externally bonded (EB) reinforcements for concrete [4-6]. This is because FRPs have shown excellent properties, better than those of conventional steel reinforcement, such as higher tensile strength, better resistance to corrosion and fire, and lower weight. FRP composites are normally applied to structural members to improve their performances (flexural and shear). The techniques most commonly used for this purpose are external bonded (EB) and near surface mounting (NSM). FRP materials in the form of plates or sheets can be applied to damaged structural elements as an external reinforcement via the EB technique, whereas those in the form of rods or strips can be used as an internal reinforcement via the NSM technique. Generally, the efficiency of the FRPs used in RC structures depends on their interface bonding behavior with concrete, which can normally be enhanced using a filling material agent such as adhesive resin.

Extensive research studies have been performed on the use of FRPs for flexural reinforcing and retrofitting SSBs [7, 8], joints [9, 10], and columns[11-12]. The results have showed that the flexural strength improvement in SSBs as a result of FRPs is significant and may reach, in some strengthening configurations, more than 90% with the EB technique[7] and even more than 130% with the NSM technique [13]. However, in ordinary RC structures, the flexural behavior and failure modes of multispan beams are considerably different from those of SSBs. This is essential because continuous beams have positive (sagging) and negative (hogging) bending

moment regions. Involving the FRP reinforcements in strengthening or retrofitting such indeterminate members makes predicting their flexural performance more complicated. In fact, the behavior benefits, failure mechanism and rate of strength gain of using FRPs in continuous beams have scarcely been explored, and to date, they remain vague concepts to most researchers and practicing engineers. Indeed, few studies have focused on strengthening continuous RC beams with EB-CFRP composites while no studies were found in the literature on strengthening continuous beams with NSM-CFRP bars. Consequently, this work primarily presents an experimental, analytical and finite element (FE) study for strengthening and repairing continuous two-span RC beams with FRP materials using the internal (NSM, side-NSM) and external (EB, side-EB) techniques. The thesis is composed of four main chapters. Each chapter is organized as a scientific research paper that is published in an international peer-reviewed journal. These papers are kept in their original journal format in this thesis.

Table II-1: Outline and objectives of the present research

Research item	Chapter 1 <sup>(*)</sup>	Chapter 2	Chapter 3	Chapter 4
Testing full-scale specimens	✓	✓	✓	✓
Finite element analysis (ABAQUS)			✓	
Simply supported RC beams	✓			
Continuous two-span RC beams		✓	✓	✓
Initial strengthening	✓	✓	✓	✓
Conventional techniques (NSM or EB)		✓	✓	✓
Proposed techniques (SNSM or S-EB)	✓		✓	✓
Effect of filling material	✓	✓		
Effect of FRP position	✓		✓	✓
Effect of FRP length	✓	✓		
Effect of FRP types		✓		
Effect of FRP arrangement			✓	
Effect of resin type				✓
Effect of FRP form				✓
Effect of steel reinforcement ratio			✓	
Moment redistribution capacity		✓	✓	✓
Comparison with literature	✓			
Comparisons: NSM with EB				✓
Comparisons: NSM with side-NSM	✓		✓	✓
Comparisons: EB with side-EB				✓
Proposed analytical model	✓	✓		
Evaluation of the exists design codes				✓
Conclusions	✓	✓	✓	✓

<sup>(\*)</sup> Chapter 1: Experimental study on strengthening of RC beams with Side Near Surface Mounted technique-CFRP bars.

Chapter 2: Assessment of the flexural behavior of continuous RC beams strengthened with NSM-FRP bars, experimental and analytical study.

Chapter 3: Experimental and numerical investigation on the effectiveness of NSM and side-NSM CFRP bars for strengthening continuous two-span RC beams.

Chapter 4: Efficiency of EB CFRP composites for flexural strengthening of continuous RC beams: A comparative study with NSM CFRP rods.

Table II-1 describes the present research and provides the research components that are considered in each chapter. The research item column refers to the main structural subjects that

are studied and investigated in this thesis. Full-scale tests were performed in all chapters to observe actual outcomes. Based on the results from the tests and the theoretical reasoning, we proposed numerical (FE) and analytical models that can be used by researchers and practicing engineers. In addition, this thesis provides comprehensive comparisons between the different strengthening techniques used nowadays in the construction industry. These comparisons provide clear answers for the most controversial topics regarding strengthening or repairing RC structures with FRP, and thereby can be used for formulating or improving current design rules.

### References

1. Eberline DK, Klaiber FW, Dunker K (1988), Bridge Strengthening with Epoxy-Bonded Steel Plates, Transportation Research Record 1180, pp.7–11.
2. Chai, Y. H., Priestley, M. J. N., and Seible, F. (1991), Seismic retrofit of circular bridge columns for enhanced flexural performance, ACI Structural Journal, Vol. 88, No. 5, pp. 572–584.
3. Meier U. Strengthening of structures using carbon fibre/epoxycomposites. Construct Build Mater 1995;9(6):341 – 51.
4. Lam L, Teng JG. Strength models for fiber-reinforced plastic-confined concrete. J Struct Eng 2002;128(5).
5. Ninoslav Pešić, Kypros Pilakoutas. Concrete beams with externally bonded flexural FRP-reinforcement: analytical investigation of debonding failure. Composites: Part B 34 (2003) 327–338.
6. Li LJ, Guo YC, Liu F, Bungey JH. An experimental and numerical study of the effects of thickness and length of CFRP on performance of repaired reinforced concrete beams. Constr Build Mater 2006;20(10):901–9.
7. Salama ASD, Hawileh RA, Abdalla JA. Performance of externally strengthened RC beams with side-bonded CFRP sheets. Composite Structures 212 (2019) 281–290
8. Sharaky IA, Baena M, Barris C, Sallam HEM, Torres L. Effect of axial stiffness of NSM FRP reinforcement and concrete cover confinement on flexural behaviour of strengthened RC beams: Experimental and numerical study. Engineering Structures 173 (2018), 987–1001.
9. Jawdhari A, Peiris A, Harika I. Experimental study on RC beams strengthened with CFRP rod panels. Engineering Structures 173 (2018) 693–705
10. Obaidat YT, Abu-Farsakh GAFR, Ashteyat AM. Retrofitting of partially damaged reinforced concrete beam-column joints using various plate-configurations of CFRP under cyclic loading. Construction and Building Materials 198 (2019) 313–322
11. Lignola GP, Prota A, Manfredi G, Cosenza E. Experimental performance of RC hollow columns confined with CFRP. J Compos Construct 2007;11(1). 1090-0268.
12. Shaikh FUA, Alishahi R. Behaviour of CFRP wrapped RC square columns under eccentric compressive loading. Structures 20 (2019) 309–323
13. Akter Hosen Md, Jumaat MZ, Saiful Islam ABM. Side Near Surface Mounted (SNSM) technique for flexural enhancement of RC beams. Materials & Design 2015; 83 : 587–597.





# CHAPTER I: EXPERIMENTAL STUDY ON STRENGTHENING OF RC BEAMS WITH SIDE NEAR SURFACE MOUNTED TECHNIQUE-CFRP BARS

*Published in Composite Structures, <https://doi.org/10.1016/j.compstruct.2019.111716>*

---

This chapter aims at studying the possibility of strengthening RC beams with FRP bars at their sides instead of their soffits. The side-NSM technique is introduced as a convenient alternative to the NSM one in order to overcome the limitations and shortcomings of the NSM technique. In general, this chapter intends to verify the efficiency of using the proposed side-NSM system on SSBs in order to be used later for strengthening continuous RC beams. The experimental program of this chapter consists of six SSBs: one control beam and five others were strengthened in bending with CFRP bars. Effects of the CFRP length, the filling material type, and the strengthening position on the enhancement of the load-carrying capacity of beams were studied and discussed in detail. The experimental results of the tested beams were analyzed in terms of the load-deflection response, failure mode, ductility and energy absorption capacity. Furthermore, a comparison study between the NSM and side-NSM techniques for strengthening RC beams was presented. The tested side-NSM-CFRP beams in this chapter were compared to similar NSM-CFRP beams tested in literature. The comparison study investigates potential of the side technique to prevent the nonconventional failure modes of strengthened beams. The tensile strain in the steel and CFRP reinforcements were measured and presented at different load levels using electrical strain gauges. Finally, in the last part of this chapter, a simplified analytical model was introduced for predicting the load-deflection response of the tested side-NSM beams.

**Experimental study on strengthening of RC beams with Side Near Surface Mounted technique-CFRP bars**

Mohammad Abdallah\*<sup>1</sup>, Firas Al Mahmoud<sup>1</sup>, Rémi Boissière<sup>1</sup>, Abdelouahab Khelil<sup>1</sup> and Julien Mercier<sup>2</sup>

<sup>1</sup>*Institut Jean Lamour, UMR 7198, CNRS, Université de Lorraine, Nancy, France*

<sup>2</sup>*Freyssinet, Paris, France*

---

**Keywords:** CFRP rods, SNSM reinforcement, experimental, RC beam, flexural behavior.

**Abstract**

This paper presents an experimental program that was carried out for the purpose of studying the global flexural performance of reinforced concrete beams strengthened internally with Carbon Fiber Reinforced Polymer (CFRP) rods using the Side Near Surface Mounted (SNSM) technique. The CFRP rods were placed laterally, adjacent to the longitudinal steel bars inside precut grooves. The strengthening length and position of CFRP rods as well as the type of filling material were the main variables investigated in this study. Moreover, a detailed comparison between the Side Near Surface Mounted (SNSM) and the Near Surface Mounted (NSM) techniques for the strengthening of RC beams using CFRP rods was conducted as well; in order to validate and assess the effectiveness of the SNSM technique.

The test results showed that using the SNSM-CFRP rods technique allowed improving in a significant way the load carrying capacity of RC beams but decreased their ductility along the deflection at maximum load. The results obtained indicated that the failure mode was influenced by the length of CFRP rods and the filling material characteristics, while the strengthening position did not have significant impact. The SNSM strengthening technique can be used as an alternative method to the NSM method, and in some cases, it may be used to prevent the non-conventional failure modes, due to degradation of the NSM strengthening system, such as the pull out of CFRP-rods or premature debonding failure. The conventional analytical model accurately predicted the strength capacity and mid-span deflection of the SNSM strengthened beams.

**1.1 Introduction**

Since the 1990s, the degraded reinforced concrete (RC) structures due to exposure to natural hazards and extreme weather events have been repaired with the help of Fiber Reinforced Polymers (FRPs). A wide range of studies have been conducted on strengthening or retrofitting RC elements using externally bonded (EB) FRP laminates or/and sheets [1-4]. Despite the mechanical strengthening advantages of using the EB-FRP technique, some drawbacks, which represent genuine handicaps in its practical execution and long-term monitoring, still exist. For instance, one can mention the pretreatment process, installation time, premature debonding failure due to interfacial stresses, and the mechanical damages resulting from accidental impacts.

In the past ten years, the Near Surface Mounted (NSM) technology is viewed as a promising alternative to the *externally bonded (EB) FRP* strengthening technique; this is actually a prevailing method for strengthening existing concrete structures using FRP reinforcement [5]. The NSM technique has attracted worldwide attention due to the different advantages it offers: (1) The NSM-FRP system is quite simple and does not require extensive surface preparation work. The FRP composites (rods, strips, etc) are inserted adjacent to longitudinal steel bars and embedded inside precut grooves in the beam soffit; they are bonded to concrete with epoxy-based pastes or modified cement grouts [6]; (2) *RC members* strengthened with *NSM-FRP reinforcement* proved to be much more ductile and experienced failure at much higher level as compared to EB-FRP members [7,8]; (3) *Strengthening of RC components* with the *NSM technique* offers higher bonding efficiency and better protection for the FRP reinforcement as compared to the EB strengthening technique [9].

Several experimental studies investigating the NSM-FRP technique have underlined its potential for strengthening *reinforced concrete (RC)* beams. Almahmoud et al. [6, 10] found that the NSM method, using CFRP rods, can significantly improve the ultimate strength of RC beams by 50%, at least, over the ultimate strength of non-strengthened beam. Their experimental results also indicated that the failure mode of strengthened beam varies from degradation of the CFRP rod mounting to compressive concrete crushing and depends on the ratio of a combination of CFRP cross-section and length to the concrete compressive strength. Kreit et al. [11] presented a testing program for the purpose of assessing the flexural performance of corroded RC beams strengthened with CFRP rods using the NSM method. The experimental results showed that retrofitted beams with 36% loss in steel cross section displayed an ultimate capacity similar to that of an un-corroded control beam. Moreover, two types of failure modes were observed; one was due to failure of the tension corroded steel and the other was because of concrete cover peeling off at level of the additional reinforcement (CFRP). Sharaky et al. [12] investigated the flexural performance of NSM strengthened RC beams with partially and fully bonded CFRP and GFRP bars. The specimens strengthened with fully bonded reinforcement showed higher stiffness and greater bearing capacity than those strengthened with partially bonded reinforcement. Also, the concrete cover separation was the dominant failure mode regarding the NSM-CFRP rods beams. On the other hand, the fully bonding NSM-GFRP rods beams failed due to either debonding at the concrete-epoxy interface or concrete splitting, depending on the number of grooves used. Furthermore, Khalifa [13] made an attempt to assess the effectiveness of NSM and EB systems with CFRP reinforcement for the purpose of improving the flexural strength of RC beams under four-point loading. The beams strengthened with NSM-CFRP strips exhibited higher ultimate loads than those strengthened with EB-CFRP sheets; the difference ranged from 12% to 18%. The tested NSM beam specimens failed due to debonding of the CFRP strips along with concrete cover peeling off. For their part, Sebastian et al. [14] evaluated the structural performance of indeterminate RC beams internally reinforced with NSM-CFRP rods. The strengthened structure failed due to the peeling-off of CFRP bars in the positive moment region; in addition, the ultimate load carrying capacity of the strengthened beam was 37% higher than that of the control beam.

Although the above mentioned studies have indicated that NSM-FRP reinforcement can significantly enhance the flexural behavior of RC beams by increasing their ultimate capacity;

this strengthening system might not be feasible in several practical cases, especially when the building is operating. In this case, widths of the beams are usually occupied by partitions as masonry walls. In other cases, the NSM technique presents some restrictions in its application : (1) Only a limited number of FRP bars can be used in each specimen, on account of the effective groove spacing. The minimum clear spacing (SG) between grooves (Figure 1-1) should be greater than twice the depth of the groove, otherwise debonding failure may occur due to stress overlapping [6,15,16]; (2) Application of the NSM technique might be difficult or even impossible for some parts of structures, particularly, over the supports. Applying anchorage of FRP rods over the supports in RC beams cannot be easily performed and could impact other structural components, such as columns and joints, during preparation and/or installation; (3) The bond efficiency of NSM-FRP rods is substantially associated with the quality of the concrete cover; for instance, in corroded beams, the bottom concrete cover is highly exposed to damage due to corrosion of the longitudinal steel bars, particularly when steel bars are arranged in one layer, and therefore, putting FRP rods in such places may reduce their expected additional resistance and drive to premature failure [11, 17]; hence, a need to change the strengthening position becomes essential. (4) As stated in the above-mentioned literature, application of NSM-CFRP technique for strengthening RC beams could lead to non-conventional failure modes, i.e. peeling off and pull out failures modes, due to degradation of the strengthening system, which induces a significant reduction in the ductility of beams [9-14,18-20]. Thus, in order to overcome the NSM limitations or/and its operational obstacles, the Side Near Surface Mounted (SNSM) technique has recently been proposed as a new alternative approach for strengthening *reinforced concrete* (RC) members using fiber *reinforced* polymer (FRP) reinforcing bars. In this proposed technique the FRP elements inserted in the vertical sides of the beam instead of the bottom side. The use of the SNSM method is quite recent and very few researchers have investigated the subject so far. Indeed, Akter et al. [21] examined the structural behavior of RC beams strengthened with CFRP and steel reinforcing bars using the SNSM technique. Although the main variable studied was the additional reinforcement ratio, the test results indicated that applying 2 $\emptyset$ 8, 2 $\emptyset$ 10 and 2 $\emptyset$ 12 SNSM-CFRP rods could increase the flexural strength of beams by up to 91%, 138% and 133%, respectively, over the non-strengthened control beam. The impact of other variables, such as the CFRP length, CFRP position and type of filling material have still not been extensively studied yet. Therefore, the purpose of the present work is to investigate the global behavior of reinforced concrete beams strengthened with 2 $\emptyset$ 6 CFRP rods using the SNSM technique. This was carried out by studying three key parameters that are likely to affect the structural response, namely, strengthening length, strengthening position and filling material characteristics. A detailed comparison between the SNSM and NSM strengthening approaches was performed in terms of the failure and bearing capacity mechanisms. In addition, the test results obtained were compared with those of conventional analytical models; also, the computed flexural strength capacity and mid-span deflection of the strengthened beams were found to be in good agreement with the experimental ones.

## 1.2 Experimental program

### 1.2.1 Test beams and materials.

A total of six RC rectangular beams, including one control beam (CB), were tested to failure by applying monotonically increasing four-point bending loads. The RC beams were designed to experience flexural failure in accordance with the ACI code [15]; they were reinforced with two ordinary 12 mm diameter deformed steel bars in the tension zone and two 6 mm diameter ribbed bars in the compression zone. The deformed steel bars in the compression zone were utilized as hanger bars; and they were running along the shear zones. Closed 6-mm-diameter stirrups were provided against the maximum shear with a 150-mm center-to-center spacing. The concrete cover thickness in all tested beams was maintained at 20-mm for the vertical sides and 30-mm at the top and bottom sides. The beam geometry and steel reinforcement configuration are illustrated in Figure 1-2.

The characteristics of concrete employed in the formulation of RC beams were determined by laboratory testing of three *hardened concrete cylinder specimens* ( $D = 160$  mm and  $H = 320$  mm). The average compressive and tensile strengths as well as the modulus of elasticity of concrete at 28 days were 37.0 MPa, 3.0 MPa and 30.3 Gpa, respectively. However, in order to determine the mechanical properties of longitudinal steel bars, two steel bar specimens of diameter 12 mm were tested in tensile and the measured yield strength was 600 MPa, and the modulus of elasticity was 210 GPa.

Five beams were internally strengthened in bending with two 6-mm-diameter CFRP rods ( $56.5 \text{ mm}^2$ ) installed into two grooves, i.e. one rod in each groove, using the SNSM technique (see Figure 1-2). The longitudinal grooves ( $12 \times 12$  mm) were made with a special concrete saw. In addition, in order to ensure proper bonding between the filling material and concrete substrate, it was decided to apply an airbrush at high pressure to remove debris and fine particles. The grooves were filled up to two stages so to guarantee that the filling material is in full contact with the surface of CFRP bars. Afterwards, all strengthened beams were confined at room temperature ( $T = 20$  °C) for one week in order to obtain maximum strengthening level, depending on the filling material used, before testing.

The mechanical properties of the strengthening material were determined through axial testing of three CFRP rods by [22]. The CFRP rods tested exhibited dissimilar response to that of the conventional steel bars, principally, the linear-elastic attitude up to the failure point (brittle failure). The ultimate tensile strength and Young's modulus of the CFRP rods used were 1875MPa and 146GPa respectively.

Two types of groove-filling materials for bonding the CFRP bars to the internal concrete surface were considered in this research, namely epoxy resin and mortar. Table 1-1 shows the compressive and tensile strengths of the epoxy resin and mortar at 7 days. The compressive and tensile strengths of resin were according to the manufacture, whereas the mechanical properties of mortar were determined by laboratory testing of four specimens.

### 1.2.2 Beam strengthening

Each strengthened beam was assigned a reference code that defines its strengthening scenario. For example, BC1(270-SR) means that beam BC1 is strengthened with 270 cm long CFRP bars placed alongside the steel bars (S) and embedded in resin filling material (R).

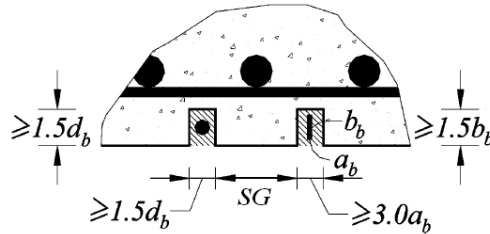
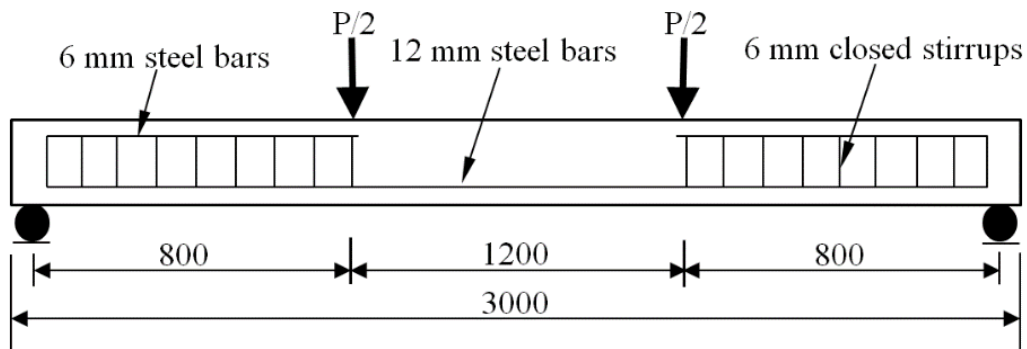
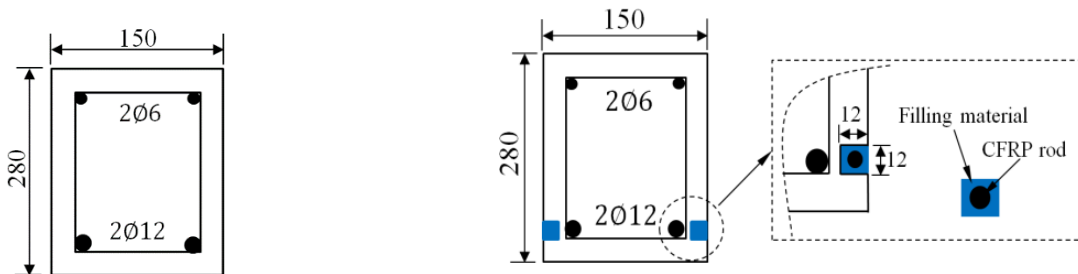


Figure 1-1: Minimum dimensions of grooves

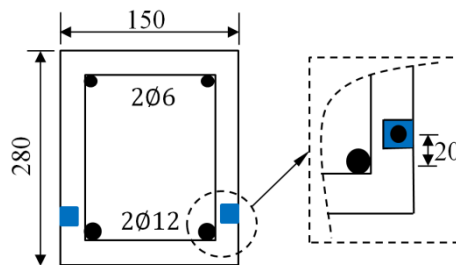


(a) Elevation view



Beam cross-section before strengthening. (CB)

Beam cross-section after strengthening with CFRP rods by using the SNSM technique.(BC1-BC4)



Beam cross-section after strengthening with CFRP rods by using the SNSM technique.(BC5)

Figure 1-2 : Test beams details and reinforcement configuration. (All dimensions are in mm)

Table 1-1: Characteristics of the filling material

Material	Compressive strength (MPa)	Tensile strength (MPa)
Epoxy resin	83	29.5
Mortar	74.6	6.2

However, the strengthening scheme of this study was designed to investigate the effectiveness of the SNSM-CFRP technique in upgrading the flexural capacity of RC beams. Therefore, the global flexural performance of the series beams BC1(270-SR), BC2(210-SR), BC3(270-SM) and BC4(210-SM), was studied with respect to the running length of CFRP rods and the type of filling material. The CFRP rods used to strengthen the above four beams were placed at the same level as the tensile steel (about 42-mm from the beam bottom surface). Beams BC1(270-SR) and BC3(270-SM) were strengthened with 270 cm long CFRP bars, whereas 210 cm long CFRP bars were employed in strengthening beams BC4(210-SM) and BC2(210-SR). The CFRP bars were embedded in resin in the case of beams BC1(270-SR) and BC2(210-SR); however, for beams BC3(270-SM) and BC4(210-SM), these bars were inserted into mortar.

Furthermore, another RC beam, namely BC5(270-UR), was strengthened with two 6 mm diameter CFRP rods embedded in resin and placed 20 mm higher than the longitudinal steel bars level (about 62 mm from the beam bottom surface), [Figure 1-2](#). The purpose was to assess effects of the position of CFRP rods on the flexural response of the beam. Indeed, the efficiency of the SNSM technique is substantially influenced by the quality of the concrete cover. Thus, a need to change the strengthening position in some competitive conditions might prove essential to ensure sufficient concrete cover for groove preparation and CFRP rebar installation. The flexural response of beam BC5(270-UR) was compared with that of beam BC1(270-SR). The test matrix of this study are summarized in [Table 1-2](#).

Table 1-2 : Strengthening details of the test beams.

Beam	Number of CFRP rod	Strengthening length (cm)	Filling Material	Strengthening Position	SL/BL <sup>(3)</sup>
CB	----	----	----	----	----
BC1(270-SR)	2 $\emptyset$ 6	270	Resin	S <sup>(1)</sup>	0.94
BC2(210-SR)	2 $\emptyset$ 6	210	Resin	S	0.56
BC3(270-SM)	2 $\emptyset$ 6	270	Mortar	S	0.94
BC4(210-SM)	2 $\emptyset$ 6	210	Mortar	S	0.56
BC5(270-UR)	2 $\emptyset$ 6	270	Resin	U <sup>(2)</sup> (+20mm)	0.94

(1) S: on the same level of the steel bars.

(2) U: above than steel level.

(3) SL/BL: is the ratio between strengthening length SL and beam length BL, where SL is the distance between the end of the CFRP bar and the applied load and BL is the distance between the support and the applied load

### 1.2.3 Instruments and test procedure.

All beams were tested under four-point loads up to failure. The main load (P) was applied using a hydraulic actuator with capacity of 400 kN and 0.3 kN/s average loading speed. The total applied load was measured by means of an attached electrical load cell. A steel beam was utilized to distribute the total applied load into two concentrated loads. Each load (P/2) acted at a point situated at 80 cm from the adjoining support.

A vertical linear variable differential transducer (LVDT) was used for each tested beam in order to monitor the vertical mid-span deflection. Regarding the strengthened beams, four electrical strain gauges in total were used for each specimen for the purpose of monitoring the strain in



the internal tensile steel bars and the adjacent CFRP rods. The strain gauges were attached to midpoint of reinforcement bars and oriented in the longitudinal direction. They were well protected with three different layers (protective paste, rubber piece and aluminum tape) after coated with polyurethane material to ensure high degree of measuring accuracy. Figure 1-3 illustrates the set up and instrumentation of beams.

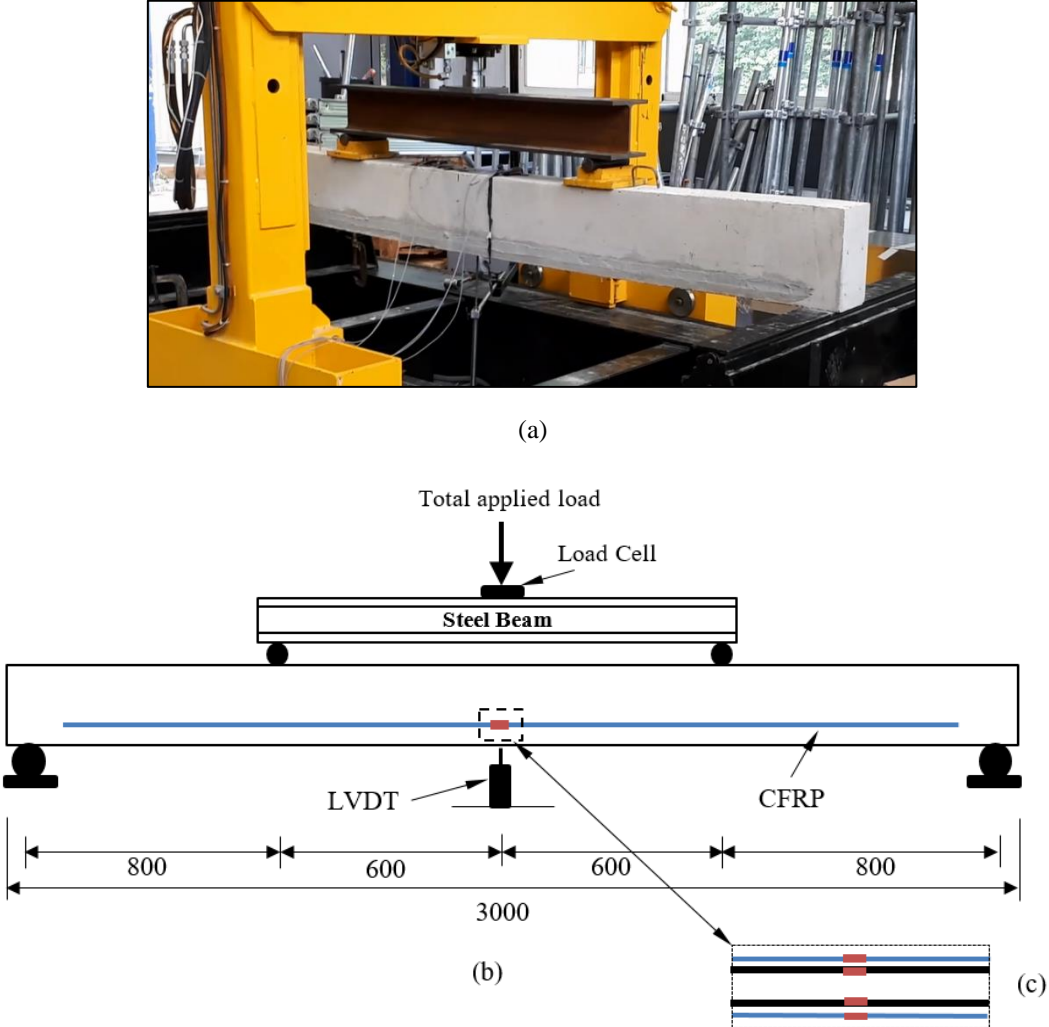


Figure 1-3 : (a) Test setup, (b) Instrumentation and (c) Strain gauges of steel and CFRP bars (top view). (All dimension are in mm)

**1.3 Results and discussion**

**1.3.1 Load-deflection response**

Figure 1-4 illustrates the curves representing the total applied load versus the mid-span deflection for the tested beams. In general, the load carrying capacities of RC beams strengthened with CFRP bars using the SNSM technique were greater than the load carrying capacity of the control beam, CB. The overall load-deflection response ( $P - \delta$ ) indicates that the tested beam specimens went through three distinct stages: elastic or pre-cracking stage (O-A), concrete cracking stage (A-B) and ultimate strength stage (B-C).



It should be clearly noted that in the elastic phase, all the beams displayed the same linear behavior and this is because of the flexural rigidity of beams as well as the bonding between the filling material and concrete were not yet been affected. The potential of CFRP rods to enhance the cracking strength of beams was negligible. The first turning point (A) represents the end of this phase, particularly, when concrete starts cracking.

In the concrete cracking stage, the slopes of strengthened beams were higher than the slope of control beam (A-B lines), which may be attributed to the fact that the CFRP bars improved the stiffness and yield load of the beams. As expected, the horizontal fine cracks on the leveled surface of grooves as well as the flexural cracks in the constant moment zone were observed in this stage. Note that these cracks spread and widened as the external load increased. The cracking phase ended at the second turning point (B), which represents the steel yielding load.

In the ultimate strength phase, the considerable change in slope of the ( $P - \delta$ ) curves as compared to the slopes in the two previous phases, was due to the intrinsic drop in the elastic modulus of tension reinforcement. It is apparent, however in this stage, that all strengthened beams presented higher load-increasing rates than that of the control beam (CB), which implies that the additional reinforcement, provided by the CFRP rods, controlled the flexural performance of the RC beams after the yielding point of tension steel was reached. At the third turning point (C), which represents the end of the ultimate strength stage, the RC beams strengthened with SNSM-CFRP rods exhibited lower ultimate mid-span deflections than that of the control beam.

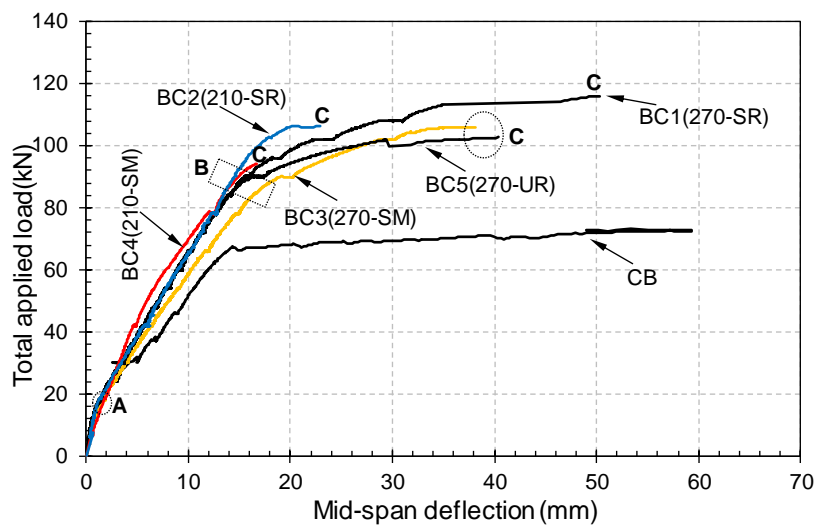


Figure 1-4 : Load vs. mid-span deflection curves

### 1.3.2 Failure mods and cracking pattern

In addition to the conventional ductile flexural failure mode of the reference beam, CB (tensile steel yielding followed by concrete crushing at the beam mid-span); three different failure modes were observed in the SNSM-CFRP beams (concrete crushing in beams BC1(270-SR) and BC5(270-UR), debonding failure in beams BC3(270-SM) and BC4(210-SM) and concrete cover peeling off in beam BC2(210-SR) ), as indicated in Table 1-3.

### 1.3.2.1 Failure mode 1

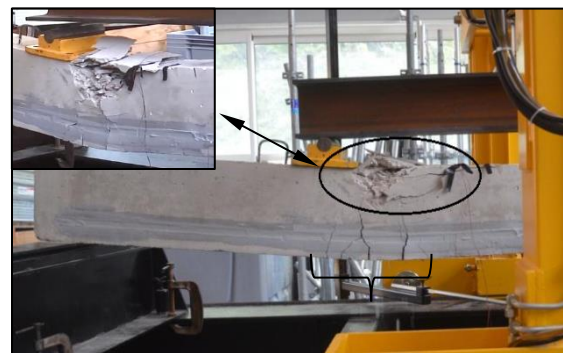
The two beams BC1(270-SR) and BC5(270-UR) experienced the same failure mode although they carried different peak loads. Failure was due to crushing of the brittle compressed concrete in the constant moment zone, close to one of the two load application points, after yielding of the tension steel reinforcement, as shown in Figure 1-5.

In the initial loading stage, horizontal fine cracks were apparent in the resin region. Afterwards, as the applied load was increased, these cracks gradually merged to the flexural cracks which propagated from the bottom side of the tested beams to the load application point. The flexural cracks growth in this set of beams (BC1(270-SR) and BC5(270-UR)) was influenced by the CFRP rod location. The flexural cracks in beam BC5(270-UR) were wider than those in beam BC1(270-SR), which is basically attributed to the displacement of the CFRP rods position to 20-mm above the steel bar level. The new position of the CFRP reinforcing bars in BC5(270-UR) created a new tensile stress level, which consequently caused the cracks to widen further and therefore to expanded upwards. Indeed, the crack pattern of this set confirms that the SNSM-CFRP reinforcing bars worked effectively as an additional tensile reinforcement [23].

However, conspicuous horizontal cracks appeared in the failure sections of both beams, as a result of compressed concrete splitting. These cracks progressively extended and widened in the direction of the mid-span.



(a)



(b)

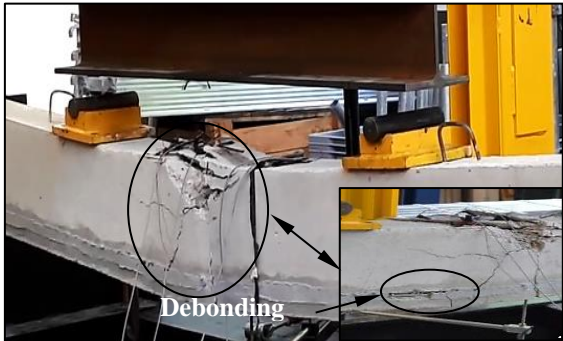
Figure 1-5 : Failure mode of beams; (a) BC1(270-SR) and (b) BC5(270-UR)

1.3.2.2 Failure mode 2

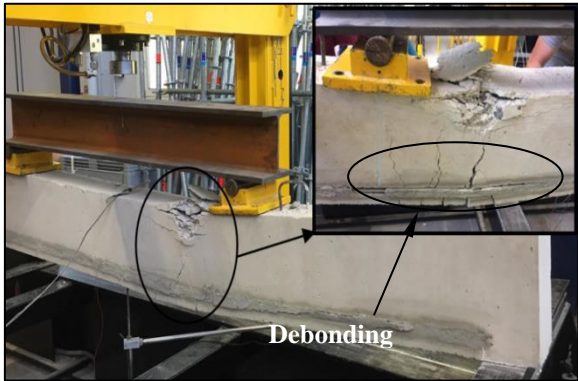
The failure mode of beams BC3(270-SM) and BC4(210-SM) was characterized by debonding between the internal surface of the groove (concrete) and mortar, as shown in Figure 1-6.

The debonding failure mechanism of this set of beams was particularly influenced by the length of CFRP rods. Instantaneous debonding failure suddenly occurred in beam BC4(210-SM), immediately after yielding of the tension steel. This was very abrupt and was followed by beam failure once the concrete at the top of the beam began to crush. On the other hand, the beam BC3(270-SM) continued to deflect but did not fail even after it reached its yielding load; it continued to resist external loads until concrete started crushing in the top fibers. At this point, cracking noises could clearly and continuously be heard, due to the mortar debonding from the concrete, until the failure load was reached. Note that the failure section of beam BC3(270-SM) was observed at the mid-span, nearly the same way as for the control beam (CB); however, failure was observed close to the load application point for beam BC4(210-SM).

Regarding the cracking mechanism, the flexural cracks in beam BC4(210-SM) were narrow but more uniformly distributed than those in beam BC3(270-SM). On the other hand, the horizontal crack due to splitting of the compressed concrete was more conspicuous in beam BC3(270-SM). It is worth mentioning that the mortar-concrete interface was affected by internal longitudinal cracks, particularly at the failure sections. These cracks prevented the flexural cracks to cross the mortar in beam BC4(210-SM) or changed the flexural cracks direction in beam BC3(270-SM). This could be attributed to the debonding failure mechanism, as stated above in each beam [24].



(a)



(b)

Figure 1-6 : Failure mode of beams: (a) BC3(270-SM) and (b) BC4(210-SM)

### 1.3.2.3 Failure mode 3

The failure mode of beam BC2(210-SR) was certainly due to brittle concrete peeling-off in the region where maximum shear occurs; this was immediately followed by the beam failure, as shown in Figure 1-7.

In the initial stage of loading, the crack pattern of beam BC2(210-SR) was almost similar to that observed in beams BC1(270-SR) and BC5(270-UR). As the applied load increased, shear cracks at the end of the additional reinforcement (CFRP bars) started to intersect the fine cracks which had previously appeared in the resin region. The intersection of the shear cracks with the minor horizontal cracks caused a significant main horizontal crack to develop and extend along the beam length at the same level as the CFRP rods. The intersection of the main horizontal crack with the bending vertical crack, which developed in the region close to the concentrated applied load, enhanced the peeling-off of the concrete cover over a significant length in the beam soffit, that is from the extremity of the CFRP bars to the region of maximum moment. In addition, one may clearly notice that visible flexural-shear cracks were formed over the failure length, particularly in the lower moment regions.

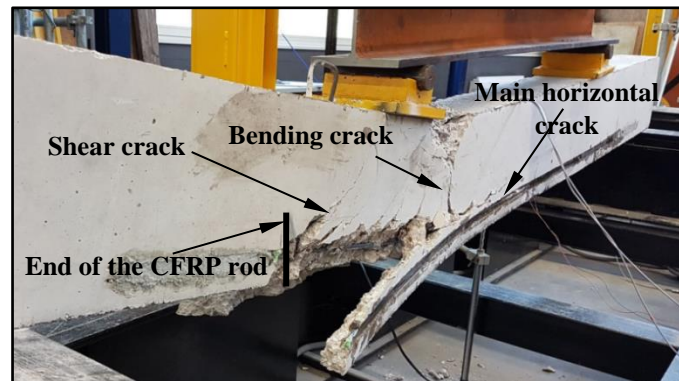


Figure 1-7 : Failure mode of beam: BC2(210-SR)

### 1.3.3 Enhancement of load carrying capacity of SNSM strengthened beams.

Table 1-3 summarizes the load carrying capacities of the tested beams representing the cracking load ( $P_{cr}$ ), yielding load ( $P_y$ ) and ultimate load ( $P_u$ ). Figure 1-8 shows the load-strain curve of the SNSM-CFRP rods. It should be noted that the CFRP load-strain curve is nearly similar to the load-deflection curve (see Figure 1-4). From Figure 1-8, it can be seen that the CFRP rods have not taken much load up to the first crack as the strains were almost zero; their potential to enhance the cracking load of the strengthened beams compared to the control beam was negligible. Afterwards, the CFRP strain curves have shown reasonable inclinations, which means that the additional bars have started to carry substantial loads, and thus significantly improved the yielding and ultimate loads of the SNSM-CFRP beams. The CFRP strains exhibited nearly linear curves up to tension steel yielding load, thereafter the strains were gradually increased up to the failure load.

In the subsequent sections, however, the effectiveness of the SNSM technique in improving the yielding and ultimate load carrying capacities of RC beams strengthened with CFRP rods is discussed with respect to the strengthening length, strengthening position and filling material

type. The ultimate load of tested beams was determined from the load–deflection curves (Figure 1-4), while the yielding load was determined according to the strain gauge measurement (Figure 1-9,  $\epsilon_{y(exp)} \approx 0.29\%$ , where  $\epsilon_{y(exp)}$  is the experimental yielding strain obtained from tensile test of the steel bars). It should be noted that the strain gauges installed on the steel rebar of beam BC3(270-SM) are stopped working during the loading process due to technical problem which may make the reported yielding load of this beam is not accurate.(see Figure 1-9)

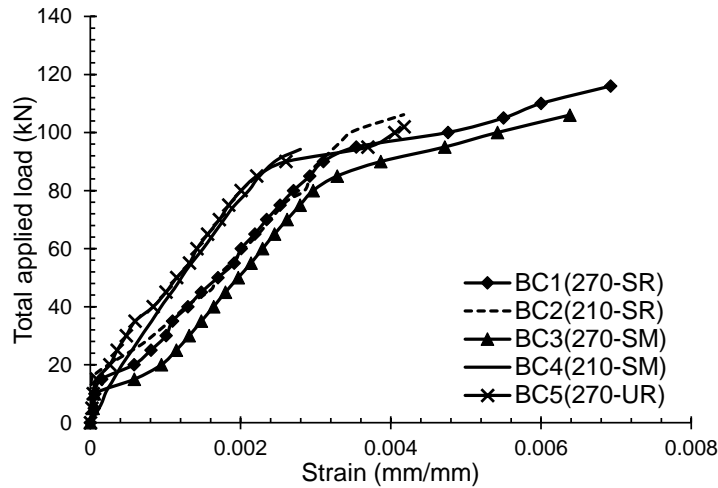


Figure 1-8 : Total applied load vs. strains of the CFRP rods

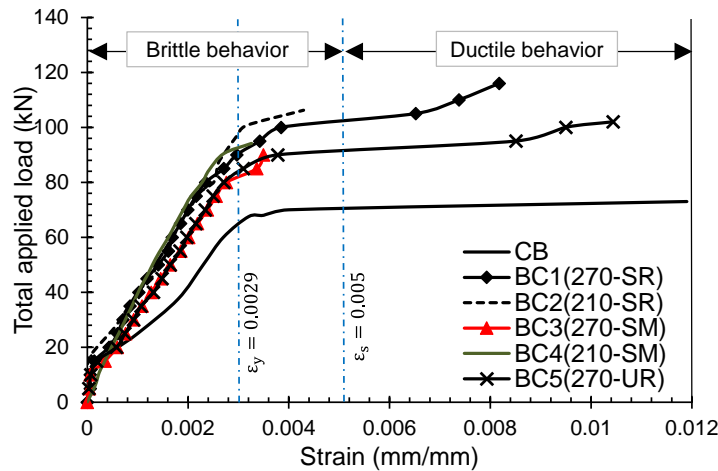


Figure 1-9 : Total applied load vs. steel strain

### 1.3.3.1 Effect of the CFRP strengthening length

The tension steel in beams BC1(270-SR) and BC2(210-SR) yielded at about 90kN and 94.5kN, respectively, which represents an increase of 40% and 47% over the yielding load of the control beam. Beam BC1(270-SR) failed due to crushing of brittle compressed concrete at loading of 116kN with an increase of about 59.3% in the failure load compared to the control beam, whereas beam BC2(210-SR) failed as a result of concrete peeling-off at loading of 106.4kN with an increase of 46.2% in the failure load. The maximum tensile strain measured on CFRP rods was 0.0069mm/mm for beam BC1(270-SR) and 0.0042mm/mm for beam BC2(210-SR); these values represent respectively about 53.9% and 32.8% of the ultimate strain of CFRP bars (see Table 1-3).

Table 1-3 : Experimental results of the test beams

Beam	Failure Mode	Cracking load $P_{cr}$ (kN)	Yielding Load $P_y$ (kN)	Failure Load $P_u$ (kN)	Strain of CFRP <sup>(1)</sup> (mm/mm)	$\chi$ <sup>(2)</sup>	Strain of steel <sup>(3)</sup> (mm/mm)	$E_{ab}$
CB	Conventional flexural failure	17.1	64.3	72.8	----	-----	0.0193	2702.5
BC1(270-SR)	1	18.3	90	116.0	0.0069	0.54	0.0082	4583.8
BC2(210-SR)	3	17.3	94.5	106.4	0.0042	0.33	0.0043	1586.1
BC3(270-SM)	2	18.0	81.8 (88)*	106.0	0.0064	0.50	0.0035	2951.2
BC4(210-SM)	2	18.8	92.4	94.1	0.0028	0.22	0.0033	972.0
BC5(270-UR)	1	17.8	83.2	102.7	0.0041	0.32	0.0104	3267.9

(1)Strain of CFRP: the recorded strain in CFRP rods at failure load of a strengthened beam.

(2) $\chi$  : Efficiency ratio of the CFRP rods = (Strain of CFRP (1) /  $\epsilon_{fu}$ ) .

$\epsilon_{fu}$ : Ultimate tensile strain of CFRP rod obtained from axial testing of three specimens= 0.0128 mm/mm.

(3)Strain of steel: recorded strain in steel bars at failure load of a strengthened beam.

(4) $E_{ab}$ : Energy absorption capacity.

\*Adjusted value, determined by considering 5% variation from BC4



Regarding beams BC3(270-SM) and BC4(210-SM), the yielding started, respectively, at 81.8 kN, which is 27.2% greater than that of CB, and at 92.4 kN, which is 43.7% higher than that of CB. The load at failure was 106 kN for beam BC3(270-SM), and at 94.1kN for beam BC4(210-SM). These failure loads represent an increase of 45.6% and 29.3% with respect to CB. As stated in the failure mode section, the debonding failure, between the filling material and concrete, occurred at an earlier stage in beam BC4(210-SM) than in beam BC3(270-SM). The recorded strain of CFRP bars at failure was 0.0064 mm/mm for beam BC3(270-SM) and 0.0028 mm/mm for beam BC4(210-SM); these values represent, respectively, about 50% and 21.9% of the CFRP rod ultimate strain.

Consequently, increasing length of the CFRP bars led to increase the failure load of the beam and the maximum measured strain of the SNSM-CFRP bars. It was noted that 60-cm of supplementary length of the CFRP rods helped to avoid non-conventional failure mode (peeling-off) or delayed the debonding failure, and therefore, the CFRP rods worked more efficiently as an additional tensile reinforcement. In other words, it may be stated that increasing the ratio between the strengthening length  $SL$  (distance between the end of the CFRP bar and the applied load) and the beam length  $BL$  (distance between the support and the applied load) significantly enhances the flexural response of the SNSM-CFRP beam. The  $\frac{SL}{BL}$  ratio of beams BC1(270-SR) and BC3(270-SM) was 0.94, whereas the  $\frac{SL}{BL}$  ratio of beams BC2(210-SR) and BC4(210-SM) was 0.56. The failure load of BC1(270-SR) was about 9.1% grater than that of BC2(210-SR), and the failure load of BC3(270-SM) was about 12.6% grater than that of BC4(210-SM). The variation between the yielding load of beams BC1(270-SR) and BC2(210-SR), which represents about 5% relative to BC1, may either refer to experimental results scattering or influence of the SNSM strengthening length, thus further experimental studies to investigate effects of the strengthening length of SNSM-CFRP bars on performance of RC beams are necessary.

#### 1.3.3.2 Effect of the filling material

The failure mode of mortar beams; i.e. BC3(270-SM) and BC4(210-SM), was characterized by debonding between the filling material and concrete substrate, whereas no signs of debonding failure were observed in the resin beams; i.e. BC1(270-SR) and BC1(270-SR), (Section 3.2). These findings are in good agreement with those reported in previous studies, on NSM-CFRP beams, which indicated that using resin as a filling material forms better bonding with concrete than using mortar [6]. Thus, the failure loads as well as the maximum measured strain of CFRP rods in mortar beams (Table 1-3) were lower than those in resin beams (BC3(270-SM) vs. BC1(270-SR) and (BC4(210-SM) vs. BC2(210-SR)).

#### 1.3.3.3 Effect of the strengthening position

As can be seen from Table 1-3, beam BC5(270-UR) yielded at 83.2kN before the yielding load of beam BC1(270-SR) (difference about 6.8kN). The beam BC5(270-UR) failed due to concrete crushing, which is similar to the failure mode of BC1(270-SR), at 102.7kN. Although, this value is about 41.1% higher than that of the control beam; it is also about 11.5% lower than the failure load of beam BC1(270-SR). The maximum tensile strain measured on CFRP rods was 0.0041mm/mm and this value represents about 32% of the CFRP ultimate strain (40.6% lower

than the maximum recorded strain of CFRP rods in BC1(270-SR)). Consequently, the slight drop in the yield and ultimate load carrying capacities of beam BC5(270-UR) compared with beam BC1(270-SR) was due to the fact that the CFRP rods in beam BC5(270-UR) caused an additional tensile stress above the steel bars level; and this led to decrease the effective moment arm of the tensile reinforcement (CFRP and steel bars) within the beam cross section.

### 1.3.4 Ductility

Design standards require adequate ductility in order to prevent brittle failure of RC members, and therefore provide warning of impending collapse. In this study, the displacement ductility index ( $\mu$ ) is obtained from the load-deflection response of the beam specimens (Figure 1-4), and it is calculated according to the deflection computation as follows [25]:

$$\mu = \frac{\delta_u}{\delta_y} \quad (1)$$

The mid-span deflection, corresponding to the beam ultimate load  $\delta_u$  and yielding load  $\delta_y$ , and the ductility index ( $\mu$ ) for the strengthened beams and control beam are given in Table 1-4.

In general, all the strengthened beams displayed less displacement ductility index ( $\mu$ ) compared to the non-strengthened beam; this is attributed to the increased tensile reinforcement (tension steel and CFRP bars). In fact, the ductility findings demonstrate effects of the brittle performance of CFRP rods and the SNSM strengthening approach as follows;

- Placing CFRP rods above the level of steel bars or using mortar instead of resin as a filling material proved to reduce the beam ductility. The decrease percent in  $\mu$ -index of beams BC3(270-SM) and BC5(270-UR), with respect to the control beam, were about 45.1% and 33% respectively, whereas the decrease percent of BC1(270-SR) beam was 26.6%.
- The large reduction in ductility values of beams BC2(210-SR) and BC4(210-SM) was due to the insufficient strengthening length (210-cm), which led to non-conventional failure modes (peeling off or early debonding failure) as a result of degradation of the strengthening system. The percentages of decrease in the  $\mu$  index of beams BC2(210-SR) and BC4(210-SM) were found equal to 66.6% and 76.7%, respectively, with respect to the control beam (CB).

However, according to tension control design principle for reinforced concrete members, adequate ductility is achieved if the strain of steel ( $\epsilon_s$ ) at the point of concrete crushing or failure of the fiber reinforced polymer (FRP) is at least equal to 0.005 [26]. Figure 1-9 depicts the load-strain curves of the longitudinal tension steel in the tested beams. It can be noted that, using SNSM-CFRP rods significantly reduces tensile strains of the adjacent steel bars as compared to those in the control beam for the same applied load. The rate of increment was almost identical for all SNSM beams up to the yielding load. Afterwards, strains of the steel bars were rapidly increased but also influenced by the failure mode of the beam. It can also be found that, after the yielding load, inclinations of the load-strain curves of steel bars were lower than those of SNSM-CFRP bars for the same beam (see Figure 1-8); which implies that the SNSM bars controlled the flexural behavior up to the failure load. As can be seen from Figure 1-9; beams



BC1(270-SR) and BC5(270-UR) meet the ductility requirement ( $\epsilon_s > 0.005$ ). The measured tensile strains of the steel bars (Table 1-3) for beams BC1(270-SR) and BC5(270-UR) at the failure load were 0.0082-mm/mm and 0.0104-mm/mm, respectively.

Based on the steel tensile strain results; the displacement ductility index  $\mu = 3$  represents the acceptable lower limit to guarantee ductile performance of the SNSM-CFRP bars strengthened beam. It should be noted that, this result corresponds to the range of  $\mu$ -index, which was proposed by [27], in order to ensure the ductile behavior of RC beams ( $3 \leq \mu \leq 5$ ). The ductile index of beams BC1(270-SR) and BC5(270-UR), obtained from Eq.(1-1), are within this reasonable range.

Table 1-4 : Mid-span deflection and ductility of the tested beams

Beam	$\delta_y^{(1)}$ (mm)	$\delta_u^{(2)}$ (mm)	$\mu^{(3)}$
CB	13.4	59.3	4.43
BC1(270-SR)	15.5	50.4	3.25
BC2(210-SR)	15.5	22.9	1.48
BC3(270-SM)	15.7 (16.5)*	38.2	2.43 (2.31)*
BC4(210-SM)	15.8	16.2	1.03
BC5(270-UR)	13.6	40.4	2.97

(1)  $\delta_y$ : Mid-span deflection of beam at level of yielding load attained from Fig.4.

(2)  $\delta_u$ : Mid-span deflection of beam at level of failure load attained from Fig.4.

(3)  $\mu$  (ductility index) = Ultimate deflection ( $\delta_u$ ) / Yielding deflection ( $\delta_y$ ).

\*According to the adjusted value (Table 1-3)

### 1.3.5 Energy absorption

The energy absorption capacity ( $E_{ab}$ ) of RC beam could be defined as the area enclosed by the load-deflection curve (Table3). It indicates to the energy absorbed per unit cross-sectional area of the specimens calculated at any deflection extreme point [28]. Figure 1-10 demonstrates influences of position and length of CFRP bars as well as the filling material type (resin or mortar) on the energy absorption capacity of the tested beams.

One observation was that, the strengthening length significantly influences the energy absorption capacity of strengthened beams compared to the other variables considered in this study. Compared to the control beam, 270-cm-long CFRP bars improved the energy absorption of the SNSM beam whatever the filling material used or position of the CFRP bars; the  $E_{ab}$  for beams BC1(270-SR), BC3(270-SM) and BC5(270-UR) increased by 69.6%, 9.2% and 20.9%, respectively. On the other hand, the energy absorption capacity of beams BC2(210-SR) and BC4(210-SM) decreased by 41.3% and 64%, respectively compared to the control beam. This considerable reduction in the  $E_{ab}$  of SNSM beams strengthened with 210-cm-long CFRP bars is principally due to their premature failure mode.

### 1.4 SNSM and NSM techniques: comparison and discussion.

Almahmoud et al. [6] carried out laboratory tests for the purpose of investigating the global behavior of reinforced concrete beams strengthened with CFRP rods using the Near Surface Mounted (NSM) technique. Their experimental work was performed on simply supported RC beams subjected to flexural loading and strengthened with CFRP rods. The study focused on

changes, such as failure modes and enhancement of ultimate strengths, in the structural performance of RC beams. However, in the present work, the mechanical characteristics of the tested specimens and CFRP bars (length, section,..etc.) were cautiously selected, and the experimental setup was carefully designed in compliance with those used in the above mentioned study. This was done for the purpose of comparing the two strengthening techniques, NSM and SNSM. For this reason, the experimental results of the three NSM-CFRP beams, i.e. S-C 6 (270-R), S-C 6 (270-M) and S-C 6 (210-R), were utilized. More details about these beams can be found in [6].

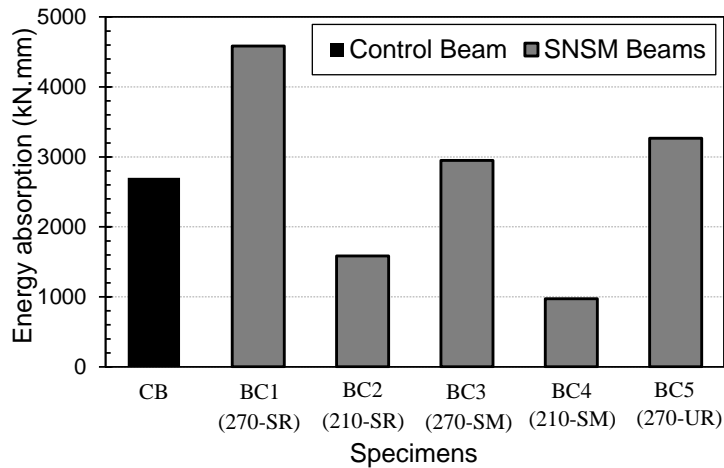


Figure 1-10 : Energy absorption of beam specimens

Table 1-5 compares the experimental results obtained with the SNSM technique with those obtained with the NSM technique in terms of the failure mode, cracking, yielding and ultimate moments as well as the ductility index ( $\mu$ ). Figure 1-11 depicts the bending moment-deflection ( $M - \delta$ ) curves of the tested SNSM beams as well as those of the NSM beams. The corresponding bending moment  $M$  of the beam is calculated by Eq. (1-2).

$$M = \frac{P}{2} \times a \quad (2)$$

Where  $P$  is total applied load at each increment of displacement obtained from the experimental tests and  $a$  is the distance between the applied point load and support,  $a = 800 \text{ mm}$ .

In general, the flexural response of RC beam specimens strengthened with CFRP rods using the SNSM technique corresponded well to the flexural response of beams strengthened with CFRP rods using the NSM technique. This is also true regarding the ultimate strength capacity, specially with regard to beams BC2(210-SR) and BC3(270-SM).

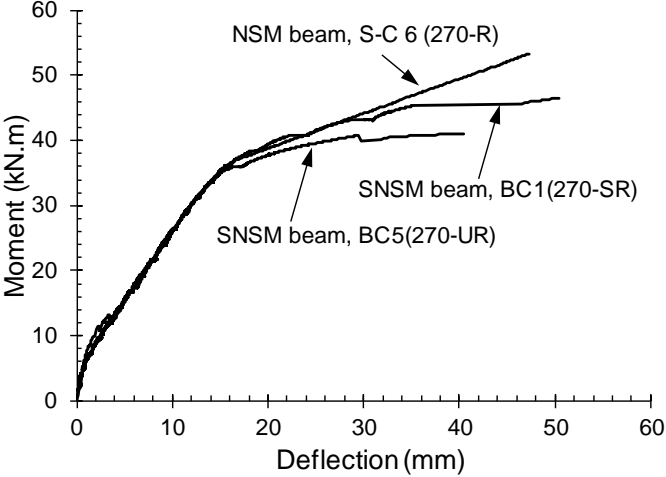
Based on Figure 1-11a, Beams BC1(270-SR) and BC5(270-UR) exhibited flexural performance similar to that of beam S-C6(270-R) in the elastic and cracking phases; however, while different slopes of the moment deflection curves were observed after tensile steel yielding.

This difference between slopes was attributed to the position of the CFRP rods, i.e. the SNSM-CFRP rods were closer to the neutral axis as a result of the implementation of the SNSM technique, and consequently, this led to reduce their carried tensile forces which means reduction in the increasing rate of the SNSM beam resisting moment. The maximum variation in the  $(M - \delta)$  curves was recorded at the failure moment. Failure of beam S-C6(270-R) occurred at 53.3 kN.m; and this value is about 6.9 kN.m (14.9%) greater than that of beam BC1(270-SR), and about 12.2 kN.m (29.7%) greater than that of beam BC5(270-UR). Although the failure moments in beams BC1(270-SR) and BC5(270-UR) are smaller than the failure moment in beam S-C6(270-R) due to the position of the additional strengthening bars; the SNSM technique used in this case helped to prevent slippage of the CFRP rods out of the strengthening system. Applying the SNSM technique caused to change the failure mode from CFRP rods pull out in S-C6(270-R) to compressed concrete crushing in BC1(270-SR) and BC5(270-UR). Figure 1-12 compares the failure mechanism of beams BC1(270-SR) and BC5(270-UR) with that of beam S-C6(270-R).

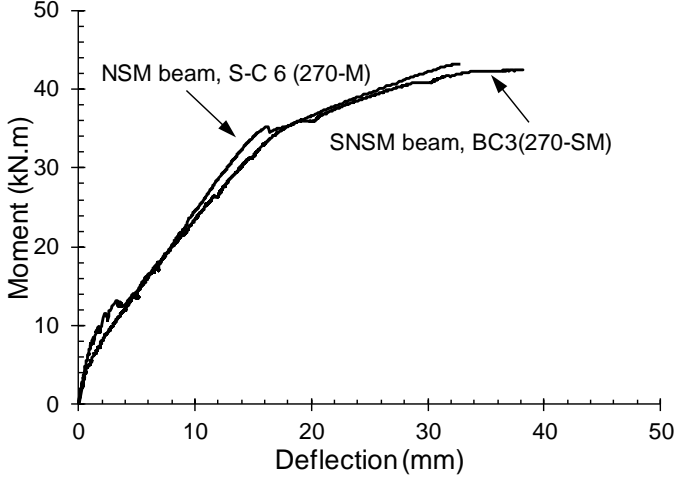
Figure 1-11b indicates that the  $(M - \delta)$  curves corresponding to beams BC3(270-SM) and S-C6(270-M) are almost identical. The ultimate bending moment capacity of beam BC3(270-SM) was 1.5 kN.m (3.4%) less than that of beam S-C6(270-M). This great convergence between the both strength capacities, despite different locations of CFRP bars, might suggest that to the proposed SNSM technique has the capacity to put off the debonding failure occurrence. Indeed, the S-C6(270-M) beam was mainly failed due to debonding failure at the mortar-concrete interface before concrete crushing, whereas debonding failure was occurred simultaneous with the compressed concrete crushing in the BC3(270-SM) beam. Figure 1-13 illustrates the debonding failure mechanism in the both beams (BC3(270-SM) and S-C6(270-M)).

Fig. 1-11c indicates that the ultimate capacity of beam S-C6(210-R) was 1.4kN.m (3.3%) higher than the ultimate capacity of beam BC2(210-SR). The S-C6(210-R) and BC2(210-SR) beams were both failed due to concrete peeling off at the end of the CFRP rods. This result confirms that, the peeling off failure is attributed more to the strengthening length than to the strengthening technique used (NSM or SMSM). The strengthening length (SL) to the beam length (BL) ratio of this set of beams ( $\frac{SL}{BL} = 0.56$ ) is consistent with the expected peeling off failure ratio suggested in [10]. However, Figure 1-14 illustrates the peeling off failure mechanism of beams S-C6(210-R) and BC2(210-SR).

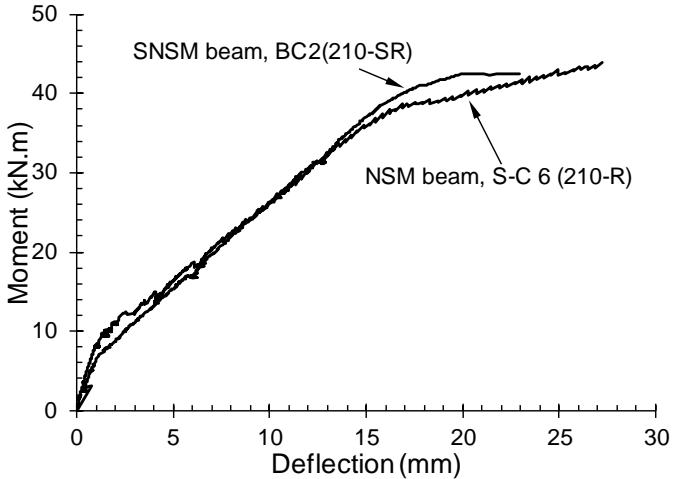
Regarding the displacement ductility, it is worth noting that beams strengthened with CFRP rods using the SNSM technique proved to be more ductile as compared to the NSM beams, except for BC2(210-SR) for which the ductility index remained the same as that of beam S-C6(210-R). The overall improvement in ductility of SNSM beams is most likely referred to the failure mode and the interaction between the additional reinforcement location and the tension steel deformation. Figure 1-15 gives a comparison between the ductility indices ( $\mu$ ) of SNSM and NSM beams.



(a) S-C6(270-R) vs. (BC1(270-SR) & BC5(270-UR))



(b) S-C6(270-M) vs. BC3(270-SM)



(c) S-C6(210-R) vs. BC2(210-SR)

Figure 1-11 : Comparisons between NSM and SNSM beams tested in chapter 1 based on the load deflection curves

Table 1-5 : Comparison between experimental results of the SNSM and NSM techniques

SNSM technique						NSM technique [6]					
Beam	Failure mode	M <sub>cr</sub> <sup>(1)</sup> (kN.m)	M <sub>y</sub> <sup>(2)</sup> (kN.m)	M <sub>u</sub> <sup>(3)</sup> (kN.m)	μ <sup>(4)</sup>	Beam	Failure mode	M <sub>cr</sub> (kN.m)	M <sub>y</sub> (kN.m)	M <sub>u</sub> (kN.m)	μ
BC1(270-SR)	Crushing of the compressed concrete nearby the load application.	7.3	36	46.4	3.3	S-C 6 (270-R)	CFRP rod pull-out	7.4	36.8	53.3	2.9
BC2(210-SR)	Concrete peeling-off at the end of CFRP rod.	6.9	37.8	42.6	1.5	S-C 6 (210-R)	Concrete peeling-off at the end of CFRP rods	8.1	38.2	44.0	1.5
BC3(270-SM)	Debonding at the mortar–concrete interface together with compressed concrete crushing.	7.2	32.7 (35.2)*	42.4	2.4 (2.3)*	S-C 6 (270-M)	Debonding at the mortar–concrete interface	8.1	35.3	43.9	1.9
BC4(210-SM)	Debonding at the mortar–concrete interface followed by compressed concrete crushing.	7.5	36.9	37.7	1	-----	-----	-----	-----	-----	----
BC5(270-UR)	Crushing of the compressed concrete near to the load application.	7.1	33.3	41.1	3	S-C 6 (270-R)	CFRP rod pull-out	7.4	36.8	53.3	2.9

(1) M<sub>cr</sub> (cracking moment) =  $\frac{P_{cr}}{2} * a$ , where P<sub>cr</sub> is the cracking load of the beam obtained from experimental test (Table 3) and a = 800mm.

(2) M<sub>y</sub> (yielding moment) =  $\frac{P_y}{2} * a$ ; where P<sub>y</sub> is the yielding load of the beam obtained from experimental test (Table 3) and a = 800mm.

(3) M<sub>u</sub> (ultimate moment) =  $\frac{P_u}{2} * a$ ; where P<sub>u</sub> is the ultimate load of the beam obtained from experimental test (Table 3) and a = 800mm.

(4) μ (ductility index): (Table 4)

\*According to the adjusted value (Table 1-3)

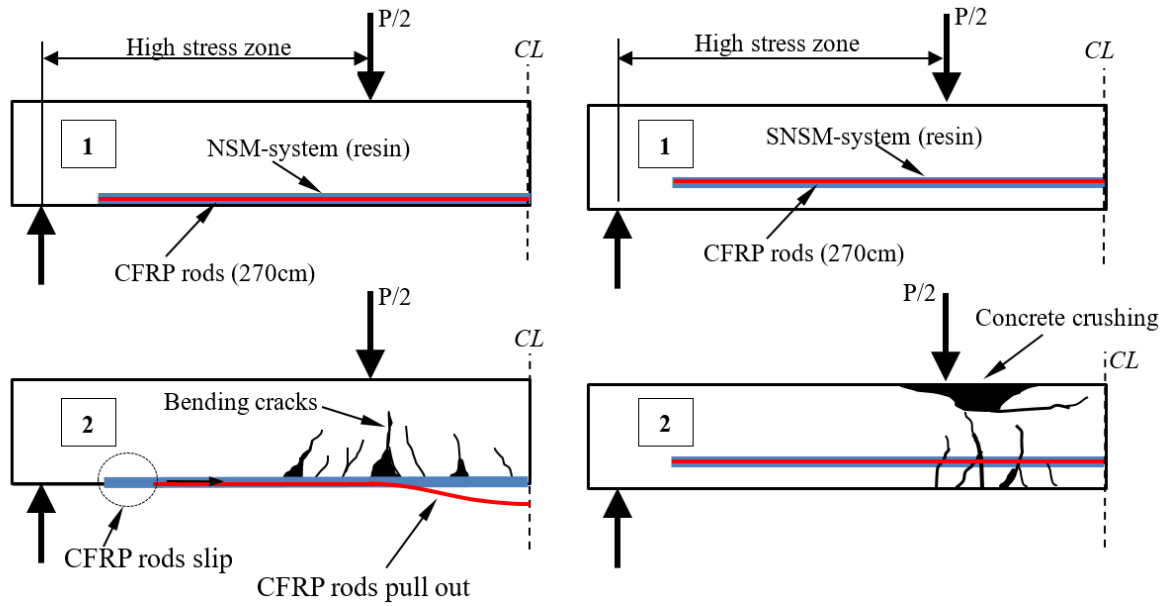


Figure 1-12 : Failure mechanism of a) S-C6(270-R) beam and b) BC1(270-SR) and BC5(270-UR) beams.

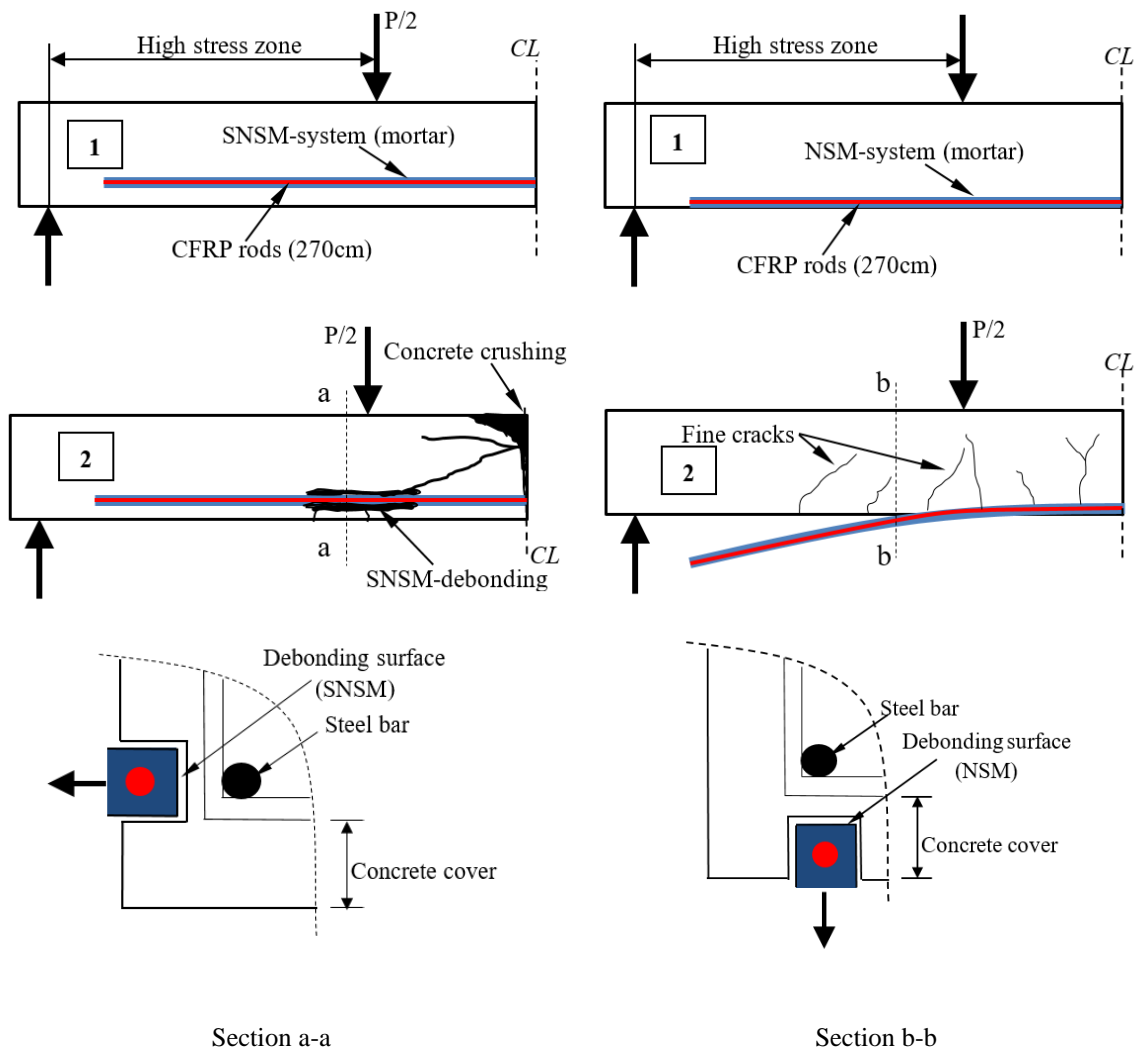


Figure 1-13 : Debonding failure mechanism of a) BC3(270-SM) beam and b) S-C6(270-M) beam

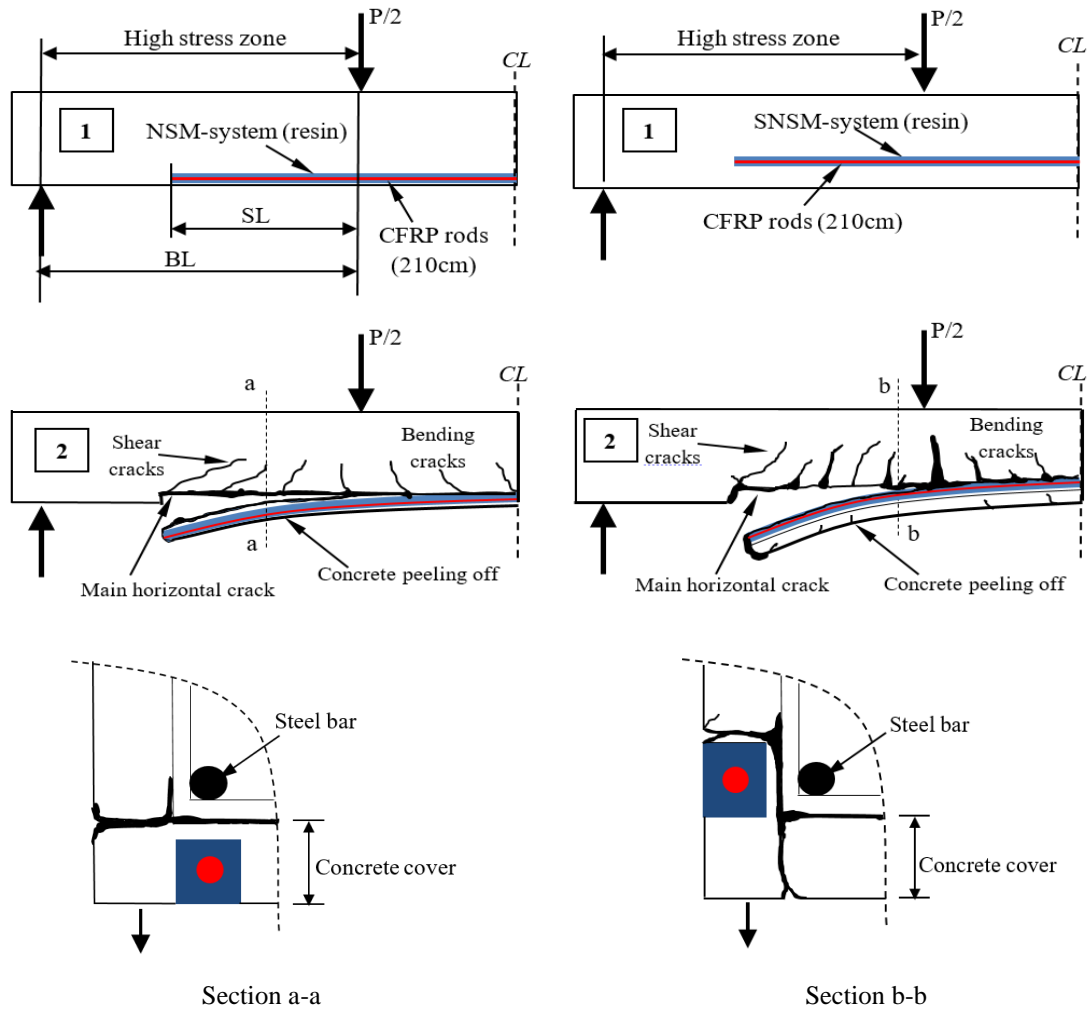


Figure 1-14 : Peeling off failure mechanism of: a) BC2(210-SR) beam and b) S-C6(210-R) beam

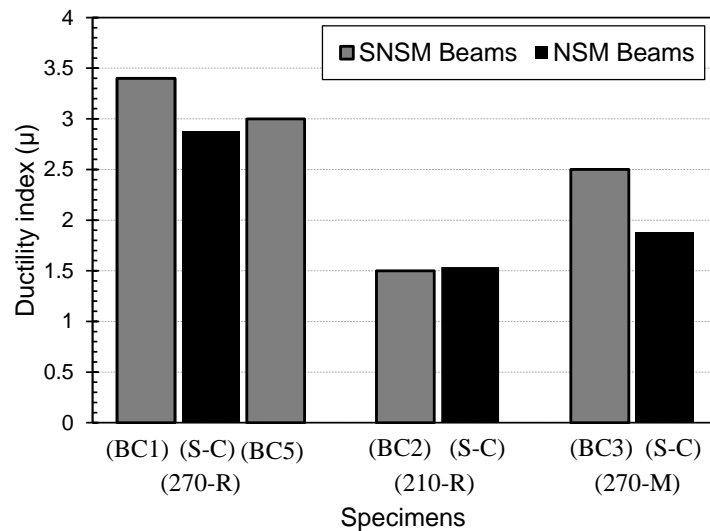


Figure 1-15 : Ductility comparison between the SNSM and NSM specimens

## 1.5 Analytical model- Application of conventional prediction techniques

### 1.5.1 Prediction of deflection response ( $(\delta)_{mid}$ )

The American Concrete Institute ACI 318-08 [26] recommendations were employed in calculating the short-term deflection of reinforced concrete beams strengthened with CFRP rods using the SNSM technique under service loads. The mid-span deflections of beams could be computed as a function of the bending moment ( $M = (P/2) \times a$ ) as expressed in Eq. (1-3). Hence, the center deflections corresponding to the cracking, yielding and ultimate moment of beams were obtained in this study according to the sequence presented in Figure 1-16.

$$(\delta)_{mid} = \frac{M}{24 E_c I_{eff}} (3L^2 - 4a^2) \quad (1-3)$$

Where,  $E_c$  is the elastic modulus of concrete ( $E_c = 4700\sqrt{f'_c}$ ) and  $I_{eff}$  is the effective moment of inertia of the entire beam. The effective moment of inertia suggested by Branson was adopted and can be determined as follows [26, 29]:

$$I_{eff} = \left(\frac{M_{cr}}{M_a}\right)^3 I_g + \left[1 - \left(\frac{M_{cr}}{M_a}\right)^3\right] I_{cr} \leq I_g \quad (1-4)$$

Where,  $M_a$  is the maximum moment calculated at the point of deflection of the beam,  $I_g$  is the gross moment of inertia,  $I_{cr}$  is the cracked moment of inertia and  $M_{cr}$  is the cracking moment.

The moment of inertia,  $I_{cr}$  of the cracked section is computed by assuming that the material has a linear elastic behavior, while neglecting the concrete below the neutral axis, as depicted in Figure 1-17. Therefore, the position of the neutral axis ( $x$ ) and the moment of inertia of the cracked section were computed using Eq. (1-5) and Eq. (1-6), respectively.

$$x = \frac{-[nA_s + n_f A_f] \mp \sqrt{[nA_s + n_f A_f]^2 + 4 \frac{b}{2} [n_f A_f d_f + nA_s d_s]}}{b} \quad (1-5)$$

$$I_{cr} = \frac{bx^3}{3} + nA_s(d_s - x)^2 + n_f A_f(d_f - x)^2 \quad (1-6)$$

Where,  $n = \frac{E_s}{E_c}$ ,  $n_f = \frac{E_f}{E_c}$ ,  $b$  is the width of the cross section,  $A_s$  is the area of tension steel,  $A_f$  is the area of SNSM CFRP bars,  $d_s$  is the effective depth of steel bars and  $d_f$  is the effective depth of the CFRP rods.

In fact, applying Eqs. (1-5) and (1-6), for deflection calculations (Eq. (1-3)), when  $M_a \gg M_{cr}$  (i.e.  $I_{eff}$  equals to  $I_{cr}$ ) was found to underestimate the deflection in the SNSM-CFRP beams. For this reason, the moment of inertia,  $I_{cr}$  was computed again while neglecting the elastic modulus of the steel reinforcement in the stage of  $\delta(M_u - M_y)$  only, Figure 1-16. This slight modification could be justified by following:



- The additional resistance of the strengthened beams to the external applied load in the ultimate strength phase (from the steel yielding load to failure load) was basically induced due to the presence of CFRP rods [6]. This can be seen in Figure 1-4 (Section 3.1) where all the strengthened beams showed load increasing rates greater than that of the control beam.
- The SNSM reinforcing bars start controlling the propagation of cracks in the strengthened beams once the tensile stress in the steel reinforcement exceeded the yielding point [21].

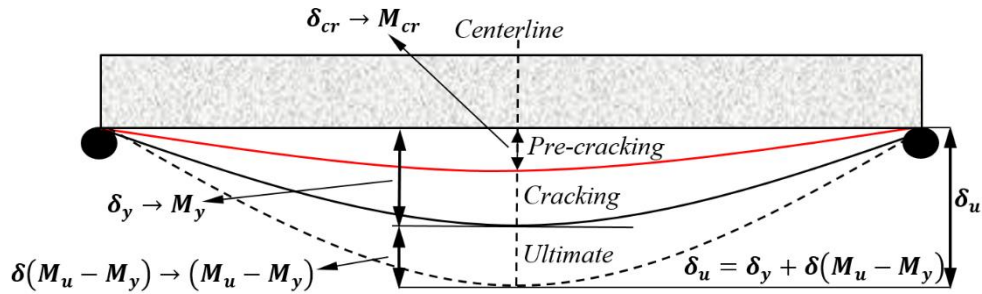


Figure 1-16 : Deflection calculation methodology

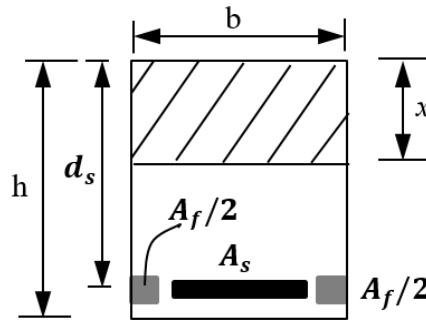


Figure 1-17 : Cracked section

### 1.5.2 Prediction of cracking moment ( $M_{cr}$ )

The predicted cracking moment ( $M_{cr} = f_t I_{tr} / y_b$ ) of the SNSM-CFRP beams was calculated by assuming that concrete fibers in the tension zone had reached their maximum tensile stress ( $\sigma = f_t$ ). Where  $f_t$  is the concrete tensile strength,  $I_{tr}$  is the un-cracked moment of inertia of the transformed section (see appendix A) and  $y_b$  is the distance between the most tensile concrete fiber and the neutral axis before cracking.

### 1.5.3 Prediction of yielding moment ( $M_y$ )

In the same way of cracking moment, the predicted yielding moment ( $M_y = f_y I_{cr} / n_y$ ) was calculated by assuming that the tension steel reinforcement had achieved the elastic behavior ( $\sigma = f_y$ ). Where  $f_y$  is the elastic limit stress of the tensile steel and ( $y = d_s - x$ ) is the distance between the steel bars and the neutral axis.

### 1.5.4 Prediction of ultimate moment ( $M_u$ )

The ultimate moment of SNSM strengthened beam is assessed by the force equilibrium conditions and the stress-strain relation of concrete in compression and steel reinforcement in

tension [15], as presented in (appendix B). The assumption includes: (1) Conventional flexural failure of strengthened beam; i.e. crushing of the compressed concrete after yielding of the tension steel reinforcement. (2) Perfect bond between the internal surface of concrete and the filling material (resin or mortar). (3) The tensile strength of concrete is totally neglected. (4) The stress-strain relation of the concrete and steel suggested by ACI-318-08 is adopted.

### 1.5.5 Performance of the analytical model.

Fig. 1-18 compares the calculated deflections of the tested RC beams at the cracking, yielding and ultimate levels with the experimental results. Overall, the analytical model gave quite a good estimation of the experiment deflections in beams strengthened with SNSM-CFRP bars. The ratio of the computed ultimate deflection to the experimental deflection ( $(\delta)_u(\text{calculated})/(\delta)_u(\text{experimental})$ ) are approximately 0.87, 0.88, 1.15, 1.24 and 1.06 for beams BC1(270-SR), BC2(210-SR), BC3(270-SM), BC4(210-SM) and BC5(270-UR), respectively.

Moreover, Fig. 1-19 shows a comparison between the experimental and the predicted bending moment-deflection relationships for the SNSM-CFRP beams. The bending moments obtained from the above analytical model and the experimental values were found to be in good agreement. The ratio of the  $M_u(\text{calculated})$  to the  $M_u(\text{experimental})$  are 1.03, 1.12, 1.13, 1.27 and 1.07 for beams BC1(270-SR), BC2(210-SR), BC3(270-SM), BC4(210-SM) and BC5(270-UR), respectively.

The significant overestimated ultimate values in beam BC4(210-SM) (1.24 for deflection and 1.27 for moment) were primarily due to the early debonding failure which is not considered in the current analytical model. Further analytical studies to include such failures are strongly recommended.

## 1.6 Conclusion:

The present study aimed to analyze the global flexural response of RC beams strengthened with CFRP rods using the SNSM technique. The experimental results obtained and the studies conducted allowed drawing the following conclusions:

- The Side Near Surface Mounted (SNSM) technique helped to improve the global flexural performance of RC beams whatever the strengthening scenario used. The load-bearing capacity of the beams BC1(270-SR), BC2(210-SR), BC3(270-SM), BC4(210-SM) and BC5(270-UR) were greater than that of the control beam by 59.3%, 46.2%, 45.6%, 29.3% and 41.1%, respectively.
- CFRP rods placed laterally adjacent to the steel bars and embedded in resin formed better resisting action to the flexural bending than those embedded in mortar or placed upper than the main tension steel. In BC1(270-SR) beam, the flexural strength increased over 59% compared to the control beam without large loss in ductility.
- The length of CFRP rods was found to have a considerable influence on the failure mode and energy absorption capacity. Two strengthened beams, i.e. BC2(210-SR) and BC4(210-SM), out of five beams showed premature failure due to the insufficient strengthening length (210 cm). The ratio of the strengthening length  $SL$  to the beam length  $BL$  of the both

beams was about 0.56. However, using mortar caused the failure mode to change from peeling-off failure in BC2(210-SR) to early debonding failure in BC4(210-SM).

- The strengthening position did not display significant impact on the failure mode. Beams BC1(270-SR) and BC5(270-UR) were both failed due to concrete crushing. However, the failure mode of beam BC3(270-SM) was debonding failure at the interface concrete–mortar because of the mortar filling material.
- According to the experimental data provided by this investigation; the Side Near Surface Mounted (SNSM) strengthening system can be used as an alternative to the Near Surface Mounted (NSM) system; it can in some cases help to avoid the non-conventional failure modes (pull-out of CFRP rods or early debonding failure). Furthermore, the SNSM-CFRP beams showed higher ductility behavior as compared to the NSM-CFRP beams.
- The computed flexural strength capacity and mid-span deflection of the strengthened beams, using the conventional prediction models, showed excellent agreement with the experimental results.

### 1.7 Appendix (A): Calculation of the transformed moment of inertia.

The moment of inertia of the transformed section of the beam strengthened with SNSM-CFRP rods was calculated based on Eq. (A.1).

$$I_{tr} = \frac{by_{nc}^3}{3} + \frac{b(h - y_{nc})^3}{3} + (n - 1)A_s(d_s - y_{nc})^2 + (n_f - 1)A_f(d_f - y_{nc})^2 \quad (A.1-1)$$

Where  $y_{nc}$  is the neutral axis depth of the transformed section; it was calculated by equating the sum of areas above and below the neutral axis as given in Eq. (A.2):

$$y_{nc} = \frac{\frac{bh^2}{2} + nA_s d_s - A_s d_s + n_f A_f d_f - A_f d_f}{bh + nA_s - A_s + n_f A_f - A_f} \quad (A.1-2)$$

### 1.8 Appendix (B): Calculation of the failure moment.

The ultimate resisting moment ( $M_u$ ) of the SNSM-CFRP bars strengthened beam was assessed by applying the equilibrium conditions ( $C = F_s + F_f$ ) and the stress-strain correlation requirements, as presented in Figure B 1-1, where  $C$ ,  $F_s$  and  $F_f$  are the compressive force, tensile steel force and tensile CFRP force, respectively.

The neutral axis location in a beam section where failure occurs can be computed as given below:

$$k_1 c^2 + k_2 c + k_3 = 0 \quad (B.1-1)$$

$$k_1 = 0.85 f'_c b \beta \quad (B.1-2)$$

$$k_2 = -(A_s f_y - \varepsilon_{cu} A_f E_f) \quad (B.1-3)$$

$$k_3 = -(A_f E_f \varepsilon_{cu} d_f) \quad (\text{B.1-4})$$

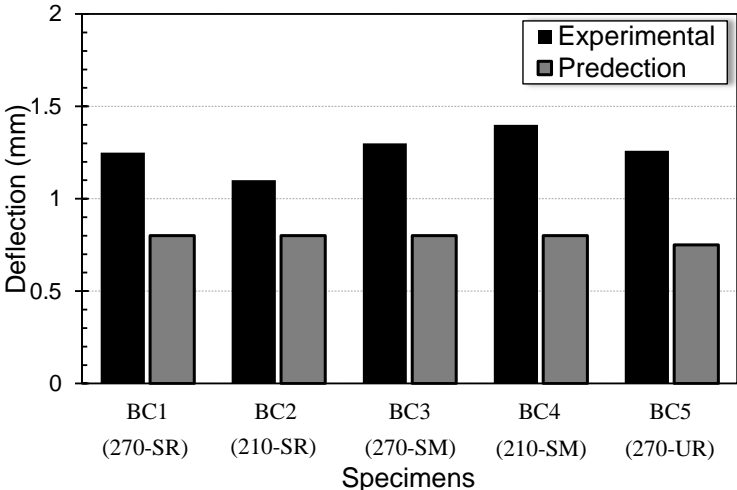
$$c = \frac{-k_2 \mp \sqrt{k_2^2 - 4k_1 k_3}}{2k_1} \quad (\text{B.1-5})$$

The ultimate compressive strain  $\varepsilon_{cu}$  in concrete was assumed equal to 0.003, based on the compressive test results; this value is similar to the one suggested by the ACI 318-08 Building Code. However, the maximum strain of CFRP rods, corresponding to the failure load, was evaluated using similar triangles as follows:

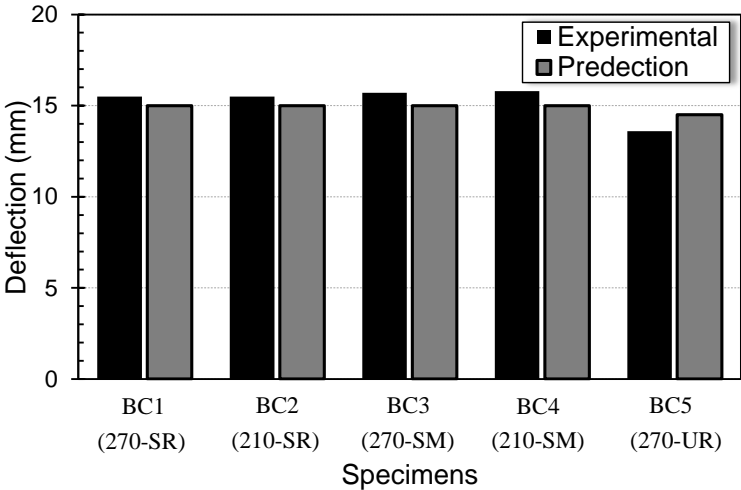
$$\varepsilon_f = \frac{\varepsilon_{cu}}{c} d_f - \varepsilon_{cu} \quad (\text{B.1-6})$$

Therefore, the ultimate moment of the SNSM-CFRP section can be expressed using the following formula:

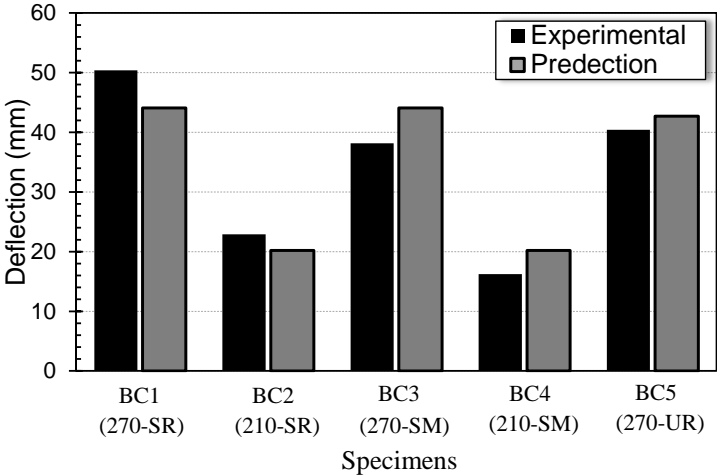
$$M_u = A_s f_y \left( d_s - \frac{\beta c}{2} \right) + \varepsilon_f A_f E_f \left( d_f - \frac{\beta c}{2} \right) \quad (\text{B.1-7})$$



(a) Cracking deflection

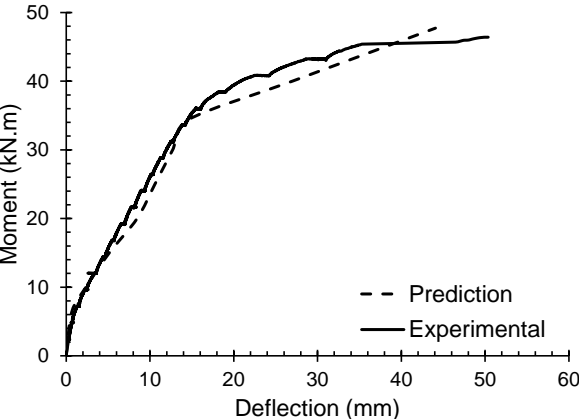


(b) Yielding deflection

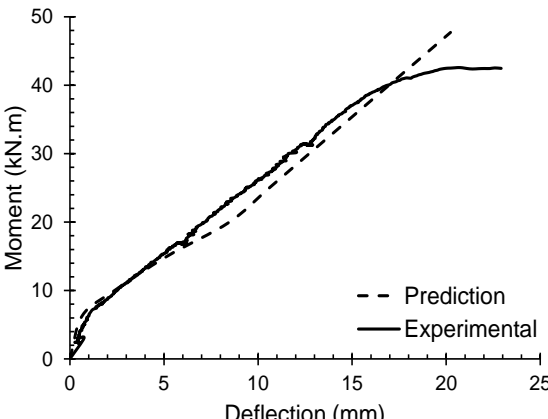


(c) Ultimate deflection

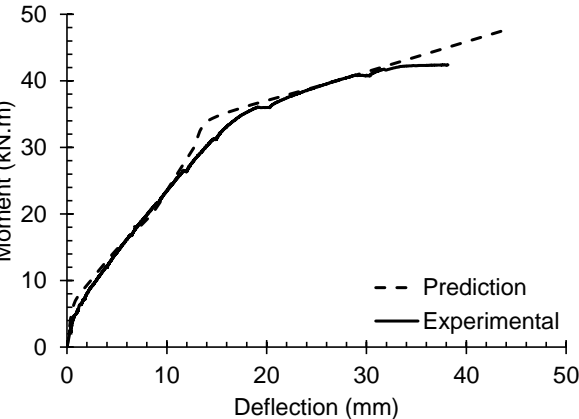
Figure 1-18 : Compression between the experimental and computed deflection.



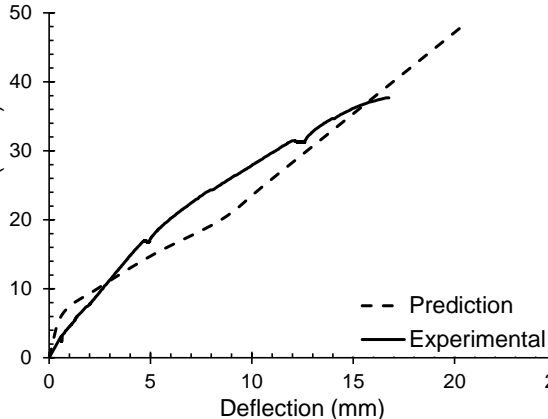
(a) Beam BC1 (270-SR)



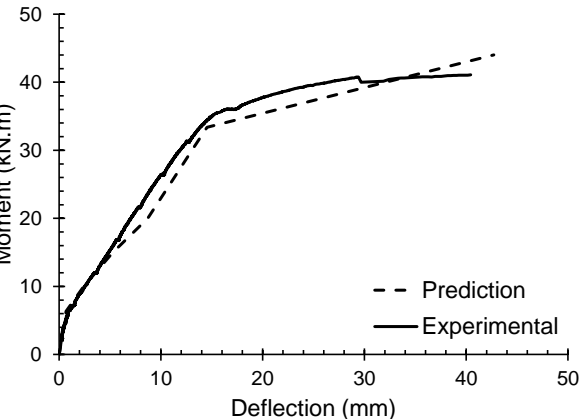
(b) Beam BC2 (210-SR)



(c) Beam BC3 (270-SM)



(d) Beam BC4 (210-SM)



(e) Beam BC5 (270-UR)

Figure 1-19 : Comparison between experimental and theoretical moment-deflection curves

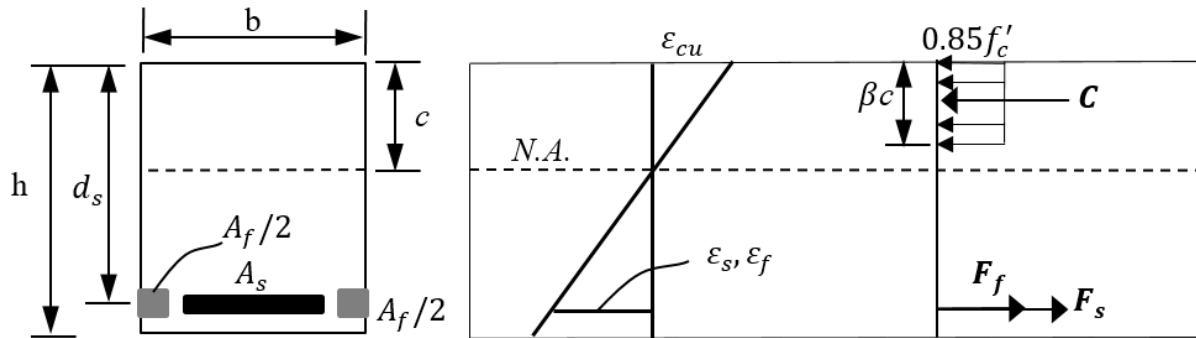


Figure B 1-1 : Strain, stress and forces of the cross section

## 1.9 References

1. Lam L, Teng JG. Strength models for fiber-reinforced plastic-confined concrete. *J Struct Eng* 2002;128(5).
2. Li LJ, Guo YC, Liu F, Bungey JH. An experimental and numerical study of the effects of thickness and length of CFRP on performance of repaired reinforced concrete beams. *Constr Build Mater* 2006;20(10):901–9.
3. Onal Mustafa M. Strengthening reinforced concrete beams with CFRP and GFRP. *Adv Mater Sci Eng* 2014:1–8.
4. Nayak AN, Kumaria A, Swain RB. Strengthening of RC beams using externally bonded fibre reinforced polymer composites. *Structures* 2018;14:137–52.
5. Zhang SS, Yu T, Chen GM. Reinforced concrete beams strengthened in flexure with near-surface mounted (NSM) CFRP strips: current status and research needs. *Compos B* 2017;131:30–42.
6. Al-Mahmoud F, Castel A, François R, Tourneur C. Strengthening of RC members with near-surface mounted CFRP rods. *Compos Struct* 2009;91:138–47.
7. Hassan T, Rizkalla S. Investigation of bond in concrete structures strengthened with near surface mounted carbon fiber reinforced polymer strips. *J Compos Constr* 2003;7(3):248–57.
8. Barros JA, Ferreira DR, Fortes AS, Dias SJ. Assessing the effectiveness of embedding CFRP laminates in the near surface for structural strengthening. *Constr Build Mater* 2006;20(7):478–91.
9. De Lorenzis L, Teng JG. Near-surface mounted FRP reinforcement: an emerging technique for strengthening structures. *Compos Part B-Eng* 2007;38(2):119–43.
10. Al-Mahmoud F, Castel A, François R. Failure modes and failure mechanisms of RC members strengthened by NSM CFRP composites – analysis of pull-out failure mode. *Compos B* 2012;43:1893–901.
11. Kreit A, Al-Mahmoud F, Castel A, François R. Repairing corroded RC beam with near surface mounted CFRP rods. *Mater Struct* 2011;44(7):1205–17.

12. Sharaky IA, Torres L, Comas J, Barris C. Flexural response of reinforced concrete (RC) beams strengthened with near surface mounted (NSM) fibre reinforced polymer (FRP) bars. *Compos Struct* 2014;109:8–22.
13. Khalifa AM. Flexural performance of RC beams strengthened with near surface mounted CFRP strips. *Alexandria Eng J* 2016;55:1497–505.
14. Sebastian WM, Vincent J, Starkey S. Experimental characterisation of load responses to failure of a RC frame and a NSM CFRP RC frame. *Constr Build Mater* 2013;49:962–73.
15. ACI. Guide for the design and construction of externally bonded FRP systems for strengthening concrete structures. Farmington Hills: American Concrete Institute, ACI 440.2R-08; 2008.
16. De Lorenzis L, Nanni A. Characterization of FRP rods as near surface mounted reinforcement. *J Compos Constr, ASCE* 2001;5(2):114–21.
17. Almassri B, Kreit A, Al Mahmoud F, François R. Mechanical behaviour of corroded RC beams strengthened by NSM CFRP rods. *Compos B* 2014;64:97–107.
18. De Lorenzis L, Micelli F, La Tegola A. Passive and active near surface mounted FRP rods for flexural strengthening of RC beams. *Proceeding of ICCI 02, San Francisco, 10-12 June 2002*.
19. De Lorenzis L, Nanni A. Bond between near-surface mounted fiber-reinforced polymer rods and concrete in structural strengthening. *ACI Struct J* 2002;99(2):123–32.
20. De Lorenzis L, Nanni A, La Tegola A. Flexural and shear strengthening of reinforced concrete structures with near surface mounted FRP rods. *Proceeding of the 4<sup>th</sup> international Conference on Advanced Composites Materials in Bridges and Structures. (ACMBS) Ottawa. 2000. p. 521–8*.
21. Akter Hosen Md, Jumaat Mohd Zamin, Saiful Islam ABM. Side Near Surface Mounted (SNSM) technique for flexural enhancement of RC beams. *Mater Des* 2015;83:587–97.
22. Al-Mahmoud F, Castel A, François R, Tourneur C. Effect of surface preconditioning on bond of carbon fiber reinforced polymer rods to concrete. *Cem. Concr. Compos.* 2007;29(9):677–89.
23. Nadim Hassoun M, Al-Manaseer A. *Structural concrete: theory and design*. John Wiley & Sons; 2012.
24. Al-Mahmoud F, Castel A, François R, Tourneur C. Anchorage and tension-stiffening effect between near-surface-mounted CFRP rods and concrete. *Cem Concr Compos* 2011;33:346–52.
25. Mukhopadhyaya P, Swamy RN, Lynsdale C. Optimizing structural response of beams strengthened with GFRP plates. *J Compos Construct, ASCE* 1998;2(2):87–95.
26. ACI. *Building code requirements for reinforced concrete*. American Concrete Institute, ACI 318, Farmington Hills, Michigan; 2008.
27. Maghsoudi AA, Akbarzadeh H. Flexural ductility of HSC members. *Struct Eng Mech* 2006;24(2).
28. Gopalaratnam VS, Gettu R. On the characterization of flexural toughness in fiber reinforced concretes. *Cement Concr Compos* 1995;17(3):239–54.



29. Branson DE. Instantaneous and time-dependent deflections of simple and continuous reinforced concrete beams. HPR Report No. 7, Part 1, Alabama Highway Department, Bureau of Public Roads, Alabama. 1965.



## CHAPTER 2: ASSESSMENT OF THE FLEXURAL BEHAVIOR OF CONTINUOUS RC BEAMS STRENGTHENED WITH NSM-FRP BARS, EXPERIMENTAL AND ANALYTICAL STUDY

*Published in Composite Structures, <https://doi.org/10.1016/j.compstruct.2020.112127>*

---

As discussed in chapter one, extensive research studies have been performed on the use of NSM-FRPs rods to flexural reinforce and retrofit SSBs while no studies were found in the literature on strengthening continuous beams with NSM-FRP bars. Therefore, this chapter aims to present and discuss results from loading to failure five continuous two-span RC beams strengthened with FRP rods by means the NSM technique. The beams were initially strengthened with FRP bars at both their hogging and sagging regions. In general, the experimental parts of this chapter study influence of the type (carbon or glass), ratio and length of the FRP bars as well as the effects of the filling material characteristics (resin or mortar) on the flexural performance of the continuous RC beams. The experimental results of the tested beams were analyzed in terms of the load-deflection response, ductility and energy absorption capacity, failure modes and cracking behavior. Capacity of the strengthened beams to redistribute moment was also examined and discussed. The effectiveness of the FRP bars and their influence on strains of steel and concrete was investigated. The analytical part in this chapter aims to introduce a nonlinear analysis approach that can accurately predict the moment-curvature curves of NSM-FRP bars beams and their load-carrying capacity. The analytical model employs the nonlinearity behaviors of the constitute materials.

**Assessment of the flexural behavior of continuous RC beams strengthened with NSM-FRP bars, experimental and analytical study**

Mohammad Abdallah\*<sup>1</sup>, Firas Al Mahmoud <sup>1</sup>, Abdelouahab Khelil <sup>1</sup>, Julien Mercier <sup>2</sup> and Belal Almassri <sup>3</sup>

<sup>1</sup>*Institut Jean Lamour, UMR 7198, CNRS, Université de Lorraine, Nancy, France*

<sup>2</sup>*Freyssinet, Paris, France*

<sup>3</sup>*Civil Engineering Department, Palestine Polytechnic University, Hebron, Palestine*

---

**Keywords:** Continuous RC beam, Strengthening, NSM-FRP rods, Flexural.

**Abstract**

This paper deals with strengthening statically indeterminate reinforced concrete (RC) beams with carbon and glass Fiber Reinforced Polymers (FRP) rods by using the Near Surface Mounted (NSM) technique. The test program consisted of six two-span beams; one control beam, which had exploited for comparison purposes, and five others initially strengthened in flexure with NSM-FRP rods in both hogging and sagging regions. The main test parameters were type, ratio and length of the FRP bars as well as characteristics of the filling material. The study presents and discusses their impacts on the global flexural behavior of continuous RC beam that mainly includes investigating the overall capacity, failure mode, moment redistribution and ductility state.

All NSM-FRP strengthened beams displayed higher overall capacity than the control beam; the test results showed that implementing the NSM technique in an appropriate way could significantly improve the yielding capacity and load-carrying capacity of RC beams without large decrease in the ductility index or the moment redistribution degree despite the non-conventional failure mode. The beam failure was primary affected by the strengthening length; terminating the FRP bars before the zero moment point caused to change the failure mode from pull out of the FRP bars to premature peeling off of the concrete cover. On the other hand, moment redistribution and ductility of the NSM-FRP beams were negatively affected by: (I) Increasing the FRP reinforcement, (II) Decreasing the FRP length or (III) Using mortar as a filling material instead of epoxy-resin. Adopting a nonlinear analysis of the cross-sections could accurately quantify the moment–curvature and the ultimate load of the NSM-FRP continuous beams.

**2.1 Introduction**

Statically indeterminate reinforced concrete (RC) members such as continuous beams are the most widely used structural form. RC continuous beams are preferred for uniform girder bridges and buildings located in sever environments or in areas exposed to high seismic hazards; they have the potential to enhance the structural integrity and rigidity; furthermore, they can offer redistribution of moments due to the structural redundancy, which permits exploiting the available reserve strength. The convenient analysis of indeterminate members is based on the elastic theory; the ACI-318 code [1] allows designers to reduce the factored moments at critical sections in any span of conventional continuous flexural members for any assumed loading

arrangement by up to a maximum of 20%. However, because of the mechanical deterioration of reinforced concrete, continuous beams as the other structural members may require repairing or strengthening either for increasing their service life or enhancing their loading and deformation capacities. Over the past three decades, externally bonding Fiber Reinforced Polymers (EB-FRP) was the most common technique for the flexural strengthening of RC beams; the FRP laminates or plates are externally bonded to the tension sides of the beam with an epoxy-resin adhesive material. The literature review reveals that there are many studies were conducted using the experimental approach on strengthening simply supported beams with EB-FRP technique [2–5], while a very few research has studied behavior of EB-FRP continuous beams [6–8]. In general, the essential weakness reported for using this technique is the premature failure of beam due to separation or/and tensile rupture of the FRP laminates, this can significantly restrict the capacity enhancement of the beam and subsequently drive to significant reduction in its ductility state. In order to avoid the prematurity failure of continuous beams with EB-FRP, the ACI 440.2R guideline [9] recommends that the external strengthening should be terminated at  $d/2$  or at least at 150-mm minimum beyond the inflection point (I.P.), where  $d$  is the beam's effective depth.

Ashour et al. [6] carried out a series of experimental tests to study performance of continuous RC beams strengthened in flexure with EBlaminate; they investigated influences of length, thickness, position as well as form of the CFRP. The study revealed that increasing the CFRP length could raise the beam load-carrying capacity by up to twice that of the un-strengthened beam unless tensile rupture failure of the bonded laminate occurs. In addition, strengthening both the sagging (positive moment) and hogging (negative moment) regions was found to be the most effective arrangement of the EB-CFRP for enhancing the beam's load-carrying capacity. On the other hand, increasing thickness of the CFRP was found to reduce ductility of the beam. Tensile rupture of the CFRP sheets, CFRP sheet separation and brittle peeling failure of concrete cover were the failure modes observed, however, increasing the length of CFRP sheets to cover the entire tension regions was found not effective to prevent the peeling off failure.

Aiello et al. [7] studied the moment redistribution of continuous RC beams strengthened with EB-CFRP laminate. They suggested to strengthen solely the beam's soffits in order to achieve a sufficient degree of moment redistribution similar to that in un-strengthened beam. However, strengthening both the positive and negative moment zones was found again the most effective arrangement of EB-CFRP to improve the beam's load-carrying capacity. The tested beams were failed due to detaching of the CFRP together with concrete crushing.

More recent, Akbarzadeh et al. [8] investigated the flexural behavior and moment redistribution of reinforced high strength concrete (RHSC) two-span beams externally bonded with CFRP sheets. The test results indicated that the ultimate strength of the RHSC beam increased with the number of the CFRP layers, the ultimate load capacity increased up to 60% with three layers, whereas the moment redistribution decreased from 16.1% to 1.5% in the un-strengthened and strengthened beam, respectively. They also found out that increasing the number of CFRP layers affected the beam's ductility adversely and caused failure mode to change from tensile rupture to debonding failure.

Recently, a new strengthening technology called Near Surface Mounted (NSM) has attracted much researchers and practical applications for strengthening and repairing RC beams with Fiber Reinforced Polymer (FRP) composites. The NSM-FRP is a cost-effective and short period technique. Applying this technology might be utilized by embedding the strengthening strips or rods with suitable paste into precut grooves in the concrete cover of the deficient item which might experience high damage or cracks [10]. The NSM-FRP offers several advantages over the aforementioned conventional EB-FRP, owing to the fact that the additional reinforcement is located inside the strengthened members which provides an advanced level of strengthening that is less prone to premature failure, high bonding efficiency as well as better protection for the FRP against external agents [11]. Furthermore, the RC members strengthened with NSM-FRP reinforcement exhibited better ductility, durability and fatigue performance [12, 13].

The experimental studies investigating the NSM-FRP bars technique have underlined its potential for improving the flexural performance of simply supported RC beams [eg. 14–19]. As reported in [16], the failure mode of NSM beam can vary from degradation of the NSM system to compressive concrete crushing and depends on the ratio of a combination of FRP cross-section and length to the concrete compressive strength. The degradation of the NSM system could lead to non-conventional failure modes such as pull out of the FRP bars [20–21] or peeling off of the concrete cover [13, 22–23]. Almahmoud et al. [20, 22] recommended that the ratio of the strengthening length to the beam length (SL/BL) should be greater than 0.56 in order to prevent the peeling off failure.

Although the NSM-FRP technique for strengthening RC members is attracting more and more attention nowadays, most of the research efforts on application this technology have focused on simply supported beams where the FRP-composites are applied in sagging moment region; there has been very limited research on the use of FRP-composites in hogging regions, e.g. RC frame [24] and slabs [25]. Consequently, further research studies on the use of NSM-FRP for strengthening continuous RC beams are a pressing need for the purpose of; (1) investigating the possibility of addressing this technique to improve the beam flexural strength, particularly in dealing with the negative bending moment (2) exploring the differences in the strengthening mechanism, especially with regard to the failure of the NSM system, and (3) checking the eventuality of moment redistribution and ductility level in such strengthened structures.

In this paper, CFRP and GFRP bars are employed for strengthening continuous RC beams. Thereby, in what follows, tests to failure of one ordinary RC beam and five NSM-FRP bars beams are studied. The principle aims of this research may be summarized as follows:

- To present findings from loading to failure of five two-span RC beams strengthened with FRP rods by means the NSM technique. These findings including analysis and discussion of enhancement of load-carrying capacity, energy absorption capacity, failure modes, cracking patterns, ductility ratio, moment redistribution and strain analysis.
- To study and discuss important influential factors such as type, ratio and length of the FRP bars as well as the effects of the filling material characteristics (resin or mortar) on the global flexural performance of the strengthened continuous RC beams.

- To predict the moment–curvature curves and the ultimate carrying load of NSM-FRP bars beams by taking advantage of the nonlinear analysis of cross-section.

**2.2 Materials**

**2.2.1 Concrete and filling material**

Six wooden moulds were prepared for casting the RC beams. Each mould had 150-mm width, 250 mm depth and 6000 mm length. Twenty-four hours after casting the concrete, the wooden strips were removed and the beams were sorted for 28 days in a confined room (T = 20 °C, RH = 60%). The mechanical properties of the vibrated ready-mix concrete employed in the formulation of beams were determined by laboratory testing of eight hardened concrete cylinder specimens. The concrete cylinders were made at the time of beams casting and kept with the beam specimens under the same conditions. Each cylinder had 160 mm diameter and 320 mm height. They were tested in compression in order to determine the compressive strength ( $f'_c$ ) and the modulus of elasticity ( $Ec$ ) of concrete, while other cylinders were tested in tensile to determine the concrete tensile strength. The modulus of elasticity of concrete was determined from the compressive stress–strain curves, i.e.  $Ec$  was defined as the slope of the line drawn from zero stress to a compressive stress equal to  $0.45f'_c$  [1]. The stress–strain curve of concrete was obtained by attaching strain gauges onto the concrete cylinders. However, the compressive and tensile strength as well as the modulus of elasticity of concrete at 28 days were 39(SD: 1.43) MPa, 3(SD: 0.16) MPa and 29.2(SD: 0.67) GPa; respectively, where (SD: value) is the standard deviation.

Two types of filling materials were studied: epoxy resin and mortar (see Figure 2-1). Characteristics of these materials after 7 days are reported in Table 2-1.

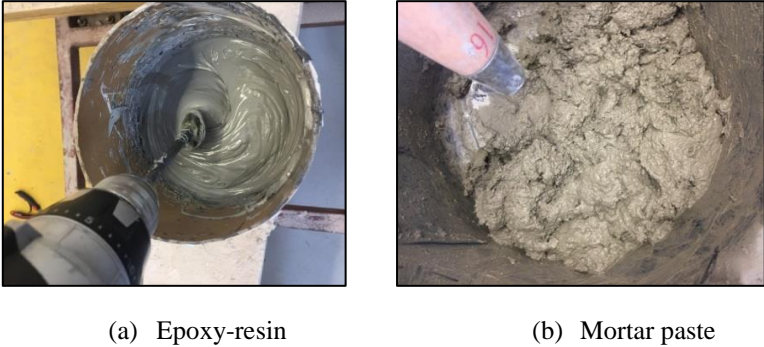


Figure 2-1 : Filling materials for bonding the NSM-FRP bars to concrete

Table 2-1 : Characteristics of the filling material

Material	Compressive strength (MPa)	Tensile strength (MPa)	Elastic modulus (GPa)
Epoxy resin [22]	83	29.5	4.94
Mortar [16]	74.6	6.2	31.4

**2.2.2 Steel and FRP reinforcement**

In all beam specimens, a 14 mm diameter deformed steel bar was used for flexural reinforcement and a 8 mm diameter ribbed bar was used for shear reinforcement. Three representative specimens of 14-mm diameter were tested in tensile in order to measure the

mechanical properties of the steel reinforcing bars; the average yield strength and Young’s modulus were 572.6 MPa and 192.5 GPa, respectively. The average experimental yielding strain of tested steel bars  $\epsilon_{y(exp)}$  was about 0.3%.

Two types of fiber reinforced polymer rods were studied, namely, carbon and glass. The manufactured CFRP bars have a smooth surface whereas the GFRP bars have a coarse surface as shown in Figure 2-2. With a view to enhance the bonding strength between the CFRP bars and the filling material; they were coated with 0.2/0.3-mm coarse sand, as recommended in [26]; this was carried out by applying a thin layer of freshly epoxy-resin before sprinkling the sand material. The mechanical properties of FRP bars according to manufacturer are presented in Table 2-2.

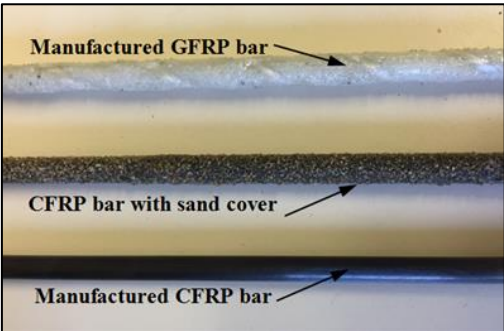


Figure 2-2 : FRP reinforcements

Table 2-2 : Characteristics of the FRP bars

Material	Diameter (mm)	Ultimate strength (MPa)	Modulus of elasticity (GPa)	Strain at failure (%)
CFRP	6	2800	165	1.7
CFRP	10	2000	165	1.4
GFRP	6	896	46.0	1.9

### 2.3 Experimental program

#### 2.3.1 Beam details

Six large-scale continuous two-span beams were loaded to failure, including one control beam and five beams strengthened with FRP bars by using the Near Surface Mounted (NSM) technique. Each tested beam was reinforced with two deformed steel bars of 14-mm diameter placed at the top and bottom part of the cross section, i.e. the reinforcement ratio of tensile steel ( $\rho_s \cong 1\%$ ) to the compression steel ( $\rho'_s \cong 1\%$ ) was kept constant through the entire beam ( $\rho_s/\rho'_s=1$ ). In addition, in order to prevent shear failure, closed nominal stirrups of 8 mm bar diameter uniformly spaced at 100 mm were provided along the complete length of each beam. The beam specimens had the same geometrical dimensions; 150 mm of width, 250 mm of depth, 2800 mm of effective span length and 6000 mm of total beam length. Dimensions, steel reinforcement layout as well as the support and loading arrangement of the tested beams are illustrated in Figure 2-3.



### 2.3.2 Test description

Table 2-3 provides the denominations and details of the control and strengthened beams. The test variables highlighted in this experimental study include the type, ratio (R) and length (L) of the FRP bars as well as the characteristics of the filling material (F).

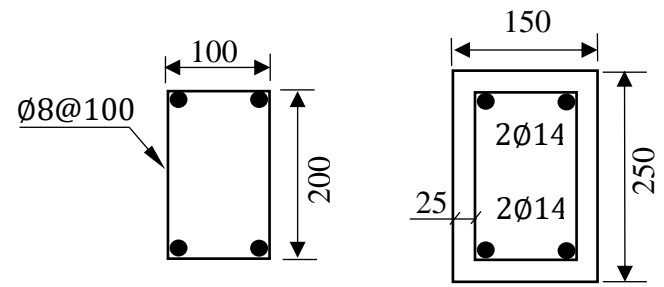
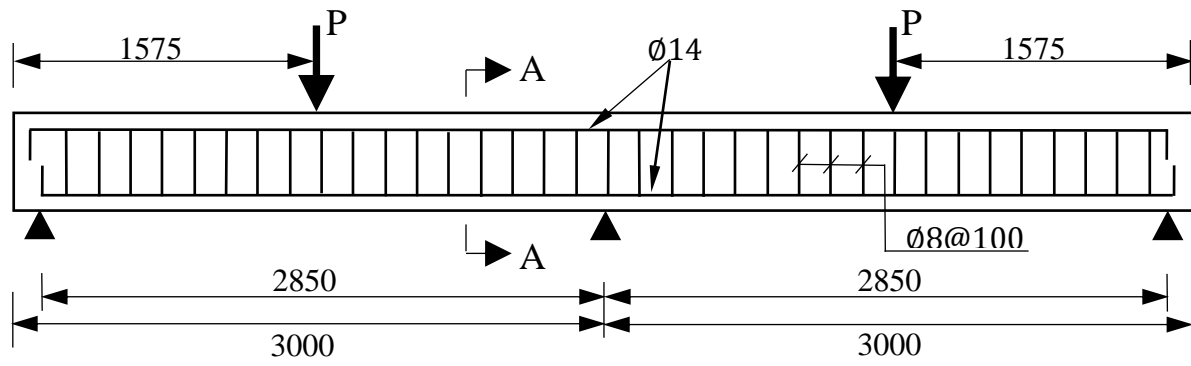
Figure 2-4 shows the general elevation view of the NSM-FRP specimens and their cross sectional details. Beam CB was tested as a reference beam; it had no FRP reinforcement, while the other beams, namely BC1, BG1, BC2-R, BC3-L and BC4-F were initially strengthened with FRP bars at both their hogging and sagging regions. The hogging-to-sagging reinforcement area that included the NSM-FRP bars was also maintained equal to one in all tested beams. In all cases, the FRP bars inserted in the sagging regions did not extend over the external supports. The beams noted BC were strengthened with CFRP bars while the beam noted BG was strengthened with GFRP bars. The numbers assigned to the beams were used only for organizational purpose.

Although there are no sufficient experimental works/guidelines regarding applying NSM-FRP bars for strengthening statically indeterminate RC beams, the strengthening scenario applied for beam BC1 took into account the generic recommendations from both the operational and theoretical [9] point of view. Two  $\emptyset 6$  CFRP bars ( $\frac{A_f}{A_s} = 18.4\%$ , where  $A_f$  and  $A_s$  are the area of FRP bars and the adjacent tension steel bars, respectively) were inserted in resin-adhesive material and they were run into the positive and negative moment spans. The CFRP bars in both regions were stopped beyond the theoretical inflection point (point of zero moment), as shown in Figure 2-4b.

The only difference between BC1 and BG1 is the FRP bars type. Glass Fiber Reinforced Polymer (GFRP) were employed to strengthening beam BG1. The purpose of BG1 was to study the flexural response of continuous beam in relation to the NSM reinforcement material type.

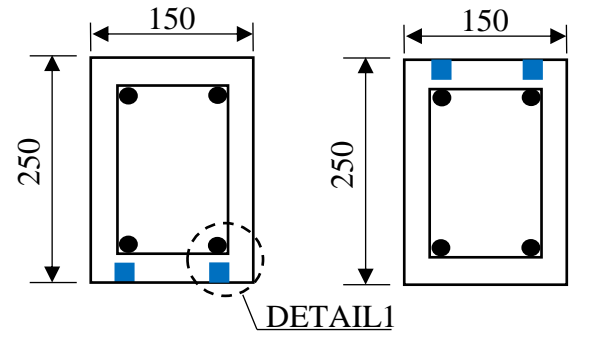
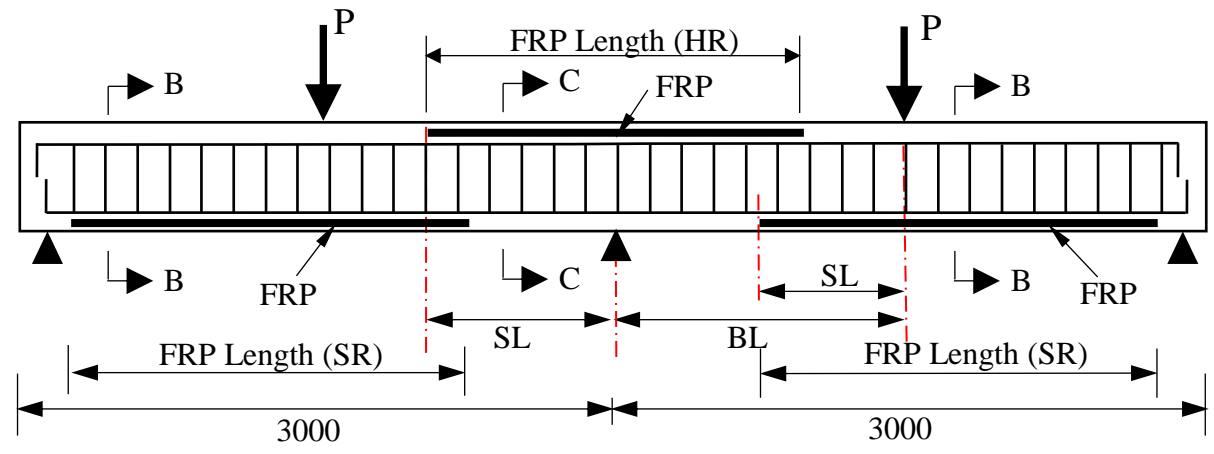
Beam BC2-R was equipped with 1 $\emptyset 10$  CFRP bar ( $\frac{A_f}{A_s} = 25.5\%$ ). It was tested to overview influences of increasing the CFRP section/ratio on improvement the load-carrying capacity of the beam. The length of CFRP bars and the filling material used in BC2-R were identical to those used in BC1.

Beams BC3-L and BC4-F were tested in order to investigate impacts of the running length of CFRP bars and characteristics of the filling material, respectively, on the response of the NSM-CFRP continuous beams, in particular to monitor the failure mode changes in the NSM system. The above two beams employed 2 $\emptyset 6$  CFRP bars ( $\frac{A_f}{A_s} = 18.4\%$ ) in each bending region; these bars were stopped just before the theoretical inflection points in beam BC3-L (see Figure 2-4b), however, the bars were inserted in mortar instead of epoxy-resin in beam BC4-F.



Section A-A

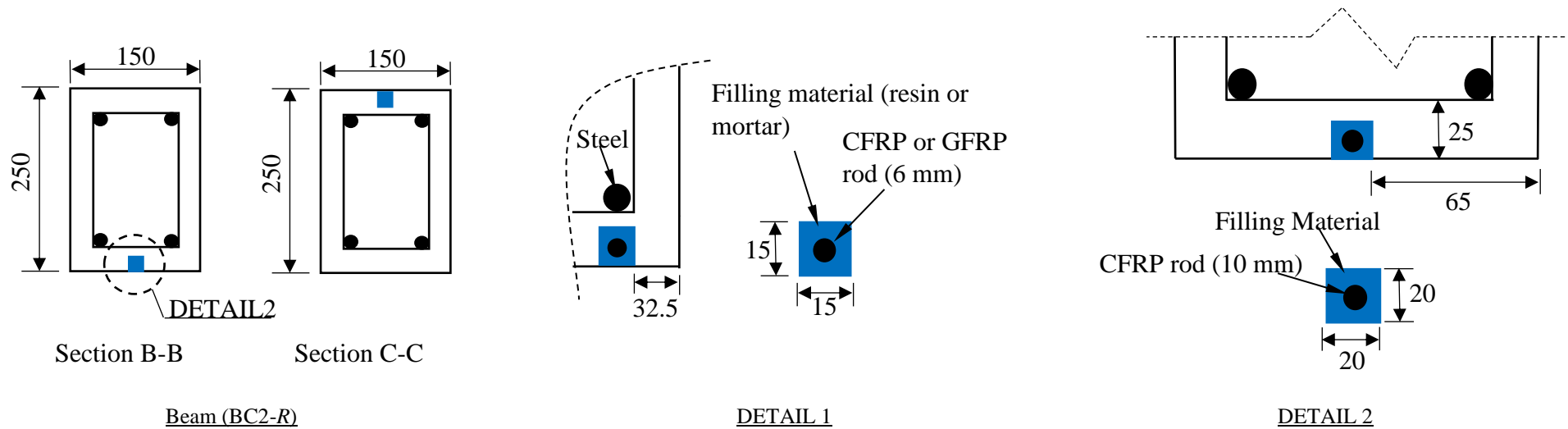
Figure 2-3 : Dimensions, steel reinforcement layout as well as support and load arrangement of tested beams.



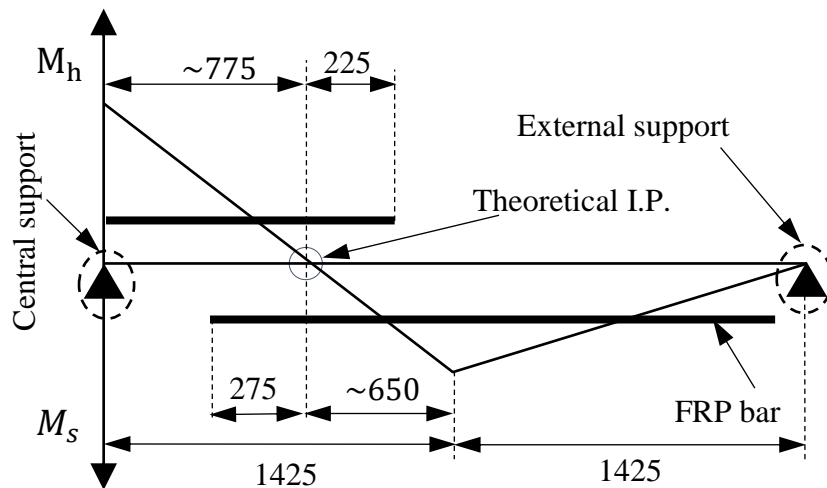
Section B-B

Section C-C

Beams (BC1, BG1, BC3-L, BC4-F)



(a) Elevation view of the beam specimens and cross sections details



(b) Layout of FRP bars in beams BC1, BG1, BC2-R and BC4-F.

- All dimensions are in mm.
- Longitudinal and transverse steel reinforcement same for all beam specimens.
- External point load applied at center of each span.
- 25-mm concrete cover was maintained for all sides of each tested beam.
- FRP bars in HR (hogging region) laid symmetrically about the central support.
- In all cases, FRP bars in SR (sagging region) start from the face of support without any anchorage over the external supports.
- For beam BC3-L, the CFRP bars terminated before the inflection point, i.e. length of CFRP bars in SR was reduced by 300 mm towards the external support, whereas length of the CFRP bars in HR was reduced by 500 mm (250mm from each end towards the center support).

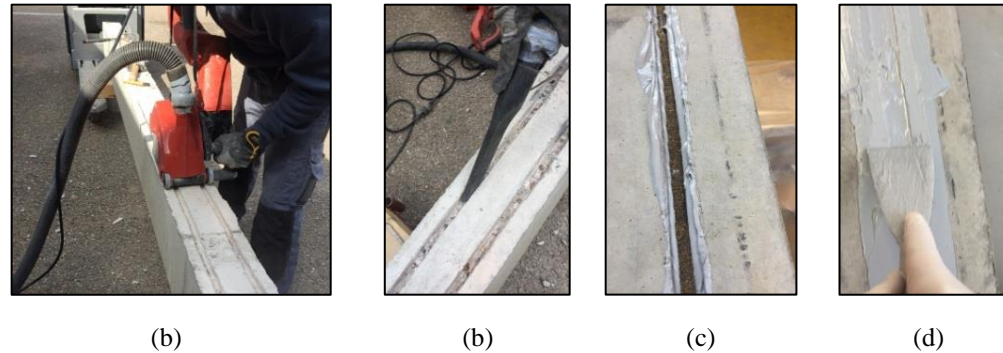
Figure 2-4 : Beam specimens strengthened with FRP rods by using the NSM technique

Table 2-3 : Test matrix and details of the control and strengthened beams

Beam	FRP Type	Hogging Region strengthening			Sagging Region strengthening			$A_f/A_s^{(2)}$	Filling Material	Test variable
		No.	Length	SL/BL <sup>(1)</sup>	No.	Length	SL/BL			
CB	----	----	----	----	----	----	----	----	----	Control beam
BC1	CFRP	2Ø6	2.0	0.70	2Ø6	2.3	0.65	18	Resin	Strengthening /CFRP bars
BG1	GFRP	2Ø6	2.0	0.70	2Ø6	2.3	0.65	18	Resin	Strengthening/GFRP bars
BC2-R	CFRP	1Ø10	2.0	0.70	1Ø10	2.3	0.65	26	Resin	CFRP bar section/ratio
BC3-L	CFRP	2Ø6	1.5	0.53	2Ø6	2.0	0.44	18	Resin	CFRP bar length
BC4-F	CFRP	2Ø6	2.0	0.70	2Ø6	2.3	0.65	18	Mortar	Filling material

(1) SL: is the distance between end of the FRP bars and the external point load. BL: is the distance between the center support and the external point load.

(2) Ratio of the FRP reinforcement ( $A_f$ ) to the tension steel reinforcement ( $A_s$ ). (%)



(a) Making the grooves by using a special concrete saw; (b)Cleaning the groove by using a standard vacuum; (c) Inserting the FRP bars after half-filled the grooves with filling material; and (d) Leveling the surface after filling the grooves by using a hand scraper tool.

Figure 2-5 : Strengthening procedure of NSM-FRP bars

### 2.3.3 Groove preparation and strengthening procedure

Figure 2-5 illustrates the grooves preparation and the strengthening method applied procedure. After 28 days from casting the concrete, longitudinal grooves were made in the concrete cover on the tension surfaces of beams by using a special concrete saw. The concrete saw consists of two diamond blades which are capable of setting any desired distance between them (up to 150 mm). Hence, it was necessary to use a hammer with hand chisel to remove the remaining concrete lugs that formed during the sawing, this made the groove's lower/top surface rougher as well. The grooves dimension were 15-mm (greater than  $1.5d_b = 9$  mm) in both width and depth for beams strengthened with  $\emptyset 6$ -mm FRP bars, whereas the grooves were widen to 20 mm (greater than  $1.5d_b = 15$ mm) in both width and depth for the beam strengthened with  $\emptyset 10$  mm CFRP bar. The dimensions of these grooves are in accordance with the recommendations of [9, 16] to avoid premature failure of beam as a result of collapse of the strengthening system. For beams BC1, BG1, BC3-L and BC4-F, the clear distance between grooves (i.e. 55 mm) was larger than twice the depth of the groove (i.e. 30 mm); however, in beam BC2-R one groove was made at mid-length of the bottom/top side of the cross section. The grooves were cleaned with the help of a standard vacuum to remove debris and fine particles. This was done to ensure perfect bonding between the filling material and concrete substrate. In addition, in order to guarantee that the filling material is in-full contact with the surface of FRP bar; the groove was firstly half-filled with resin/mortar and then the FRP rod was gently applied. Eventually, more filling material was added in order to fill the groove and a hand scraper tool was used for finishing the surfaces.

### 2.3.4 Test setup and instrumentation

Figure 2-6 presents the test setup with the various monitoring devices used in order to collect information for discussion effectiveness of the NSM technique for strengthening indeterminate RC beams. Each continuous beam was loaded to failure with two concentrated loads separated by a distance of 2850-mm; i.e. each load ( $P$ ) was applied at the middle point of each span. The total applied load ( $P_t = 2P$ ), center reaction ( $R_c$ ), mid-spans deflections ( $\delta$ ) as well as strains of the steel bars ( $\epsilon_s$ ), FRP bars ( $\epsilon_f$ ) and concrete ( $\epsilon_c$ ) were recorded during the loading.

Two hydraulic actuators were used to load the beams with capacity of 400 kN and 0.3 kN/s average loading speed for each. A 200 kN load cell was utilized as an intermediate support in order to measure the reaction at any level of the applied load. The vertical mid-spans deflection of each beam were measured by means of two vertical linear variable differential transducer (LVDTs). The tensile strains of reinforcing bars (steel and FRP) at different locations and compressive strains of concrete at central support and mid-span of the beams were measured by using electrical strain gauges with base lengths of 13 mm and 63 mm, respectively. The strain gauges were installed internally on the reinforcement bars. Figure 2-7 shows locations of the strain gauges used in each tested beam. All the strain gauges were coated with polyurethane material to ensure high level of measuring accuracy. Protection of the strain gauges attached to the reinforcing bars was made by using protective paste, rubber piece and aluminum tape, as shown in Figure 2-7c.

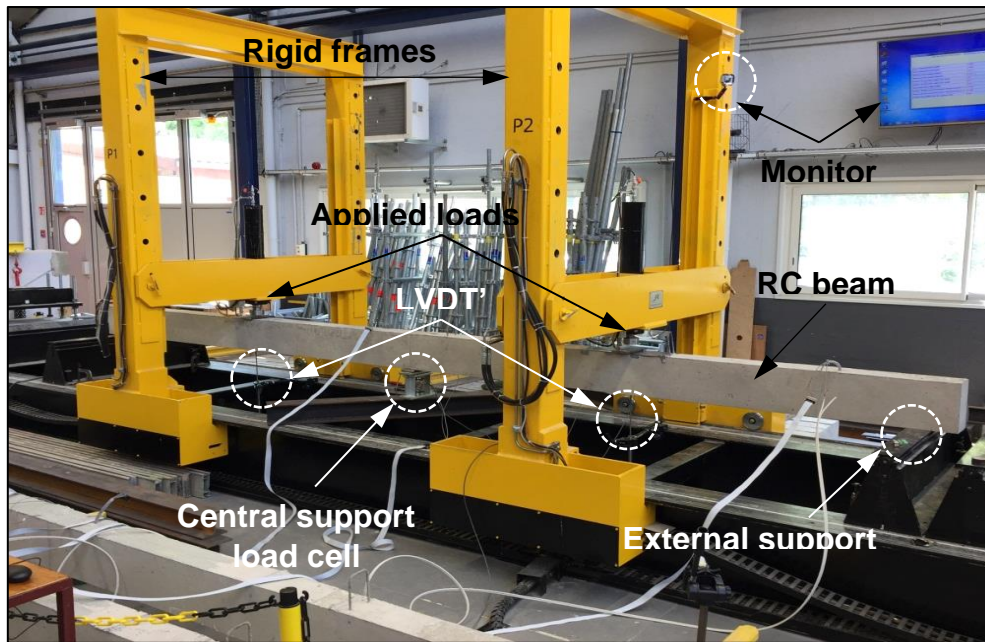


Figure 2-6 : Test setup and the instrumentations used for testing beams

## 2.4 Results and discussion

The global performance of tested beams was measured in terms of the load–deflection response, energy absorption capacity, failure mode and overall capacity, cracking maps and cracking behaviors, beam ductility, moment redistribution as well as load–strain response as described in the following subsequent sections. The provided comparison rates were computed according to the following equations, unless stated otherwise;

$$\text{Increasing (\%)} = \frac{x_s - x_r}{x_r} \times 100\% \quad (1)$$

$$\text{Decreasing (\%)} = \frac{x_r - x_s}{x_r} \times 100\% \quad (2)$$

Where,  $x_s$  and  $x_r$  are values (eg.; load, displacement,..etc) of a strengthened beam and control beam, respectively.

### 2.4.1 Load-deflection response

Fig. 2-8 shows the total applied loads ( $Pt$ ) versus the average midspans deflection ( $\delta$ ), obtained from LVDT1 and LVDT2 for beams CB, BC1, BG1, BC2-R, BC3-L and BC4-F. Points A, B, C and D initially represent the concrete cracking, steel yielding, ultimate and failure loads of the beam, respectively. These points were determined based on the slope changes of the  $Pt - \delta$  curves. Overall, compared to the reference beam CB, the NSM-FRP beams showed higher yield and ultimate loads, while the cracking loads were almost similar.

As can be seen from the  $Pt - \delta$  curves, four distinct stages could be discerned during the loading process, namely the elastic stage (O-A), concrete cracking stage (A-B), ultimate strength stage (B-C) and failure stage (C-D).



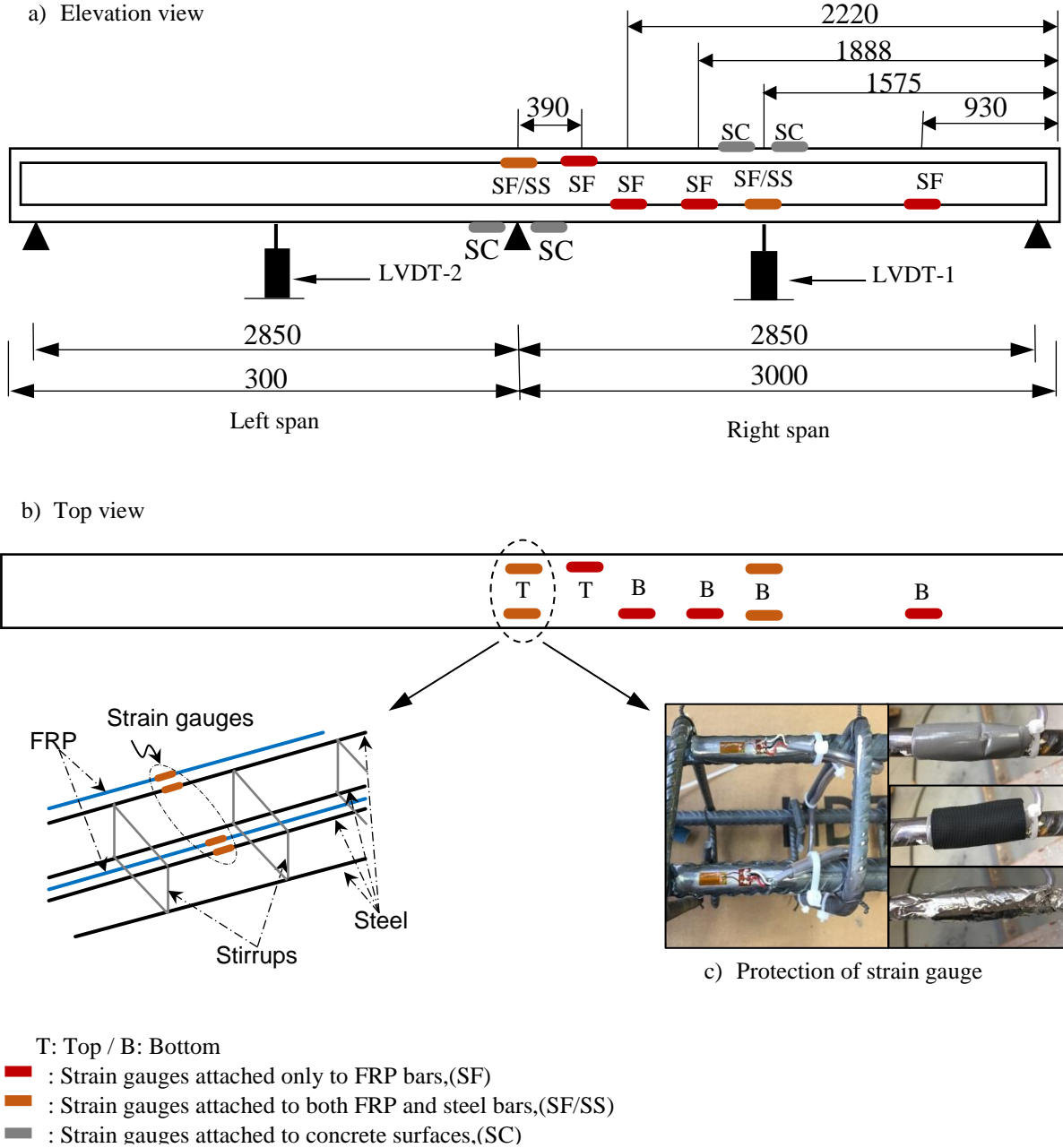


Figure 2-7 : Locations of strain gagues on steel bars, FRP bars and concrete

In the elastic stage, the FRP showed marginal contribution in improving the behavior of strengthened beams. All beams displayed approximately same behavior indicating similar stiffness. In the cracking stage and prior to the yielding of the tension steel, the NSM-FRP beams showed improvement in stiffness and yielding load as compared to the control beam regardless type, length and ratio of the FRP bars or the filling material used. After yielding of the tension steel, all NSM-FRP beams exhibited higher load-increasing rates up to the ultimate load than that of the control beam, these results may provide evidence for: (1) the SNSM-FRP bars worked effectively as an additional tensile reinforcement, (2) the NSM-FRP bars controlled the flexural performance in the ultimate strength stage, and (3) the NSM-FRP bars enhanced the flexural response of beams by reducing the loss in stiffness.

As indicating in Figure 2-8, stiffnesses of beams BG1 and BC4-F were lower than that of beam BC1 in the ultimate strength stage, this is a direct result of the mechanical properties of the strengthening bars (CFRP/GFRP) and the filling material (resin/mortar). Indeed, the modulus of elasticity of GFRP is much lower than that of the CFRP, and the tensile strength of mortar is much lower than that of the resin. On the other hand, increasing section or decreasing length of the CFRP bars turned out not significantly affecting the beam's stiffness; the  $P_t - \delta$  response of beams BC2-R and BC3-L, up to their peak loads, were almost similar to the  $P_t - \delta$  response of beam BC1.

After the ultimate load was attained (i.e. failure stage), significant decrease in the NSM beams resisting load and stiffness were observed, the decreasing rate as well as the maximum mid-span deflection were principally influenced by the beam's failure mode.

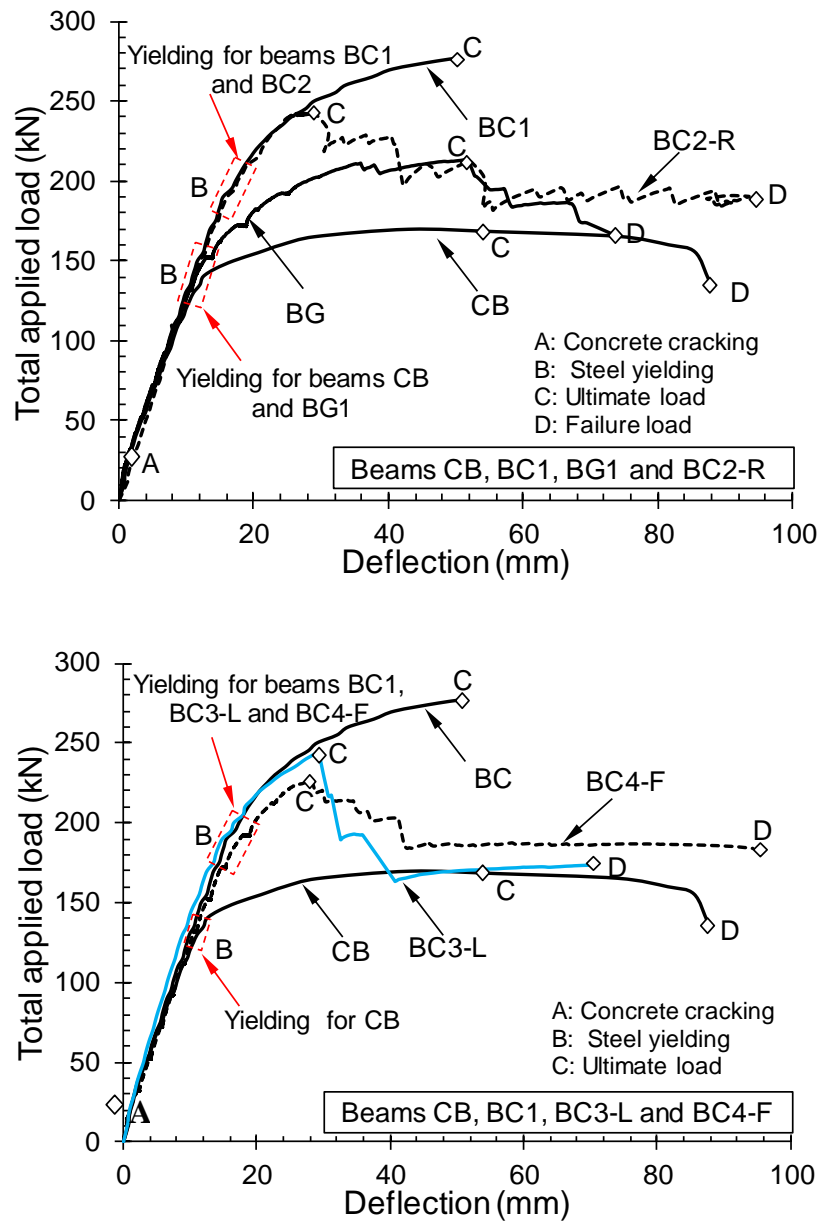


Figure 2-8 : Load-deflection response of tested beams



### 2.4.2 Energy absorption capacity

The energy absorption of RC member indicates to the transformation of mechanical energy to internal potential energy; it considers indicative of structural integrity [27]. The area under the load–deflection curve could be defined as the energy absorption capacity,  $E_{ab}$ . Therefore, the  $E_{ab}$  of tested beams was calculated based on the area under the  $P_t - \delta$  curves up to the ultimate load (Figure 2-8). The main observation was that, the adequate using of NSM-FRP bars for strengthening continuous RC beams could improve the energy absorption capacity. The  $E_{ab}$  of beams BC1 and BG1 was increased by 28.1% ( $E_{ab} = 10356.6\text{kN}\cdot\text{mm}$ ) and 8.2% ( $E_{ab} = 8740.7\text{kN}\cdot\text{mm}$ ), respectively compared to that of CB ( $E_{ab} = 8082.8\text{kN}\cdot\text{mm}$ ), while it decreased by 43.9% ( $4537.8\text{kN}\cdot\text{mm}$ ) in beam BC2-R, 40.6% ( $E_{ab} = 4799.2\text{kN}\cdot\text{mm}$ ) in beam BC3-L and 48.8% ( $E_{ab} = 4137.8\text{kN}\cdot\text{mm}$ ) in beam BC4-F. These results might also give indications about the ductility performance of strengthened beams, as will be discussed later (Section 4.5).

### 2.4.3 Failure mode and overall capacity

In this section, values of the ultimate load and maximum mid-span deflection of tested beams were determined from the load–deflection curves (Figure 2-8), while the yielding load of tension steel at the central support was accurately determined according to the strain gauge measurement.

The control beam CB, underwent a classical ductile flexural failure. This failure was characterized by plastic hinge formation at both intermediate support and mid-span sections followed by concrete crushing in the compression parts (see Figure 2-9). After the yielding load of tension steel at the central support was reached ( $P_y = 132.3\text{ kN}$ ), the beam's resistance to the external applied load slowly increased up to the ultimate load ( $P_u = 169.7\text{ kN}$ ), and then decreased until the average vertical displacement ( $\delta$ ) reached 87.6 mm.

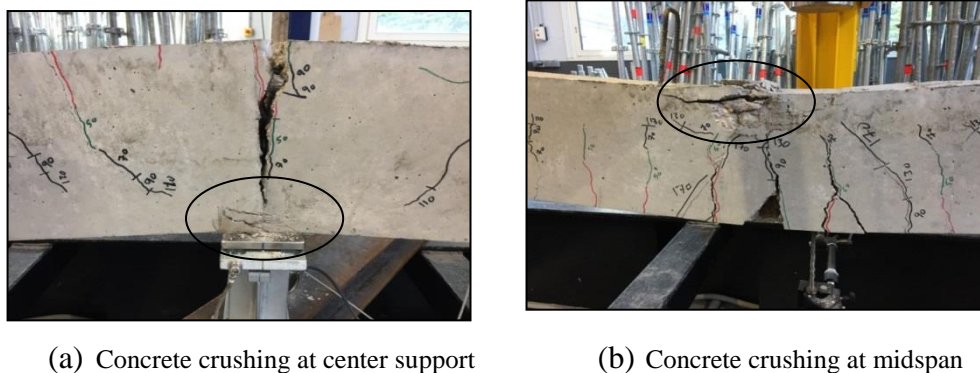


Figure 2-9 : Conventional flexural failure of control beam, CB.

The beam BC1 primarily failed due to pull out of the CFRP bars close to the central support in the upper part of the beam, see Figure 2-10. This failure occurred due to debonding between the strengthening bars and the resin filling material. The pull out of CFRP rods was sudden and accompanied with an explosive sound; it was followed by the beam failure. The tension steel at the central support yielded at a load of 195.1 kN (47.5% increasing), and the ultimate load occurred at 277.1 kN (63.3% increasing). The mid-span deflection at the beam failure was 50.6 mm (42.2% decreasing).

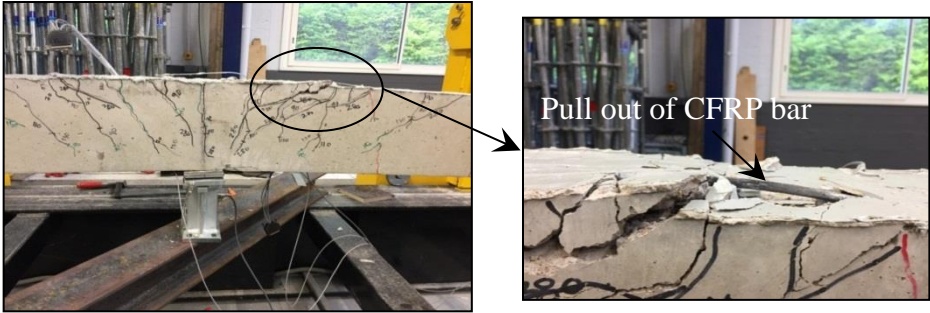
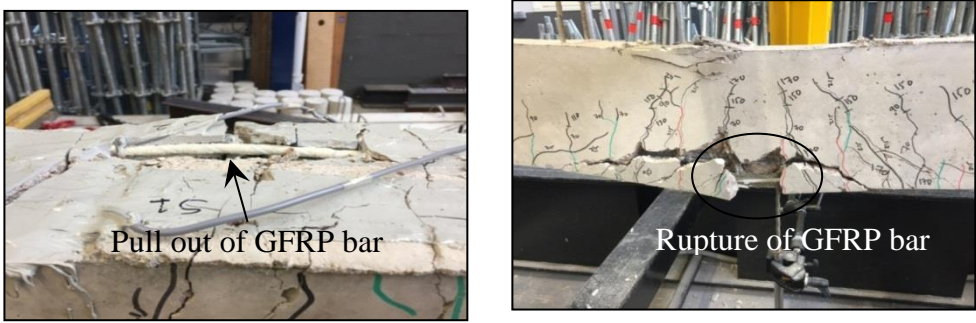


Figure 2-10 : Failure mode of beam BC1

The failure of beam BG1 was due to pull out of GFRP bar at the hogging region followed instantly by tensile rupture of GFRP bar in one of the sagging regions, as shown in Figure 2-11. The pull out failure of this beam was nearly at the same position as that observed in BC1. The rupture of GFRP bar was abrupt and accompanied by concrete ripping at the beam soffit. Considering the ultimate tensile strength of the GFRP bars, the pull out failure at central support of beam BG1 may turn brought the rupture failure at mid-span, which was not occurred in case of BC1. The tension steel at central support yielded at a load of 150.2 kN (13.5% increasing), and the ultimate applied load recorded at 213.3 kN (25.7% increasing). The mid-span deflection at the beam failure was 73.7 mm (about 15.9 % decreasing).

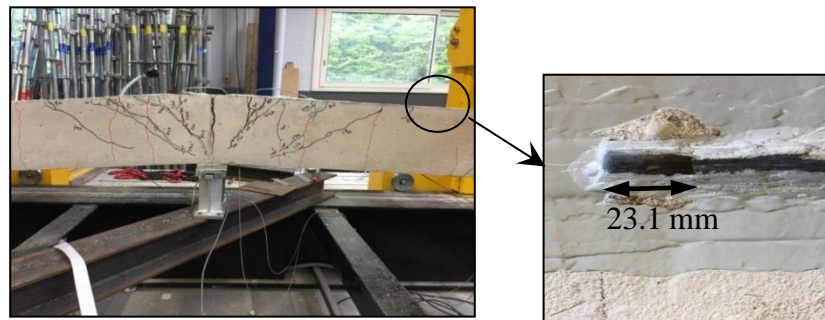


(a) GFRP rod pull out at center support      (b) Rupture of GFRP bar at midspan

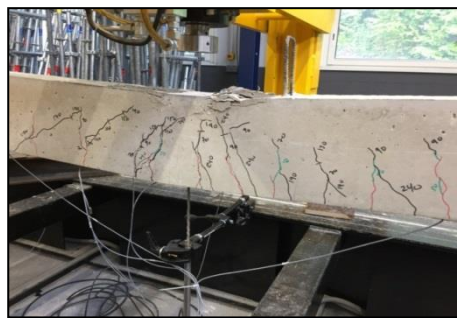
Figure 2-11 : Failure mode of beam BG1

The initial observation purported that beam BC2-R failed conventionally due to concrete crushing (Figure 2-12a and Figure 2-12b). However, it was essential to check the constancy of the embedded CFRP bar due to: (1) the cracking noises which was clearly heard after yielding of the tension steel before the beam failure, (2) the intensive transverse cracks which emerged in the resin material particularly at the hogging region, and (3) the load bearing capacity of this beam ( $1\varnothing 10$  CFRP bar,  $A_f = 78.5 \text{ mm}^2$ ) was lower than that of beam BC1 ( $2\varnothing 6$  CFRP bars,  $A_f = 56.5 \text{ mm}^2$ ). Therefore, a small hammer along with a hand chisel were carefully used, and it was found that one ends of the CFRP bar in the hogging region was moved about 23.1 mm from its original position towards the central support (Fig. 2-12a). This means a debonding failure occurred between the CFRP bar and epoxy-resin. Compared to beams BC1 and BG1, the movement of the CFRP bar during the debonding failure in beam BC2-R was confined within the groove ( $20 \times 20 \text{ mm}$ ) without slippage out of the NSM system. The tension steel at central support of this beam yielded at a load of 218 kN, which is 64.8% greater than that of the CB,

and its peak load was reported at 242.1 kN, which is 42.7% greater than the CB. The maximum midspan deflection at the end of the test was about 93.5 mm, which represents a 6.7% increase in comparison with the CB.



(a) Center support



(b) Mid-span

Figure 2-12 : Failure mode of beam BC2-R

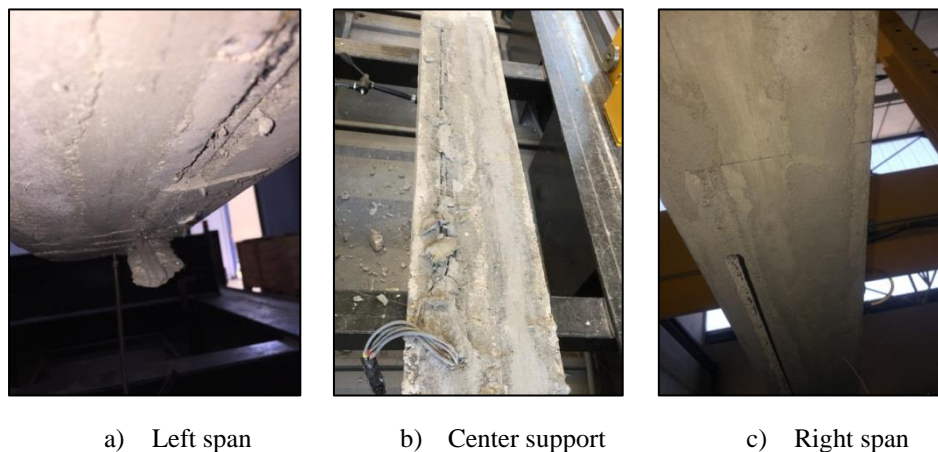
In Beam BC3-L, the CFRP bars were stopped just before the theoretical inflection points, i.e. no extension length was applied, in order to study the impact of length and anchorage of the CFRP bars on the beam behavior. Indeed, BC3-L exhibited brittle concrete cover peeling off that included the CFRP bars in the hogging region and in both the sagging regions, as shown in Figure 2-13. The peeling off failure was firstly observed within one of the sagging regions followed immediately by failure of the hogging region. This failure happened as a consequence of the following reasons: (1) the confined concrete between the NSM and steel was exposed to tensile and shear stresses induced by the force transferred from the CFRP to the end of the anchorage zone [28]. (2) CFRP bars, cut off before the I.P., i.e. low-tension stress and high shear zone, caused a major stress concentration which in turn formed main inclined crack at the end of NSM bars (see Fig. 2-13), and (3) the intersection between the inclined crack at the end of CFRP bars with the fine horizontal cracks which previously appeared at level of the steel reinforcement caused to develop a horizontal main crack extending from the maximum moment zone to the extremity of CFRP bars. The tension steel at central support yielded at a load of 200 kN and the peak load was reported at 244.4 kN; these values represent, respectively, increasing of 51.2% and 44% over than those of the control beam. The maximum midspan deflection of this beam at the end of the test was 70.2 mm, which is 19.9% lower than the CB.





Figure 2-13 : Failure mode of beam BC3-L

Beam BC4-F failed by debonding between the filling material (mortar) and concrete at the groove lateral faces in the hogging and sagging regions, as shown in Figure 2-14. The mortar remained attached to the rough surface of the grooves only, i.e. lower or top surface according to position of the groove. The increase in the yield load (172 kN), load-carrying capacity (226.2 kN) and the maximum midspan deflection (94.3 mm) provided by the strengthening system of this beam were about 30.2%, 33.3% and 7.6%, respectively, with respect to the CB.



a) Left span

b) Center support

c) Right span

Figure 2-14 : Failure mode of beam BC4-F

#### 2.4.4 Cracking maps and cracking behavior

The first cracks initiated nearly simultaneously at the intermediate support and in the mid-span region in all NSM beams. With further increasing of the applied load, these cracks deployed, widened and extended to the compressive regions. Meanwhile, more flexural cracks started and distributed along the beams. In case of beam BC3-L, additional horizontal cracks had formed; these cracks were at level of the tension steel bars and extended from the central support and the applied load points toward the ends of the CFRP bars (see Figure 2-13). From the initiation of loading until yielding of the tension steel (either in hogging or sagging regions), the flexural cracks did not cross the filling material in all strengthened beams. However, after steel yielding was attained, transverse flexural cracks relative to the beam's length propagated within the adhesive resin, indicating that the additional reinforcement (FRP rods) controlled the cracking until the failure load was attained. These transverse cracks were much more distributed in BC2-R; which is essentially due to the position and ratio of the CFRP reinforcement and to its groove dimension. On the contrary, concerning BC4-F, no propagation of the transverse cracks was

observed in mortar although the beam continued to resist external loads after the yielding load was reached. Instead of that, the mortar-concrete interface was clearly affected by visible longitudinal cracks along the groove length indicating debonding failure occurred (see Figure 2-14).

At failure of beams, concrete crushing (limited/full) was noticed at the load application points and at the central support for all tested beams, except for BC3-L due to its premature peeling off failure. In this beam (i.e. BC3-L), concrete cover separation together with the NSMCFRP bars over significant lengths in the tension zones of beam was happened. However, for beams BC1 and BG1 local ripping of concrete was observed in the site where the FRP bars were pulled out or ruptured.

Figure 2-15 displays the crack maps of tested beam specimens at failure; the cracks are congested in the tension zones and at the failure positions. As can be seen from Fig. 2-15, using NSM-FRP rods for strengthening continuous RC beams leads to a higher number of the cracks in the sagging and hogging regions, and consequently the corresponding average crack spacing in each zone is significantly reduced. Table 2-4 presents the number of the cracks including flexural, shear and inclined flexural-shear that appeared in each zone of each tested beam as well as their average spacing, where  $N_s^{cr(max)}$  = maximum number of cracks in the sagging regions, i.e. the largest number of cracks in the left or right span,  $N_h^{cr}$  = total number of cracks in the hogging region,  $S_s^{avg}$  = average crack spacing in the sagging regions and  $S_h^{avg}$  = average crack spacing in the hogging region. Compared to the control beam, the number of cracks increased by 62.5%, 100%, 81.3%, 125% and 112.5% in the positive region and by 200%, 137.5%, 100%, 175% and 200% in the negative region for beams BC1, BG1, BC2-R, BC3-L and BC4-F, respectively, while the average crack spacing decreased by 47.3%, 47.5%, 28.2%, 40%, 34.6% in the positive region and by 47.2%, 65.7%, 61%, 32.7%, 52.9% in the negative region.

The load-flexural crack width diagrams of strengthened and unstrengthened beams are shown in Figure 2-16. The crack width was measured in the hogging region using a special microscope with accuracy of 0.05-mm. As can be seen from Figure 2-16, the NSM-FRP bars restricted development of the crack width; the crack width was significantly reduced in the NSM-FRP specimens. Beams strengthened with CFRP bars, i.e. BC1, BC2-R, BC3-L and BC4-F, exhibited lower crack widths than the beam strengthened with GFRP bars, i.e. BG1, for the same applied load. On the other hand, increasing section of CFRP bars (BC2-R) or using mortar as a filling material (BC4-F) instead of resin, slightly increased the crack width in comparison with that observed in BC1, while decreasing the length of CFRP bars (BC3-L) had displayed greater impact. However, as the load is approached the yielding, the crack width values of the NSM-CFRP beams were almost conformed. The crack widths after the yielding load was not totally measured due to safety concerns.

#### 2.4.5 Beam ductility

The ductility index ( $\mu$ ) was calculated according to Eq. (2-3) in order to measure ductility of the strengthened beam with respect to the unstrengthened control beam. The results obtained are concluded in Table 2-5.

$$\mu = \frac{\delta_u}{\delta_y} \quad (2-3)$$

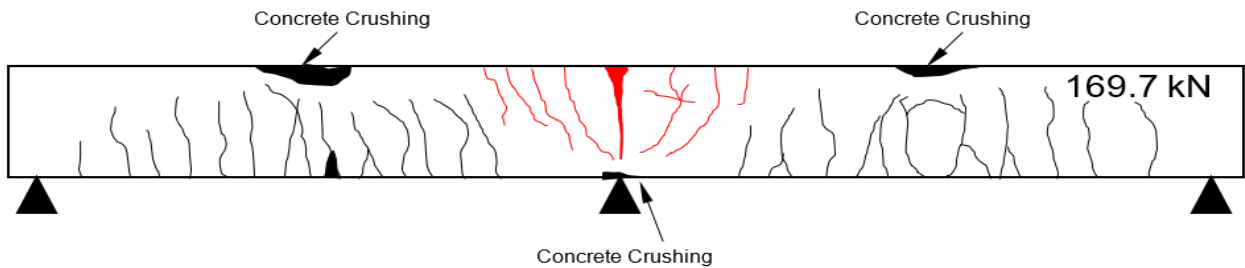
where  $\delta_u$  and  $\delta_y$  are the average mid-spans deflection of beam at ultimate and yielding load, respectively, these deflection values were obtained from the load–deflection response (see Fig. 2-8).

As expected, using NSM-CFRP bars for strengthening RC beams tends to reduce the beam ductility. The ductility index of beams BC, BC2-R, BC3-L and BC4-F were decreased by 31.3%, 66.7%, 62.5% and 60.4%, respectively, compared to the control beam. These findings provide evidence that increasing the area of CFRP bars, terminating the CFRP bars before the inflection point or using mortar as a filling material significantly decreased the beam ductility. However, the greater ductility index among the tested strengthened specimens was found for beam incorporating GFRP bars, i.e. BG1, and this can be explained as that the elastic modulus and tensile strain of GFRP were, respectively, lower and higher than those of CFRP. The  $\mu$ -index of this beam (BG1) slightly decreased by about 14.6% than the  $\mu$ -index of the control beam.

Table 2-4 : Cracks number and average crack spacing of strengthened and unstrengthened beams.

Beam	$N_s^{cr(max)}$ <sup>(1)</sup>	$n_s$ <sup>(2)</sup>	$N_h^{cr}$ <sup>(3)</sup>	$n_h$ <sup>(4)</sup>	$S_s^{avg}$ <sup>(5)</sup>	$x_s$ <sup>(6)</sup>	$S_h^{avg}$ <sup>(7)</sup>	$x_h$ <sup>(8)</sup>
CB	16	1	8	1	136	1	163	1
BC1	26	1.6	24	3	71.7	0.53	86.1	0.53
BG1	32	2	19	2.4	71.4	0.53	55.9	0.34
BC2-R	29	1.8	16	2	94.7	0.70	63.6	0.39
BC3-L	36	2.3	22	2.8	81.6	0.60	109.7	0.67
BC4-F	34	2.1	16	2	89	0.65	76.7	0.47

- (1)  $N_s^{cr(max)}$ : Maximum total number of cracks in the sagging regions (left span or right span, which is greater).  
(2)  $n_s$ : Ratio of  $N_s^{cr(max)}$  of a NSM beam to  $N_s^{cr(max)}$  of CB.  
(3)  $N_h^{cr}$ : Total number of cracks in the hogging region.  
(4)  $n_h$ : Ratio of  $N_h^{cr}$  of a NSM beam to  $N_h^{cr}$  of CB.  
(5)  $S_s^{avg}$ : Average crack spacing in the sagging regions;  $S_s^{avg} = \frac{\text{total spacings length (left and right spans)}}{\text{total number of spacing (left and right spans)}} \cdot (\text{mm})$   
(6)  $x_s$ : Ratio of  $S_s^{avg}$  of a NSM beam to  $S_s^{avg}$  of CB.  
(7)  $S_h^{avg}$ : Average crack spacing in the hogging region;  $S_h^{avg} = \frac{\text{total spacings length in the negative region}}{\text{number of spacings}} \cdot (\text{mm})$   
(8)  $x_h$ : Ratio of  $S_h^{avg}$  of a NSM beam to  $S_h^{avg}$  of CB.



(a) Control beam, CB

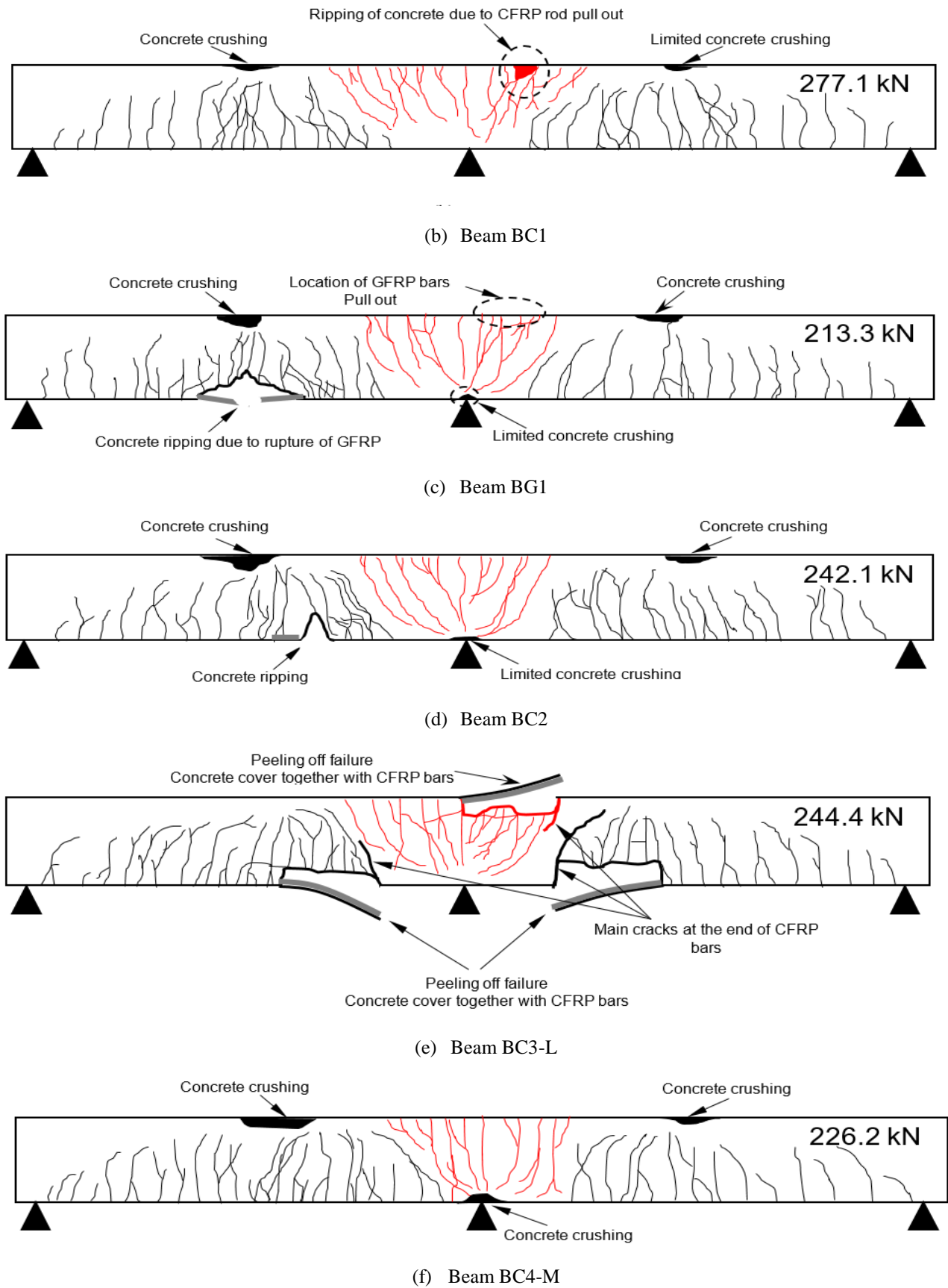


Figure 2-15 : Cracks maps of tested beam specimens

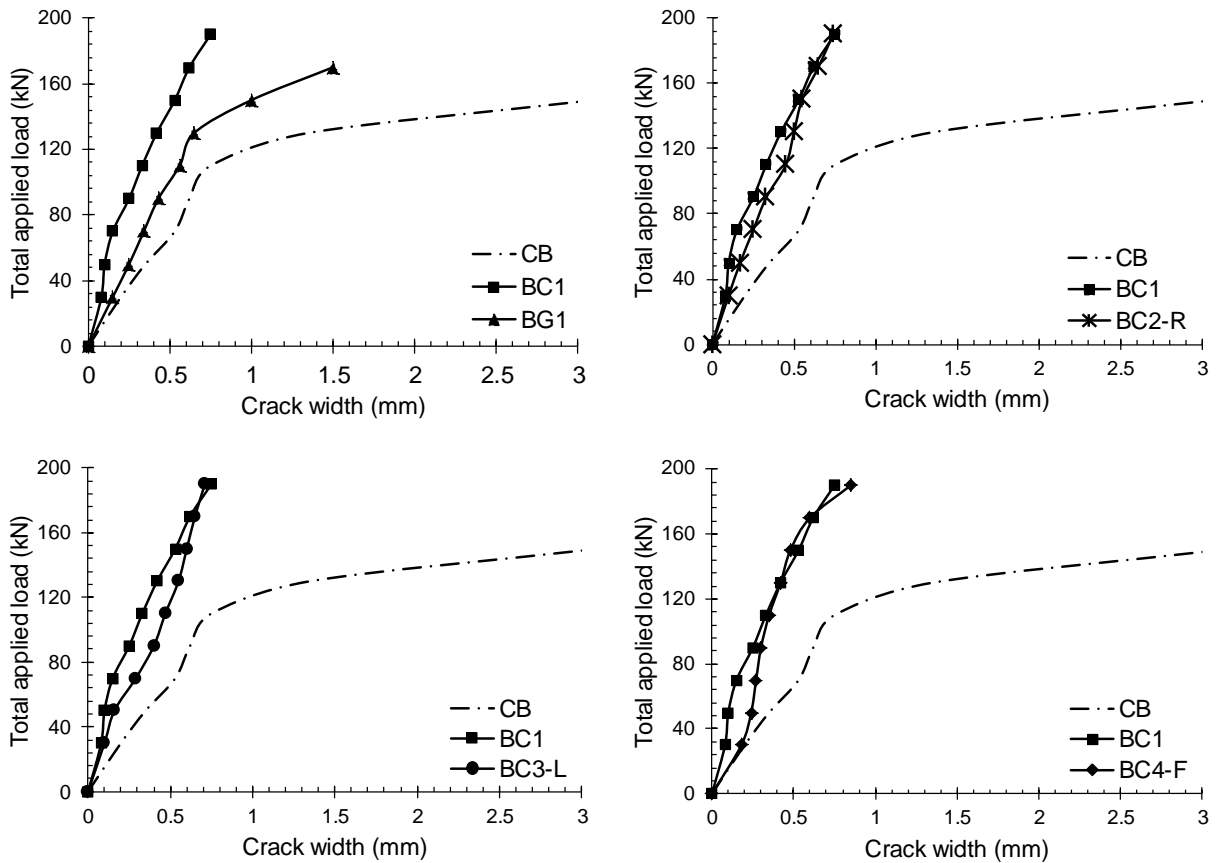


Figure 2-16 : Total applied load vs. crack width at hogging region of tested beams

Table 2-5 : Ductility index of tested beams.

Beam	$\mu^{(1)}$	$\lambda^{(2)}$
CB	4.8	1
BC1	3.3	0.69
BG1	4.1	0.85
BC2-R	1.6	0.33
BC3-L	1.8	0.38
BC4-F	1.9	0.40

(1) Ductility index.

(2) Ratio of ductility index of a strengthened beam to the ductility index of control beam.

### 2.4.6 Moment redistribution

Moment redistribution in conventional steel reinforced concrete beam could be referred to the structural redundancy and nonlinear behavior of reinforced concrete. Quantifying the moment redistribution in ordinary indeterminate RC beams is complex as it depends on several factors such as the quantity, arrangement and mechanical characteristic of internal steel, loading arrangement, geometry of the member as well as the width of supports; in fact, it becomes more complicated for beams strengthened with FRP bars. For continuous two-span beam that is symmetrical in reinforcement and loading in each span, moment transfer from the intermediate support to the mid-span region could occur [eg. 29–32]. The existing building codes such as ACI 318–14 [1], Eurocode 2 [33] and AS 3600 [34] allow taking advantage of the linear elastic analysis with moment redistribution (15–30%) for conventional structural designs; this means



reducing the moment of critical sections while increasing that of other sections in order to satisfy static equilibrium. These codes often tend to be conservative and do not allow the moment redistribution for beams reinforced or retrofitted with FRP materials due to: (1) the brittle behavior of FRP, (2) the bonding conditions between these materials and concrete substrate, and (3) the required level of ductility for moment redistribution in such members is still unclear, although several experimental studies on EB-FRP strengthened beams indicated that moment redistribution is possible to some extent [35].

Figure 2-17 presents the measured central support reaction of tested beams with respect to the total applied load at different levels, along comparison with the elastic reaction which computed by considering a uniform flexural stiffness throughout the entire length of beams. For beams CB, BC1 and BG1, the elastic model cannot accurately reflect the evolution of the actual reaction, especially after formation of the concrete cracking. At the ultimate load, the actual reaction of these beams was lower than the elastic reaction indicating sign of load/moment redistribution occurs from the central support to the mid-span section. Beams BC2-R, BC3-L and BC4-F exhibited a low to moderate load redistribution behavior until failure. The actual reaction at the ultimate load in beams BC2-R and BC4-F, turned out to be slightly lower than the elastic reaction, while it was slightly greater than the elastic reaction in beam BC3-L.

Table 2-6 reports the data obtained at the ultimate load level ( $P_u$ ) of each tested beam; these are the experimental flexural moment in the hogging region ( $M_h^{Exp}$ ) and sagging region ( $M_s^{Exp}$ ), the corresponding hypothetical flexural moments ( $M_h^{Th}$ ,  $M_s^{Th}$ ), the central support reaction  $R_c$  as well as the moment redistribution ratio ( $\beta$ ). The  $M_h^{Exp}$  and  $M_s^{Exp}$  were determined by means of Eqs. (2-4) and (2-5), respectively, while the  $M_h^{Th}$  and  $M_s^{Th}$  were computed according to the linearly elastic statement, as given in Eqs. (2-6) and (2-7), respectively, where L designates to the beam's span length ( $L = 2850$  mm). The moment redistribution ratio ( $\beta$ ) corresponding to the ultimate load was calculated for both regions based on Eq. (2-8). Moreover, Figure 2-18 gives a comparison between the experimental and elastic bending moment for the tested beams at the ultimate load.

$$M_h^{Exp} = \frac{(P_u - 2R_c) \times L}{4} \quad (2-4)$$

$$M_s^{Exp} = \frac{(P_u - R_c) \times L}{4} \quad (2-5)$$

$$M_h^{Th} = \frac{3P_u L}{32} \quad (2-6)$$

$$M_s^{Th} = \frac{5P_u L}{64} \quad (2-7)$$

$$\beta (\%) = \left( \frac{M^{Th} - M^{Exp}}{M^{Th}} \right) \times 100\% \quad (2-8)$$

Table 2-6 and Figure 2-18 indicate that the moment redistribution ratio ( $\beta$ ) of control beam was equal to 20.53% at the central support and -12.43% at the mid-span. The beams BC1 and BG1 had, respectively, a moment redistribution ratio of 19.59% and 17.89% at the central support

and  $-11.83\%$  and  $-10.74\%$  at the mid-span. For the rest of strengthened beams, the moment redistribution ratio was significantly decreased due to the increase in the cross-sectional area of the CFRP bars (BC2-R), insufficient length of CFRP bars (BC3-L) or the mortar filling material used (BC4-F). Beams BC2-R, BC3-L and BC4-F had a moment redistribution ratio of  $10.79\%$ ,  $-6.43\%$  and  $3.31\%$  at the central support and  $-6.68\%$ ,  $3.86\%$  and  $-1.98\%$  at the mid-span, respectively. These results demonstrate that; although limited to some specimens, moment migration from the hogging into the sagging region was occurred in beams strengthened with a sufficient length of NSM-FRP bars, while opposite process took place in case of beam BC3-L. However, by comparing the above moment redistribution values with those reported in previous studies on strengthening continuous RC beam with externally bonding sheets [7,8], it may state that applying the NSM-FRP technique allows more moment redistribution value at the ultimate load than the conventional externally bonding FRP technique. Accordingly, further studies on NSM-FRP indeterminate RC beams are strongly recommended in order to provide more reasonable and effective design guidelines allowing moment redistribution in practical engineering.

In conclusion, in addition to the above mentioned factors identified in ordinary indeterminate RC beams; the amount of moment redistribution in NSM-FRP bars strengthened continuous beams depends on quantity and length of the FRP bars as well as on the characteristic of the filling material. Within the framework of this study, the  $18\%$  ratio of  $\frac{A_f}{A_s}$  was found suitable to achieve moment redistribution in strengthened beam approximately similar to that of unstrengthened beam as long as the failure mode is not caused by peeling off of concrete cover or debonding between the filling material and concrete.

### 2.4.7 Strain analysis

Strains of tension steel bars, FRP bars and concrete at center support and mid-span of tested beams are presented in Figs. 2-19 and 2-20, respectively. The positive strain values represent the tensile strain of steel and FRP reinforcements and the negative strain values represent the compressive strain of concrete. From an overall view of using NSM-FRP bars for strengthening RC beams, the tensile strains of adjacent steel and the compressive strains of extreme concrete fibers are reduced as compared to those of the control beam for the same applied load.

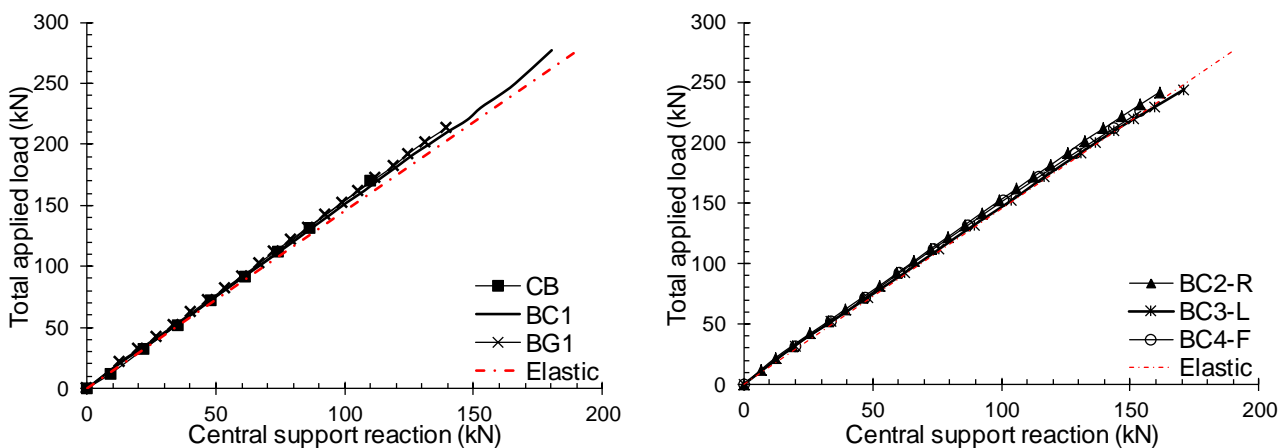


Figure 2-17 : Total applied load versus central support reaction of tested beams.

### 2.4.7.1 Load-strain response of tension reinforcement (steel and FRP)

As can be discerned from Figs. 2-19 and 2-20, the strain values of tension reinforcing bars at both central support and mid-span of beams were affected by two characteristic points: the first point represents the concrete cracking load; it was approximately similar for all beams, while the second point represents yielding of the tension steel which was influenced by the strengthening scenario applied to the beam. On the average, the yielding loads of beams strengthened with NSM-CFRP bars, i.e. BC1, BC2-R, BC3-L and BC4-F, were significantly greater than that of the beam strengthened with NSM-GFRP bars, i.e. BG1.

Table 2-6 : Total applied load, central support reaction, bending moments and moment redistribution of tested beams at level of peak applied load

Beam	ultimate load $P_u$	Central support reaction <sup>[1]</sup> $R_c$	Flexural moment at hogging			Flexural moment at sagging			$\alpha$ <sup>[7]</sup>
			$M_h^{Exp}$ <sup>[2]</sup>	$M_h^{Th}$ <sup>[3]</sup>	$\beta(\%)$ <sup>[6]</sup>	$M_s^{Exp}$ <sup>[4]</sup>	$M_s^{Th}$ <sup>[5]</sup>	$\beta(\%)$ <sup>[6]</sup>	
CB	169.7	110.1	36	45.3	20.53	42.5	37.8	-12.43	1.66
BC1	277.1	180.3	59.5	74	19.59	69	61.7	-11.83	1.66
BG1	213.3	139.5	46.8	57	17.89	52.6	47.5	-10.74	1.67
BC2-R	242.1	161.4	57.6	64.7	10.97	57.5	53.9	-6.68	1.65
BC3-L	244.4	171	69.5	65.3	-6.43	52.3	54.4	3.86	1.67
BC4-F	226.2	154.1	58.4	60.4	3.31	51.4	50.4	-1.98	1.67

[1] Central reaction measured by attached load cell at ultimate load  $P_u$ . (Both in kN)

[2] Experimental ultimate negative moment calculated according to Eq. 2-4. (kN.m)

[3] Theoretical ultimate negative moment calculated according to Eq. 2-6. (kN.m)

[4] Experimental ultimate positive moment calculated according to Eq. 2-5. (kN.m)

[5] Theoretical ultimate negative moment calculated according to Eq. 2-7. (kN.m)

[6] Moment redistribution calculated according to Eq. 2-8.

[7] Ratio between hogging and sagging moment redistribution.

The tensile strain in the tension reinforcement was almost zero up to the cracking load, however, as the cracking initiated in the concrete sections, the tensile stresses were become mainly carried by steel and FRP bars, and this engendered an abrupt increase in their tensile strains. From the cracking load to the yield load, in hogging or sagging regions, the increment rate of steel strain was approximately identical for all NSM beams, and the load–strain curves of steel exhibited almost a linear response; afterwards, the strain in steel was rapidly increased up to the ultimate load.

Up to yielding of tension steel, the tensile strain in the NSM-FRP bars were far below their ultimate strain. The lowest increment rate of tensile strain of FRP bars, between the cracking and yield loads, was reported in beam BC2-R; this was mainly due to the large area of strengthening material. On the other hand, the largest increment rate was reported in beam BG1; this could certainly be assigned to the fact that the elastic modulus of GFRP is significantly lower than that of CFRP. The increment rates of strain of CFRP bars in beams BC1, BC3-L and BC4-F were relatively similar, despite the strengthening length or the filling material type.

Inclinations of load–strain curves of NSM-FRP bars in the ultimate strength phase (from yield load to ultimate load of the beam) were appreciably higher than those of steel bars for the same

strengthened beam; which implies that the additional reinforcement provided by NSM-FRP controlled the flexural performance of beams up to failure.

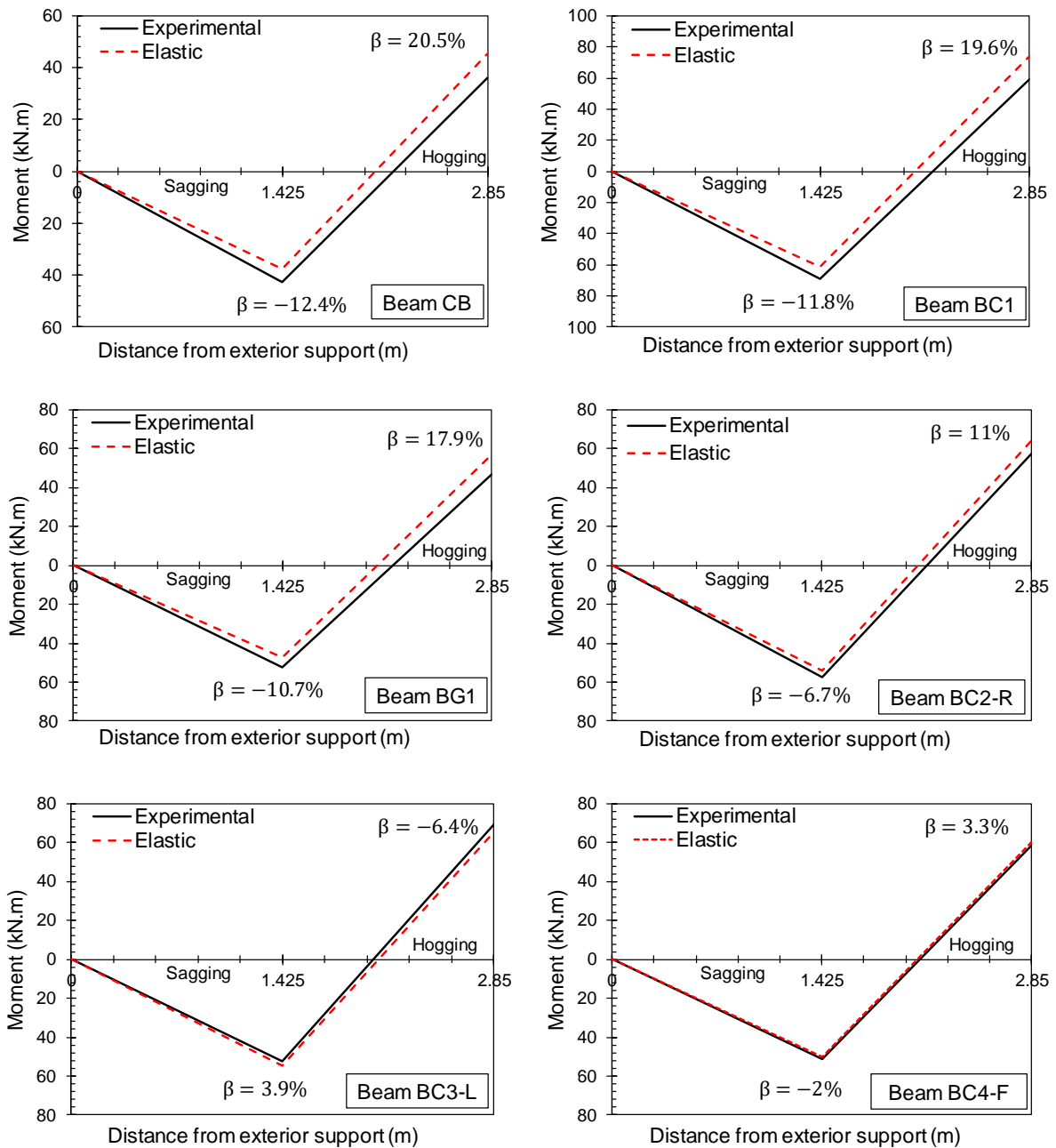


Figure 2-18 : Experimental and elastic bending moment of tested beams at the ultimate load.

#### 2.4.7.2 Load-strain response of compressive concrete

In both the central support and the mid-span regions, the compressive strain of concrete for beams strengthened with NSM-FRP bars was lower than that of the control beam for the same applied load, in particular for beams strengthened with CFRP rods (see Figure 2-19 and Figure 2-20). In general, the maximum compressive strain of concrete ranged from 0.21% to 0.31% and from 0.21% to 0.44% at the central support and mid-span, respectively.

A close look at the load–strain curves of concrete obtained at the central support indicates that all strengthened beams, except for BC2-R, exhibited a nearly linear attitude up to the peak load of beam, without clear signs of affection by cracking of concrete or yielding of tension steel.

On the other hand, in the mid-span section, the load–strain curves of concrete were about influenced by the cracking of concrete and the yielding of tension steel, except for beam BC3-L, where the load–strain response remained linear with no visual changes noted in the slopes, same as to that observed at the central support, due to the premature peeling off failure. However, regarding the rest of beams, i.e. BC1, BG1, BC2-R and BC3-F, it can be seen some changes in the slope of the concrete load–strain curves, and the nonlinear properties of concrete at compression can be noticed as well.

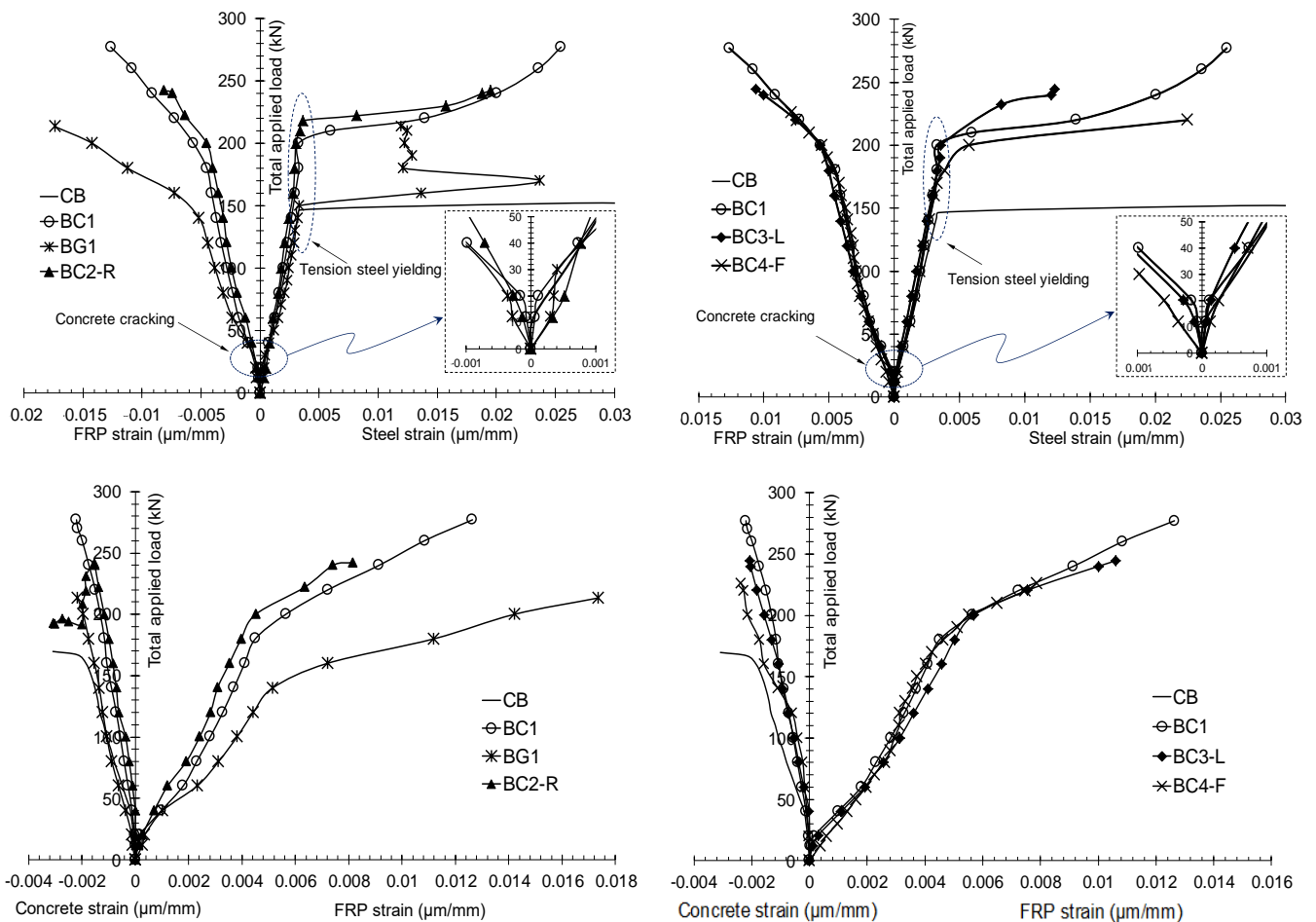


Figure 2-19 : Strains of tension steel bars, FRP bars and compressive concrete at central support.

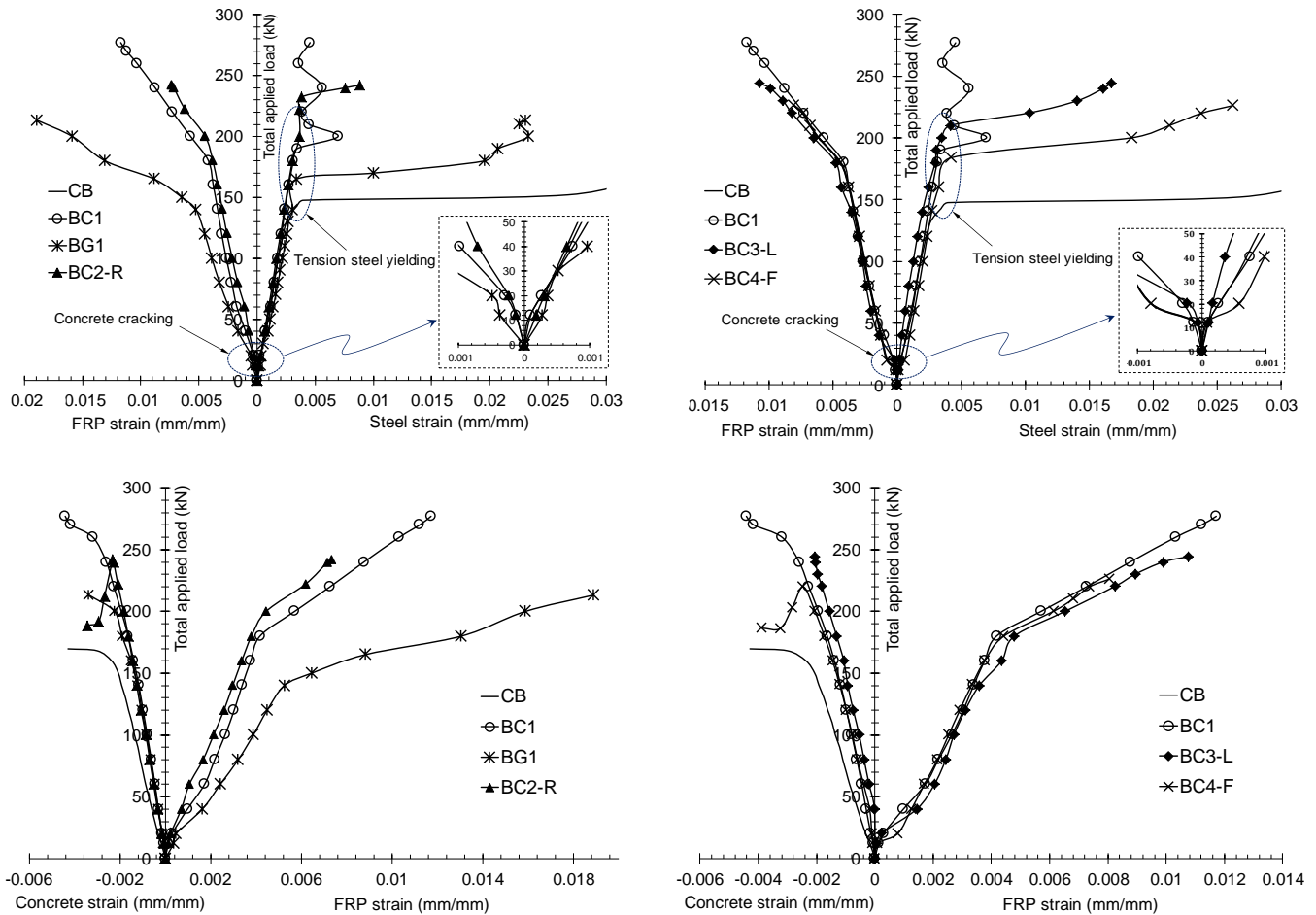


Figure 2-20 : Strains of tension steel bars, FRP bars and compressive concrete at right mid-span.

### 2.4.7.3 Longitudinal strain of NSM-FRP bars

Figure 2-21 illustrates the variation in the longitudinal tensile strain of the strengthening FRP bars for several load levels. The strains are presented for half of the beam length; from the exterior support of right span to the central support. The maximum strain values were reported in the central support and mid span sections, while the minimum strain values were those at the ends of FRP bars. The relationship between the maximum and minimum strains in each region, at low load levels, was relatively linear and it became non-linear as the loads approached the ultimate value. When the flexural strength capacity of the central support section was reached, the maximum measured strain of CFRP in beam BC1 was 0.0126, and about 59% of that strain occurred after the yielding initiation in the steel reinforcement. As for beams BG1, BC2-R, BC3-L and BC4-F, the above percentage was 67.1%, 28.3%, 46.4% and 41.2%, respectively. These results indicate that the contribution of NSM-FRP to the load carrying capacity of the beam is influenced by the strengthening scenario applied to the beam, as will be discussed in the next section.

### 2.4.7.4 Effectiveness of NSM-FRP bars

Table 2-7 presents the maximum recorded tensile strain of NSM-FRP bars ( $\epsilon_{FRP}^{max}$ ) obtained from the experimental investigations conducted on beams BC1, BG1, BC2-R, BC3-L and BC4-F. Table 2-7 indicates that increasing the CFRP reinforcement, or using mortar instead of resin



as a filling material, decreases the tensile strain of CFRP; i.e. decreases the probability of using more capacity of CFRP. The mobilization levels of NSM-CFRP rods ( $\varepsilon_{FRP}^{max}/\varepsilon_{FRP}^{ult}$ ) at peak load of beams BC1, BC2-R and BC4-F were respectively equal to 74%, 59%, 46% at the central support and to 69%, 52%, 46% at the mid-span. The reduction in using of CFRP bars in beam BC3-L as compared to those in beam BC1 was due to the insufficient strengthening length, which led to premature peeling off failure at both hogging and sagging regions; this failure mode usually restricts effectiveness of the strengthening materials. The mobilization level of CFRP bars in beam BC3-L was about 62% and 63% at the central support and mid-span, respectively. As a result of the mechanical characteristic of GFRP bars, the greater ( $\varepsilon_{FRP}^{max}/\varepsilon_{FRP}^{ult}$ ) among the tested beams was reported for beam BG1, which was about 92% at the central support and about 100% at the mid-span.

According to the American guideline ACI 440.2R [9], the debonding strain of NSM-FRP may vary from  $0.6 \varepsilon_{FRP}^{ult}$  to  $0.9 \varepsilon_{FRP}^{ult}$ , depending on many factors, such as the member dimensions, steel and FRP reinforcement ratios, and surface roughness of the FRP bar. This guideline recommends the maximum strain of NSM-FRP, for beam failed due to debonding, to be equal to  $\varepsilon_{FRP}^{max} = 0.7 \varepsilon_{FRP}^{ult}$  for calculating the nominal capacity of strengthened RC sections.

Hassan et al. [36] proposed two equations to estimate stress of NSMFRP bars in terms of the maximum tensile strength of concrete and resin. The two equations might be expressed in the following forms in order to calculate the  $\varepsilon_{FRP}^{max}$  in beams failed due to concrete cover separation and FRP-resin debonding, respectively:

$$\varepsilon_{FRP}^{max} = \frac{4mL_d f_{ct}}{G_1 d_{FRP} E_{FRP}} \quad (2-9)$$

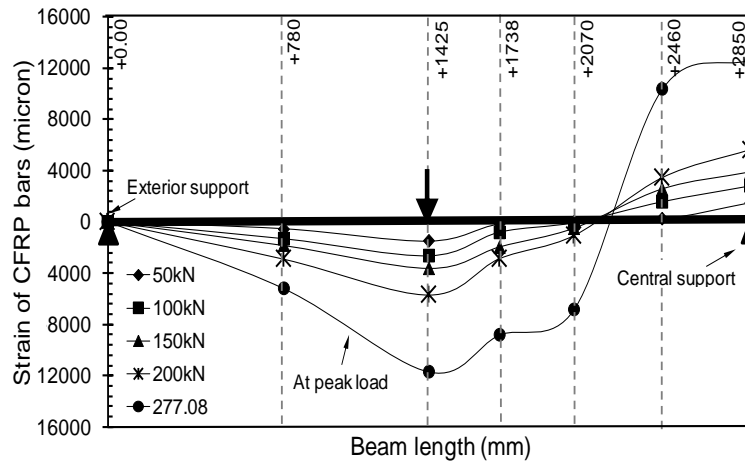
$$\varepsilon_{FRP}^{max} = \frac{4mL_d f_a}{G_2 d_{FRP} E_{FRP}} \quad (2-10)$$

where  $G_1$  and  $G_2$  = coefficients function determined according to the ratio of adhesive to the diameter of FRP bar,  $m$  = the coefficient of friction between adhesive and FRP bar,  $L_d$  = the embedment length of FRP bar,  $f_{ct}$  = the maximum tensile strength of concrete,  $f_a$  = the maximum tensile strength of resin,  $d_{FRP}$  = the diameter of FRP bar and  $E_{FRP}$  = the modulus of elasticity of FRP.

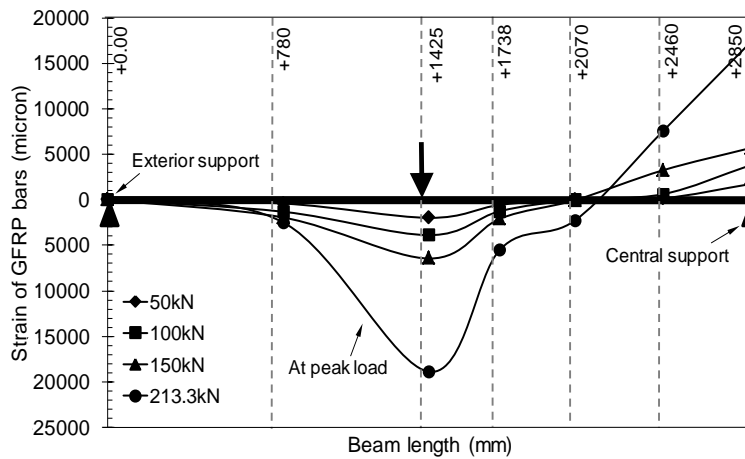
Comparing the values of  $\varepsilon_{FRP}^{max}$  obtained from the current tests with the above techniques is also presented in Table 2-7. It should be noted that these mentioned techniques were developed based only on simply supported NSM beams. In addition, the recommendation provided by the ACI 440.2R guideline is not applicable in the case of peeling off failure, i.e. beam BC3-L, while the both techniques did not take into account the failure mechanism of beam BC4-F. However, the debonding strain recommended by the ACI 440.2R guideline showed a good correlation with the experimentally measured ones, particularly for beams where the adhesive resin was used to bond the FRP bars.

## 2.5 Nonlinear analysis of strengthened sections

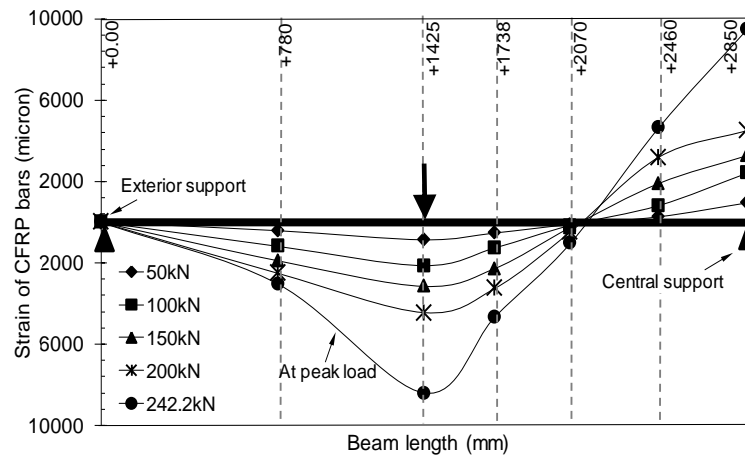
In this part, a nonlinear analysis of strengthened reinforced concrete (RC) beam sections was developed in order to construct and compare the theoretical moment-curvature ( $M - \phi$ ) curves of NSM-FRP bars beams with the experimental curves, furthermore, to predict the peak loads of tested beams.



a) Beam BC1

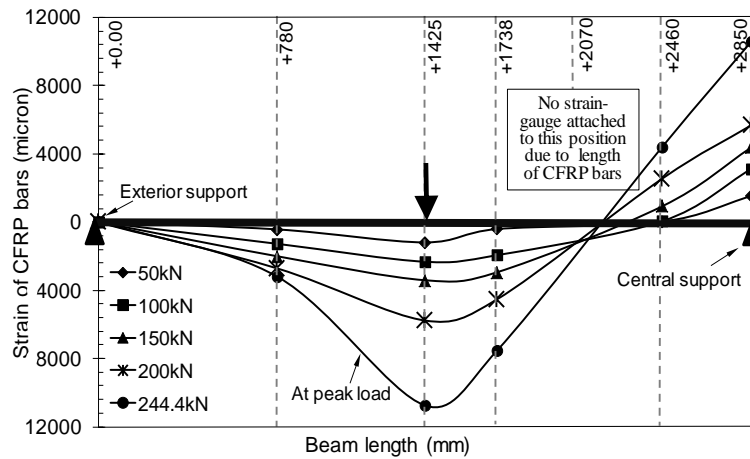


b) Beam BG1

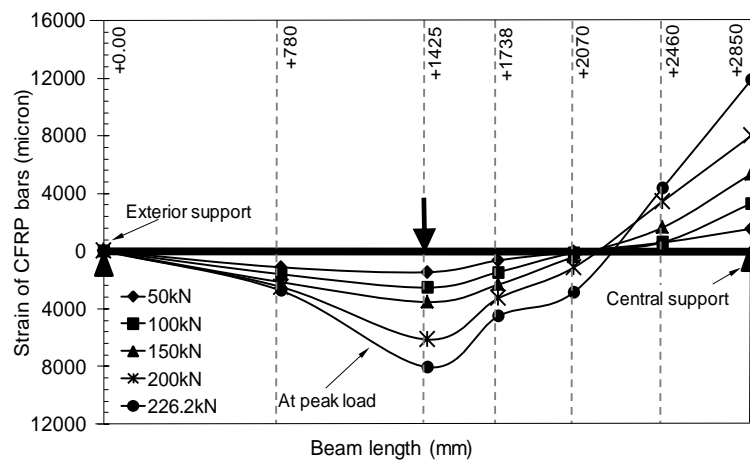


c) Beam BC2-R





a) Beam BC3-L



b) Beam BC4-F

Figure 2-21 : Variation in longitudinal strain of FRP bars at different loads.

This analytical approach employs the following assumptions: (1) the nonlinearity behaviors of concrete and steel as described by [37–39]; (2) the linear behavior of the strengthening material as described by [26]; (3) the tensile strength of concrete was neglected; (4) the differences between mechanical properties of concrete and filling material at the level of grooves were neglected, this because the resin/mortar occupies a small fraction of the beam cross-section [40]; (5) the collapse of the cross-section occurred when one of the ultimate strain of concrete or FRP was reached; (6) the moment–curvature ( $M - \varnothing$ ) curves were derived from the fundamental principles of equilibrium for the forces and moments acting on the cross-section of beam (Eq. 2-11) as well as the strain compatibility conditions for the used materials (Eqs. 2-12 and 2-15) as depicted in Figure 2-22.

This prediction model depends on the gradual increase of curvature and on the step-by-step numerical integration. The sectional-rotation ( $\varnothing$ ) considered as the control value, i.e. later, for any desired value of curvature ( $\varnothing_i$ ) within the admissible limit, the sectional-neutral axis ( $X_i$ ) will be computed from the compressed edge of concrete by applying the force (stress  $\times$  area) equilibrium equation (Eq. 2-11), thus with the known pair of ( $\varnothing_i, X_i$ ) the correspondent bending

moment  $M(\phi_i, X_i)$  established with relation to  $X_i$  could be estimated by using Eq. (2-16), where  $\sigma_c$  = the compressive strength of concrete,  $\sigma_s$  = the stress of steel in tension,  $\sigma'_s$  = the stress of steel in compression,  $\sigma_f$  = the stress of FRP bars,  $A_s$  = the area of tension steel,  $A'_s$  = the area of compressed steel and  $A_f$  = the area of FRP bars. This firstly requires to write all expressions of stresses of the cross-section in terms of  $\phi_i$  and  $X_i$ . It is worth mentioning that this prediction strategy has been analytically verified by [41] for prediction of  $M - \phi$  for ordinary RC beams. However, the analysis steps along with the constitutive laws of three materials (concrete, steel and FRP) are presented as follows:

$$F_{ci} + F'_{si} = F_{si} + F_{fi} \quad (2-11)$$

Where,  $F_{ci}$ ,  $F'_{si}$ ,  $F_{si}$  and  $F_{fi}$  are the compressive force of concrete, compressive force of steel, tensile force of steel and tensile force of FRP bars, respectively, at  $i$  operation ( $i = 1, 2, 3, \dots, n$ : number of operations to reach the beam failure).

$$\varepsilon_{ci} = \phi_i X_i \quad (2-12)$$

$$\varepsilon_{si} = \phi_i (d_s - X_i) \quad (2-13)$$

$$\varepsilon'_{si} = \phi_i (X_i - d'_s) \quad (2-14)$$

$$\varepsilon_{fi} = \phi_i (d_f - X_i) \quad (2-15)$$

Where,  $\phi_i$ ,  $X_i$ ,  $\varepsilon_{ci}$ ,  $\varepsilon_{si}$ ,  $\varepsilon_{fi}$  and  $\varepsilon'_{si}$  are the rotation of the cross-section, neutral axis of the cross-section, strain of the most compressed concrete fibers, strain of tension steel, strain of FRP bars, and strain of compression steel, respectively, at  $i$  operation. The symbols  $d_s$ ,  $d_f$  and  $d'_s$  refer to the effective depth of tension steel, FRP and compression steel, respectively.

$$M(\phi_i, X_i) = b \int_0^{X_i} \sigma_c(\phi_i, X_i) x dx + \sigma_s(\phi_i, X_i) A_s (d_s - X_i) + \sigma'_s(\phi_i, X_i) A'_s (X_i - d'_s) + \sigma_f(\phi_i, X_i) A_f (d_f - X_i) \quad (2-16)$$

- (1) The constitutive law of stress–strain relationship of concrete adopts the Kent-Scott-Park model [39] as given in Eq. (2-17); this model takes into account the confinement effects from the steel stirrups, where  $K$  and  $Z$  are, respectively, the strength and strain coefficients of the Kent-Scott-Park model;  $\varepsilon_c$  is the concrete strain;  $\rho'_s$  is the shear reinforcement ratio per unit volume of confined concrete;  $f'_y$  is the yielding strength of the steel stirrups;  $h''$  is the width of the confined concrete zone measured to the outside periphery of the steel stirrups; and  $s$  is the center to center spacing of the steel stirrups. Combined with Eq. (2-12); the compressed stress of concrete (Eq. (2-17)) could be simply written as a nonlinear function of  $\phi_i$  and  $X_i$  as given in Eq. (2-18).

$$\sigma_c = \begin{cases} K f'_c \left( \frac{2\varepsilon_c}{0.002K} \right) - \left( \frac{\varepsilon_c}{0.002K} \right)^2 & \varepsilon_c \leq 0.002k \\ K f'_c [1 - Z(\varepsilon_c - 0.002K)] & \varepsilon_c > 0.002k \end{cases} \quad (2-17)$$

In which,

$$K = 1 + \frac{\rho'_s f'_y}{f'_c} \text{ and } Z = \frac{0.5}{\frac{3+0.29f'_c}{145f'_c-1000} + 0.75\rho'_s \sqrt{\frac{h''}{s}} - 0.002K}$$

$$\sigma_c(\phi_i, X_i) = \begin{cases} K f'_c \left( \frac{2\phi_i X_i}{0.002K} \right) - \left( \frac{\phi_i X_i}{0.002K} \right)^2 & \phi_i X_i \leq 0.002K \\ K f'_c [1 - Z(\phi_i X_i - 0.002K)] & \phi_i X_i > 0.002K \end{cases} \quad (2-18)$$

(2) In previous relevant works published in the literature [eg. 40, 42], the steel reinforcement generally considered as a linear-perfectly plastic material, i.e. without including state of the steel reinforcement in the strain-hardening stage. In the current approach, however, the stress strain ( $\sigma_s - \varepsilon_s$ ) relationship of steel reinforcement was modeled by accommodating the nonlinear function proposed by Richard and Abbott [38], as given in Eq. (2-19), for the tension and compression steel. This expression allows modeling the hardening effect of steel by including its plastic modulus,  $E_{sp}$  (see Eq. (2-20)); hence, this can improve the accuracy of the analytical verification. In Eq. (2-19), the exponent  $n$  is a positive value, which controls the transition of stress–strain curve from elastic to plastic stage; it was taken  $n = 10$  and it has been determined by matching the Richard and Abbott curve with the tensile test curve of steel bars used in the present study, as shown in Figure 2-23. By substituting Eqs. (2-13) and (2-14) separately into Eq. (2-19), the stress of steel in tension and compression parts of the cross-section could be rewritten in terms of  $(\phi_i, X_i)$  as given in Eqs. (2-21) and (2-22), respectively.

$$\sigma_s = \frac{(E_s - E_{sp})\varepsilon_s}{\left[ 1 + \left( \frac{(E_s - E_{sp})\varepsilon_s}{f_y} \right)^n \right]^{\frac{1}{n}}} + E_{sp}\varepsilon_s \quad (2-19)$$

$$E_{sp} = \frac{\sigma(0.05) - f_y}{0.05 - \varepsilon_h} \quad (2-20)$$

Where;  $E_s$  = the elastic modulus of steel,  $\sigma(0.05)$  = the stress of steel at 0.05 strain, and  $\varepsilon_h$  = the strain of steel at the beginning of strain hardening zone.

$$\sigma_s(\phi_i, X_i) = \frac{(E_s - E_{sp})\phi_i(d_s - X_i)}{\left[ 1 + \left( \frac{(E_s - E_{sp})\phi_i(d_s - X_i)}{f_y} \right)^n \right]^{\frac{1}{n}}} + E_{sp}\phi_i(d_s - X_i) \quad (2-21)$$

$$\sigma'_s(\phi_i, X_i) = \frac{(E_s - E_{sp})\phi_i(X_i - d'_s)}{\left[1 + \left(\frac{(E_s - E_{sp})\phi_i(X_i - d'_s)}{f_y}\right)^n\right]^{\frac{1}{n}}} + E_{sp}\phi_i(X_i - d'_s) \quad (2-22)$$

(3) The mechanical behavior of strengthening material was considered linear-elastic up to failure, the stress–strain relationship of FRP bars is depicted in Figure 2-24 (see also Eq. (2-23)). By the same substituting methodology, applied above for concrete and steel, the expression of stress of FRP bars could be written in the form given in Eq. (2-24) by employing Eq. (2-16):

$$\sigma_f = E_f \varepsilon_f \quad (2-23)$$

$$\sigma_f(\phi_i, X_i) = E_f \phi_i(d_f - X_i) \quad (2-24)$$

(4) Pivotal to the calculation of the ultimate flexural capacity of the beam is estimation the failure occurrence. Beam failure was assumed to occur when the ultimate strain of either concrete or strengthening material was reached. The ultimate compressive strain  $\varepsilon_{cu}$  in concrete was assumed to be equal to 0.003, based on the compressive test results; this value is similar to the one suggested by the ACI 318-code [1]. The ultimate strain of FRP bars was taken according to the measured strains obtained from the experimental investigations (see Section 4.6), i.e. ( $\varepsilon_{FRP}^{max}$ ) equal to 0.0126, 0.0174, 0.0082, 0.0108 and 0.0079 for beams BC1, BG1, BC2-R, BC3-L and BC4-F, respectively.

(5) Once the ultimate moment of a strengthened section was obtained, the ultimate load capacity ( $P_u^{Th}$ ) of the beam could be determined through equilibrium considerations of the internal loads ( $M_s$  = sagging moment,  $M_h$ = hogging moment and  $v$  = shear) and external loads ( $P_e$  = external reaction,  $P_c$  = center reaction,  $P$  = applied load) of the beam, as illustrated in Figure 2-25 and expressed by Eq. (2-25).

$$P_u^{Th} = 2P = \frac{4}{L}(M_h + 2M_s) \quad (2-25)$$

Table 2-7 : Compression between experimental and analytical maximum strain of FRP bars

Beam	Failure mode	Maximum measured stain ( $\epsilon_{FRP}^{max}$ )				Computed stain		
		Over central support	$\frac{\epsilon_{FRP}^{max}}{\epsilon_{FRP}^{ult}}$	Mid-span	$\frac{\epsilon_{FRP}^{max}}{\epsilon_{FRP}^{ult}}$	ACI [9]	Hassan et. al [36]	
						(value) <sup>(2)</sup>	Central support (value) <sup>(3)</sup>	Mid-span (value) <sup>(3)</sup>
BC1	Pull out of the CFRP bars over the central support	0.0126 <sup>(1)</sup>	0.74	0.0117	0.69	0.0119 (0.94)	0.0103 (0.82)	0.0126 (1.08)
BG1	Pull out of GFRP bar over the central support followed immediately by tensile rupture of GFRP bar at mid-span sections.	0.0174 <sup>(1)</sup>	0.92	0.0189	1	0.014 (0.81)	0.0419 (2.4)	0.0512 (2.71)
BC2-R	Debonding at CFRP-resin interface in the hogging region	0.0082 <sup>(1)</sup>	0.59	0.0073	0.52	0.0098 (1.23)	0.0058 (0.71)	0.0071 (0.97)
BC3-L	Peeling off in hogging and sagging regions	0.0106	0.62	0.0108	0.63	N.A. <sup>(4)</sup>	0.008 (0.75)	0.007 (0.65)
BC4-F	Debonding at mortar-concrete interface in hogging and sagging regions	0.0079 <sup>(1)</sup>	0.46	0.0078 <sup>(1)</sup>	0.46	0.0119 (1.51-1.53)	0.0022 (0.28)	0.0026 (0.33)

(1) Experimental debonding strain. (2) Ratio of computed debonding strain according to recommendation of ACI 440.2R to the experimental debonding strain. (3) Ratio of computed strain according to Hassan et. al equations to the correspondent experimental strain. (4) N.A.: Recommendation of ACI is not applicable in case of peeling off failure, BC3-L.

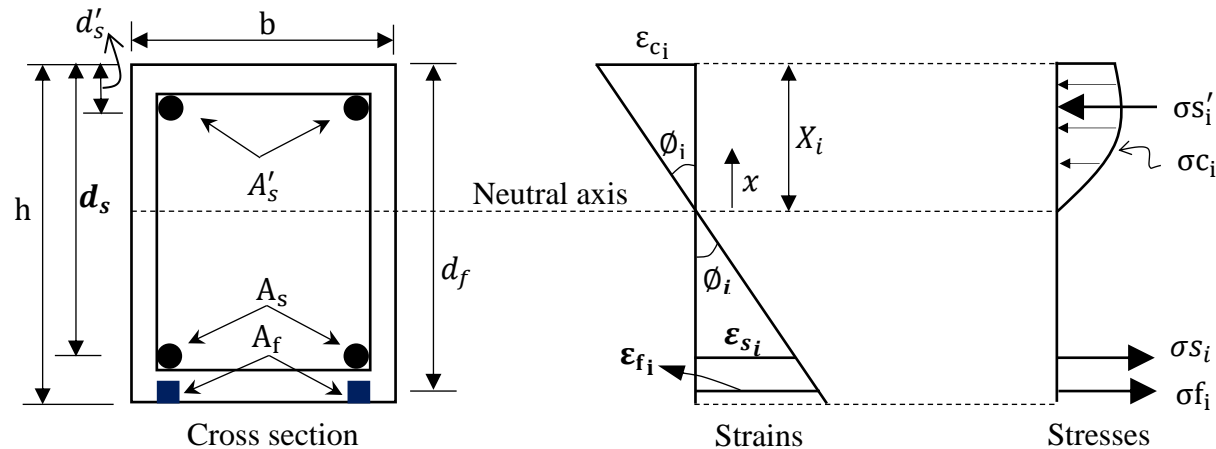


Figure 2-22 : Beam cross-section, strains and stresses.

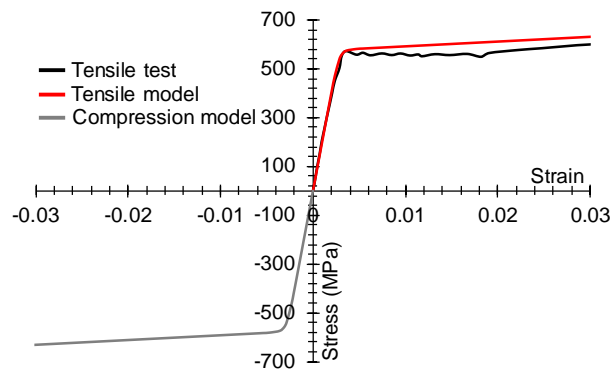


Figure 2-23 : Stress strain of steel

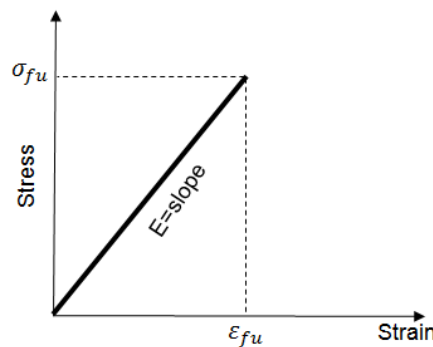


Figure 2-24 : Stress strain of FRP.

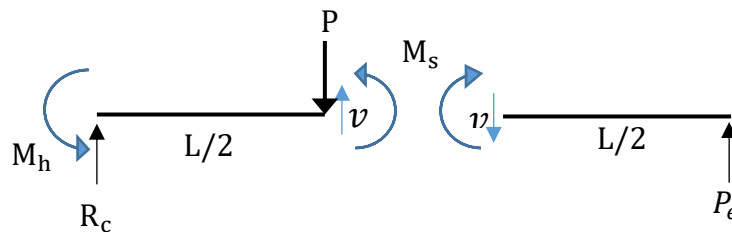


Figure 2-25 : External and internal loads.

Figure 2-26 compares the moment curvature diagrams of strengthened beams, as obtained from the above analytical model (Eq. (2-16)), with the experimental diagrams. The analytical ( $M - \emptyset$ ) curves were constructed with the help of the Excel program, and the increasing value of  $\emptyset$  was  $1 \times 10^{-6}$ . Figure 2-26 shows that the predicted ( $M - \emptyset$ ) curves are compatible with the experimental ( $M - \emptyset$ ) curves, which verifies accuracy of the reported test results. Table 2-8 presents a comparison between the computed and the experimental load-carrying capacity of strengthened beams. The ratio of analytical ultimate load  $P_u^{Th}$  to the experimental ultimate load  $P_u^{Exp}$  is close to one; the ratio  $P_u^{Th}/P_u^{Exp}$  for beams BC1, BG1, BC2-R, BC3-L and BC4-F was found equal to 0.93, 0.90, 1.01, 0.98 and 0.96, respectively. However, the analytical ultimate moment, load-carrying capacity and ratio of  $P_u^{Th}/P_u^{Exp}$  corresponding to the ultimate strain of NSM-FRP rods, obtained by adopting the ACI 440.2R [9] recommendation and by the equations developed by Hassan et al. [36], are presented for each beam in the tables accompanying Figure 2-26.

Chapter 2: Assessment of the flexural behavior of continuous RC beams strengthened with NSM-FRP bars, experimental and analytical study

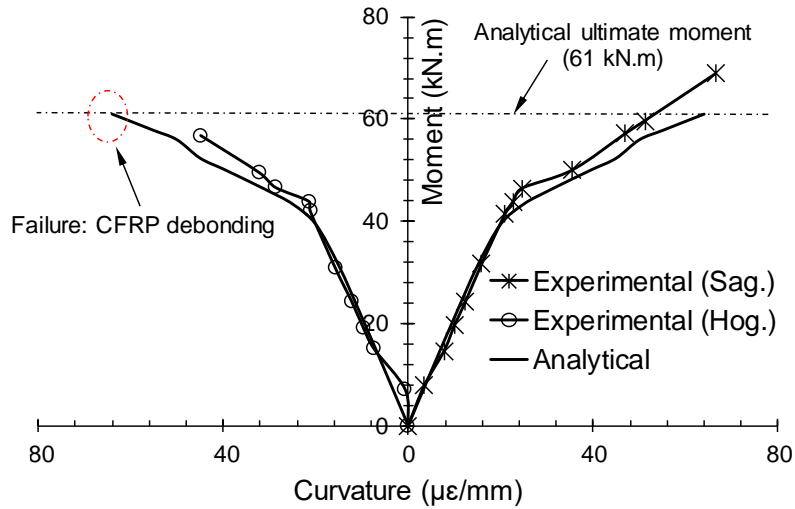
Method	FRP strain <sup>(1)</sup>	$M_u$ (kN.m) <sup>(2)</sup>	$P_u^{Th}$ (kN) <sup>(3)</sup>	$P_u^{Exp}$ (kN) <sup>(4)</sup>	$P_u^{TH}/P_u^{Exp}$
ACI 440.2R	0.0119	59.6	250.9	277.1	0.91
Hassan et al.	0.0103	56.3	237.1	277.1	0.86

(1) Computed ultimate strain of FRP according to [9] or [36].

(2) Analytical ultimate moment due to adopting (1).

(3) Analytical ultimate load.

(4) Experimental ultimate load.



a) Beam BC1

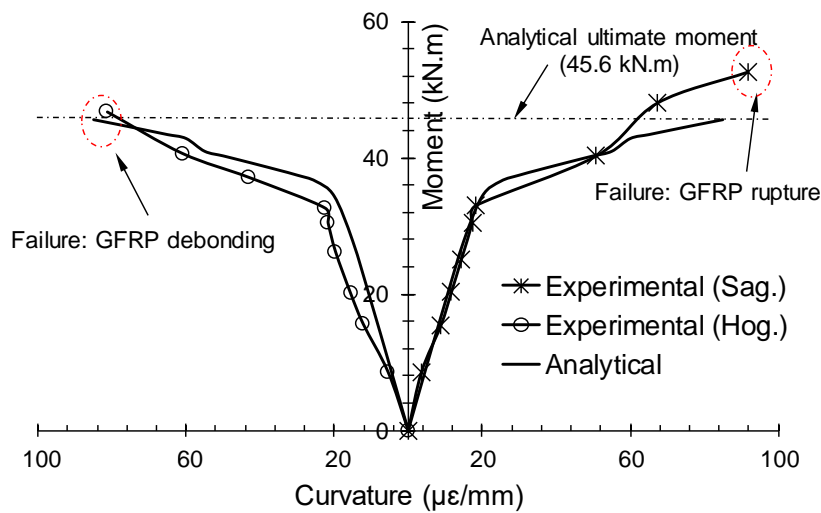
Method	FRP strain <sup>(1)</sup>	$M_u$ (kN.m) <sup>(2)</sup>	$P_u^{Th}$ (kN) <sup>(3)</sup>	$P_u^{Exp}$ (kN) <sup>(4)</sup>	$P_u^{TH}/P_u^{Exp}$
ACI 440.2R	0.014	43.4	182.7	213.3	0.86
Hassan et al.	0.0512	45.9	193.3	213.3	0.91

(1) Computed ultimate strain of FRP according to [9] or [36].

(2) Analytical ultimate moment due to adopting (1).

(3) Analytical ultimate load.

(4) Experimental ultimate load.

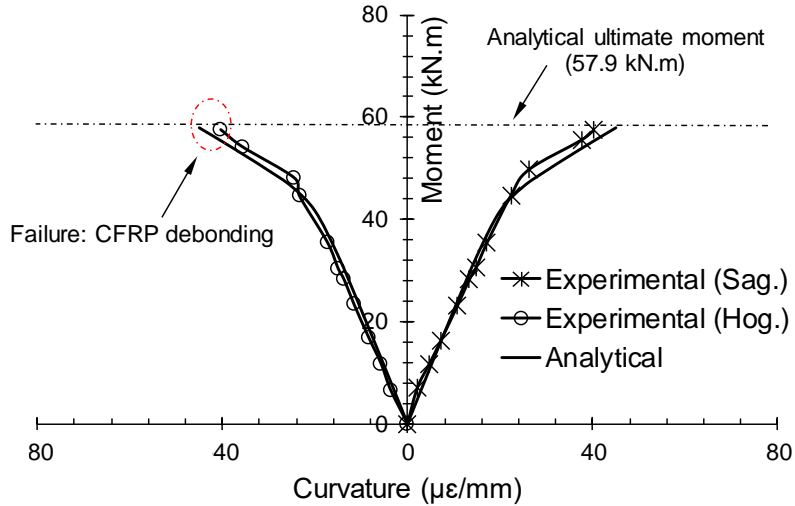


b) Beam BG1

Chapter 2: Assessment of the flexural behavior of continuous RC beams strengthened with NSM-FRP bars, experimental and analytical study

Method	FRP strain <sup>(1)</sup>	$M_u$ (kN.m) <sup>(2)</sup>	$P_u^{Th}$ (kN) <sup>(3)</sup>	$P_u^{Exp}$ (kN) <sup>(4)</sup>	$P_u^{TH}/P_u^{Exp}$
ACI 440.2R	0.0098	62.7	264	242.1	1.09
Hassan et al.	0.0058	50.4	212.2	242.1	0.88

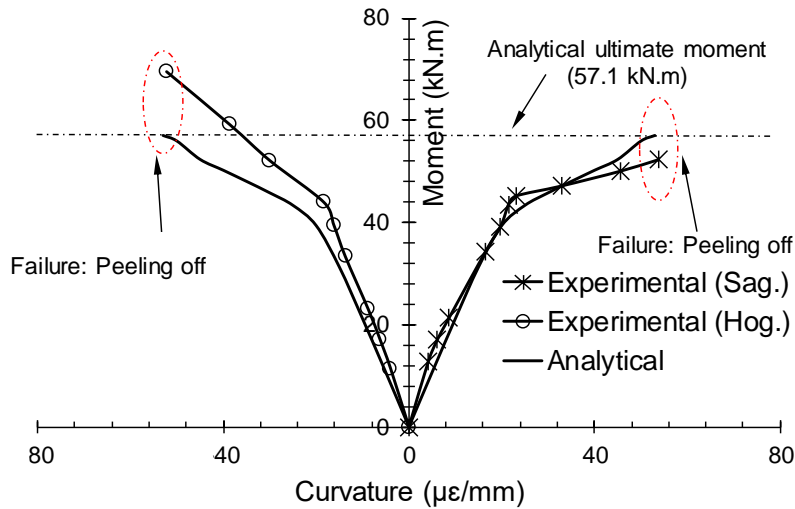
- (1) Computed ultimate strain of FRP according to [9] or [36].
- (2) Analytical ultimate moment due to adopting (1).
- (3) Analytical ultimate load.
- (4) Experimental ultimate load.



c) Beam BC2-R

Method	FRP strain <sup>(1)</sup>	$M_u$ (kN.m) <sup>(2)</sup>	$P_u^{Th}$ (kN) <sup>(3)</sup>	$P_u^{Exp}$ (kN) <sup>(4)</sup>	$P_u^{TH}/P_u^{Exp}$
ACI 440.2R	----	----	----	244.4	----
Hassan et al.	0.007	48.9	205.9	244.4	0.84

- (1) Computed ultimate strain of FRP according to [9] or [36].
- (2) Analytical ultimate moment due to adopting (1).
- (3) Analytical ultimate load.
- (4) Experimental ultimate load.



d) Beam BC3-L



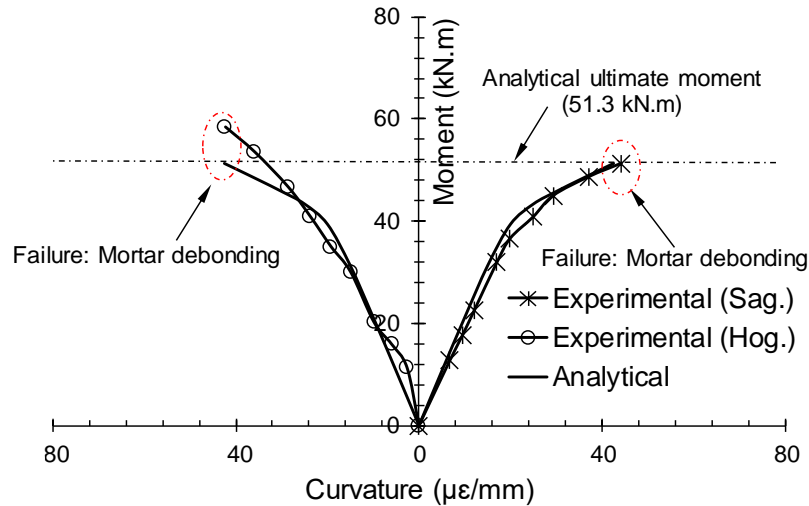
Method	FRP strain <sup>(1)</sup>	$M_u$ (kN.m) <sup>(2)</sup>	$P_u^{Th}$ (kN) <sup>(3)</sup>	$P_u^{Exp}$ (kN) <sup>(4)</sup>	$P_u^{Th}/P_u^{Exp}$
ACI 440.2R	0.0119	58.4	245.9	226.2	1.09
Hassan et al.	0.0022	27.3	114.9	226.2	0.51

(1) Computed ultimate strain of FRP according to [9] or [36].

(2) Analytical ultimate moment due to adopting (1).

(3) Analytical ultimate load.

(4) Experimental ultimate load.



e) Beam BC4-F

Figure 2-26 : Experimental and prediction of moment curvature diagrams of strengthened beam

Table 2-8 : Experimental and theoretical ultimate load of strengthened beams.

Beam	$P_u^{Exp}$	$P_u^{Th}$	$P_u^{Th}/P_u^{Exp}$
BC1	277.1	256.8	0.93
BG1	213.3	192	0.90
BC2-R	242.1	243.8	1.01
BC3-L	244.4	240.4	0.98
BC4-F	226.2	216	0.96

## 2.6 Conclusion

From the analysis and discussion of the experimental results provided in this research, the following conclusions can be outlined:

- The contribution of NSM-FRP to improving the load carrying capacity of statically indeterminate two-span RC beams was limited by the debonding of the FRP bars at the intermediate support or by the peeling off of the concrete covers. The improvement of the load carrying capacity of beams BC1, BG1, BC2-R, BC3-L and BC4-F was 63.3%, 25.7%, 42.7%, 44% and 33.3%, respectively, over the load carrying capacity of the control beam, CB.
- The debonding failure between NSM-CFRP bars and resin was observed earlier in beam BC2-R than in beam BC1 due to the increase in CFRP reinforcement. The load carrying capacity and ductility of BC2-R decreased by about 12.6% and 51.5%, respectively, with respect to those detected in BC1.
- Terminating CFRP bars before the inflection point caused the failure mode to change from debonding to premature peeling off of the concrete cover, which caused a 11.8%

decrease in the load carrying capacity of beam BC3-L and a 45.5% drop in the ductility as compared to those observed in beam BC1.

- Using mortar instead of resin formed less bonding strength at the concrete-filling material interface. Thus, the load carrying capacity of beam BC4-F decreased by about 18.4% and the ductility state by about 42.4% in comparison with beam BC1.
- Although the mechanical properties (tensile strength and elastic modulus) of GFRP were considerably lower than the mechanical properties of CFRP, using NSM-GFRP bars for strengthening continuous RC beams led to appreciable improvement in the load carrying capacity. The load carrying capacity of beam BG1 was about 77% of that of beam BC1, similarly, the ductility state showed about 24% improvement.
- The experimental results obtained showed that the moment redistribution achieved at the beam ultimate load varying with quantities and layout of the FRP bars. The beam strengthened with GFRP bars (i.e. BG1) showed approximately similar moment redistribution to its counterpart beam with CFRP bars (i.e. BC1), however, the both beams achieved degree of moment redistribution nearly similar to that in the un-strengthened beam, CB. On the other hand, redistribution of moment negatively affected in beams BC2-R, BC3-L and BC4-F by; increasing the CFRP ratio, decreasing the CFRP length or using mortar as filling material instead of epoxy resin, respectively.
- In comparison with the control beam, using the FRP bars increased the number of the cracks in hogging and sagging regions of the NSM continuous beams, whereas the average crack spacing and crack width were significantly decreased.
- Compared to control beam, utilizing the FRP bars in the NSM continuous beam reduced the tensile strains of the adjacent steel and the compressive strains of extreme concrete fibers for the same applied load.
- The non-linear analysis of strengthened section could be used to predict the moment–curvature diagram of NSM continuous beam, in addition to predict the beam ultimate load.

## 2.7 References

1. ACI. Building code requirements for structural concrete and commentary. American Concrete Institute, ACI 318-14, Farmington Hills, MI., September 2014.
2. Arduini M, Di Tommaso A, Nanni A. Brittle Failure in FRP plate and sheet bonded beams. *ACI Struct J* 1997;94(4):363–70.
3. Teng JG, Chen JF, Smith ST, Lam L. FRP strengthened RC structures. New York: Wiley; 2002.
4. Hollaway LC, Teng JG. Strengthening and rehabilitation of civil infrastructures using FRP composites. Cambridge, U.K.: Woodhead; 2008.
5. Salama ASD, Hawileh RA, Abdalla JA. Performance of externally strengthened RC beams with side-bonded CFRP sheets. *Compos Struct* 2019;212:281–90.
6. Ashour AF, El-Refaie SA, Garrity SW. Flexural strengthening of RC continuous beams using CFRP laminates. *Cem Concr Compos* 2004;26:765–75.

7. Aiello M. A., Valente L., and Rizzo A.. Moment Redistribution In Continuous Reinforced Concrete Beams Strengthened With Carbon-Fiber-Reinforced Polymer Laminates. *Mechanics of Composite Materials*, Vol. 43, No. 5, 2007.
8. Akbarzadeh H, Maghsoudi AA. Experimental and analytical investigation of reinforced high strength concrete continuous beams strengthened with fiber reinforced polymer. *Mater Des* 2010;31:1130–47.
9. ACI Committee 440. Guide for the design and construction of externally bonded FRP systems for strengthening concrete structures. ACI 440.2R-17, Farmington Hills, MI. 2017.
10. De Lorenzis L. Strengthening of RC structures with near surface mounted FRP rods PhD Thesis Italy: University of Lecce; 2002.
11. De Lorenzis L, Rizzo A, La Tegola A. A modified pull-out test for bond of near surface mounted FRP rods in concrete. *Compos B Eng* 2002;33(8):589–603.
12. Rosenboom O, Rizkalla S. Behavior of prestressed concrete strengthened with various CFRP systems subjected to fatigue loading. *J Compos Constr* 2006;10(6):492–502.
13. Almassri B, Kreit A, Al Mahmoud F, François R. Mechanical behaviour of corroded RC beams strengthened by NSM CFRP rods. *Compos B Eng* 2014;64:97–107.
14. Hassan T, Rizkalla S. Investigation of bond in concrete structures strengthened with near surface mounted carbon fiber reinforced polymer strips. *J Compos Constr* 2003;7(3):248–57.
15. Barros JA, Ferreira DR, Fortes AS, Dias SJ. Assessing the effectiveness of embedding CFRP laminates in the near surface for structural strengthening. *Constr Build Mater* 2006;20(7):478–91.
16. Al-Mahmoud F, Castel A, François R, Tourneur C. Strengthening of RC members with near-surface mounted CFRP rods. *Compos Struct* 2009;91:138–47.
17. Sharaky IA, Torres L, Comas J, Barris C. Flexural response of reinforced concrete (RC) beams strengthened with near surface mounted (NSM) fibre reinforced polymer (FRP) bars. *Compos Struct* 2014;109:8–22.
18. Almassri B, Al Mahmoud F, Francois R. Behaviour of corroded reinforced concrete beams repaired with NSM CFRP rods, experimental and finite element study. *Compos B Eng* 2016;92:477–88.
19. Reda RM, Sharaky IA, Ghanem M, Seleem MH, Sallam HEM. Flexural behavior of RC beams strengthened by NSM GFRP Bars having different end conditions. *Compos Struct* 2016;147:131–42.
20. Al-Mahmoud F, Castel A, François R. Failure modes and failure mechanisms of RC members strengthened by NSM CFRP composites–Analysis of pull-out failure mode. *Compos Part B Eng* 2012;43(4):1893–901.
21. De Lorenzis L, Nanni A. Bond between near-surface mounted fiber-reinforced polymer rods and concrete in structural strengthening. *ACI Struct J* 2002;99(2).
22. Al-Mahmoud F, Castel A, François R, Tourneur C. RC beams strengthened with NSM CFRP rods and modeling of peeling-off failure. *Compos Struct* 2010;92(8):1920–30.

23. Radfar S, Foret G, Saeedi N, Sab K. Simulation of concrete cover separation failure in FRP plated RC beams. *Constr Build Mater* 2012;37:791–800.
24. Sebastian WM, Vincent J, Starkey S. Experimental characterisation of load responses to failure of a RC frame and a NSM CFRP RC frame. *Constr Build Mater* 2013;49:962–73.
25. Dalfré G. M. and Barros J. A.O. Flexural Strengthening of RC Continuous Slab Strips Using NSM CFRP Laminates. *Advances in Structural Engineering* Vol. 14 No. 6 2011.
26. Al-Mahmoud F, Castel A, François R, Tourneur C. Effect of surface preconditioning on bond of carbon fiber reinforced polymer rods to concrete. *Cem Concr Compos* 2007;29(9):677–89.
27. Hanoon AN, Jaafar MS, Hejazi F, Abdul Aziz FNA. Energy absorption evaluation of reinforced concrete beams under various loading rates based on particle swarm optimization technique. *Eng Optim* 2017;49(9):1483–501.
28. Sabaua C, Popescu C, Sas G, Schmidt JW, Blanksvärd Th, Täljsten B. Strengthening of RC beams using bottom and side NSM reinforcement. *Compos B* 2018;149:82–91.
29. Lou T, Lopes SMR, Lopes AV. Effect of relative stiffness on moment redistribution in reinforced high-strength concrete beams. *Mag Concr Res* 2017;69:716–27.
30. Akiel MS, El-Maaddawy T, El Refai A. Serviceability and moment redistribution of continuous concrete members reinforced with hybrid steel-BFRP bars. *Constr Build Mater* 2018;175:672–81.
31. Mahroug MEM, Ashour AF, Lam D. Tests of continuous concrete slabs reinforced with carbon fibre reinforced polymer bars. *Compos B Eng* 2014;66:348–57.
32. Visintin P, Mohamad Ali MS, Xie T, Sturm AB. Experimental investigation of moment redistribution in ultra-high performance fibre reinforced concrete beams. *Constr Build Mater* 2018;166:433–44.
33. BS EN 1992-1-1:2004. Eurocode 2: Design of concrete structures - Part 1–1: General rules and rules for buildings. London, UK: British Standards Institution; 2004.
34. AS 3600-2009. Concrete structures. Sydney, Australia: Australia Standards; 2009.
35. Li L, Zheng W, Wang Y. Review of moment redistribution in statically indeterminate RC members. *Eng Struct* 2019;196:109306.
36. Hassan T, Rizkalla S. Bond mechanism of near-surface-mounted fiber reinforced polymer bars for flexural strengthening of concrete structures. *ACI Struct J* 2004;101(6):830–9.
37. Goldberg JE, Richard RM. Analysis of nonlinear structures. *ASCE J Struct Div – Proc Am Soc Civ Eng* 1963;89:333–51.
38. Richard RM, Abbott BJ. Versatile elastic-plastic stress-strain formula. *ASCE J Eng Mech Div – Proc Am Soc Civ Eng* 1975;101:511–5.
39. Scott BD, Park R, Priestley MJN. Stress-strain behavior of concrete confined by overlapping hoops at low and high strain rates. *J Am Concr Inst* 1982;79:13–27.
40. Yanga Yaqiang, Fahmyb Mohamed FM, Cuid Jing, Pana Zhihong, Shie Jianzhe. Nonlinear behavior analysis of flexural strengthening of RC beams with NSM FRP laminates. *Structures* 2019;20:374–84.

41. Simão PD, Barros H, Ferreira CC, Marques T. Closed-form moment-curvature relations for reinforced concrete cross sections under bending moment and axial force. *Eng Struct* 2016;129:67–80.
42. Sharaky IA, Torres L, Sallam HEM. Experimental and analytical investigation into the flexural performance of RC beams with partially and fully bonded NSM FRP bars/strips. *Compos Struct* 2015;122:113–26.



### CHAPTER 3 : EXPERIMENTAL AND NUMERICAL INVESTIGATION ON THE EFFECTIVENESS OF NSM AND SIDE-NSM CFRP BARS FOR STRENGTHENING CONTINUOUS TWO-SPAN RC BEAMS.

*Published in Journal of Building Engineering, <https://doi.org/10.1016/j.jobbe.2021.102723>*

---

This chapter aims to study the possibility of using the side-NSM-CFRP bars technique for strengthening continuous RC beams; furthermore, to study influence of steel ratio in the negative hogging region as well as the CFRP bars arrangement on the flexural behavior of continuous beams internally strengthened using the NSM and side-NSM techniques. This chapter comprises two parts: an experimental and numerical part. The experimental part includes testing an additional two continuous beams. In the numerical part, the computer software ABAQUS version was used to model the tested beams and to expand this research by implementing a parametric study. In total, twenty-one two-span beams were numerically (FE) simulated and investigated. The conventional perfect bond model (PBM), modified perfect bond with a reduction in the tensile strength of CFRP (MPBM), and the cohesive zone model (CZM) were considered to simulate the bond relationship between the CFRP and concrete substrate. The experimental and FE analysis results of the beams were primarily discussed in terms of the load-carrying and moment redistribution capacities.

**Experimental and numerical investigation on the effectiveness of NSM and side-NSM CFRP bars for strengthening continuous two-span RC beams**

Mohammad Abdallah\*<sup>1</sup>, Firas Al Mahmoud<sup>1</sup>, M. Idriss Tabet-Derraz<sup>1,2</sup>, Abdelouahab Khelil<sup>1</sup> and Julien Mercier<sup>3</sup>

<sup>1</sup>*Institut Jean Lamour, UMR 7198, CNRS, Université de Lorraine, Nancy, France*

<sup>2</sup>*EOLE laboratory, Department of Civil Engineering, Faculty of Technology, University of Tlemcen, Algeria*

<sup>3</sup>*Freyssinet, Paris, France*

---

**Keywords:** NSM; Side-NSM; strengthening; continuous RC beam; FEA.

**Abstract**

This paper aims to present and analyze the results of an ongoing research project on the use of NSM and side-NSM-FRP composites for the purpose of increasing the load-carrying capacity of two-span continuous RC beams. This research study comprises two parts; an experimental part and a finite element (FE) part. First, three large-scale two-span beams were statically investigated; one control beam and two other beams initially strengthened in bending with two 6 mm diameter CFRP bars. Second, a three dimensional (3D) FE model was developed, using the computer software ABAQUS, in order to predict the flexural performance of the tested beams and to investigate the influence of the models applied to the CFRP-resin-concrete interfaces. The results obtained indicated that the side-NSM-CFRP bars system is a convenient alternative to the conventional one for strengthening continuous beams. For some strengthening configurations, the side-NSM technique proved to be more efficient than the NSM technique, particularly when the CFRP bars were applied solely in the hogging region or the sagging regions. The moment redistribution of strengthened beams was negatively affected when the steel reinforcement ratio in the hogging region was increased. Nevertheless, the moment redistribution degree was significantly affected by the position and arrangement of the CFRP bars. The 3D-FE analysis developed with the cohesive zone model can capture the main aspects observed from the experiments.

**3.1 Introduction**

Strengthening or retrofitting of reinforced concrete (RC) structures is required due to material deterioration, upgrading initial designs or restoring the lost strength of structural members as a result of accidents or natural hazards such as earthquakes. The near surface mounted (NSM) is presently one of the most promising techniques used for strengthening and repairing RC beams. By this technology, the fiber reinforced polymers (FRPs), in different forms (rods, strips, laminate, etc.) could be embedded with an adhesive-epoxy resin or mortar into pre-sawn grooves in the bottom/top concrete covers of the beam

The NSM-FRP technique has proven its advantages in improving the flexural strength of RC beams as compared to the traditional externally bonding technique (EB-FRP) [1-3]. Comprehensive research studies have been conducted for the purpose of experimentally and numerically investigating the behavior of simply supported RC beams strengthened or repaired



with NSM-FRP bars [4-8]. The results of the experimental investigations indicated that the effectiveness of applying the NSM-FRP bars depends on several factors such as continuity, bonding length and characteristics of the FRP reinforcements along with the mechanical properties of the filling material. On the other hand, the numerical investigations revealed that predicting the flexural performance of beams strengthened with NSM-FRP composites, using computer programs based on the finite element (FE) analysis, depends on the constitutive model used for simulating the behavior of the interface between the FRP and filling material, as well as between the filling material and concrete. In other words, the proper simulation of the interaction between the strengthening system and concrete is essential for creating reliable finite element models (FEMs) for such strengthened structural members. To this end, the available approaches reported in literature can be classified into two main categories: (1) Perfect bond between the CFRP bars and concrete/filling material. This approach ignores the development of shear stresses in the interface materials, and the slip between the reinforcement elements and concrete. Almassri et al. [9] found out that by fully embedded the CFRP bars into concrete; the nonconventional failure mode of NSM beams, in particular the concrete cover separation, could be simulated. Sharaky et al. [10] on the other hand, indicated that the perfect bond between concrete and resin could give accurate FE results, compared to the experimental ones, for the beams that experimentally failed at the concrete-epoxy interface or the CFRP-epoxy interface, while less precise FE results were recorded for the beams failed due to concrete cover separation. (2) The interface contact; this approach is widely used in the literature [10-14] for simulating the probability of debonding between CFRP and concrete in the FE analysis. Shomali et al [14] found out that modeling the cohesive layer for the CFRP-concrete interface provides a good estimation of load-deflection behavior compared with the experimental results. However, in this formulation, the interaction behavior between CFRP and concrete can be simulated using a single bond-slip law to represent the overall response of the strengthening components. The bond-slip law is defined by three main parameters: (i) stiffness ( $k$ ); (ii) ultimate bond strength ( $\tau_m$ ); and (iii) ultimate slip ( $s_m$ ) at debonding.

However, as reported in previous study carried out by the authors on simply supported beams [15], the NSM system might be not feasible or even impossible to set up in several practical cases, starting from the imposed architectural constraints to those related to the dimensions and reinforcement of the beam itself. The same mentioned study showed that inserting the CFRP rods laterally, adjacent to the longitudinal steel bars inside the pre-cut grooves instead of the beam soffit, as so called the side near surface mounted (side-NSM) technique, could be a convenient method for addressing problems linked to the use of the classical NSM strengthening technique. The side-NSM beams exhibited improvement in the flexural capacity up to 59% over than that of the corresponding unstrengthened beam. In addition, the ductility performance of the side-NSM beams was better than that of the NSM beams. This was principally due to the application of the side technique which caused change or delay the nonconventional failure mode of beams such as CFRP bars pull-out. More recent, the side-NSM technique for strengthening medium-scale simply supported beams was investigated by Haddad et al [16]. The experimental results of their study confirmed efficiency of the side-NSM technique in improving the overall mechanical performances of RC beams, in particular for beams strengthened with CFRP strips at variable profiles (trapezoidal and parabolic profile).

In addition to the limitations of using the NSM technique for strengthening simply supported beams, the need for changing the strengthening position is essential for the continuous RC beams. This is because the continuous RC beams are commonly used in parking garages, overpasses and bridges. In these cases, the side surfaces of the beam are more accessible than the top or bottom surfaces; therefore, using the side-NSM technique for strengthening these types of structures is more feasible. However, in other cases, particularly in ordinary RC buildings, applying NSM-CFRP reinforcements on the top of the beam in the continuous connection cannot be easily performed due to the presence and continuity of the columns, while applying the CFRP reinforcements laterally, in the top part of the beam/connection, might be more rational. Furthermore, the RC beams used in residential buildings are usually narrow, which limits the amount of the FRPs that can be provided; hence, the side surfaces can be utilized along with the top or bottom faces to accommodate the appropriate amount of FRPs.

Although most *in-situ* RC beams are statically indeterminate constructions, the application of NSM/side-NSM techniques for strengthening indeterminate RC structures has hardly been studied, and the published design guidelines provide limited provisions regarding the NSM-FRP continuous beams. To date, the behavior benefits, failure mechanism and rate of strength gain of using the NSM/side-NSM CFRP bars strengthening techniques in continuous beams have scarcely been explored and still remain vague concepts to most researchers and practicing engineers. A very recent study [17] showed that, in addition to the above mentioned factors identified for strengthening simply supported beam, the effectiveness of using the NSM technique in continuous RC beam depends on the anchorage length of CFRP bars beyond the inflection point IP (zero moment point). As stated in [17], terminating the CFRP bars before the IP caused a change in the failure mode from debonding to premature detachment of the concrete cover, which caused a 12% decrease in the load-carrying capacity and a 46% drop in the beam ductility as compared to the values observed in a beam employed sufficient strengthening length. Furthermore, a significant reduction in the ability of the beam to redistribute moment at failure was observed. To the best of the authors' knowledge, there are no studies in the literature that have been performed for investigating the flexural behavior and failure mode of continuous RC beam strengthened with the side-NSM-CFRP bars.

The present paper concerns with the global performance of RC beams continuous over two spans of 2850 mm each, and strengthened in bending with CFRP bars by using the NSM and the side-NSM technique. In the initial sections of this paper, three full-scale of two-span beams were statically tested: one control beam and two strengthened beams. Several comparative studies were conducted between the tested beams in terms of failure mode and location, flexural capacity, ductility state and moment redistribution level. A three-dimensional (3-D) finite element model for each tested beam was then created using the ABAQUS software [18]. Three combinations of bond model and behavior of CFRP bars were investigated; namely: (i) the perfect bond with full tensile strength of the CFRP ( $\sigma_{FRP}^{max} = \sigma_{FRP}^{ult}$ ); (ii) the modified perfect bond with a reduction in the tensile strength of the CFRP ( $\sigma_{FRP}^{max} = \alpha\sigma_{FRP}^{ult}$ ), where  $\alpha < 1$ ; and (iii) the cohesive zone bond model. These models were initially used for exploring impacts of the different interfacial models on the prediction of the ultimate capacity of strengthened NSM and side-NSM beams. For comparison and validation purposes, the results of the FE beams

were compared with the experimental results. Accordingly, the cohesive zone model was adopted for assessing effects of the reinforcement ratio and arrangement, as selected parameters, on the flexural capacity and moment redistribution degree of continuous beams strengthened internally according to the NSM/side-NSM CFRP bars techniques.

### 3.2 Experimental work

#### 3.2.1 Experimental program

For the experimental investigation, three rectangular two-span RC beams were fabricated and tested. One beam was considered as a control beam, and the two others were initially strengthened with  $\varnothing 6$  CFRP bars. The beams were built at the same time with the same size, concrete and steel. The total length, span length, width and depth of each beam were 6000 mm, 2850 mm, 150 mm and 250 mm, respectively. The tested beam specimens were reinforced with the same reinforcement amount composed of two steel bars of 14 mm diameter in flexural and closed stirrups of 8 mm bar diameter in shear. The shear stirrups were uniformly spaced, at equal intervals of 100 mm, along the beam length, as illustrated in Figure 3-1. The clear concrete cover of the tested beams was maintained at a depth of 25 mm on all sides.

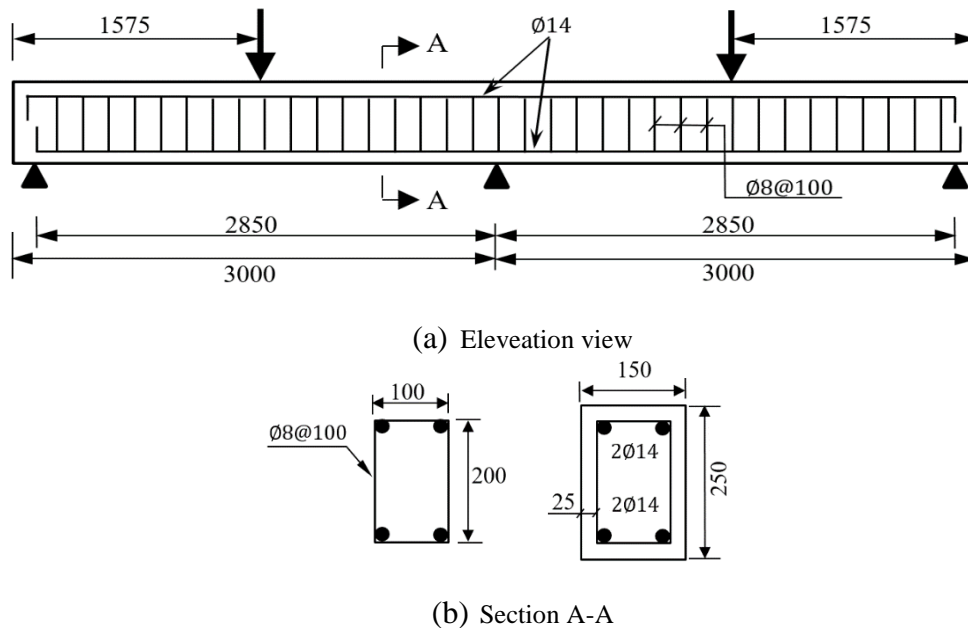


Figure 3-1 : Dimensions, steel layout as well as support and load arrangement of tested beams. (All dimensions are in mm)

Table 3-1 provides the designations and details of the control and strengthened beams. Note that beam CB-E was not reinforced with CFRP bars; it was tested for comparison purposes, while beams BC1-E-NSM and BC2-E-SNSM were strengthened with CFRP rods in the hogging and sagging regions. The only difference between the above strengthened beams was the position of the CFRP bars. The NSM technique was used for strengthening beam BC1-E-NSM and the side-NSM technique was used for strengthening beam BC2-E-SNSM. The CFRP bars in the hogging region of each beam were placed symmetrically about the central support; however, the CFRP bars in the sagging regions started from the face of the support without any anchorage over the external supports, as is clearly indicated in Figure 3-2. In order to avoid the

premature peeling off failure mode of beam, the strengthening length to the beam length ratio (SL/BL) was taken equal to 0.7 and 0.65 in the hogging and sagging regions, respectively, where SL is the distance between the end of the CFRP and the applied load and BL is the distance between the support and the applied load [6,15,19]. In addition, the area of CFRP reinforcement ( $A_f$ ) to the area of the tension steel reinforcement ( $A_s$ ) was selected equal to 18% [17] in both hogging and sagging regions. Therefore, the axial stiffness ratio [10] ( $1 + \frac{E_f \times A_f}{E_s \times A_s}$ ) of tested beams was approximately 1.16, where  $E_f$  and  $E_s$  are the Young's modulus of CFRP and steel, respectively. The letter (E) assigned to the beam's name is used to refer to the experimental testing of the beam.

The groove preparation applied procedure is described elsewhere [17]. Indeed, grooves measuring 15 mm in both width and depth were made, these dimensions are in accordance with the recommendations of the ACI 440.2R guideline [19], i.e. greater than  $1.5d_{CFRP}$ , in order to avoid premature collapse of the strengthening system. In beam BC1-E-NSM, the clear distance between the grooves was maintained at 55 mm, which is larger than twice the depth of the groove (30 mm). A surface sand coating was applied to modify the surface state of the initially smooth CFRP rods, as recommended by [20].

Table 3-1 : Test matrix and details of the control and strengthened beams

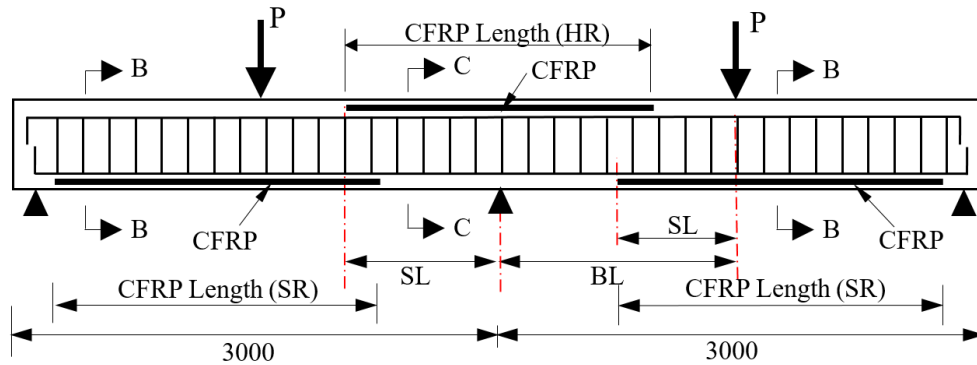
Beam	FRP Type	Hogging region strengthening			Sagging region strengthening			$A_f/A_s^{(3)}$	Filling Material	Strengthening technique
		No.	Length <sup>(1)</sup>	SL/BL <sup>(2)</sup>	No.	Length <sup>(1)</sup>	SL/BL			
CB-E	----	----	----	----	----	----	----	----	----	----
BC1-E-NSM	CFRP	2Ø6	2.0	0.70	2Ø6	2.3	0.65	18	Resin	NSM
BC2-E-SNSM	CFRP	2Ø6	2.0	0.70	2Ø6	2.3	0.65	18	Resin	Side-NSM

(1) Length in m; (2) SL: is the distance between end of the FRP bars and the external point load. BL: is the distance between the center support and the external point load; (3) Ratio (%) of the FRP reinforcement ( $A_f$ ) to the tension steel reinforcement ( $A_s$ ).

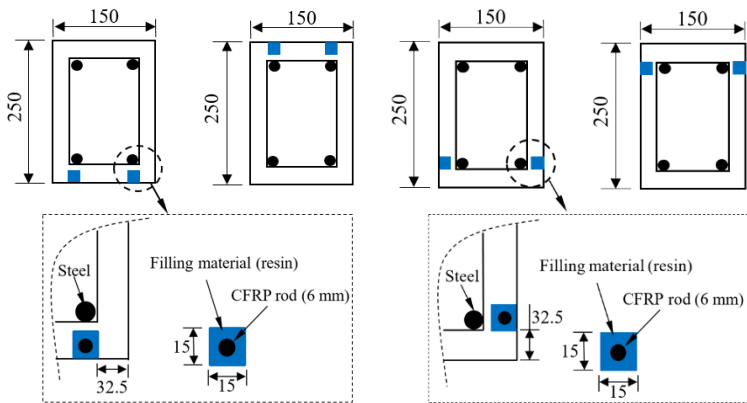
The characteristics of the steel reinforcement and concrete, which were utilized in the formulation of the tested beams, were determined experimentally. Three representative specimens of steel were tested in tension; the average yield strength and Young's modulus obtained were 572.6MPa and 192.5GPa, respectively. Eight specimens of hardened concrete cylinders, with dimensions of 160 mm in diameter and 320 mm in height, were tested in compression/tension at 28 days; the average compressive strength, tensile strength and elastic modulus obtained were equal to 39MPa, 3MPa and 29.2GPa, respectively. As indicated by the manufacturer, the tensile strength and modulus of elasticity of CFRP bars were 2800MPa and 165GPa, respectively.

The beams were tested to destruction under two concentrated loads separated by a distance of 2850 mm; one load ( $P$ ) was placed at middle of each span. Two hydraulic actuators were used to load the beams with a load capacity of 400 kN and an average loading speed 0.3 kN/s each. However, in order to measure the reaction at any level of the applied load, a 200 kN load cell was used as an intermediate support. Two vertical linear variable differential transducer (LVDTs) were used for each beam to monitor the vertical mid-span deflections, as presented in

Figure 3-3. In addition, eight strain gauges, each with a base length of 13 mm, were installed on the CFRP bars, at different positions for the purpose of measuring the variation in the longitudinal tensile strain of the strengthening bars.

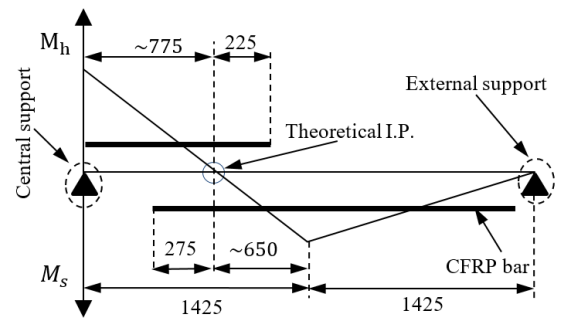


(a) Elevation view of the beam specimens and arrangement of the CFRP bars



(b) Cross section (B-B & C-C) in beam BC1-E-NSM

(c) Cross section (B-B & C-C) in beam BC2-E-SNSM



(d) Layout of CFRP bars in strengthened beams

Figure 3-2 : Beam specimens strengthened with CFRP rods. (All dimensions are in mm)



Figure 3-3 : Test setup and the instrumentations used for testing beams.



### 3.2.2 Main test results and discussion

Table 3-2 provides a summary of the main experimental results of the tested beams in terms of load-carrying capacity ( $P_u$ ), attained central reaction at the ultimate load level ( $R_c$ ), ultimate bending moment in the hogging ( $M_h^{Exp}$ ) and sagging ( $M_s^{Exp}$ ) regions, moment redistribution ratio ( $\beta$ ), ductility index ( $\mu$ ) and energy absorption capacity ( $E_{ab}$ ). The ductility index ( $\mu$ ) is defined as the ratio of the deflection at ultimate load to the deflection at which the steel starts yielding. The energy absorption capacity  $E_{ab}$  is calculated based on the area under the load-deflection curve (Figure 3-4). This section also presents and discusses the experimental results regarding the longitudinal strain, effectiveness and bond strength of the CFRP bars.

#### 3.2.2.1 Load deflection response

Figure 3-4 displays the relationship between the total applied load and the average deflection at the midspan points of the CB, BC1-E-NSM and BC2-E-SNSM specimens. It is clearly indicated from Figure 3-4 that the two strengthened beams exhibited a higher load-carrying capacity than that of the unstrengthened control beam, although the side-NSM system turned out to be slightly less efficient than the NSM system in enhancing the flexural strength capacity of RC beam. The beam BC1-E-NSM failed at a load of 277.1kN, which represents a 63.3% increase over the ultimate load of the control beam, CB-E (169.7kN), while the beam BC2-E-SNSM failed at a load of 250.1kN which corresponds to a 47.4% increase over than that of the control beam.

The reason behind the 9.7% reduction in the load-carrying capacity of beam BC2-E-SNSM with respect to that of beam BC1-E-NSM is attributed to the position of the CFRP bars. In the side strengthened beam, the CFRP bars were closer to the neutral axis, which led to decrease the effective depth of the tension reinforcements (CFRP and steel). As a result of that, the effective moment arm of the tensile reinforcements decreased within the beam cross section. It is worth mentioning that the reported percentage drop of the ultimate load for the continuous beam specimens tested in the present study is approximately similar to that previously reported for simply supported beams. As stated in [15], inserting the CFRP bars in the vertical sides of the beam instead of the bottom side decreases the load-carrying capacity by about 12.9%.

Compared with the conventional NSM system, Figure 3-4 also indicates that placing the additional CFRP reinforcement alongside the tension steel bars proved to increase the average midspan deflection of the strengthened beam, thereby improving the displacement ductility index ( $\mu$ ) and energy absorption capacity ( $E_{ab}$ ) (see Table 3-2). Among all the tested beams, beam BC2-E-SNSM exhibited the highest deflection ( $\delta_u = 58.9$  mm) at the ultimate load level ( $P_u$ ), while beam BC1-NSM presented the lowest value ( $\delta_u = 50.58$  mm). The midspan deflection of beam BC2-E-SNSM at the end of the test ( $\delta_f$ ) was 63.9 mm, whereas it was 50.6 mm for beam BC1-E-NSM. These two results of deflection are about 27.1% and 42.2% lower than the deflection at the midspan of the control beam ( $\delta_f = 87.6$ mm), respectively.

#### 3.2.2.2 Failure mode and cracks pattern

Figure 3-5 shows the classical flexural failure of control beam specimen; concrete crushing after yielding of tension steel.

The typical failure mode of beams strengthened with NSM/side-NSM CFRP bars was due to the yielding of the tension steel reinforcement followed by debonding of the strengthening components. The debonding failure of beam BC1-E-NSM was brittle as a consequence of the sudden pulling-out of the CFRP bars in the hogging region close to the central support, with minor concrete crushing at the applied load points, as illustrated in Figure 3-6. On the other hand, the debonding failure of beam BC2-E-SNSM was characterized by cracking of the epoxy-resin cover and fracture in the concrete at the hogging and sagging regions, with a high-intensity concrete crushing at the applied load points and minor concrete crushing at the central support, as depicted in Figure 3-7. In beam BC2-E-SNSM, longitudinal cracks appeared after yielding of the tension steel at the resin-concrete interface in the hogging and sagging regions. These cracks gradually merged to the adjacent flexural cracks which had previously formed in the regions close to the points of loading and over the central support. It should be noted that wide flexural cracks emerged in the hogging regions of beams CB-E and BC1-E-NSM before failure. These wide cracks were not observed in the case of beam BC2-E-SNSM.

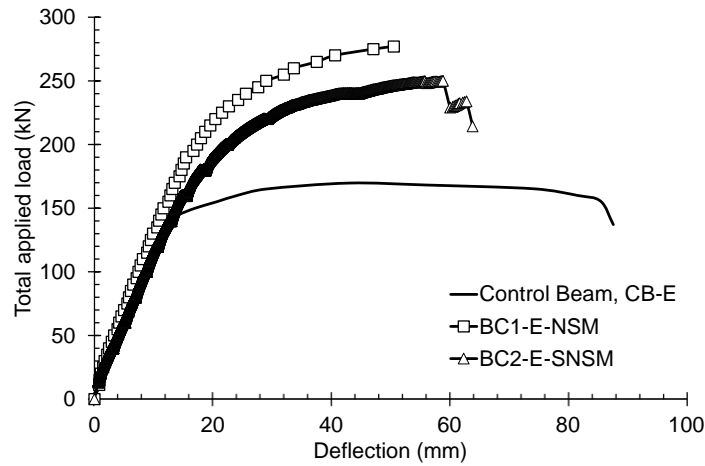


Figure 3-4 : Load deflection curve of tested beams

Table 3-2 : Main experimental results of control, NSM and SNSM beam.

Beam	Ultimate load ( $P_u$ )	Central support reaction <sup>[1]</sup> $R_c$	Flexural moment at hogging ( $M_h$ )			Flexural moment at sagging ( $M_s$ )			$\mu$ <sup>[7]</sup>	$E_{ab}$ <sup>[8]</sup>
			$M_h^{Exp}$ <sub>[2]</sub>	$M_h^{Th}$ <sup>[3]</sup>	$\beta$ (%) <sup>[6]</sup>	$M_s^{Exp}$ <sup>[4]</sup>	$M_s^{Th}$ <sup>[5]</sup>	$\beta$ (%) <sup>[6]</sup>		
			CB-E	169.7	110.1	36	45.3	20.53		
BC1-E-NSM	277.1	180.3	59.5	74	19.59	69	61.7	-11.83	3.3	10356.6
BC2-E-SNSM	250.1	166.6	59.3	67	11.49	59.4	55.6	-6.92	3.6	11242.1

(1) Central reaction measured by attached load cell at ultimate load  $P_u$ . (Both in kN); (2) Experimental ultimate negative moment calculated by:  $M_h^{Exp} = \frac{(P_u - 2R_c) \times L}{4}$ , where L is the beam length. (kN.m); (3) Theoretical ultimate negative moment calculated by:  $M_h^{Th} = \frac{3P_u L}{32}$ . (kN.m); (4) Experimental ultimate positive moment calculated by:  $M_s^{Exp} = \frac{(P_u - R_c) \times L}{4}$ . (kN.m); (5) Theoretical ultimate positive moment calculated by:  $M_s^{Th} = \frac{5P_u L}{64}$ . (kN.m); (6) Moment redistribution calculated by:  $\beta$  (%) =  $\left( \frac{M^{Th} - M^{Exp}}{M^{Th}} \right) \times 100\%$ . ; (7) Ductility index; (8) Energy absorption capacity. (KN.mm).

A small hammer and a chisel were cautiously used to check the constancy of the embedded CFRP bars in the hogging regions of beams BC1-E-NSM and BC2-E-SNSM. It was found that, in each beam, one extremity of the CFRP bars moved from its initial position towards the central

support, indicating that debonding failure occurred at the resin-CFRP interface. This displacement of CFRP bars was more conspicuous in beam BC1-E-NSM than in beam BC2-E-SNSM.

Interestingly, it was noticed that in the strengthened beams, the flexure cracks extended beyond the inflection points, i.e. zero moment points, as a result of applying the CFRP bars (Figure 3-6 and Figure 3-7). Compared to the control beam, the number of the cracks in beam BC1-E-NSM was higher by 200% and 62.5% in the hogging and sagging region, respectively; whereas the number of the cracks in beam BC2-E-SNSM was higher by 250% in the hogging region and 193.8% in the sagging region.

Table 3-3 presents the flexural crack width values in the hogging region over the central support of tested beams. The crack width was measured up to the beam's yielding load point using a special microscope with an accuracy of 0.05 mm. Table 3-3 demonstrates that the position of the additional reinforcement has limited impact on the development of the crack width. The measured crack width in beam BC2-E-SNSM was turned out to be slightly larger than that in beam BC1-E-NSM for the same applied load.

#### 3.2.2.3 Experimental bending moments and moment redistribution

The total applied load versus the bending moments of tested beams CB-E, BC1-E-NSM and BC2-E-SNSM at the critical sections (sagging and hogging regions) are presented in Figure 3-8a. The mid-span bending moment (sagging moment) is shown with a positive sign and the intermediate bending moment (hogging moment) is shown with a negative sign. In order to assess the amount of moment redistribution, the elastic bending moment was computed by considering a uniform flexural stiffness throughout the entire length of the beam. Moreover, the experimental bending moment at any level of the applied load was calculated based on equilibrium considerations of the beam using the measured central support reaction (Figure 3-8b). As can be observed in Figure 3-8b, the experimental central support reaction, in beams CB-E and BC1-E-NSM, suddenly shifted from the elastic reaction once the tension steel yielding load was reached. This involved more loads transferred to the external supports, leaving the central support with less load. The sudden shift could mainly be accredited to the wide cracks that appeared over or near to the middle support, which changed the reaction system of continuously supported beams (see section 2.2.2).

Furthermore, as can be seen in Figure 3-8a, the elastic model cannot accurately reflect the evolution of the actual bending moment. The actual bending moment of the beams at a low load level showed a nearly linear development; however, when the load increased, the actual bending moment exhibited a different evolution from the elastic moment with nonlinear behavior. At the ultimate load, the experimental negative and positive moments of the tested beams were, respectively, lower and larger than the elastic moments, indicating moment transfer occurred from the inner support towards the midspan. In general, among the tested beams, the experimental bending moment values of the side-NSM beam (i.e. BC2-E-SNSM) were the closest to the elastic bending moment values. For example, the experimental hogging moment at the failure load, calculated from the measured central support reaction of beams CB-E, BC1-E-NSM and BC2-E-SNSM, were 36kN.m, 59.5kN.m and 59.3kN.m, respectively. These results



Chapter 3: Experimental and numerical investigation on the effectiveness of NSM and side-NSM CFRP bars for strengthening continuous two-span RC beams.

represent 79.47%, 80.41% and 88.51% of the calculated elastic moment of 45.3kN.m (for CB-E), 74kN.m (for BC1-E-NSM) and 67kN.m (for BC2-E-SNSM).



(a) Central support

(b) Left span

(c) Right span

Note: (1)Number of the cracks in the hogging region: 8; (2)Number of the cracks in the sagging region (maximum number): 16

Figure 3-5 : Failure mode of control beam, CB-E



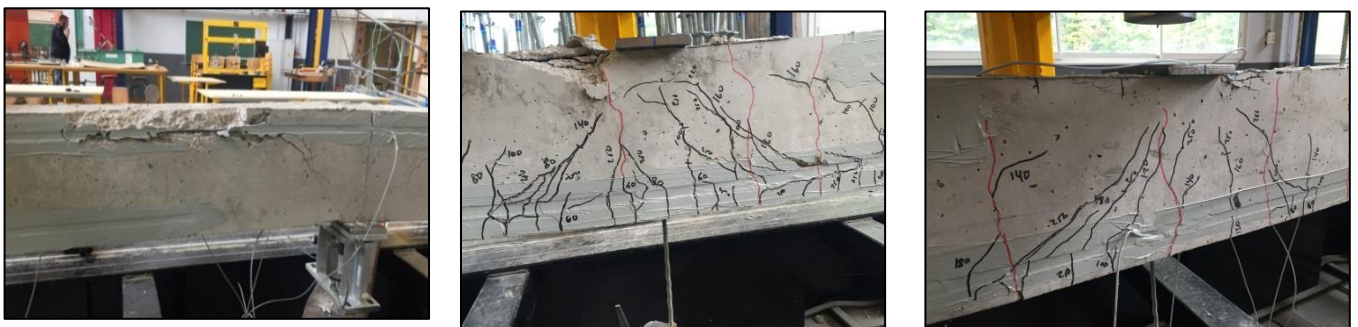
(a) Central support

(b) Left span

(c) Right span

Note: (1)Number of the cracks in the hogging region: 24; (2)Number of the cracks in the sagging region (maximum number): 26

Figure 3-6 : Failure mode of beam BC1-E-NSM



(a) Central support

(b) Left span

(c) Right span

Note: (1)Number of the cracks in the hogging region: 28; (2)Number of the cracks in the sagging region (maximum number): 47

Figure 3-7 : Failure mode of beam BC2-E-SNSM

The moment redistribution could refer to the ability of an indeterminate RC structure to form a sufficient number of hinges under increasing the applied load. These hinges usually allow

transferring the moment in accordance with their formation and position. In this study, the capacity of the tested beams to redistribute moment was assessed and presented in Table 3-2. The control beam and the beam strengthened with NSM-CFRP bars exhibited almost similar trends to redistribute moment. They failed, however, at different loads. On the other hand, in accordance with the reinforcement ratio adopted in this experimental program, it was found that placing the CFRP bars laterally, adjacent to the steel reinforcement using the side-NSM technique, decreases the moment redistribution capacity of the beam. The moment redistribution ratio ( $\beta$ ) of the control beam was 20.5% at central support and -12.4% at midspan; however, beams BC1-E-NSM and BC2-E-SNSM had respectively moment redistribution of 19.6% and 11.5% at the central support, and -11.8% and -6.9% at mid-span.

Table 3-3 : Crack width of tested beams at different load levels.

CB-E		BC1-E-NSM		BC2-E-SNSM	
$P_t$ (kN)	$w_{cr}$ (mm)	$P_t$ (kN)	$w_{cr}$ (mm)	$P_t$ (kN)	$w_{cr}$ (mm)
30	0.2	30	0.08	30	0.15
50	0.35	50	0.1	50	0.21
70	0.53	70	0.15	70	0.26
90	0.62	90	0.25	90	0.3
110	0.75	110	0.33	110	0.43
130	1.35	130	0.42	130	0.55
150	3.1	150	0.53	150	0.61
-----	-----	170	0.62	170	0.76

#### 3.2.2.4 Longitudinal strain and effectiveness of the CFRP bars

Figure 3-9a and Figure 3-9b show the variation in the longitudinal tensile strain of the CFRP bars for beams BC1-NSM and BC2-SNSM respectively, at different load levels. The strains are presented for half of the beam length, i.e. from the exterior support of the right span to the interior support. Owing to the configuration of the CFRP bars in beam BC1-E-NSM, it was expected that the CFRP bars in the critical sections would demonstrate a high strain response at the ultimate load level in comparison with the CFRP bars in beam BC2-E-SNSM. Such anticipation has not been exhibited by beam BC1-E-NSM, as can be discerned from Figure 3-9. Although the two strengthened beams failed at different loads, the maximum measured tensile strain of CFRP bars over the central support, in beams BC1-E-NSM and BC2-E-SNSM, were found equal to 0.0126 mm/mm and 0.0123 mm/mm, respectively. This can be justified by the fact that the failure of the two strengthened beams was primarily due to the collapse of the strengthening systems (i.e. debonding failure). However, regarding the remaining strain-gauges attached to the longitudinal direction of CFRP bars, the CFRP strains (Figure 3-9) measured in beam BC1-E-NSM at the ultimate load level exhibited a relative increase in comparison with the CFRP strain measured in beam BC2-E-SNSM for the same position of the gauge. The main observation pertained to the strain value at the elastic inflection point, i.e. at a length of 2070 mm from the external support. Indeed, at the ultimate load level, the increase in the tensile strain of CFRP bars at that point was clearly visible in beam BC1-E-NSM compared to that reported in beam BC2-E-SNSM. This increasing in the ultimate strain could be imputed to the amount of moment redistribution as well as to the wide cracks that formed before the beam's failure;

these cracks changed the location of the inflection point in beam BC1-E-NSM to a new position beyond the elastic one.

The effectiveness of the CFRP bars for strengthening continuous RC beams was evaluated for beams BC1-E-NSM and BC2-E-SNSM on the basis of the utilization level ( $\frac{\epsilon_{CFRP}}{\epsilon_{CFRP}^{ult}}$ ) in the critical sections, as reported in Table 3-4. As can be noticed from Table 3-4, none of the specimens reached the ultimate CFRP rupture strain (0.017 mm/mm) and the reported debonding strain was marginally affected by the position of CFRP reinforcement. The ( $\frac{\epsilon_{CFRP}}{\epsilon_{CFRP}^{ult}}$ ) of NSM-CFRP bars at the ultimate load was 74.3% at central support and 68.9% at midspan section. On the other hand, the ( $\frac{\epsilon_{CFRP}}{\epsilon_{CFRP}^{ult}}$ ) of side-NSM-CFRP bars at the ultimate load was about 72.2% at central support and 69.8% at midspan section.

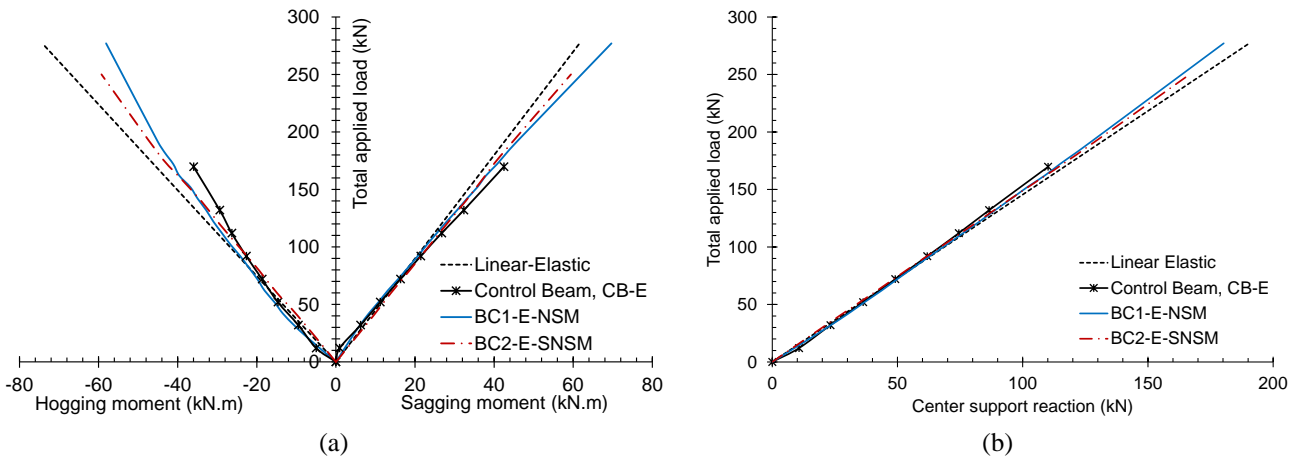


Figure 3-8 : Total applied load versus (a) bending moment; (b) central support reaction

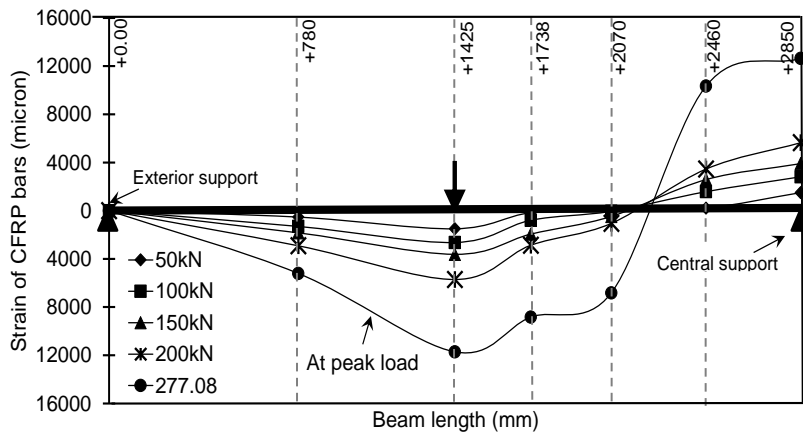
### 3.2.2.5 Bond analysis of the CFRP bars

In general, the bond strength of NSM-FRP bars ranges from 3.5MPa to 20.7MPa [21-22], which is influenced by many factors such as the groove size, section type, surface state and development length of the CFRP bars as well as by the mechanical properties of the filling material. The ACI 440.2R guideline [19], for instance, recommends the average bond strength as 6.9MPa for calculating the development length of the NSM-FRP bars. However, in the present paper, the experimental average bond stress ( $\tau$ ), between two consecutive strain gauges, was calculated according to Eqs. (3-1) and (3-2) by taking into account the measured experimental strain (see Figure 3-9), where  $i$  refers to number of the strain gauge and  $\sigma$ ,  $\epsilon$ ,  $E_{CFRP}$ ,  $l$ ,  $d_{CFRP}$ ,  $A_{CFRP}$  are, respectively, the tensile stress, strain, modulus of elasticity, length, diameter, and area of the CFRP bars.

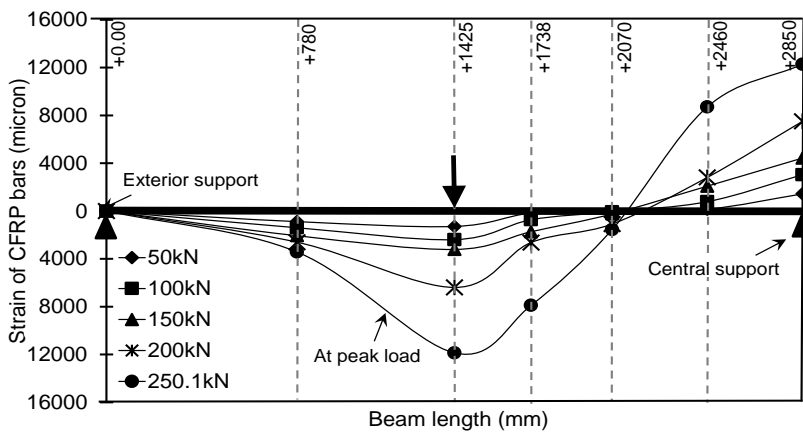
$$\sigma_{((i+1)-i)} \times A_{CFRP} = \tau_{((i+1)-i)} \times (l_{(i+1)} - l_i) \times d_{CFRP} \times \pi \quad (3-1)$$

$$\tau_{((i+1)-i)} = \frac{(\epsilon_{(i+1)} - \epsilon_i) \times E_{CFRP} \times d_{CFRP}}{4 \times (l_{(i+1)} - l_i)} \quad (3-2)$$

Figure 3-10 indicates that the bond stress increases with the applied load. The maximum values of  $\tau$  reported for beams BC1-E-NSM and BC2-E-SNSM were 6.4MPa and 5.6 MPa, respectively. These values were recorded at the same location of failure in the beam, i.e. in the hogging regions between the central support and end of the CFRP composite. The slight decrease in the  $\tau$  value at the ultimate load for beam BC2-E-SNSM with respect to the  $\tau$  value for beam BC1-E-NSM could be assigned to the drop in the measured strains resulting from the change of the position of CFRP bars, as discussed in the previous section.

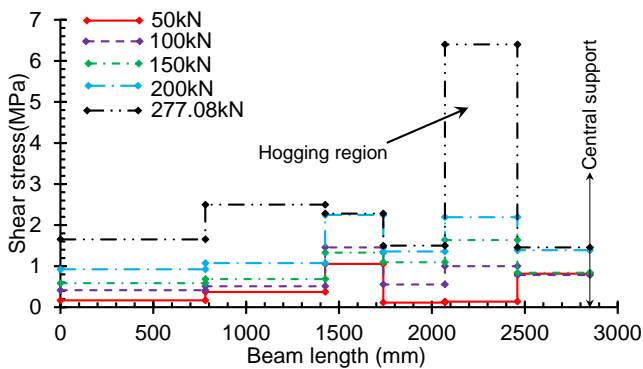


(a) BC1-E-NSM

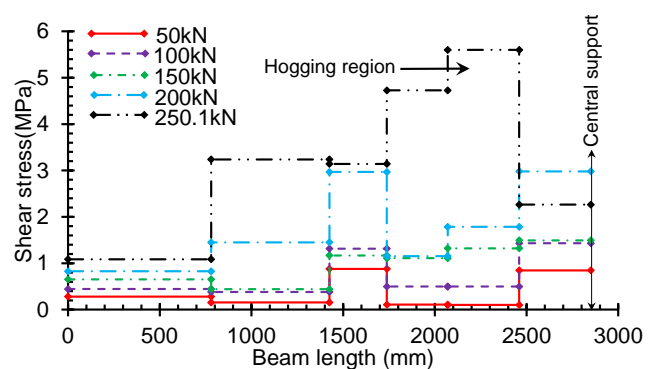


(b) BC2-E-SNSM

Figure 3-9 : Variation in longitudinal strain of FRP bars at different loads.



(a) BC1-E-NSM



(b) BC2-E-SNSM

Figure 3-10 : Experimental average shear stress



Table 3-4 : Tensile strains of CFRP bars at different load levels.

Load (kN)	BC1-E-NSM				BC2-E-SNSM			
	Central support		Mid-span		Central support		Mid-span	
	$\epsilon_{CFRP}$ (Micron)	$\frac{\epsilon_{CFRP}}{\epsilon_{CFRP}^{ult}}$	$\epsilon_{CFRP}$ (Micron)	$\frac{\epsilon_{CFRP}}{\epsilon_{CFRP}^{ult}}$	$\epsilon_{CFRP}$ (Micron)	$\frac{\epsilon_{CFRP}}{\epsilon_{CFRP}^{ult}}$	$\epsilon_{CFRP}$ (Micron)	$\frac{\epsilon_{CFRP}}{\epsilon_{CFRP}^{ult}}$
50	1500	0.088	1497.5	0.088	1493	0.088	1290	0.076
100	2812	0.165	2640	0.155	3039	0.179	2393	0.141
150	3907	0.230	3628	0.213	4435	0.261	3207	0.189
200	5647	0.332	5707	0.336	7510	0.442	6389	0.376
250.1	9948	0.585	9399	0.553	12278	0.722	11862	0.698
277.1	12639	0.743	11717.5	0.689	----	----	----	----

### 3.3 Numerical investigation

The objective of this section is to utilize the FE package ABAQUS version 6.13 [18] for creating an efficient and reliable 3D model that can simulate and predict the behavior of continuous RC beams strengthened internally with CFRP bars. In addition, for investigating the effect of using different models of CFRP/resin-concrete interface on predicting the ultimate strength capacity of strengthened beams.

The ABAQUS-standard software uses a non-linear procedure that is suitable for FE analysis and computer-aided engineering. FE failure analysis was performed to model the tested three beams; one of the beams was control beam (CB-E) and the other two beams, namely BC1-E-NSM and BC2-E-SNSM, were strengthened with CFRP bars using the NSM and side-NSM technique, respectively. Dynamic explicit analysis in ABAQUS with the quasi-static approach was employed by applying a very slow loading in order to make the model converges to the static solution. The dynamic analysis is more commonly used than the static analysis in investigating the highly non-linear behavior of cohesive contact in ABAQUS. This type of analysis also been applied to other problems such as external CFRP strengthening impact [23], cracks and failure of concrete [24] and push out tests simulations [25]. The accuracy and reliability of the results of the FE dynamic analysis approach were checked for each model during the loading process by comparing the total kinetic energy with the total internal energy. As recommended in the ABAQUS manual [26]; the ratio of the kinetic energy to the internal energy must be less than 5%.

According to the experimental tests, both the geometric and material nonlinearity were considered in the numerical solutions. The analysis was operated by means of the displacement control method in order to overcome the convergence difficulties as well as the rigid body modes when two bodies are disconnected in contact pairs [27].

The RC beam is composed of four components: concrete, steel reinforcement, CFRP bars and epoxy-resin adhesive. These components were modeled as separate parts; however, the constitutive laws that are described in the following sections allow identifying their interactions.

### 3.3.1 Material properties

#### 3.3.1.1 Concrete

The classical concrete damage plasticity (CDP) available in ABAQUS [18] library was adopted to model the complex nonlinear behavior of concrete in the simulation test of RC beams. This material model, which has widely been used, provided accurate results [28-30]. The CDP offers the best modeling of the real behavior of concrete and other quasi-brittle materials. It is generally, suitable for material with different yield strength in tension and compression. The CDP assumes the flow rule of non-associated plasticity, which is in accordance with the assumption that the plastic potential function and the yield surface do not coincide with each other. The software ABAQUS uses the Drucker-Prager hyperbolic function for the flow potential. The concrete damage plasticity model assumes that the main failure modes of concrete are cracking in tension and crushing in compression.

In relation to the mechanical properties applied for simulating concrete, the experimental results obtained from the compressive and tensile tests of eight concrete cylinder specimens were used, as reported in section 2.1. The compressive stress-strain relationship for concrete (Figure 3-11a) was constructed based on the strain readings from the attached strain-gauges on the surface of the tested concrete cylinders. On the other hand, for the full behavior of concrete under uniaxial tensile stress, the modified model, developed by Wahalathantri et al. [31], was used, as given in Figure 3-11b.

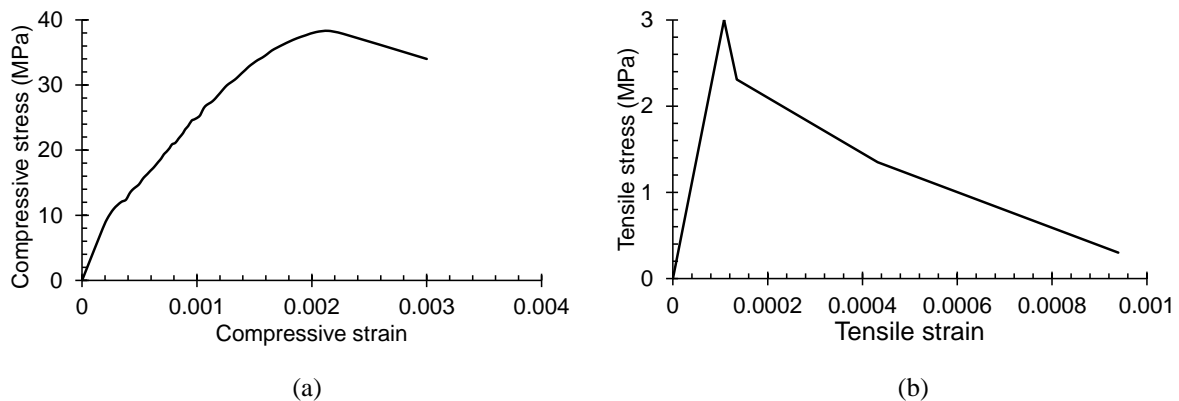


Figure 3-11 : Response of concrete to uniaxial loading in (a) compression and (b) tension

In the concrete damage plasticity model, concrete degradation is characterized by two independent variables, namely the degradation of concrete under compression ( $d_c$ ) and degradation of concrete under tension ( $d_t$ ). It is important to know that when the damage variable is equal to zero, the concrete is not damaged; whereas when it is equal to one, the concrete is totally damaged [28]. Calculation of the quantities  $d_c$  and  $d_t$  was performed according to the recommendations of Alfarah et al. [32]; as given by Eqs. (3-3) and (3-4), respectively.

The calibration of the CDP model was done according to the recommendations of [10, 26, 33]. The dilatation angle ( $\psi$ ), flow potential eccentricity ( $\epsilon$ ), stress ratio ( $\sigma_{b0}/\sigma_{c0}$ ) and  $K_c$  are the main parameters that define respectively the concrete internal friction angle, the rate at which the hyperbolic flow potential approaches its asymptote, the ratio of the biaxial compressive

yield stress to the uniaxial compressive yield stress, and the ratio of the second stress invariant on the tensile meridian. The values of the aforementioned parameters were taken as  $\psi = 36$ ,  $\epsilon = 0.1$ ,  $\frac{\sigma_{bo}}{\sigma_{co}} = 1.16$  and  $K_c = 0.667$ .

$$d_c = 1 - \frac{\sigma_c}{\sigma_{c\text{ ult}}} \quad (3-3)$$

$$d_t = 1 - \frac{\sigma_t}{\sigma_{t\text{ ult}}} \quad (3-4)$$

### 3.3.1.2 Steel and CFRP reinforcement

The elastic modulus, yielding and ultimate strengths of the steel bars were determined experimentally, as previously discussed in section 2.1. The nonlinear tensile stress-strain relationship obtained from the uniaxial tests, on three representative specimens, was assigned to the steel rebar as indicated in Figure 3-12. The software ABAQUS could then establish the behavior of the multi-axial stress state. A Poisson's ratio of 0.3 was used for the steel reinforcement, and the bond between the steel bars and concrete was assumed to be perfect by using the embedded region contact. This can be justified by the sufficient anchorage length of the steel bars and plenty of friction between the steel and concrete.

According to the manufacturer's instructions, the tensile stress-strain behavior of CFRP reinforcement is linearly elastic up to failure, as illustrated in Figure 3-13. The elastic modulus, ultimate strength and Poisson ratio of the CFRP bars used were equal to 165GPa, 2800MPa and 0.35, respectively.

### 3.3.1.3 Epoxy-resin filling material

The stress-strain relationship of the epoxy-resin material was considered as a bi-linear curve in the FE model [27]. The tensile resistance, modulus of elasticity and Poisson ratio of the resin were taken as 29.5MPa, 4.94GPa and 0.37, respectively.

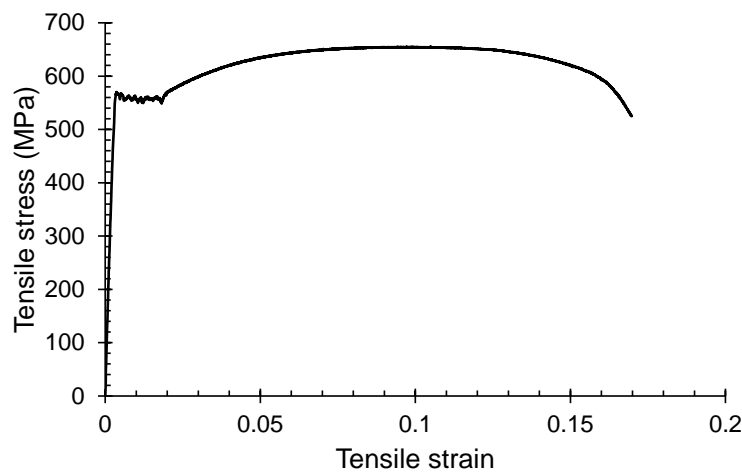


Figure 3-12 : Constitutive model of steel reinforcement

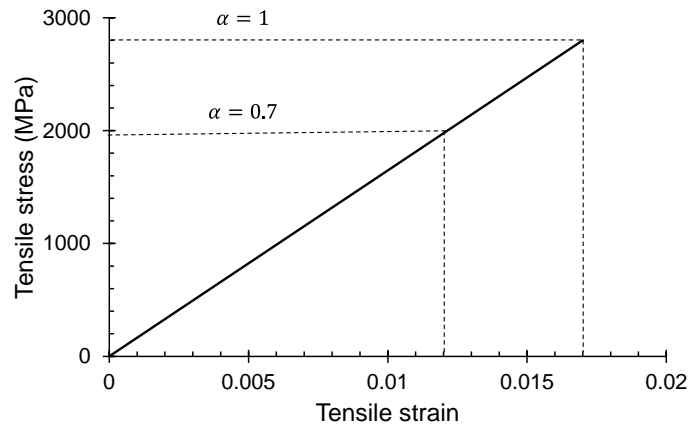


Figure 3-13 : Constitutive model of CFRP reinforcement

### 3.3.2 Interaction and contact conditions

In general, it is important to take into account the interaction between the components of the FE model (concrete, steel,...etc.) in order to accurately simulate the behavior of the tested beams. The prediction of the flexural performance of RC beams strengthened with FRP composites using computer programs, based on the FE analysis, is strongly associated with the constitutive model used to simulate the bond behavior between the strengthening components (CFRP bars and resin) and concrete. The bond behavior influences the ultimate strength of the strengthened beam as well as its serviceability aspects such as cracks formation and spacing. In this study, the embedded element option, available in the ABAQUS software, was used to describe the contact between the steel reinforcements and concrete, so one may consider that all degrees of freedom of the nodes of the steel bars and stirrups were subjected to the nodes of concrete. Regarding the interaction between the additional reinforcement/resin and concrete, two different bond models were separately assumed: the perfect bond model (PBM) and the cohesive zone model (CZM). These two models are discussed in the following sections.

#### 3.3.2.1 Perfect bond model (PBM)

This approach ignores the development of shear stresses in the interface materials and the slip between the reinforcing elements. Furthermore, it does not include fracture of the bond. Researchers usually use this assumption to simplify the modeling behavior [9, 10, 34]. The overall concept of the PBM can be described as follows: (i) The contact between resin and concrete is taken as a perfect bond; and (ii) The CFRP bars are embedded into the epoxy resin using the embedded contact option, (Figure 3-14).

In the present study, the PBM was modified by reducing the nominal tensile strength and strain of CFRP by a debonding factor,  $\alpha$  ( $0.5 < \alpha < 1$ ) [17] in order to take into account the sliding/fracture that occur between the CFRP/filling material and concrete. Therefore, within the framework of this research, a value of 0.7 was selected for the parameter  $\alpha$  according to the utilization level of the CFRP bars (see section 2.2.4). The modified PBM was used to validate the mechanical properties of the materials (CFRP, resin,..etc.) and to verify accuracy of the experimental results.



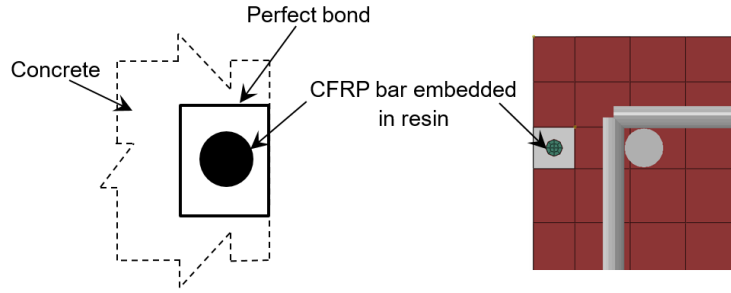


Figure 3-14 : Perfect bond model

### 3.3.2.2 Cohesive zone model (CZM)

In this approach, the overall response of the strengthening system (NSM or SNSM) was modelled as a very thin cohesive layer of 1 mm in thickness. The cohesive layer was created by using the offset option available in ABAQUS; and it is located between the CFRP bar and concrete, as depicted in Figure 3-15. The cohesive layer was tied to the concrete surface, nevertheless, the probability of debonding in the numerical analysis could be obtained by giving the implemented cohesive zone the values of the parameters those define the bond-slip curve. According to [22, 35], there is no data available on the relative slip at the resin-concrete interface. Therefore, the only bond-slip curve used in this research is the one shown in Figure 3-16 [1], where  $\tau_m$  is the maximum shear strength,  $s_m$  is the ultimate slip,  $a$  is a curve-fitting parameter obtained by equating the area underneath the ascending branch of the experimental curve to the value of  $(\frac{\tau_m s_m}{1+a})$ , and  $G_{cr}$  is the fracture energy which is defined as the area under the bond-slip curve.

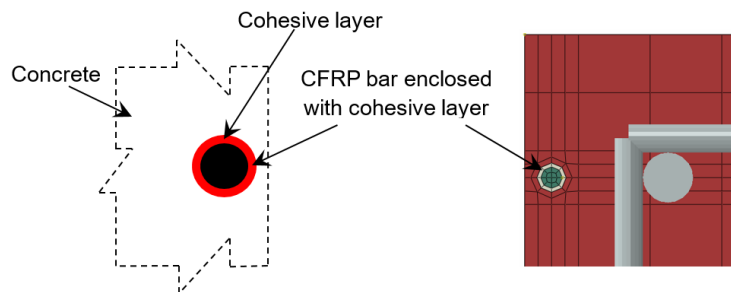


Figure 3-15 : Cohesive zone model

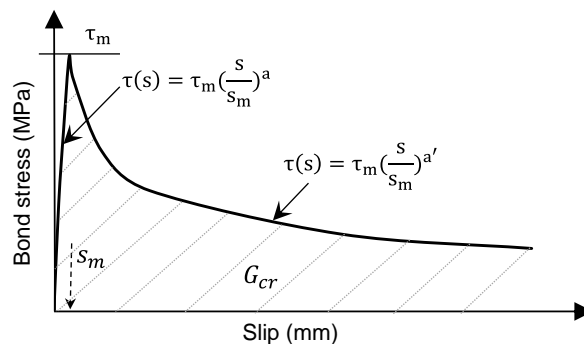


Figure 3-16 : Bond slip law

Several experimental tests were carried out on the basis of the direct pull out test to evaluate the bond stress-slip relationship of the NSM-FRP system [21, 22, 36, 37]. In fact, the results concerning the maximum shear strength have ranged from 3.5 to 20.7MPa. Results from pull out tests on 25×25 mm groove specimens, which were conducted by Al Mahmoud et al. [36], have suggested values for the  $\tau_m$ ,  $s_m$  and  $a$  parameters; giving  $\tau_{max} = 12.2/0.4$ ,  $s_m = 0.16/0.05$  and  $a = 0.74/0.04$ . For their part, De Lorenzis et al. [22] carried out a series of experimental pull out tests in order to investigate the effect of several factors, such as the groove size (14mm-24mm), groove-filling material (epoxy/cement) and type of the FRP (CFRP/GFRP) on the bond performance of NSM-FRP bars in concrete. The reported maximum shear strength  $\tau_m$  for the CFRP bars specimens with epoxy-filled grooves was found between 7.24MPa and 16.56MPa, while the measured ultimate slip  $s_m$  was between 0.034 mm and 0.372 mm. Furthermore, the experimental pull out tests conducted by Capozucca [37] on 20×20 mm groove specimens showed that the bond strength  $\tau_m$  value when failure occurred at the epoxy-CFRP rod interface was about 7.2MPa, while the bond strength value when the failure takes place at the epoxy-concrete interface was about 3MPa. Seracino et al. [38] proposed an expression (Eq. 3-5) to calculate the interface shear stress of NSM-plate-to-concrete joints, while considering the geometry of debonding based on the statistical analysis of experimental values. Applying Eq. (3-5), in the present study, gives  $\tau_m = 7.9$ MPa.

$$\tau_{max} = (0.802 + 0.078\varphi)fc^{0.6} \text{ (MPa)} \quad (3-5)$$

where  $\varphi$  is the aspect ratio of the interface failure plane calculated from Eq. (3-6), and  $fc$  is the concrete compressive strength.

$$\varphi = \frac{\text{Groove depth}+1}{\text{Groove width}+2} \text{ (mm)} \quad (3-6)$$

However, the numerical simulation showed that the value of  $\tau_m = 12.2$  MPa significantly overestimated the ultimate strength of the tested beams, since the CFRP rupture induced the failure instead of the interfacial debonding that was observed in the experiments (Figure 3-17). Hence, the  $\tau_m$  was reduced to 6MPa by taking advantage of the computed bond strength from the experimental study (see section 2.2.5); based on the fact that the bending tests are more adequate to describe and define the actual bond-slip law.

The quadratic traction function, which is similar to the cohesive contact approach that is available in literature [39], was adopted to indicate the initial damage of the cohesive layer, as given in Eq. (3-7), where  $\sigma_n$  is the cohesive normal tensile stress,  $\tau_s$  and  $\tau_t$  are the shear stresses of the interface. The characters  $n$ ,  $s$ , and  $t$  refer to the stress directions. The initial values of the above stresses were taken as  $\sigma_n^0$ : tensile strength of concrete = 3MPa and  $\tau_s^0 = \tau_t^0 = 6$ MPa. The evolution of the interface damage was expressed in terms of energy release [23], and the value of the calibrated fracture energy  $G_{cr}$  used in this FE study was 15mJ/mm<sup>2</sup>.

$$\left(\frac{\sigma_n}{\sigma_n^0}\right)^2 + \left(\frac{\tau_s}{\tau_s^0}\right)^2 + \left(\frac{\tau_t}{\tau_t^0}\right)^2 = 1 \quad (3-7)$$

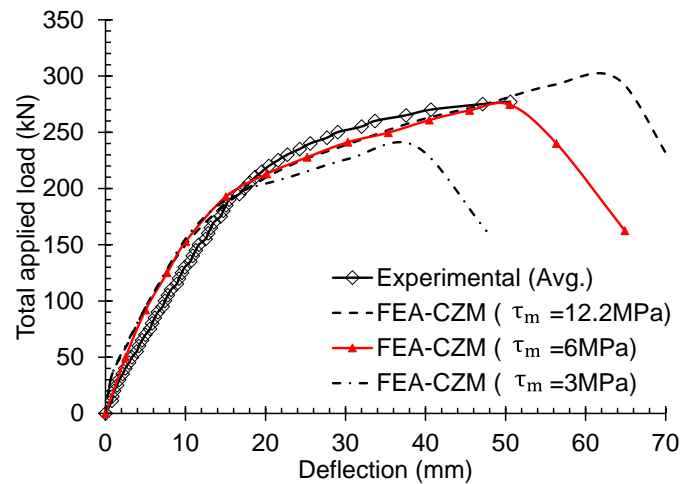


Figure 3-17 : Comparison between the experimental results and FEA results with different value of maximum shear stress for beam BC1-E/N-NSM

### 3.3.3 Finite element modelling of tested beams

Three combinations of bond models and behavior of CFRP bars were examined and analyzed. These are the perfect bond with the full tensile strength of CFRP ( $\sigma_{FRP}^{max} = \sigma_{FRP}^{ult}$ ), the modified perfect bond with 70% tensile strength of CFRP ( $\sigma_{FRP}^{max} = 0.7\sigma_{FRP}^{ult}$ ), and the cohesive zone bond model.

Figure 3-18 shows the boundary conditions, steel skeleton and meshing of the beam model. By taking advantage of the double symmetry of the beam specimen, a symmetry simplification was introduced, as shown in Figure 3-18a. Only a quarter of the beam, involving two CFRP rods (one rod in the hogging region and the other rod in the sagging region), was modeled (Figure 3-18b). This helped to make the numerical modeling easier and to reduce the computational time as well. To guarantee the stability of the model, symmetric boundary conditions were applied to the surfaces of the symmetric plans. All the nodes of surface 1, as shown in Figure 3-18b, were prevented from moving along the X axis and from turning about the Y and Z axes ( $U_x = R_y = R_z = 0$ ); while for the nodes of surface 2, the translational displacement along the Z axis as well as the rotational displacement about the X and Y axes were restrained ( $U_z = R_x = R_y = 0$ ).

The convergence of the numerical solution was checked through the use of coarse (50 mm) and fine mesh (20 mm) sizes. The numerical load-deflection curves of beam BC1-E-NSM was compared with the experimental one, as shown in Figure 3-19. As can be seen from Figure 3-19 the difference between the FE load-deflection curves is not large. This is certainly due to the interface region between the CFRP bars and concrete, in the both referred mesh trials, was also refined with a mesh size of 3 mm in order to achieve accurate results (see Fig. 3-15). However, the mesh size of 20 mm was selected as an overall size for the all specimen models throughout this paper, while reducing the mesh size in the region around the CFRP bars to 3 mm. To mesh the components of the beam, different types of mesh elements available in the ABAQUS library were used. Concrete, resin and CFRP bars were meshed with an eight-node 3D hexahedral brick element with reduced integration stiffness, (C3D8R). The steel bars and stirrups were meshed

with a two-node 3D truss element type (T3D2). The cohesive layer was meshed with an eight-node 3D cohesive element (COH3D8).

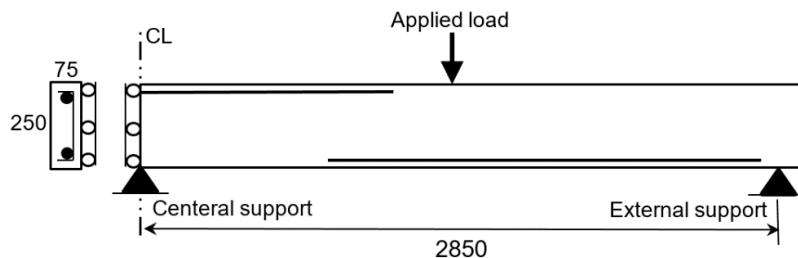
In this FE analysis study, the loading was downward implemented displacement applied on the top surface of the beam, at the mid-span, as a distributed load over a surface similar to that of the loading plate that was employed in the experiments ( $100 \times 150\text{mm}$ ). This load was defined as an imposed displacement and applied as a loading rate by using the smooth amplitude function in order to reduce the dynamic analysis time.

Henceforth, for organizational purposes, the letter (E) which was assigned to the beam's name in the experimental sections has been replaced with the letter (N) in the following sections in order to indicate that the beam is numerically investigated.

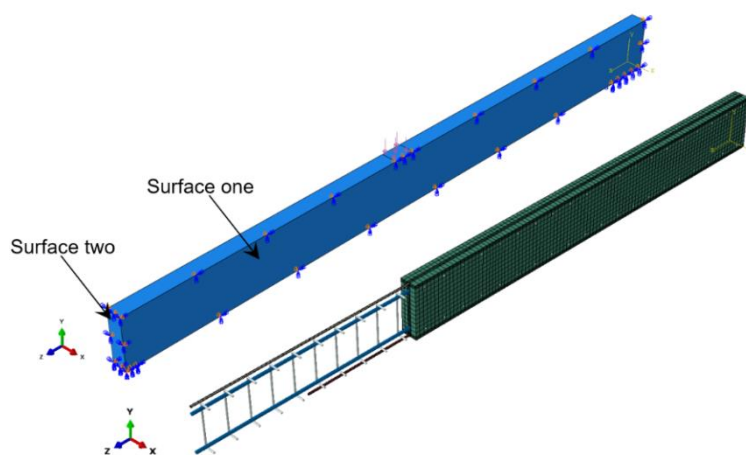
### 3.3.4 Finite element results and discussion

#### 3.3.4.1 Load deflection response

Figure 3-20 shows the load-deflection ( $P - \delta$ ) curves obtained from the experiments and finite element (FE) analysis, for the control and strengthened beams (CB-E, BC1-E-NSM and BC2-E-SNSM). In general, there is a good correlation between the numerical and experimental results in terms of the ultimate load and deflection. As expected, the largest difference between the numerical and experimental results was reported when the conventional PBM ( $\alpha = 1$ ) was employed, whereas a quite satisfactory convergence was observed when using the modified PBM ( $\alpha = 0.7$ ) and the CZM.



(a) Symmetry simplification (Dimensions in mm)



(b) Boundary conditions, steel Skelton and finite element mesh of quarter beam

Figure 3-18 : Detail and boundary condition of the FE beam (all dimension are in mm)

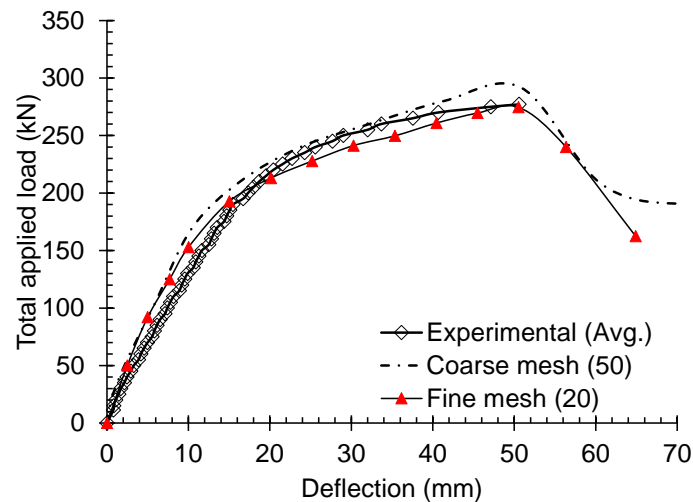


Figure 3-19 : Effect of the mesh size

For the control beam, [Figure 3-20a](#), the excellent agreement between the experimental and the FE analysis results is clear. The stiffness and flexural load capacities of the beam were well predicted by the numerical model. The little difference between stiffness of the experimental curve and that of the FE curve is probably attributed to: (i) The perfect bond assumed between concrete and steel reinforcement, and (ii) the presented average deflection; i.e here, at any level of the applied load the experimental deflection of the beam was computed as the average value of the left and right span deflections.

Regarding the strengthened beams ([Figure 3-20b](#) and [Figure 3-20c](#)), the results obtained from the FE analysis, using the different bond models, were identical to the experimental results found before the concrete cracking load. However, from the concrete cracking load up to the steel yielding load, the ( $P - \delta$ ) curves obtained from the perfect bond FE models (either the conventional or the modified one) appeared to be stiffer than the experimental curve. This FE stiffness was slightly smaller when the CZM was employed. In the ultimate strength stage, i.e. from the steel yielding load to the failure load, the conventional PBM overestimated the stiffness and load-carrying capacity of the beam because the PBM ignores the shear stress/strain between the CFRP/resin and concrete which mainly occur in this stage. On the other hand, the stiffness and load-carrying capacity values of the modified PBM (PBM,  $\alpha = 0.7$ ) and CZM were considerably close to the experimental values. The predicted ultimate load and deflection ( $P_u$  and  $\delta_u$ ) of beam BC1-N-NSM were within the error bands (9.8-0.19)%, (2.1-0.5)% and (0.1-0.2)%, respectively, for PBM, modified PBM and CZM. For beam BC2-N-SNSM, the values of  $P_u$  and  $\delta_u$  were within the error bands (15.6-11.4)%, (2.3-5.5)% and (0.7-5.2)%, respectively, for PBM, modified PBM and CZM. These results justify the reduction that was applied to the nominal tensile strength of the CFRP bars, as discussed in section 3.2.1, and validate the bond-slip law that was assumed in assessing the behavior of the interface bond between the strengthening bars and concrete, as discussed in section 3.2.2.

It is worth mentioning that, although the modified PBM ( $\alpha = 0.7$ ) is valid within the framework of this research, the great correspondence between the experimental and FE analysis results for the strengthened beams (BC1-E-NSM and BC2-E-SNSM) in terms of the ultimate load and deflection proves the accuracy of the experimental results, in particular the readings from the

strain gauges, and the constitutive models used for modeling steel, concrete, CFRP and resin materials.

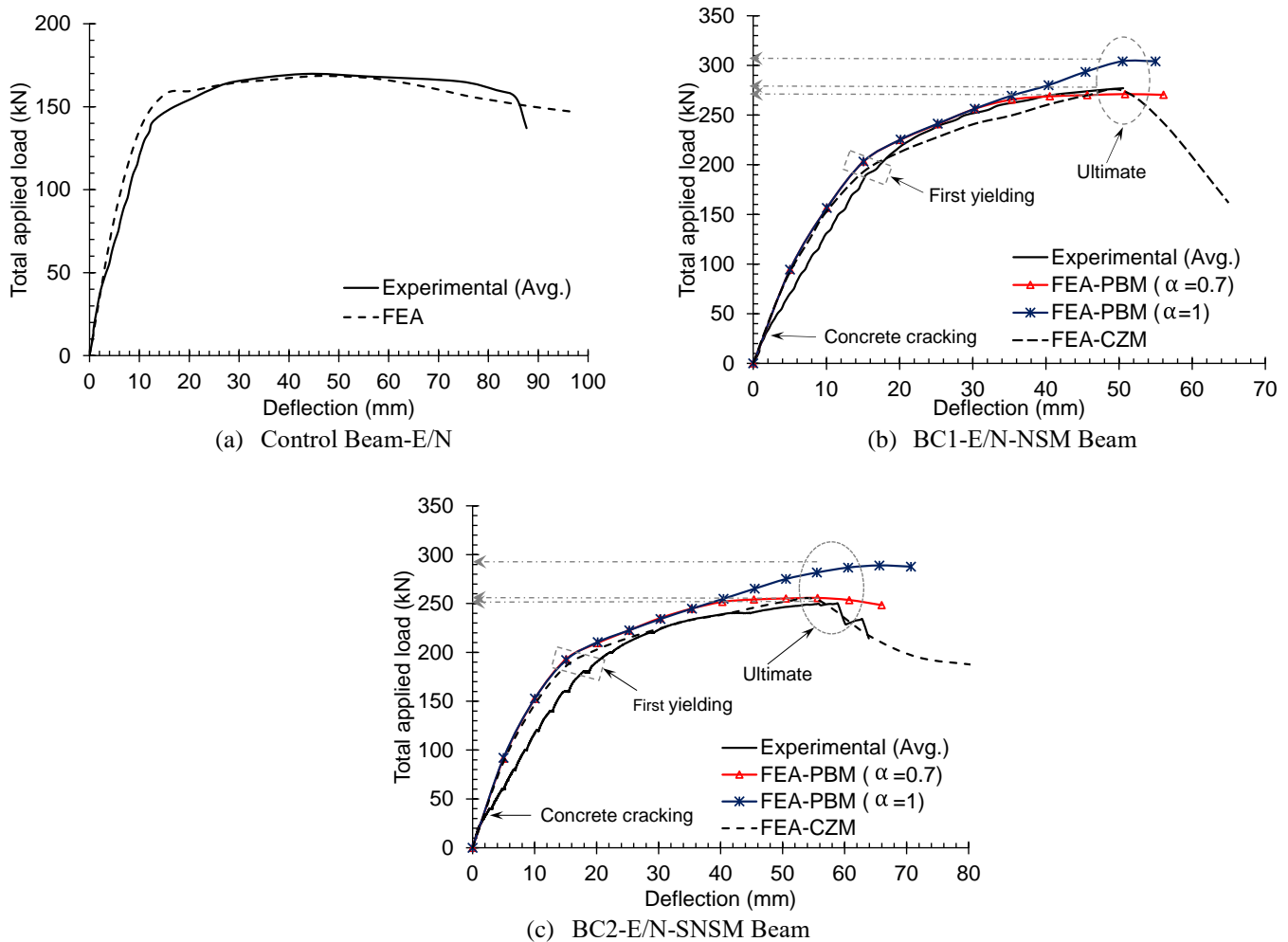


Figure 3-20 : The experimental and numerical load deflection curves of tested beams.

### 3.3.4.2 Cracks pattern and failure modes

Figure 3-21 shows the cracking maps and failure modes of strengthened beams (BC1-N-NSM and BC2-N-SNSM) obtained from the FE analysis using the cohesive zone model (CZM). As can be seen from Figure 3-21, adopting the CFRP bars for strengthening continuous RC beams significantly increases the number of the cracks in the hogging and sagging regions, especially for the beam strengthened with side-NSM CFRP bars. The crack patterns observed from the experimental tests (Figure 3-5 and Figure 3-7) and those from the numerical simulations were quite similar, which confirms that the CZM can successfully capture the mechanism of fracture in the beams.

In general, the prediction of the nonconventional failure modes, such as debonding/pull out of the CFRP bars using the FE analysis, is more complicated. However, the cohesive zone model proposed in this study can still capture to some extent these failure modes, as illustrated in Figure 3-21, in which the red color represents the cracked elements that describe the mode of failure. As explained earlier, the proposed CZM was principally applied to exemplify the interaction between the strengthening components and concrete. Consequently, the two FE



beams showed that failure occurred in the cohesive layer indicating debonding. The reported maximum FE shear stress/slip of the CFRP bar in the hogging region of beams BC1-E-NSM and BC2-E-SNSM were 5.96 MPa/6.01 mm and 5.55 MPa/5.38 mm, respectively.

### 3.3.4.3 Central support reaction and moment redistribution

The evolution of the actual central supports reactions gives an indication for redistribution of the moment in the statically indeterminate RC beams. Hence, Figure 3-22 presents the central support reaction of the tested beams obtained from the experimental and FE analysis results versus the total applied load at different load levels, in addition to a comparison of the elastic reactions which were computed by considering a uniform flexural stiffness throughout the entire length of the beam. From Figure 3-22, the great convergence between the experimental results and the FE analysis results is clear. For beams CB-N, BC1-N-NSM and BC2-N-SNSM, the central support reaction at the ultimate load level were 110.2 kN, 180.9 kN and 167.1 kN, respectively, whereas the measured reactions from the tests at the same load level were 110.1 kN, 180.3 kN and 166.6 kN, respectively. Consequently, the computed moment redistribution degree ( $\beta$ ) for the FE beam models were very close to those reported in Table 3-2 (see also Table 3-5 and Table 3-6).

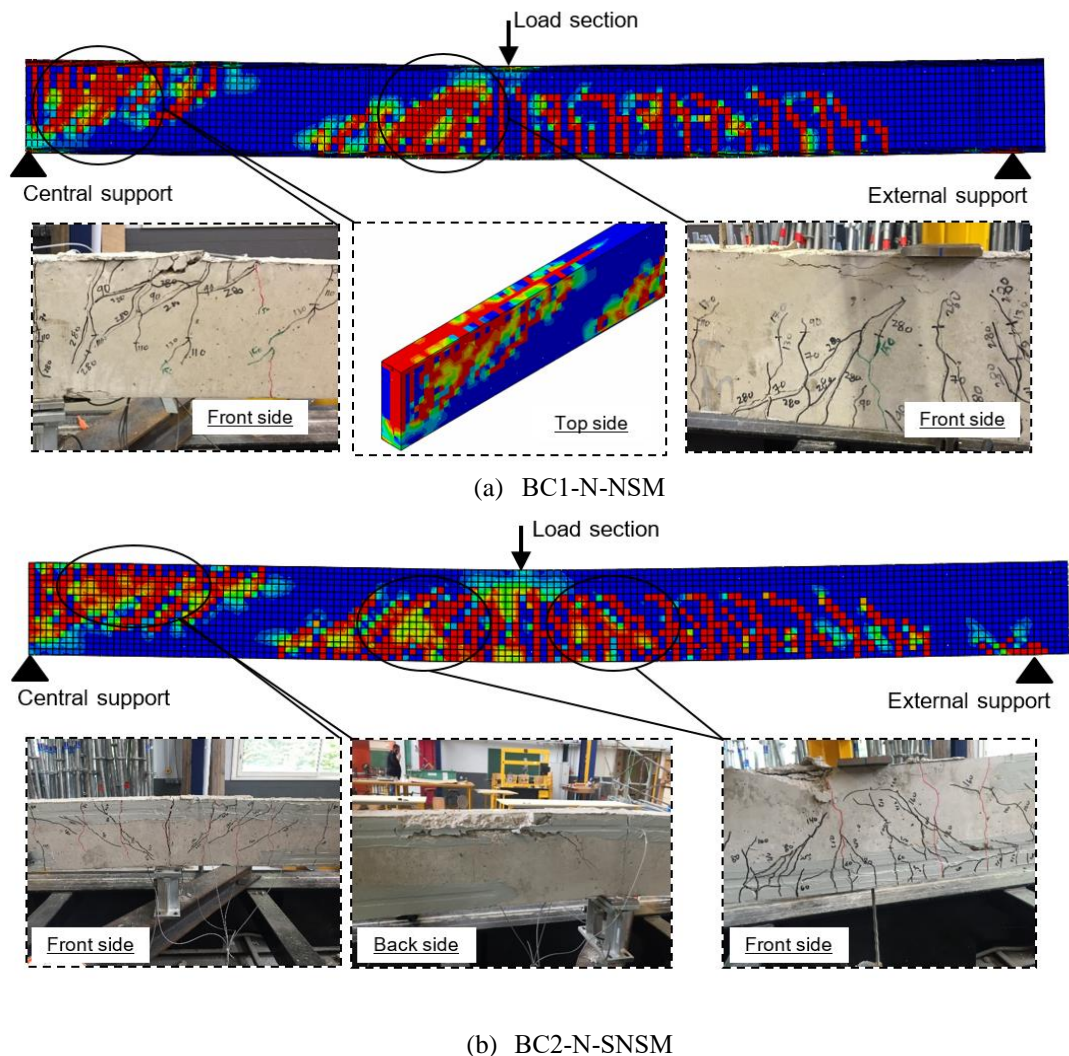


Figure 3-21 : Cracks maps and failure of strengthened beams

### 3.3.4.4 Effectiveness of the CFRP bars

As stated in the experimental sections of this paper (section 2.2.4), it was found that changing the position of the strengthening can slightly influence the effectiveness of the CFRP bars at the ultimate load level. Figure 3-23 presents the tensile stresses of the CFRP bars at the ultimate load in the strengthened beam specimens, as obtained from the FE analysis (CZM). The FE stresses correspond well to the experimental stresses. The maximum tensile stress of the CFRP bars in both beams was reported in the hogging region; and the CFRP bars effectiveness ( $\frac{\sigma_{max}^{CFRP}}{\sigma_{ult}^{CFRP}}$ ) was about 72% for beam BC1-N-NSM and about 68.8% for beam BC2-N-SNSM.

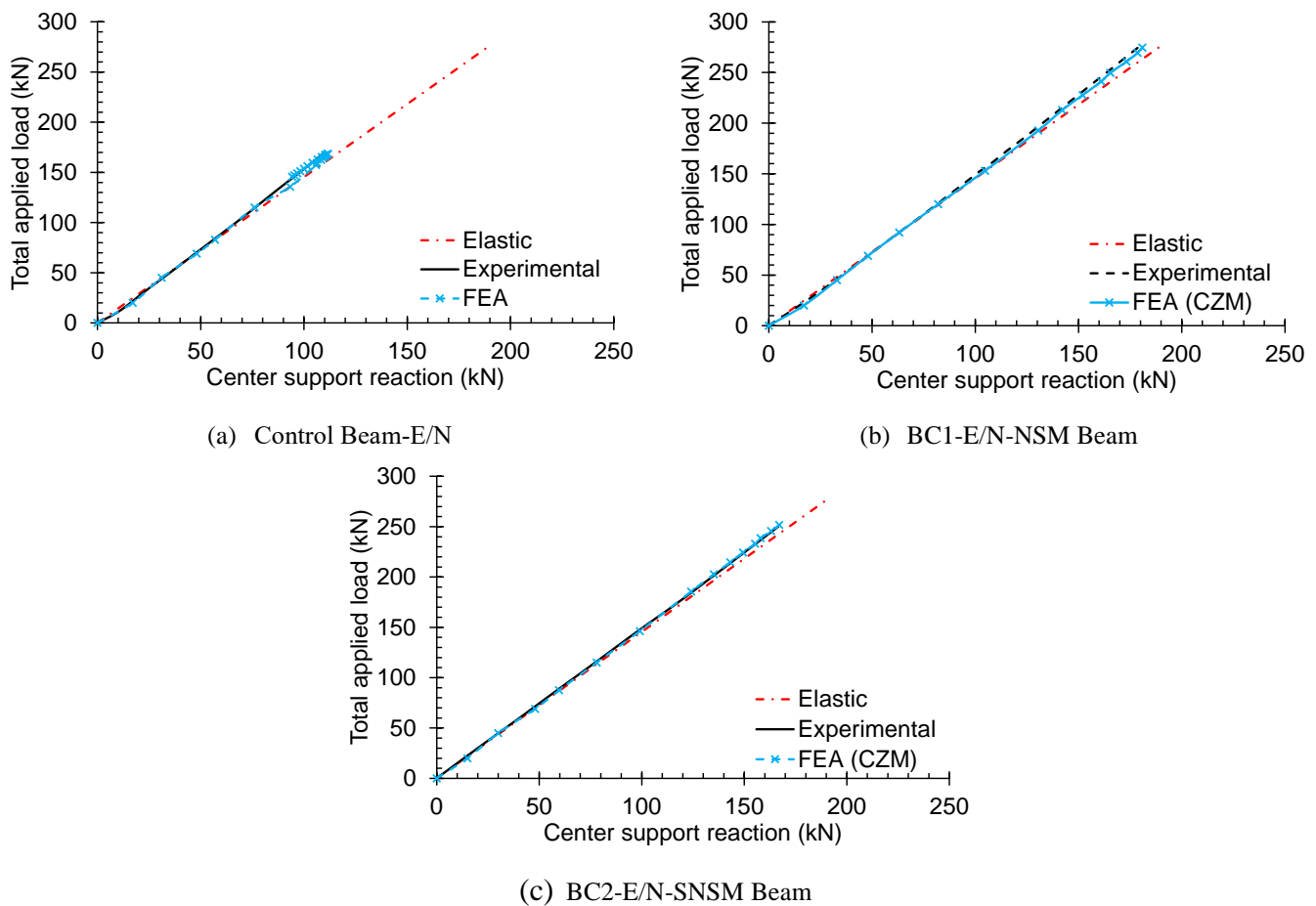


Figure 3-22 : The experimental and FEA results of central support reaction of tested beams

### 3.3.5 Parametric study-Arrangement of the reinforcement

Based on the above discussion, it can be asserted that the CZM is suitable for analyzing behavior of continuously RC beams strengthened with CFRP bars by means the NSM and side-NSM techniques. The main parameters influencing the behavior of statically indeterminate RC beams are the amount and arrangement of the tension reinforcements. Consequently, the proposed CZM model is employed in this section for studying the effects of these parameters on the load-carrying capacity and moment redistribution of strengthened two-span continuous RC beams.

The parametric study was conducted with distinct strengthening arrangements in the negative and positive moment regions of beams, as summarized in Table 3-5a, Table 3-5b and Table



3-5c, where  $A_f^H$  and  $A_f^S$  are the area of CFRP bars in the hogging and sagging regions, respectively. The dimensions, positive steel reinforcement ratio ( $\rho_s^S=1\%$ ), load and support conditions of the FE beams were all similar to those used in the experimental program (Figure 3-1).

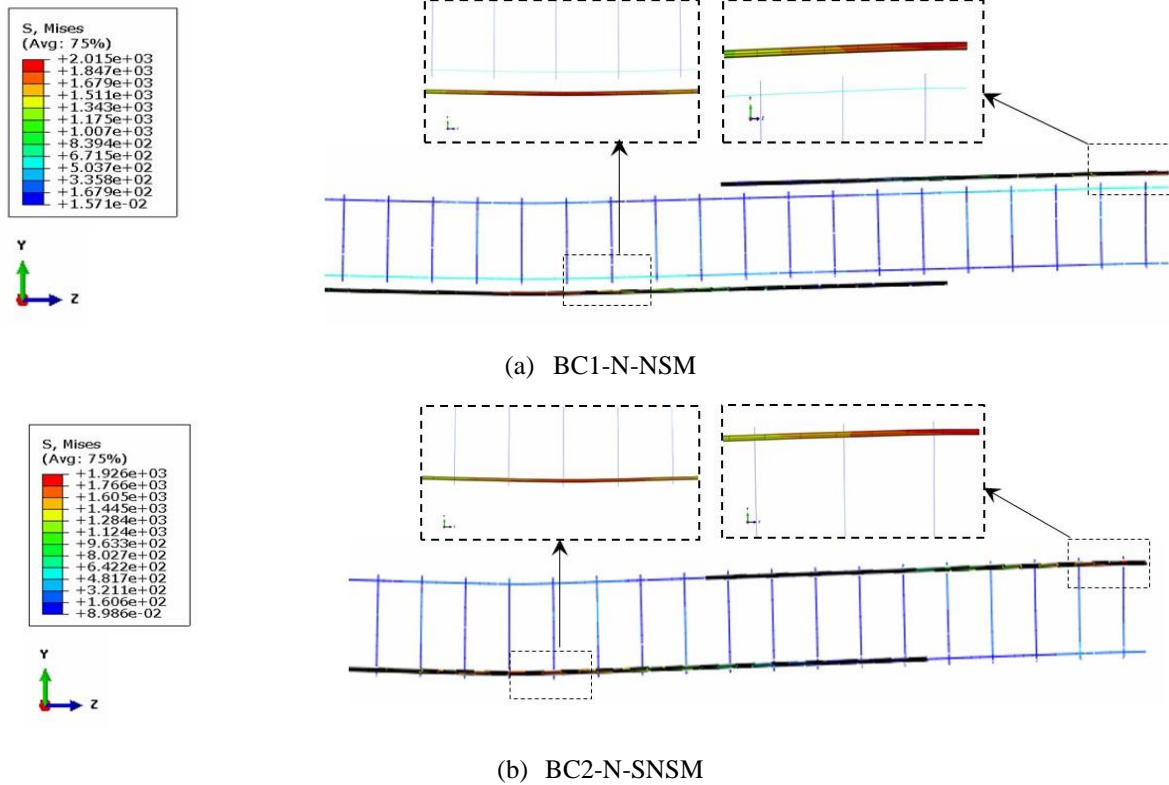


Figure 3-23 : The FEA (CZM) tensile stress of CFRP bars in the strengthened beams at the ultimate load level

A total of 21 strengthened beams were investigated. The FE beam specimens had different steel reinforcement ratios in the hogging region, i.e.  $\rho_s^H = 0.5\%$ ,  $1\%$  and  $1.25\%$ . For each steel ratio, the applied strengthening arrangements were classified into three groups: a) The hogging region ( $x-0$ ), b) The sagging region ( $0-x$ ) and c) The hogging and sagging region ( $x-x$ ), where  $x$  refers to the number of CFRP bars.

In order to ensure the validation of the adopted cohesive zone model for studying the influences of the strengthening and reinforcement arrangement on the behavior of continuous RC beams, an additional beam namely BC1-N-NSM-(0-2) from Table 3-5b was also experimentally tested. This beam was strengthened with CFRP bars in the sagging regions only. The experimental load-deflection curve of this beam (BC1-N-NSM-(0-2)) is plotted in Figure 3-24, and its failure mode is presented in the Appendix.

Figure 3-24 shows the load-deflection curves of all simulated beams whereby it was easy to perceive the ductile failure of side-NSM beams compared to the NSM beams. Table 3-6a, Table 3-6b and Table 3-6c summarize the FE results according to the different steel reinforcement ratios used in the hogging region. In Tables 6a-c,  $P_u$  and  $\delta_u$  are respectively the ultimate load and deflection,  $R_c$  is the central reaction at the ultimate load level,  $\beta_H$  and  $\beta_S$  are respectively the moment redistribution degree in the hogging and sagging region; and  $\lambda$  is the load-carrying

Chapter 3: Experimental and numerical investigation on the effectiveness of NSM and side-NSM CFRP bars for strengthening continuous two-span RC beams.

capacity index that is defined as the ratio of the ultimate load of the strengthened beam to that of the control beam. Two criteria were assumed to describe the failure modes obtained from the FE analysis: (i) The flexural failure (F), indicating yielding of the tension steel followed by concrete crushing; the concrete crushing was assumed to takes place when its compressive strain exceeds the value 0.003. (ii) The damage of the cohesive layer, indicating interfacial debonding failure (D).

Table 3-5a : Resume of the strengthening arrangements,  $\rho_s^H = 0.5\%$ . (2D10)

Beam	Hogging region strengthening			Sagging region strengthening			$A_f^H$ mm2	$A_f^H/A_s^H$ (%)	$A_f^S$ mm2	$A_f^S/A_s^S$ (%)
	No.	Length	SL/BL	No.	Length	SL/BL				
Control Beam-N-(0-0)	----	----	----	----	----	----	0	0	0	0
BC1-N-NSM-(0-2)	----	----	----	2Ø6	2.3	0.65	0	0	56.5	18
BC1-N-NSM-(2-0)	2Ø6	2.0	0.70	----	----	----	56.5	36	0	0
BC1-N-NSM-(2-2)	2Ø6	2.0	0.70	2Ø6	2.3	0.65	56.5	36	56.5	18
BC2-N-SNSM-(0-2)	----	----	----	2Ø6	2.3	0.65	0	0	56.5	18
BC2-N-SNSM-(2-0)	2Ø6	2.0	0.70	----	----	----	56.5	36	0	0
BC2-N-SNSM-(2-2)	2Ø6	2.0	0.70	2Ø6	2.3	0.65	56.5	36	56.5	18

Table 3-5b : Resume of the strengthening arrangements,  $\rho_s^H = 1\%$ . (2D14)

Beam	Hogging region strengthening			Sagging region strengthening			$A_f^H$ mm2	$A_f^H/A_s^H$ (%)	$A_f^S$ mm2	$A_f^S/A_s^S$ (%)
	No.	Length	SL/BL	No.	Length	SL/BL				
Control Beam-N-(0-0)	----	----	----	----	----	----	0	0	0	0
BC1-N-NSM-(0-2)	----	----	----	2Ø6	2.3	0.65	0	0	56.5	18
BC1-N-NSM-(2-0)	2Ø6	2.0	0.70	----	----	----	56.5	18	0	0
BC1-N-NSM-(2-2)	2Ø6	2.0	0.70	2Ø6	2.3	0.65	56.5	18	56.5	18
BC2-N-SNSM-(0-2)	----	----	----	2Ø6	2.3	0.65	0	0	56.5	18
BC2-N-SNSM-(2-0)	2Ø6	2.0	0.70	----	----	----	56.5	18	0	0
BC2-N-SNSM-(2-2)	2Ø6	2.0	0.70	2Ø6	2.3	0.65	56.5	18	56.5	18

Table 3-5c : Resume of the strengthening arrangements,  $\rho_s^H = 1.28\%$ . (2D16)

Beam	Hogging region strengthening			Sagging region strengthening			$A_f^H$ mm2	$A_f^H/A_s^H$ (%)	$A_f^S$ mm2	$A_f^S/A_s^S$ (%)
	No.	Length	SL/BL	No.	Length	SL/BL				
Control Beam-N-(0-0)	----	----	----	----	----	----	0	0	0	0
BC1-NSM-N-(0-2)	----	----	----	2Ø6	2.3	0.65	0	0	56.5	18
BC1-NSM-N-(2-0)	2Ø6	2.0	0.70	----	----	----	56.5	14.1	0	0
BC1-NSM-N-(2-2)	2Ø6	2.0	0.70	2Ø6	2.3	0.65	56.5	14.1	56.5	18
BC2-SNSM-N-(0-2)	----	----	----	2Ø6	2.3	0.65	0	0	56.5	18
BC2-SNSM-N-(2-0)	2Ø6	2.0	0.70	----	----	----	56.5	14.1	0	0
BC2-SNSM-N-(2-2)	2Ø6	2.0	0.70	2Ø6	2.3	0.65	56.5	14.1	56.5	18

Chapter 3: Experimental and numerical investigation on the effectiveness of NSM and side-NSM CFRP bars for strengthening continuous two-span RC beams.

Table 3-6a : FEA results of the strengthening arrangements,  $\rho_s^H = 0.5\%$ . (2D10)

Beam	$P_u$	$\delta_u$	$\lambda$	$R_c$	$\beta_H$	$\beta_S$	$\sigma_{CFRP}^{max}$	$\frac{\sigma_{CFRP}^{max}}{\sigma_{CFRP}^{ult}}$	Shear stress*		Failure mode
									H	S	
CB-N-(0-0)	143.5	40.4	1	86.8	49.6	-28.8	----	----	----	----	F
BC1-N-NSM-(0-2)	199.1	47.4	1.39	116.1	55.7	-33.4	1783	0.64	----	5.96	D in S
BC1-N-NSM-(2-0)	185.1	55.9	1.29	124.7	7.4	-4.4	2156	0.77	4.95	----	F
BC1-N-NSM-(2-2)	227.8	47.3	1.59	147.1	22.3	-12.6	2158	0.77	5.82	5.96	D in S and H
BC2-N-SNSM-(0-2)	202.8	55.7	1.41	117.5	57.7	-34.6	1796	0.64	----	4.44	F
BC2-N-SNSM-(2-0)	185	63.6	1.29	118.7	24.5	-14.7	1877	0.67	4.11	----	F
BC2-N-SNSM-(2-2)	230.5	55.7	1.61	144	33.5	-20.1	2020	0.72	5.12	4.33	F

F: flexural; D: debonding; S: sagging and H: hogging. \*Maximum shear stress induced in the cohesive zone

Table 3-6b : FEA results of the strengthening arrangements,  $\rho_s^H = 1\%$ . (2D14)

Beam	$P_u$	$\delta_u$	$\lambda$	$R_c$	$\beta_H$	$\beta_S$	$\sigma_{CFRP}^{max}$	$\frac{\sigma_{CFRP}^{max}}{\sigma_{CFRP}^{ult}}$	Shear stress*		Failure mode
									H	S	
CB-N-(0-0)	169.5	45.6	1	110.2	20.1	-12	----	----	----	----	F
BC1-NSM-N-(0-2)	227.9	47.3	1.34	142.4	33.6	-20.1	1886	0.67	----	5.91	D in S
BC1-NSM-N-(2-0)	202.3	55.6	1.19	143.3	-10.8	6.7	1981	0.71	4.51	----	F
BC1-NSM-N-(2-2)	277.5	50.5	1.64	180.9	19	-11.3	2015	0.72	5.96	5.73	D in H
BC2-SNSM-N-(0-2)	231.4	55.8	1.37	144.1	34.5	-20.7	1867	0.67	----	5.08	F
BC2-SNSM-N-(2-0)	214.2	63.8	1.26	147.5	-0.6	0.4	2135	0.76	4.58	----	F
BC2-SNSM-N-(2-2)	251.8	55.8	1.49	167.1	12.9	-7.6	1926	0.69	5.55	5.84	D in S and H

F: flexural; D: debonding; S: sagging and H: hogging. \*Maximum shear stress induced in the cohesive zone

Table 3-6c : FEA results of the strengthening arrangements,  $\rho_s^H = 1.28\%$ . (2D16)

Beam	$P_u$	$\delta_u$	$\lambda$	$R_c$	$\beta_H$	$\beta_S$	$\sigma_{CFRP}^{max}$	$\frac{\sigma_{CFRP}^{max}}{\sigma_{CFRP}^{ult}}$	Shear stress*		Failure mode
									H	S	
CB-N-(0-0)	183.9	55.7	1	126.9	-1.4	0.8	----	----	----	----	F
BC1-NSM-N-(0-2)	242.3	47.4	1.32	156	23.3	-14	1887	0.67	----	5.23	F
BC1-NSM-N-(2-0)	217.7	56	1.18	158.3	-21.1	12.7	2025	0.72	4.95	----	F
BC1-NSM-N-(2-2)	281.1	56	1.53	191.7	2.9	-1.8	2128	0.76	5.57	5.91	D in S
BC2-SNSM-N-(0-2)	244.1	55.8	1.33	157.2	23.2	-13.9	1897	0.68	----	4.86	F
BC2-SNSM-N-(2-0)	226.6	63.9	1.23	160.1	-10.2	6.1	2031	0.72	4.96	----	F
BC2-SNSM-N-(2-2)	269.3	56.9	1.46	181.8	6.6	-4	1964	0.70	5.10	5.02	F

F: flexural; D: debonding; S: sagging and H: hogging. \*Maximum shear stress induced in the cohesive zone

The FE analysis results indicated in Table 3-6a, Table 3-6b and Table 3-6c can point out the following observations:

- I. The arrangement of the CFRP and amount of the steel reinforcement had significant effects on the moment redistribution of continuous RC beams, and they can even change the direction of redistribution.
- II. The increase in the steel reinforcement ratio in the hogging region ( $\rho_s^H$ ) caused a decrease in the positive moment redistribution of continuous RC beams, regardless of the strengthening technique used. However, for beams reinforced with the same  $\rho_s^H$ , strengthening only the sagging moment regions was found to increase the moment redistribution. This can be explained by the fact that the flexural stiffness of the sagging region was greater than that of the hogging region.

- III. With regard to the moment redistribution capability in the ultimate state for beams strengthened in the hogging moment regions only, it was found that using the side-NSM CFRP bars slightly decreased stiffness of the hogging region in comparison with the NSM CFRP bars.
- IV. Applying the CFRP bars in both hogging and sagging regions of the beam was found to be the most effective strengthening arrangement for improving the beam's load-carrying capacity. Compared to the control beam specimens, the ultimate load of beam BC1-N-NSM-(2-2) was improved by about 59%, 64% and 53% for  $\rho_s^H = 0.5\%$ , 1% and 1.28%, respectively. Similarly, the ultimate load of beam BC2-N-SNSM-(2-2) was improved by about 61%, 49% and 46% for  $\rho_s^H = 0.5\%$ , 1% and 1.28%, respectively.
- V. The side-NSM technique was relatively more efficient than the bottom/top NSM technique when the CFRP bars were applied only in the hogging region or the sagging region. For example, for a reinforcement ratio of 1%, the value of  $\lambda$  was found equal to 19% and 34%, for NSM beams (BC1-NSM-(2-0) and BC1-NSM-(0-2)), and 26% and 37%, for side-NSM beams (BC2-SNSM-(2-0) and BC2-SNSM-(0-2)).
- VI. The contribution of CFRP bars to the load-carrying capacity of the beams was limited by the occurrence of concrete crushing or by the damaged strengthening system. It was also observed that the utilization level of the CFRP bars ( $\sigma_{CFRP}^{max}/\sigma_{CFRP}^{ult}$ ) at the ultimate load ranged from 64% to 77%, which confirmed the relatively low influence of the steel reinforcement ratio ( $\rho_s^H$ ), strengthening arrangement and strengthening position on the effectiveness of the CFRP bars.

### 3.4 Conclusion

The present study aimed to analyze the global flexural response of statically indeterminate RC beams strengthened with CFRP rods using the NSM and side-NSM techniques. According to the obtained results, the following conclusions could be drawn:

- All strengthened continuous RC beam either tested or FE modeled using the NSM and side-NSM CFRP bars techniques exhibited improvement in their load carrying capacity with respect to that of the un-strengthened beams, regardless of the CFRP arrangement or steel reinforcement ratio used. The highest increase of beam's load-carrying capacity ( $\lambda$ ) was achieved when the strengthening configuration composed CFRP bars in both hogging and sagging regions. However, when a relatively low steel reinforcement ratio was employed in the hogging region ( $\rho_s^H = 0.5\%$ ), this strengthening configuration showed a slightly lower load-carrying capacity of the side-NSM beams in comparison with the NSM beams. This difference increased to about 10% when the hogging's steel ratio was raised to 1% and 1.28%.
- For all the strengthening configurations adopted in this research study, the increase of load-carrying capacity ( $\lambda$ ) of beams strengthened with NSM-CFRP bars varied between 18% and 64%, whereas an increase in  $\lambda$  between 23% and 61%, was registered for beams strengthened with side-NSM-CFRP bars.
- In comparison with the NSM-CFRP bars strengthening technique, insertion of CFRP bars in the lateral sides adjacent to the steel bars using the side-NSM technique proved to considerably increase the number of cracks in the hogging and sagging regions.

However, with the both strengthening techniques, the crack widths of beams were almost identical under the same applied load.

- The moment redistribution degree ( $\beta$ ) of strengthened RC beams decreased as the steel reinforcement amount in the hogging region increased. In addition, the experimental and FE results showed that the  $\beta$  was significantly affected by the position and arrangement of the CFRP bars.
- The three-dimensional FE analysis developed with the cohesive zone bond model, presented in this study, can capture the main aspects observed from the experiments, for both NSM and side-NSM beams, regarding the load-carrying capacity, cracks pattern, performance of the CFRP bars and the beam's moment redistribution.

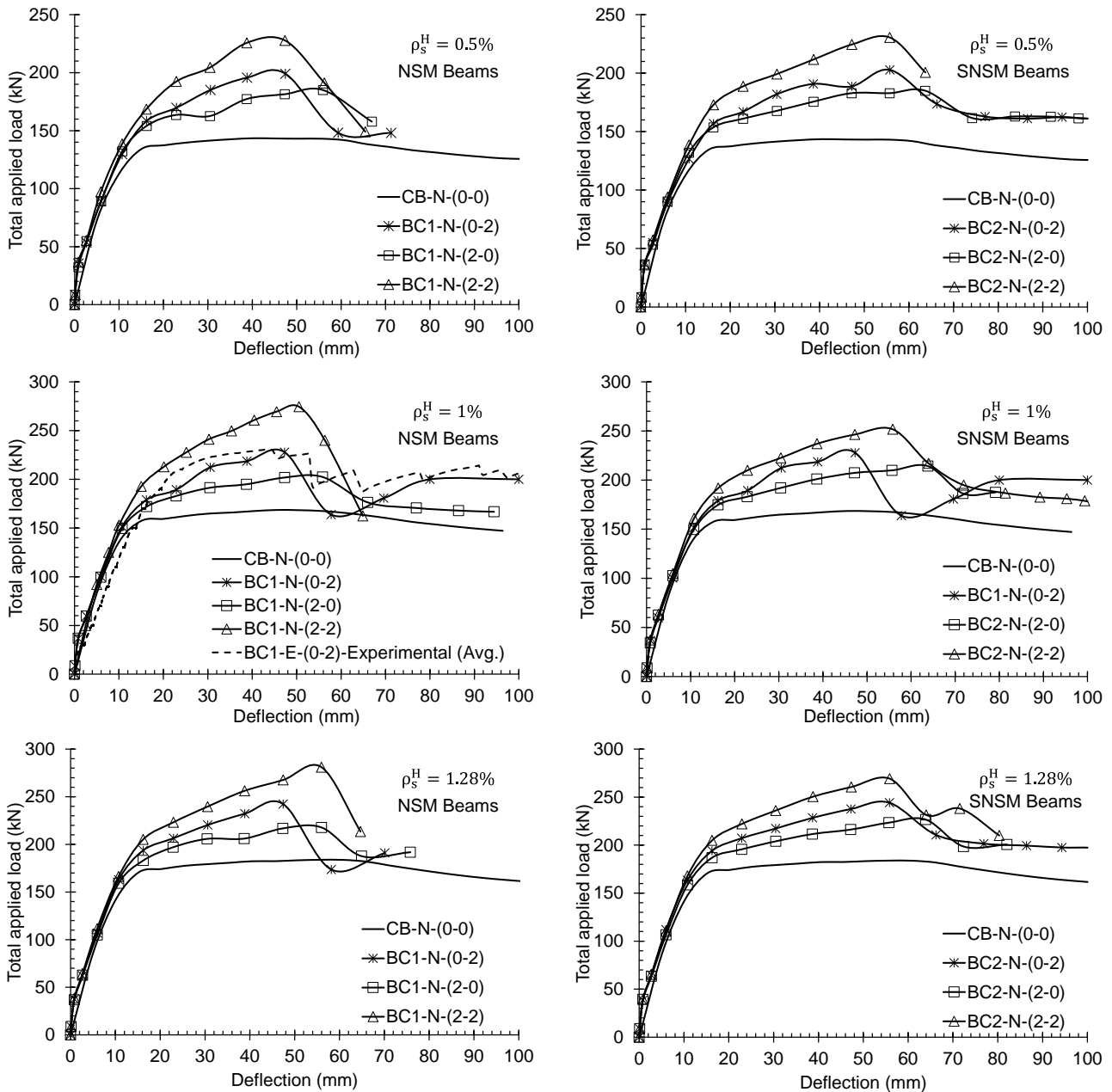


Figure 3-24 : Load-deflection curves of FE beams

### 3.5 Appendix

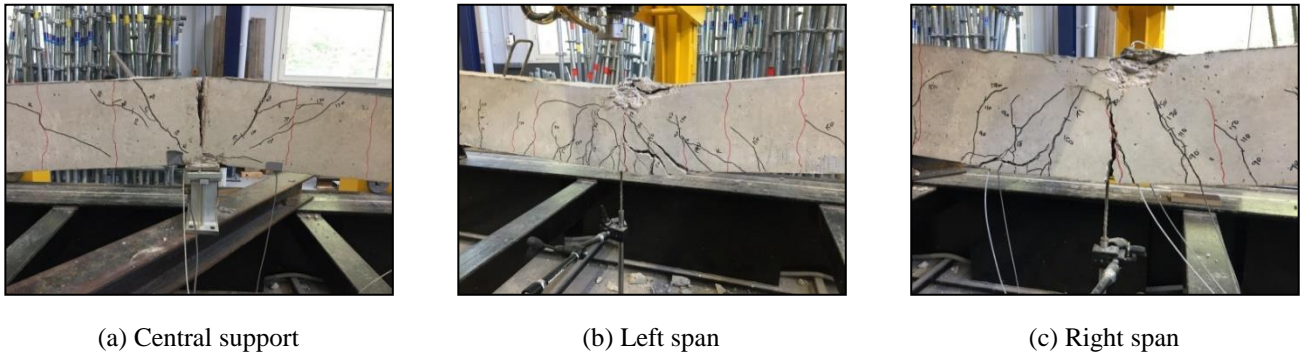


Figure A-1 : Failure mode of beam BC1-E-NSM-(0-2)

### 3.6 References

1. De Lorenzis L, Teng JG. Near-surface mounted FRP reinforcement: an emerging technique for strengthening structures. *Composites Part B-Engineering* 2007; 38(2):119-143.
2. Khalifa AM. Flexural performance of RC beams strengthened with near surface mounted CFRP strips. *Alexandria Eng J* 2016;55:1497–505.
3. Ayesha Siddika, Abdullah Al Mamun Md, Rayed Alyousef, Mugahed Amran YH. Strengthening of reinforced concrete beams by using fiber-reinforced polymer composites: A review. *Journal of Building Engineering* 25 (2019) 100798.
4. Al-Obaidi S, Saeed Y M., Rad FN, Flexural strengthening of reinforced concrete beams with NSM-CFRP bars using mechanical interlocking *Journal of Building Engineering*, 31 (2020) 101422.
5. Akter Hosen Md, Jumaat MZ, Alsubari B, Ramli Sulong NH , Ibrahim Z, Johnson Alengaram U, Hashim H. Effect of bonding materials on the flexural improvement in RC beams strengthened with SNSM technique using GFRP bars. *Journal of Building Engineering* 32 (2020) 101777.
6. Al-Mahmoud F, Caste A I, François R, Tourneur C. Strengthening of RC members with near surface mounted CFRP rods. *Composite Structures* 2009; 91:138-147
7. Al-Mahmoud F, Castel A, François R. Failure modes and failure mechanisms of RC members strengthened by NSM CFRP composites – analysis of pull-out failure mode. *Compos B* 2012;43:1893–901.
8. Dias SJE, Barros JAO, Janwaen W. Behavior of RC beams flexurally strengthened with NSM CFRP laminates, *Composite Structures*, 201(2018), 363-376.
9. Almassri B, Al Mahmoud F, Francois R. Behaviour of corroded reinforced concrete beams repaired with NSM CFRP rods, experimental and finite element study. *Compos B Eng* 2016;92:477–88.
10. Sharaky IA, Baena M, Barris C, Sallam HEM, Torres L. Effect of axial stiffness of NSM FRP reinforcement and concrete cover confinement on flexural behaviour of strengthened RC beams: Experimental and numerical study. *Engineering Structures* 173 (2018), 987–1001.
11. Ferracuti B, Savoia M, Mazzotti C. A numerical model for FRP–concrete delamination. *Composites Part B: Engineering*, 37(2006), 356-364.

12. Chen G, Teng J, Chen J. Finite-element modeling of intermediate crack debonding in FRP-plated RC beams. *Journal of Composites for Construction*, 15(2011), 339–53.
13. Arruda MRT, Firmo JP, Correia JR, Tiago C. Numerical modelling of the bond between concrete and CFRP laminates at elevated temperatures, *Engineering Structures*, 110 (2016), 233-243.
14. Shomali A, Mostofinejad D, Esfahani MR. Experimental and numerical investigation of shear performance of RC beams strengthened with FRP using grooving method. *Journal of Building Engineering* 31 (2020) 101409
15. Abdallah M, Al Mahmoud F, Boissière R, Khelil A, Mercier J. Experimental study on strengthening of RC beams with Side Near Surface Mounted technique-CFRP bars. *Composite Structures* 234 (2020) 111716. <https://doi.org/10.1016/j.compstruct.2019.111716>.
16. Haddad RH, Yagmour EM. Side NSM CFRP strips with different profiles for strengthening reinforced concrete beams. *Journal of Building Engineering* 32 (2020) 101772.
17. Abdallah M, Al Mahmoud F, Khelil A, Mercier J, Almassri B. Assessment of the flexural behavior of continuous RC beams strengthened with NSM-FRP bars, experimental and analytical study, *Composite Structures*, 242 (2020) 112127.
18. ABAQUS version 6.13, 2013. Computer software, Assault Systems, Waltham. MA.
19. ACI Committee 440. Guide For The Design And Construction Of Externally Bonded FRP Systems For Strengthening Concrete Structures. American Concrete Institute, 2017, Farmington Hills, MI., USA.
20. Al-Mahmoud F, Castel A, François R, Tourneur C. Effect of surface preconditioning on bond of carbon fiber reinforced polymer rods to concrete. *Cem Concr Compos* 2007;29(9):677–89.
21. Hassan T, Rizkalla S. Investigation of bond in concrete structures strengthened with near surface mounted carbon fiber reinforced polymer strips. *J Compos Constr.*, 2003; 7(3):248–57
22. De Lorenzis L.; Lundgren K; Rizzo A. Anchorage Length of Near-Surface-Mounted FRP Bars for Concrete Strengthening—Experimental Investigation and Numerical Modeling, *ACI Structural Journal*, 101 (2004), 269-278
23. Tahnat YBA., Dwaikat MMS, Samaaneh MA. Effect of using CFRP wraps on the strength and ductility behaviors of exterior reinforced concrete joint. *Composite Structures*, 201 (2018), 721–739.
24. Algaard W, Lyle J, Izzat C. Perforation of composite floor. 5<sup>th</sup> European LS-DYNA Users Conference, 2005, Birmingham, UK, May
25. Nguyen HT, Kim SE. Finite element modeling of push-out tests for large stud shear connectors, *Journal of Constructional Steel Research*, 65(2009), 1909-1920.
26. ABAQUS, 2013, ABAQUS Analysis User's Manual Version 6.13, Assault Systems.

27. Omran HY, El-Hacha R. Nonlinear 3D finite element modeling of RC beams strengthened with prestressed NSM-CFRP strips, *Construction and Building Materials*, 31(2012), 74–85.
28. Lubliner J, Oliver J, Oller S, Oñate E. A plastic-damage model for concrete, *Int. J. Solids Structures*. 25(1989), 229–326.
29. Lee J, Fenves GL, Plastic-damage model for cyclic loading of concrete structures, *Journal of Engineering Mechanics*, 124 (1998), 892–900.
30. Bezerra LM, Cavalcante OO, Chater L, Bonilla J. V-shaped shear connector for composite steel-concrete beam, *Journal of Constructional Steel Research*, 150(2018), 162-174.
31. Wahalathantri BL, Thambiratnam DP, Chan THT, Fawzia S. A material model for flexural crack simulation in reinforced concrete elements using ABAQUS. First International conference on engineering, designing and developing the built environment for sustainable wellbeing, 2011, Brisbane, Australia, April.
32. Alfarah B, López-Almansa F, Oller S. New methodology for calculating damage variables evolution in plastic damage model for RC structures, *Engineering Structures*. 132 (2017), 70–86.
33. Rezazadeh M, Costa I, Barros J. Influence of prestress level on NSM CFRP laminates for the flexural strengthening of RC beams, *Composite Structures*, 116(2014), 489-500.
34. Abouali S, Shahverdia M, Ghassemieh M, Motavallia M. Nonlinear simulation of reinforced concrete beams retrofitted by nearsurface mounted iron-based shape memory alloys, *Engineering Structures*, 187(2019), 133–148.
35. Hawileh RA. Nonlinear finite element modeling of RC beams strengthened with NSM FRP rods, *Construction and Building Materials*, 27(2012), 461–471.
36. Al-Mahmoud F, Castel A, François R, Tourneur C. Anchorage and tension-stiffening effect between near-surface-mounted CFRP rods and concrete. *Cem Concr Compos* 2011;33:346–52.
37. Capozucca R. Analysis of bond-slip effects in RC beams strengthened with NSM CFRP rods, *Composite Structures*, 102(2013), 110–123.
38. Seracino R, Saifulnaz MMR, Oehlers DJ. Generic debonding resistance of EB and NSM plate-to-concrete joints, *Journal of Composites for Construction*, 11(2007), 62–70.
39. Obaidat YT, Heyden S, Dahlblom O. The effect of CFRP and CFRP/concrete interface models when modeling retrofitted RC beams with FEM. *Composite Structures*, 92(2010), 1391–1398.



## CHAPTER 4 : EFFICIENCY OF EB CFRP COMPOSITES FOR FLEXURAL STRENGTHENING OF CONTINUOUS RC BEAMS: A COMPARATIVE STUDY WITH NSM CFRP RODS.

*Published in Structures, <https://doi.org/10.1016/j.istruc.2021.08.073>*

---

As the previous two chapters (2&3) presented the flexural behavior of continuous RC beams strengthened internally with FRP bars using the NSM or side-NSM techniques, this chapter aims to strengthen continuous two-span RC beams with EB-CFRP. First, the influence of the CFRP reinforcements on the beam behavior was investigated according to their position (side or top/bottom), form (sheet or plate), layer number (one or multiple layers); and weight (350 g/m<sup>2</sup>, 700 g/m<sup>2</sup> and 1100 g/m<sup>2</sup>). The experimental program of chapter four consists of six large-scale two-span beams. The test results were discussed through the load-carrying capacity and failure mode of the beams as well as the reinforcements strain. The crack maps of all tested beams at failure were drawn and discussed. The relationships between the axial stiffness ratio and yielding load of beams as well as between the EB-CFRP area and debonding strain were introduced. Furthermore, this chapter investigates, in detail, the capacity of EB-CFRP continuous beams to redistribute the bending moment in the stage between the concrete cracking and the first steel yielding. Second, this chapter evaluates the effectiveness of the current design codes (ACI 440.2R-08, CNR-DT 200 R1/2013 and *fib* Bulletin 14) in determining the flexural strength of continuous beams strengthened externally with CFRP sheets or plates. Third, it presents a comprehensive comparison study between the NSM and EB techniques in strengthening continuous RC beams.

**Efficiency of EB CFRP composites for flexural strengthening of continuous RC beams:  
A comparative study with NSM CFRP rods**

Mohammad Abdallah\*<sup>1</sup>, Firas Al Mahmoud<sup>1</sup>, Abdelouahab Khelil<sup>1</sup> and Julien Mercier<sup>2</sup>

<sup>1</sup>*Institut Jean Lamour, UMR 7198, CNRS, Université de Lorraine, Nancy, France*

<sup>2</sup>*Freyssinet, Paris, France*

---

**Keywords:** EB; NSM; strengthening; continuous RC beam; comparison.

**Abstract**

This paper presents an experimental study of the use of carbon fiber-reinforced polymer (CFRP) composites to strengthen two-span reinforced concrete (RC) beams. Six large-scale beams were strengthened in hogging and sagging regions according to the external bonding (EB) technique and then statically tested to investigate the impact of the CFRP position, CFRP form, CFRP layers, and weight of carbon fibers on the flexural performance of continuous beams. The experimental results of the strengthened beams were carefully studied in terms of load-carrying capacity, failure modes, cracking patterns, moment redistribution, and reinforcement strain and compared with the results of an unstrengthened control beam. The efficiency of the EB technique in strengthening continuous RC beams was assessed through a comparative study with the near surface mounted (NSM) technique. For this purpose, another two beam specimens strengthened with NSM-CFRP bars were considered.

Based on the experimental results, a general improvement in the flexural performance of strengthened beams was observed. By applying the EB-CFRP composites, the yield and ultimate load capacity could be improved up to 59.1% and 49.8% respectively. The results also showed that increasing the carbon fiber weight was found to be effective in improving the strength capacity of beams and it may be used as an alternative to multiple sheet layers. Comparisons regarding the global flexural performance allow confirming the higher efficiency of the NSM system in comparison to the EB one.

**4.1 Introduction**

Fiber-reinforced polymers (FRPs) are increasingly being used in the field of civil engineering due to their mechanical strengthening advantages. Among the various composite materials available, carbon fiber-reinforced polymers (CFRPs) are considered the most used and are widely preferable. In general, CFRPs have a high tensile strength and modulus of elasticity and exhibit excellent resistance to corrosion and creep rupture [1]. CFRP materials in the form of plates or sheets can be applied to damaged structural elements as an external reinforcement via the external bonding (EB) technique [2], whereas those in the form of rods are used as an internal reinforcement via the near surface mounted (NSM) technique [3]. Generally, the efficiency of the CFRPs used in reinforced concrete (RC) structures depends on their interface bonding behavior with concrete, which can normally be achieved using an epoxy-resin agent. Such bonding behavior is essentially affected by the mechanical properties of the CFRP and the adhesive epoxy-resin materials, as well as the roughness of the concrete surface [4, 5]. Regarding the latter, both the EB and NSM techniques have different construction processes, implying different bond strength levels.

Although CFRP materials were used for the first time more than 50 years ago to strengthen RC members, only a limited number of research studies have investigated the use of such materials to strengthen statically indeterminate members, such as continuous beams [6-9]. Extensive research studies have been performed on the use of CFRPs to reinforce and retrofit simply supported beams (SSBs) [10-16], joints [17-19], and columns [20-22]. It has been found that the flexural strength improvement in SSBs as a result of CFRPs is significant and may reach, in some strengthening configurations, more than 90% with the EB technique [10] and even more than 130% with the NSM technique [23]. However, regardless of the strengthening technique that is used, an essential drawback that has been reported is the nonconventional failure mode of the SSBs due to delamination and/or the tensile rupture of the EB-CFRP sheets/plates or pull-out of the NSM-CFRP rods. Under certain circumstances, such a nonconventional failure mode may occur at an early load stage in the form of concrete cover separation [24] or peeling-off failure [25], either of which can prevent the desired flexural strength enhancement in the beam. A number of end anchorage systems have been suggested to prevent such a premature failure in EB-CFRP sheet beams, such as U-strap [26], L-shaped jackets [27], and CFRP splay anchors [28], as well as in NSM-CFRP rod beams, such as end-steel plates [29]. Some of these systems, however, are not convenient to implement in current constructions and may require a prior manufacturing process. In contrast, the ACI 440.2R guideline [30] recommends that, on the one hand, FRP laminates should be terminated at least at a distance equal to the development length ( $l_{df}$ ) past the point along the span corresponding to the cracking moment ( $M_{cr}$ ) in the SSBs. In continuous beams, on the other hand, FRP laminates should be terminated at  $d/2$  or at least 150 mm beyond the inflection point (point of zero moment), where  $d$  is the cross-sectional effective depth.

A general review of the literature on strengthening SSBs using the EB and NSM techniques confirms their potential to enhance the flexural behavior of RC beams. However, their initial forms might not be feasible for some practical applications. These systems have several shortcomings due to the imposed architectural constraints, the insufficient dimensions of the beam itself, and the possibility of damaging other members, such as columns, during preparation and installation. Consequently, side-bonded CFRP sheets [10] and side-NSM-CFRP rods [11,23] have recently been proposed as convenient alternatives, although their effectiveness has not yet been investigated in continuous RC beams. Bilotta et al. [24] discussed the efficiency of the NSM and EB techniques in strengthening SSBs using CFRP strips and plates. The test results indicated that the NSM system is more effective than the EB system in improving the flexural strength although it is less effective in increasing the beam stiffness. Furthermore, NSM strips were found to be weakly sensitive to debonding phenomena. To the best of our knowledge, there are no published studies comparing the efficiency of the EB and NSM systems in terms of strengthening continuous RC beams.

Unlike SSBs, continuous beams have positive (sagging) and negative (hogging) bending moment regions. Therefore, their flexural behavior and failure modes are considerably different from those of SSBs and are strongly associated with the strengthening arrangement of CFRP reinforcements. Ashour et al. [6] performed a series of experimental tests to study the performance of continuous two-span RC beams strengthened in flexure with EB-CFRP sheets. The test results showed that strengthening both the sagging and hogging regions is the most

effective arrangement to enhance the beams' load-carrying capacity. The tested strengthened specimens exhibited about 25% improvement in the ultimate load compared to their unstrengthened counterparts, and they failed because of the tensile rupture of the CFRP sheets, CFRP sheet separation, and brittle peeling failure of the concrete cover. The same strengthening arrangement was adopted by Akbarzadeh et al. [7] to experimentally study the influence of multilayer CFRP sheets on the flexural response of reinforced high-strength two-span beams. The authors found that increasing the number of layers can change the failure mode from tensile rupture to intermediate crack (IC) debonding of the CFRP sheets. The beam strengthened with three layers of CFRP sheets exhibited about 60% improvement in the load-carrying capacity compared to the control beam. Ali et al. [8] examined the flexural capacity and failure modes of continuous RC beams with three spans externally strengthened in the positive and negative moment regions with different lengths and layers of CFRP sheets. They concluded that the ultimate load of the strengthened beams increased by 16.7%–26.6% with respect to the control beam. The main failure modes observed were peeling-off and rupture of the CFRP sheets. Abdallah et al. [9] clarified that the contribution of NSM-CFRP rods to the improvement of the load-carrying capacity of statically indeterminate two-span RC beams is limited by the debonding of the CFRP bars in the negative bending moment zone or peeling-off of the concrete cover. Notably, the peeling-off failure occurred due to the insufficient CFRP rod length. However, the beam specimens were strengthened in both the hogging and sagging regions, and the improvement achieved in their load-carrying capacity ranged between 42% and 63% compared to the load-carrying capacity of the control beam.

Moment redistribution is a key feature of continuous RC beams. In ordinary indeterminate beams, moment redistribution primarily depends on the amount of tension steel reinforcement ( $\rho_s$ ) in the critical sections. Indeed, at the ultimate state, moment transfer occurs from the hogging region to the sagging region when  $\rho_s^h/\rho_s^s$  is not greater than 1.0, whereas when  $\rho_s^h/\rho_s^s$  is greater than 1.5, moment transfer occurs from the sagging region to the hogging region. When  $\rho_s^h/\rho_s^s$  falls between 1.0 and 1.5, the moment transfer is indistinct [31]. Despite being very limited, previous experimental studies on strengthening RC beams with CFRP composites have indicated that moment redistribution in such members is possible to some extent at the ultimate state [7, 9]. Nevertheless, moment redistribution not only occurs at the ultimate state but also evolves through the whole loading process, even before formation yielding of the tension steel reinforcement [31-32].

As stated above, relatively few studies have been performed on continuous RC beams strengthened with either EB-CFRP or NSM-CFRP. Most of these studies have focused on the impact of the arrangement, number of layers, and length of CFRPs on the failure modes and flexural capacity of beams. It is worth mentioning that increasing the carbon fiber weight per unit area has recently been used in the construction and rehabilitation industry as an alternative to multiple sheet layers. However, there are no available studies in the literature exploring the effectiveness of that alternative in terms of improving the performance of continuous RC beams. Therefore, the primary aim of this study is to fill in the gaps in the literature regarding strengthening continuous RC beams with EB-CFRP. Generally, this study consists of three main sections. In the first section, seven large-scale two-span beams are statically investigated: one control beam and six beams initially strengthened in terms of bending with CFRP sheets or

plates. The principle aim of the first section is to investigate the effects of important influential factors, such as (i) the CFRP reinforcement position; (ii) the CFRP form, either sheet or plate; (iii) the CFRP layer number; and (iv) the weight of the carbon fibers, on the load-carrying capacity, failure modes, cracking patterns, moment redistribution, and strain analysis of continuous beams. Because the current design guidelines have been developed to strengthen SSBs with EB-FRP laminates, the second part of this study evaluates the effectiveness of the current design codes in determining the flexural strength of continuous beams strengthened externally with CFRP sheets or plates. The experimental flexural strength capacities of the tested beams are compared with those obtained from the design formulas provided in the American ACI 440.2R-08 [30], the Italian CNR-DT 200 R1/2013 [33], and the technical report of FIB Bulletin 14 [34]. Finally, the third section assesses and compares the efficiencies of the EB and the NSM techniques. For this purpose, another two beams strengthened by means of the NSM and side-NSM-CFRP bars technique are tested and presented.

## 4.2 Experimental Program

### 4.2.1 Tested beams and material properties

The test matrix in this section consists of seven full-scale two-span RC beams: one considered as a reference beam and six externally strengthened with CFRP composites. Figure 4-1 shows the cross-sectional details, steel reinforcement layout, and applied loads of the tested beam specimens. Each specimen comprised two equal spans, each of 2850 mm. All beams had a rectangular cross section with a width of 150 mm and a height of 250 mm. The steel reinforcement arrangement was as follows:  $A_{s1} = A_{s2} = 307.9 \text{ mm}^2$ ,  $A_v = 100.5 \text{ mm}^2$ , where  $A_{s1}$  and  $A_{s2}$  are the tensile steel reinforcement amounts in the negative and positive moment regions, respectively, and  $A_v$  is the shear reinforcement of one stirrup. The steel stirrups were spaced at 100 mm center to center. The mechanical properties of the steel used as obtained from three tensile tests on representative specimens, were as follows:  $F_y = 572.6 \text{ MPa}$ ,  $E_s = 192.85 \text{ GPa}$ , and  $\varepsilon_y = 0.3\%$ , where  $F_y$ ,  $E_s$ , and  $\varepsilon_y$  are the average yielding strength, modulus of elasticity, and yielding strain of steel, respectively. The mechanical characteristics of the concrete used for formulating the beams, as obtained from testing eight cylindrical specimens (130 mm  $\times$  260 mm), were as follows:  $f'_c = 39 \text{ MPa}$ ,  $E_c = 29.2 \text{ GPa}$ , and  $f_t = 3 \text{ MPa}$ , where  $f'_c$ ,  $f_t$ , and  $E_c$  are the average compressive strength, tensile strength, and modulus of elasticity of concrete, respectively.

Figure 4-2 and Table 4-1 show the strengthening layout, specimen designations, and details of the control and strengthened beams with EB-CFRP composites. The position of the CFRP reinforcement (either bottom/top or side), the CFRP composite form (either sheet or plate), the CFRP layer number, and the weight of the CFRP sheet were the main variables investigated for this experimental program. Each continuous strengthened beam had the same positive and negative CFRP reinforcement. Each EB beam is identified throughout this paper using a reference code that describes its strengthening scenario. For example, BC1-EB1S means that beam BC1 was strengthened with one externally (E) bonded (B) sheet (S) on the top and bottom surfaces. The number next to the first two letters, BC, indicates the beam number.

In all the tested beams, EB-CFRPs were bonded to the hogging and sagging regions to achieve the highest improvement in the load-carrying capacity. In the hogging region of each specimen, the CFRP reinforcements were placed symmetrically about the central support, whereas, in the sagging regions, the CFRP reinforcements started from the face of the support without any anchorage over the external supports. The strengthening length to the beam length ratio (SL/BL) was considered equal to 0.7 and 0.65 in the hogging and sagging regions, respectively, where SL is the distance between the end of the CFRP and the applied load and BL is the distance between the support and the applied load. To avoid the premature failure of continuous beams with EB-CFRPs, the recommendations outlined in the ACI 440.2R guideline [30] regarding the strengthening length were applied, as shown in Figure 4-2b.

Beams BC1-EB1S and BC2-EB1P were tested to study the efficiency of the EB technique through the strengthening material form. Two forms of CFRP were used: sheets (S) and plates (P). Although CFRP sheets and plates have different properties, the axial stiffness ratios of the total reinforcement ( $1 + \frac{E_f \times A_f}{E_s \times A_s}$ ) of BC1-EB1S and BC2-EB1P were designed to be close to each other.

Beam BC3-EB1S-*side* was tested to evaluate the effect of the CFRP sheet's position on the flexural performance of continuous RC beams. The amount of CFRP reinforcement used in this beam was similar to that used in beam BC1-EB1S. However, in the side beam (BC3-EB1S-*side*), the CFRP sheet was cut beforehand in the longitudinal direction of the fibers into two equal halves, and each tension side of the beam was bonded with one half, as shown in Figure 4-2.

Beams BC4-EB2S, BC5-EB1S-*weight (700)*, and BC6-EB1S-*weight (1100)* were tested to measure the effect of increasing the EB-CFRP sheet's reinforcement ratio through either the number of layers or the carbon fiber weight on the flexural behavior of the beam. Beam BC4-EB2S was strengthened with two layers of CFRP sheets similar to what has been used in beam BC1-EB1S, whereas, beams BC5-EB1S-*weight(700)* and BC6-EB1S-*weight(1100)* were strengthened with one layer of CFRP sheets weighing 700 g/m<sup>2</sup> and 1100 g/m<sup>2</sup>, respectively. The longitudinal carbon fiber weight of the CFRP sheets applied to beams BC1-EB1S, BC3-EB1S-*side*, and BC4-EB2S was approximately 350 g/m<sup>2</sup>. Figure 4-3 shows the three types of CFRP sheets.

Table 4-2 shows the mechanical properties of the Foreva CFRP sheets and plates used. All data were provided by the manufacturer. CFRPs were bonded to the beams using an epoxy-resin adhesive material: Epx TFC (350, 1000) was used for the sheets, whereas Epx SC980 was used for the plates, as shown in Figure 4-4. In general, different resin types were used (i) to simulate the real procedure used by construction companies in the field and (ii) to show the workability of Epx TFC resin is higher than that of the Epx SC980 resin, making it more suitable and feasible in case of sheet strengthening. However, Epx TFC 350 is a normal adhesive that usually used for ordinary CFRP sheets (350 g/m<sup>2</sup>), in this study, it was also used for investigating efficiency of the CFRP sheet 750 g/m<sup>2</sup>, whereas Epx TFC 1000 is an epoxy based resin specifically designed to be used with CFRP sheet 1100 g/m<sup>2</sup> structural strengthening systems. Table 4-3 presents the characteristics of the resin materials.



Table 4-1 : Beams details

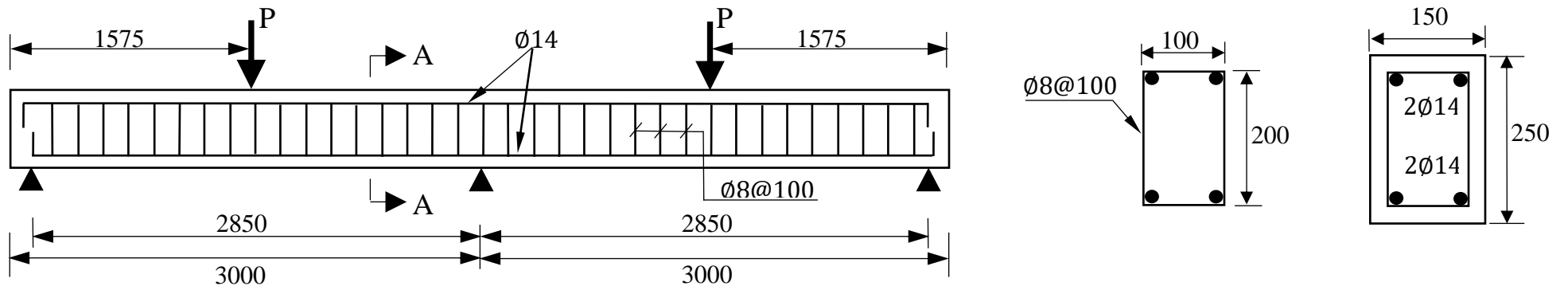
Beam	Hogging region strengthening			Sagging region strengthening			$A_s$ (mm <sup>2</sup> )	$A_f$ (mm <sup>2</sup> )	$E_f$ $\times A_f$ (kN)	$1 + \frac{E_f \times A_f}{E_s \times A_s}$
	No.	Length (m)	SL/BL	No.	Length (m)	SL/B L				
CB	----	----	----	----	----	----	307.88	----	----	1
BC1-EB1S	1	2.0	0.70	1	2.3	0.65	307.88	72	7560	1.13
BC2-EB1P	1	2.0	0.70	1	2.3	0.65	307.88	56.5	9322.5	1.16
BC3-EB1S-side	1	2.0	0.70	1	2.3	0.65	307.88	72	7560	1.13
BC4-EB2S	2	2.0	0.70	2	2.3	0.65	307.88	144	15120	1.26
BC5-EB1S-weight(700)	1	2.0	0.70	1	2.3	0.65	307.88	99	10395	1.17
BC6-EB1S-weight(1100)	1	2.0	0.70	1	2.3	0.65	307.88	187.5	19635	1.33

Table 4-2 : Characteristics of the CFRP composites

Material	Width $\times$ Depth (mm $\times$ mm)	Ultimate strength (MPa)	Modulus of elasticity (GPa)	Strain at failure (%)
CFRP-Sheet-350 g/m <sup>2</sup>	150 $\times$ 0.48	1700	105	1.7
CFRP-Sheet-700 g/m <sup>2</sup>	150 $\times$ 0.66	1700	105	1.7
CFRP-Sheet-1100 g/m <sup>2</sup>	150 $\times$ 1.25	1700	105	1.7
CFRP-Plate	50 $\times$ 1.2	2800	165	1.7

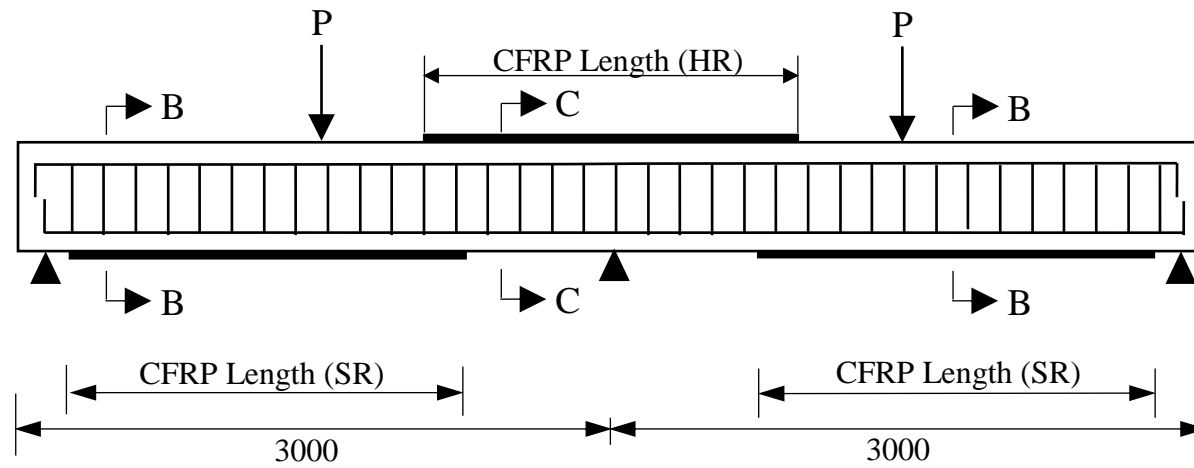
Table 4-3 : Characteristics of the epoxy-resin

Material	Compressive strength (MPa)	Tensile strength (MPa)	Elastic modulus (GPa)
Epoxy resin- SC980 [22]	83	29.5	4.94
Epoxy resin-TFC (350)	89	27	2.3
Epoxy resin-TFC (1000)	68	48	1.7



Section A-A

Figure 4-1 : Dimensions, steel reinforcement layout and support arrangement of the tested beams.



(a)



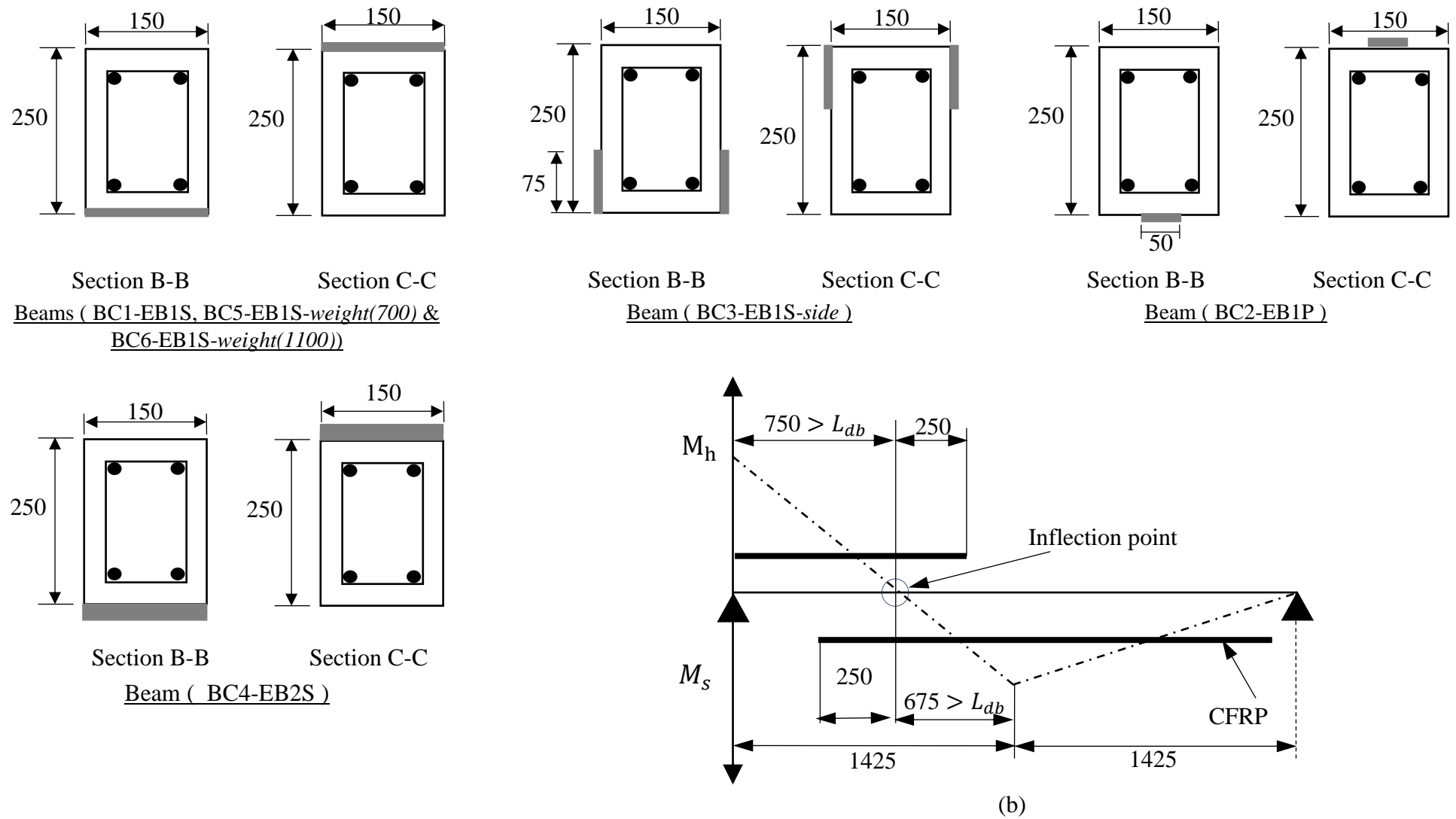


Figure 4-2 : (a) Elevation view and cross-sections of the beam specimens and (b) Length of CFRP sheets/plates in beams. (All dimensions are in mm)

### 4.2.2 Surface preparation and strengthening technique

First, a concrete surface was prepared using a mechanical grinder, as shown in Figure 4-5a. Then the surface was cleaned with compressed air to remove debris and fine particles (Figure 4-5b). Next, an initial layer of Epx TFC epoxy was added and distributed over the prepared concrete surface using a paint roller (Figure 4-5c). The CFRP sheets were saturated with an epoxy resin while being installed, and the paint roller was applied with a considerable amount of pressure to roll the CFRP sheets in the longitudinal direction of the fibers, as illustrated in Figure 4-5d. This was done to ensure proper bonding between the CFRP sheets and the concrete substrate.

Regarding the beam specimen strengthened with CFRP plates, the same procedure described above was applied. The only difference was the type of epoxy resin used; that is Epx SC980 was used for the plated beams instead of Epx TFC. The final shape of the CFRP plated beam is shown in Figure 4-5e. For all the strengthened specimens, the CFRP composites were allowed to cure for seven days before testing.

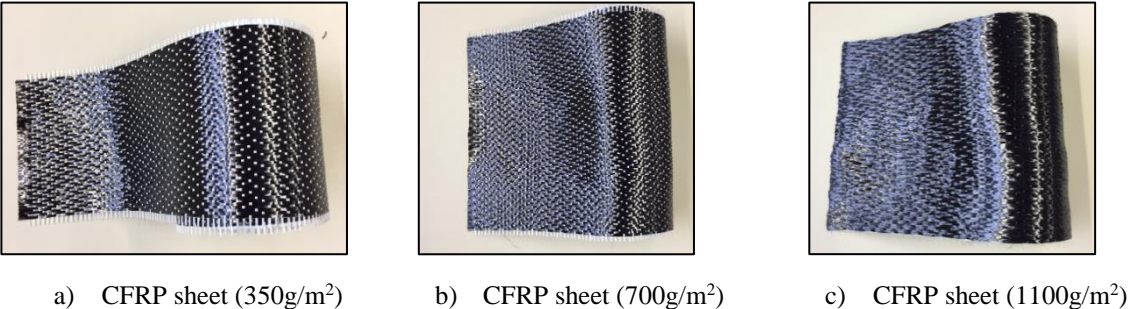


Figure 4-3 : CFRP sheets used for strengthening beams

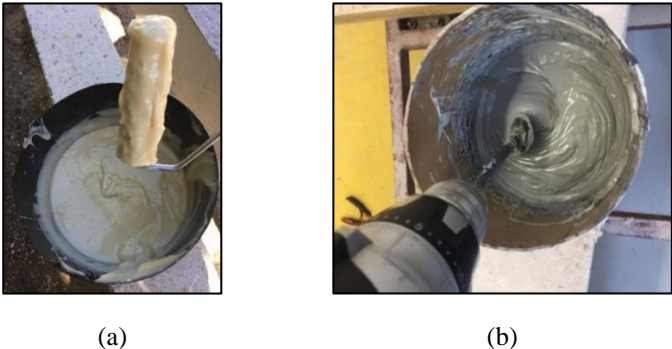


Figure 4-4 : Epoxy resin material for bonding the CFRP (a) sheets and (b) plates

### 4.2.3 Instrumentation and test setup

One control beam, four beams strengthened with one EB sheet, one beam strengthened with two-layer sheets, and one beam strengthened with one EB plate were loaded until destruction with two concentrated loads separated by a distance of 2850 mm. For the loading process, two hydraulic actuators with a capacity of 400 kN and an average loading speed of 0.3 kN/s were used. The total applied load, central support reaction, midspan deflection, and strain of the steel and CFRP were measured during the tests. The reaction at the interior support was measured using a load cell with a capacity of 200 kN, while two vertical linear variable differential transducers (LVDTs) were used for each beam to monitor the vertical midspan deflection (one

LVDT at each midspan). The tested beam specimens were instrumented with electrical strain gauges attached to the tension steel and CFRP at the central support and midspan sections to measure their tensile stresses. Figure 4-6 illustrates the instrumentations used and the bending test setup.

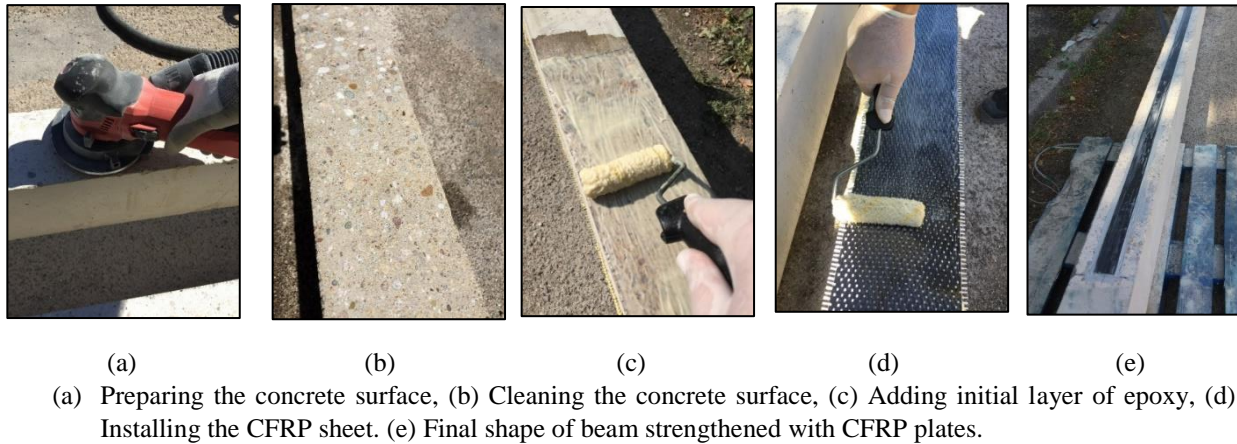


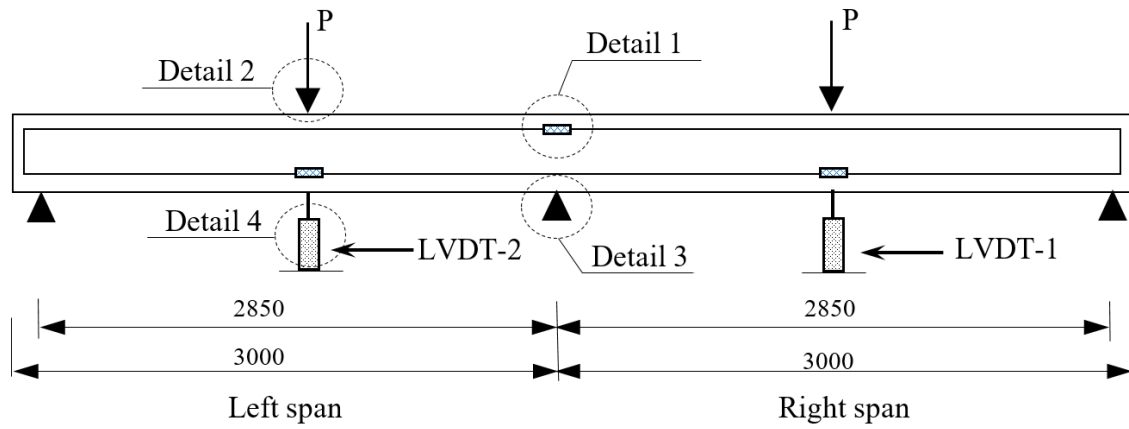
Figure 4-5 : Strengthening procedure of EB-CFRP beam specimens

### 4.3 Results and Discussion

#### 4.3.1 Load-deflection response

Figure 4-7 presents the applied load versus the midspan deflection of the control and strengthened beams. The load-deflections curves of the tested beams typically consist of three stages: the precracking of concrete, postcracking of concrete, and postyielding of steel. No noticeable variation was found between the beams at the first stage. In contrast, the comparisons provided in Fig. 4-7 show increases in the postcracking stiffness, load at yielding, and load at failure in the EB-CFRP beams in comparison to the control beam. Such increases were principally controlled by the number of layers, by the form and weight of the carbon fibers, and marginally by the position of the CFRP reinforcement. Indeed, among all the tested strengthened specimens, the highest improvement in the load-deflection response was achieved in the beam employing one layer of  $1100 \text{ g/m}^2$  CFRP sheet (BC6-EB1S-weight (1100)), whereas the lowest improvement was reported in the beam strengthened with CFRP plates (BC2-EB1P). Overall, in all the tested beams, the increasing percentages of the yield and ultimate load due to the EB-CFRP composites were found to range from 25.5% to 59.1% and from 7.6% to 49.8%, respectively.

The ultimate load of beams BC1-EB1S (219.4 kN) and BC4-EB2S (242.4 kN) was found to be about 29.3% and 42.8 higher than that of the control beam (169.7 kN), respectively. This result confirms that increasing the amount of CFRP reinforcement using multisheet layers contributes considerably to the enhancing of the load-carrying capacity of continuous beams, as one can also notice in [8].



(a) Instrumentation and arrangement of supports and loads



(b) Test setup



Detail 1 : Strain guage instillation



Detail 2 : Point load



Detail 3 : Central support



Detail 4 : LVDT

Figure 4-6 : Instrumentation and test setup

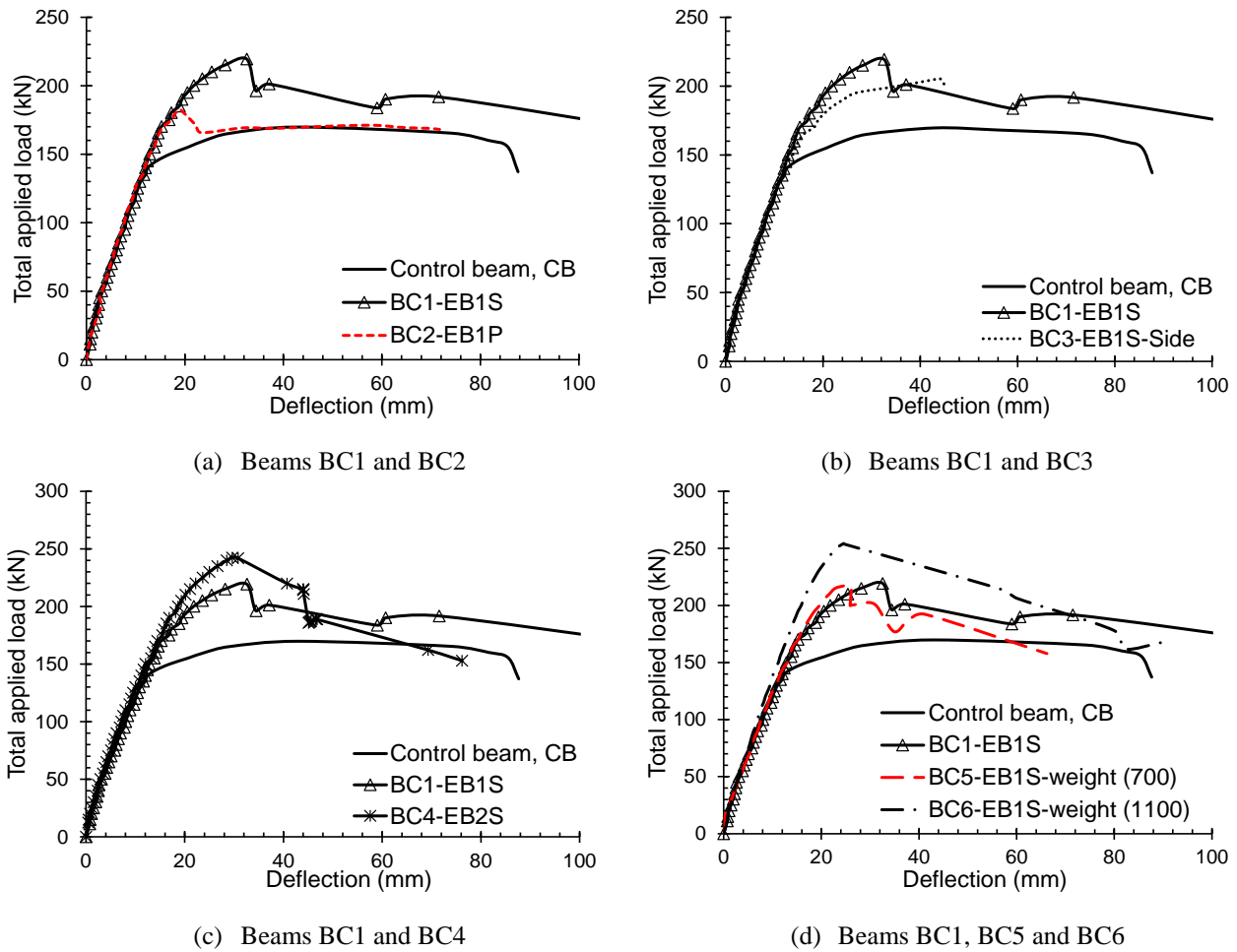


Figure 4-7 : Load deflection curves of tested beams

It has also been observed that the efficiency of the EB-CFRP plate in improving the flexural strength of continuous beams in terms of the ultimate load capacity was lower than that observed for the EB-CFRP sheets. Although the axial stiffness ratio of beam BC2-EB1P (1.16) was slightly greater than that of beam BC1-EB1S (1.13), the ultimate load capacity of BC2-EB1P (182.52 kN) was only 83% that of BC1-EB1S. This lower efficiency of the EB-CFRP plates may be attributed to the bonding surface between the CFRP and the concrete substrate. The bonding surface between the CFRP sheet and the concrete surface in beam BC1-EB1S (width of sheet: 150 mm) was about three times that between the CFRP plate and the concrete in beam BC2-EB1P (width of plate: 50 mm). Therefore, it may be concluded that the bonding area is more influential than the axial stiffness ratio when the comparison is based on the EB-CFRP form.

The load-deflection graphs (Figure 4-7) also show that the side-bonded CFRP sheet was slightly less efficient than the conventional top/bottom-bonded CFRP sheets in terms of enhancing the flexural behavior of continuous RC beams, making it a feasible alternative. Compared to beam BC1-EB1S, the decrease in the ultimate load (205.43 kN) of beam BC3-EB1S-side was only 6.4%. This difference in the load-carrying capacity is most likely due to the decrease in the effective moment arm depth of the tension reinforcements in beam BC3-EB1S-side due to the changing position of the CFRP sheet.



Because the CFRP reinforcement area was higher, it was expected that the load-carrying capacity of beam BC5-EB1S-*weight(700)* would be relatively higher than that of beam BC1-EB1S. However, this hypothesis was not confirmed by beam BC5-EB1S-*weight(700)*, as can be discerned from Figure 4-7d. Although the postyielding stiffness improved, increasing the carbon fiber weight from 350 g/m<sup>2</sup> to 700 g/m<sup>2</sup> found not to allow an additional improvement in the ultimate load capacity of the beam. The failure load of beam BC5-EB1S-*weight(700)* (217.6 kN) was about 99.2% of the failure load of beam BC1-EB1S. This can be attributed to (i) increasing the CFRP reinforcement from 72 mm<sup>2</sup> in BC1-EB1S to 99 mm<sup>2</sup> in BC5-EB1S-*weight(700)* not being sufficient to significantly increase the axial stiffness ratio, which remains very close in the two beams; and (ii) the adhesive epoxy-resin used, Epx TFC 350, not being suitable to saturate heavy and dense carbon fiber fabrics such that used in BC5-EB1S-*weight(700)*.

The impact of increasing the carbon fiber weight can be clearly seen in beam BC6-EB1S-*weight(1100)*, where the failure load (254.26 kN) increased by 49.8% over that of the control beam and even by 4.9% over that of the beam strengthened with two sheet layers (i.e. BC4-EB2S, 350 g/m<sup>2</sup>), (Figure 4-7c and Figure 4-7d). The CFRP reinforcement amount and the axial stiffness ratio of BC6-EB1S-*weight(1100)* were 1.3 and 1.06 times those in BC4-EB2S. It should be noted that a special soft adhesive (Epx TFC 1000) was used in BC6-EB1S-*weight(1100)* to ensure saturation such a heavy carbon sheet.

### 4.3.2 Failure modes

Four failure modes were observed in the tests (i) conventional flexural failure, (ii) IC debonding of CFRP plates/sheets, (iii) IC debonding of CFRP sheets in one region followed by concrete cover delamination (CCD) in the other region, and (iv) IC debonding of CFRP sheets followed by tensile rupture of the CFRP sheets. These failure modes are described in detail in the following sections.

Debonding of CFRP sheets and plates as a result of ICs at critical sections (midspan and over the central support) was the dominant failure mode observed in the strengthened beams. IC debonding appeared to be the only failure mode in beams BC2-EB1P and BC6-EB1S-*weight(1100)*, whereas it was followed by other types of failure, such as CCD, in beams BC1-EB1S, BC4-EB2S, and BC5-EB1S-*weight(700)*, as well as tensile rupture of CFRP sheets in beam BC3-EB1S-*side*. Such debonding of the CFRP composites as a results of ICs started first either at the midspan or over the central support and then developed toward the ends of the CFRP composites with the increase of the external applied load. By contrast, in the regions that failed as a result of CCD, separation of the concrete cover started at the ends of the CFRP composites due to the formation of diagonal flexural shear cracks and then propagated toward the interior critical section.

It worth noting that the separation of the EB-CFRP sheets/plates observed in the tested beams, resulting from either IC or CCD failures, occurred with concrete attached, meaning that it was accompanied by a loud noise and dust. In all the tested CFRP beams, ripping and limited crushing of the compressed concrete at the external load application sections and central support occurred before the EB-CFRP failure.

4.3.2.1 Failure mode 1: Conventional ductile flexural failure

This failure mode was illustrated by the control beam specimen (CB), as shown in Figure 4-8. This failure started by the yielding of the tension steel reinforcement followed by concrete crushing in the compression surfaces at the central support and points of the applied loads.

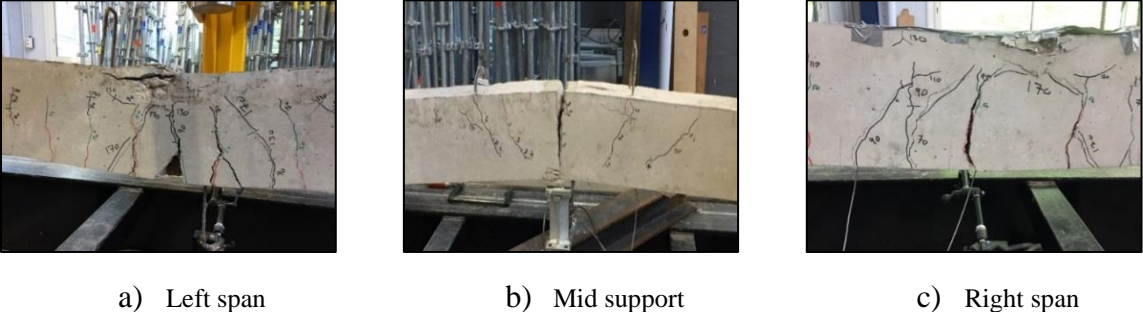


Figure 4-8 : Failure mode of control beam, CB.

4.3.2.2 Failure mode 2: IC debonding

Debonding failure of EB-CFRP resulting from an IC was demonstrated by beams BC2-EB1P and BC6-EB1S-weight(1100), as shown in Figure 4-9 and Figure 4-10, respectively.

The IC debonding in beam BC6-EB1S-weight (1100) first occurred in the left sagging region, followed by failure of the hogging and right sagging regions. In beam BC2-EB1P, the IC debonding occurred simultaneously at the hogging and left sagging regions. This IC debonding was explosive and was followed immediately by beam failure.

Interestingly, such debonding failure was not observed in the right span of beam BC2-EB1P. This was most likely associated with the IC width, which was considerably greater in the left span and over the central support than in the right span. However, the CFRP plates were rapidly affected by the development of ICs at the critical sections because of the small contact area between the EB-CFRP plate and the concrete. This led to the acceleration of the debonding phenomena, thus explaining the lower ultimate capacity of this beam in comparison to that of beam BC1-EB1S (Section 3.1).

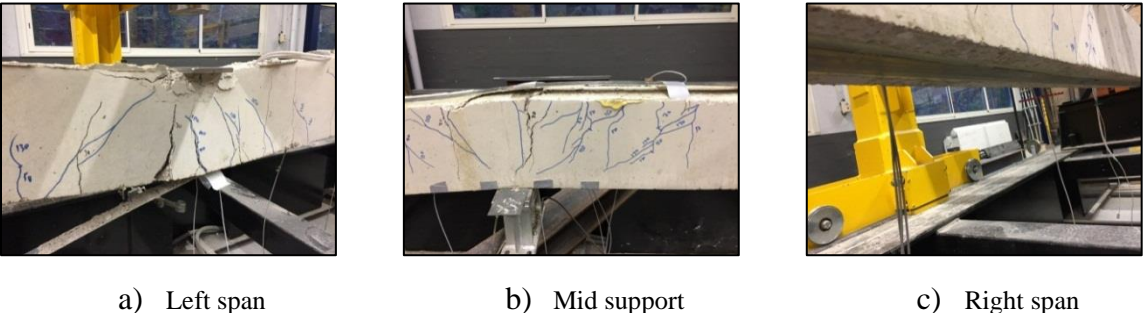


Figure 4-9 : Failure mode of beam BC2-EB1P.

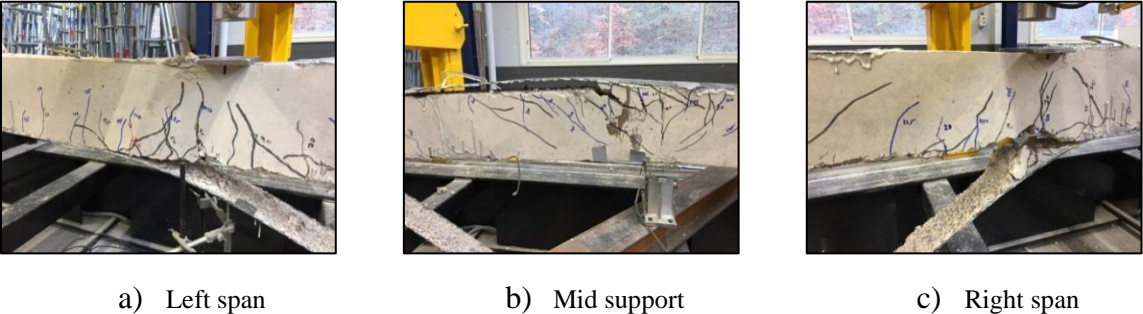


Figure 4-10 : Failure mode of beam BC6-EB1S-weight (1100).

4.3.2.3 Failure mode 3: IC debonding and CCD

Beam BC1-EB1S failed in two areas as a result of IC debonding of the EB-CFRP sheets: firstly at the negative moment zone (hogging region) close to the central support, then again in the left positive moment zone (sagging region). During later stages, the beam failed by CCD in the right positive moment zone. The failure that occurred at the hogging region was sudden and was accompanied by a loud noise, indicating rapid release of energy and significant loss in the load capacity (see Figure 4-7). In the right sagging region, however, delamination of the concrete cover started at the extremities of the CFRP sheets close to the external supports and developed toward the applied load points with the load increasing. This was accompanied by a loud cracking noise, which continued until the end of the test. Figure 4-11 shows the failure mode of beam BC1-EBS.

In beams BC4-EB2S and BC5-EB1S-weight (700), IC debonding occurred in the left sagging region and then in the hogging region, followed by CCD in the right sagging region, as shown in Figure 4-12 and Figure 4-13. This failure mode indicates that increasing the reinforcement ratio of the EB-CFRP sheets through the number of layers and carbon fiber weight (see also Section 3.2.2) is not effective in terms of preventing the IC debonding.

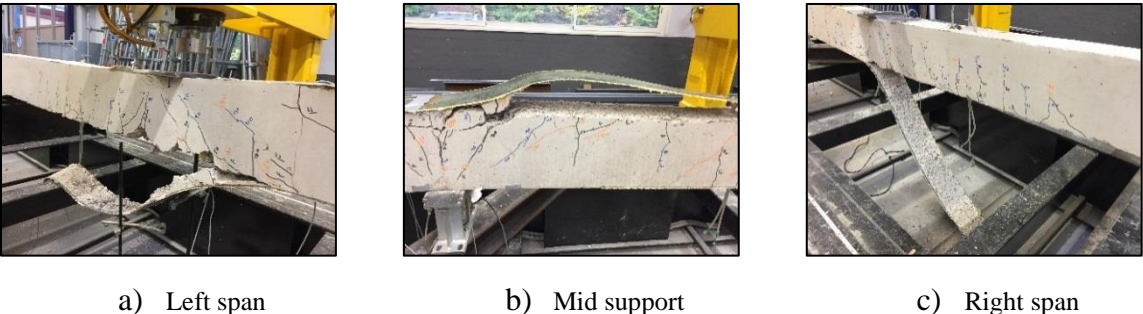


Figure 4-11 : Failure mode of beam BC1-EB1S.

4.3.2.4 Failure mode 4: IC debonding and rupture of the CFRP sheet

Beam BC3-SEB1S-side principally failed as a result of IC debonding of the EB-CFRP sheets at both the hogging and sagging regions. Debonding failure was first observed in the left sagging region, followed by failure of the hogging and right sagging regions. This IC debonding failure resulted in a tensile rupture of the CFRP sheets at the critical sections, as shown in Figure 4-14. Such an abrupt rupture of the CFRP sheets occurred because once the CFRP sheets were debonded from one side of the beam, the load suddenly transferred to the other side.



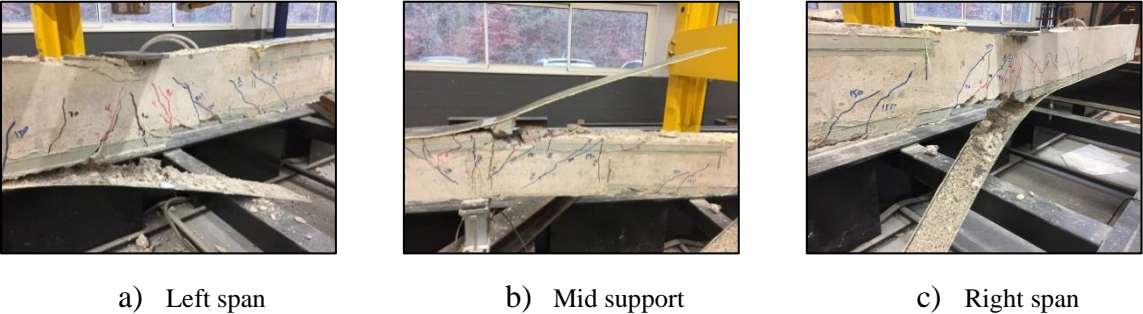


Figure 4-12 : Failure mode of beam BC4-EB2S.

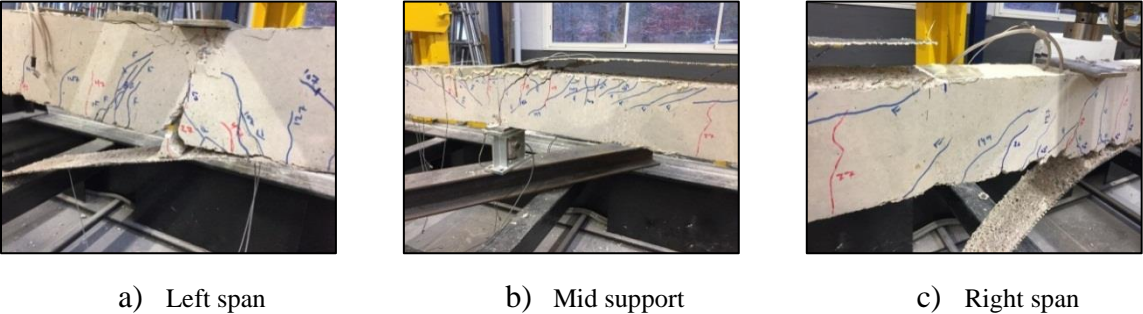


Figure 4-13 : Failure mode of beam BC5-EB1S-weight(700).

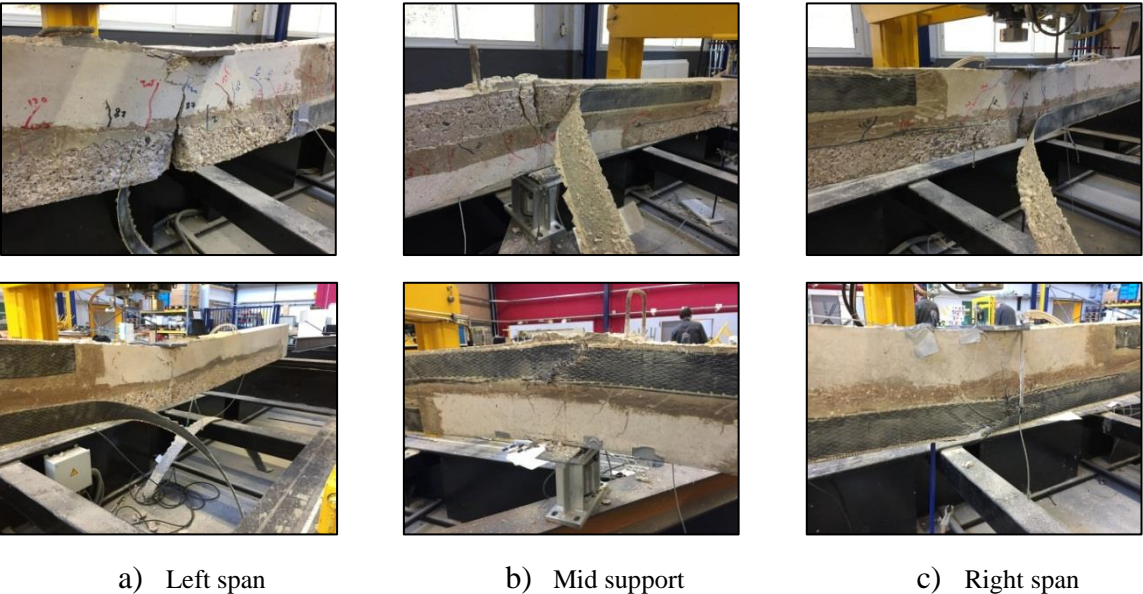


Figure 4-14 : Failure mode of beam BC3-SEB1S-side.

**4.3.3 Crack maps and crack width**

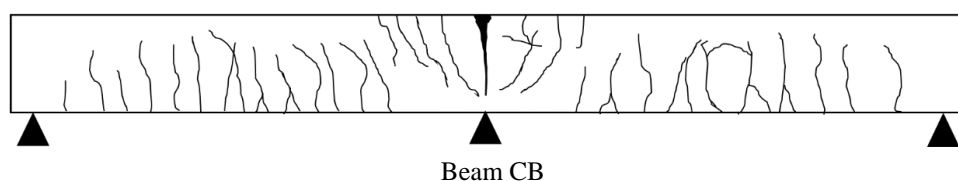
Figure 4-15 shows the cracks maps of strengthened and unstrengthened beams at the failure stage. Crack propagation was monitored and manually marked throughout the tests. The ICs at the critical sections (maximum-moment regions) are depicted by bold lines to reflect their larger width compared to other cracks. The ICs started nearly simultaneously in both the hogging and sagging regions in all the tested beams. However, as can be seen in Figure 4-15, strengthening a continuous RC beam with EB-CFRP significantly increased the number of cracks, regardless of the strengthening state. Compared to the control beam, the number of cracks increased by 189%, 200%, 63%, 125%, 213%, and 238% in the hogging region and by 125%, 44%, 19%,

19%, 44%, and 63% in the sagging region for beams BC1-EB1S, BC2-EB1P, BC3-EB1S-*side*, BC4-EB2S, BC5-EB1S-*weight* (700), and BC6-EB1S-*weight* (1100), respectively. In addition, the average crack spacing of the EB beams was found to be smaller than in the control beam. In general, the average crack spacing is calculated by summing the crack spaces divided by the number of spaces in each region, and it was found to be equal to 163, 80.2, 88.5, 88.3, 82.5, 86.6, and 86.6 mm in the hogging region and 136, 85.2, 94.3, 107.9, 115, 103.9, and 102.1 mm in the sagging region for beams CB, BC1-EB1S, BC2-EB1P, BC3-EB1S-*side*, BC4-EB2S, BC5-EB1S-*weight* (700), and BC6-EB1S-*weight*(1100), respectively.

Beams BC4-EB2S and BC6-EB1S-*weight*(1100) exhibited a higher first cracking load than that experienced by other beams due to their high axial stiffness ratio. The first cracking loads of beams CB, BC1-EB1S, BC2-EB1P, BC3-EB1S-*side*, BC4-EB2S, BC5-EB1S-*weight* (700), and BC6-EB1S-*weight* (1100) were found to be approximately 26, 30, 29, 32, 46, 30, and 52 kN respectively. Therefore, it can be concluded that the axial stiffness ratio of the EB-CFRP specimen is the key factor affecting the first crack load.

At later stages of loading, the influence of the strengthening scenarios applied could be noticed through the crack width of the specimens. Figure 4-16 shows the relationship between the total applied load and the flexural crack width in the hogging region. The crack width was measured using a special microscope with an accuracy of 0.05 mm. Generally, EB-CFRP sheets/plates have a considerable effect on reducing the width of flexural cracks. Nevertheless, the crack width of the CFRP sheet beams (i.e. BC1-EB1S, BC3-EB1S-*side*, BC4-EB2S, BC5-EB1S-*weight* (700), and BC6-EB1S-*weight* (1100)) was significantly smaller than that of the CFRP plate beam (i.e. BC2-EB1P) under the same applied load. This finding indicates that not only the axial stiffness ratio of the EB-CFRP specimen, but also the form and position of the CFRP may affect the crack development. Indeed, bonding the CFRP sheets on the side surfaces of the beam (BC3-EB1S-*side*) was found to be more efficient in decreasing the beam's crack width than the conventional top/bottom bonding technique (BC1-EB1S). This can be explained as the side-bonded sheets confine the concrete in the tension sides along the depth of the beam's cross section, which allows enhancing the tension carrying capacity of concrete between cracks.

The red points shown in Figure 4-16 represent the maximum crack width in each strengthened beam corresponding to the service load (67% ultimate load). According to ACI-319-14 [35], the allowable crack width of ordinary steel RC beams ranges between approximately 0.46 and 0.56 mm at the service load. It can be seen from Figure 4-16 that none of the CFRP sheet beams exceeded the maximum limit (0.56 mm). Moreover, beams BC3-EB1S-*side*, BC4-EB2S, BC5-EB1S-*weigh* (700), and BC6-EB1S-*weigh* (1100) did not even exceed the lower crack width limit (0.46 mm). These results highlight the great benefits of using EB-CFRP sheets and their strengthening configurations adopted in this study to meet the serviceability requirements of continuous RC beams in comparison to the control and EB-CFRP plate beam.



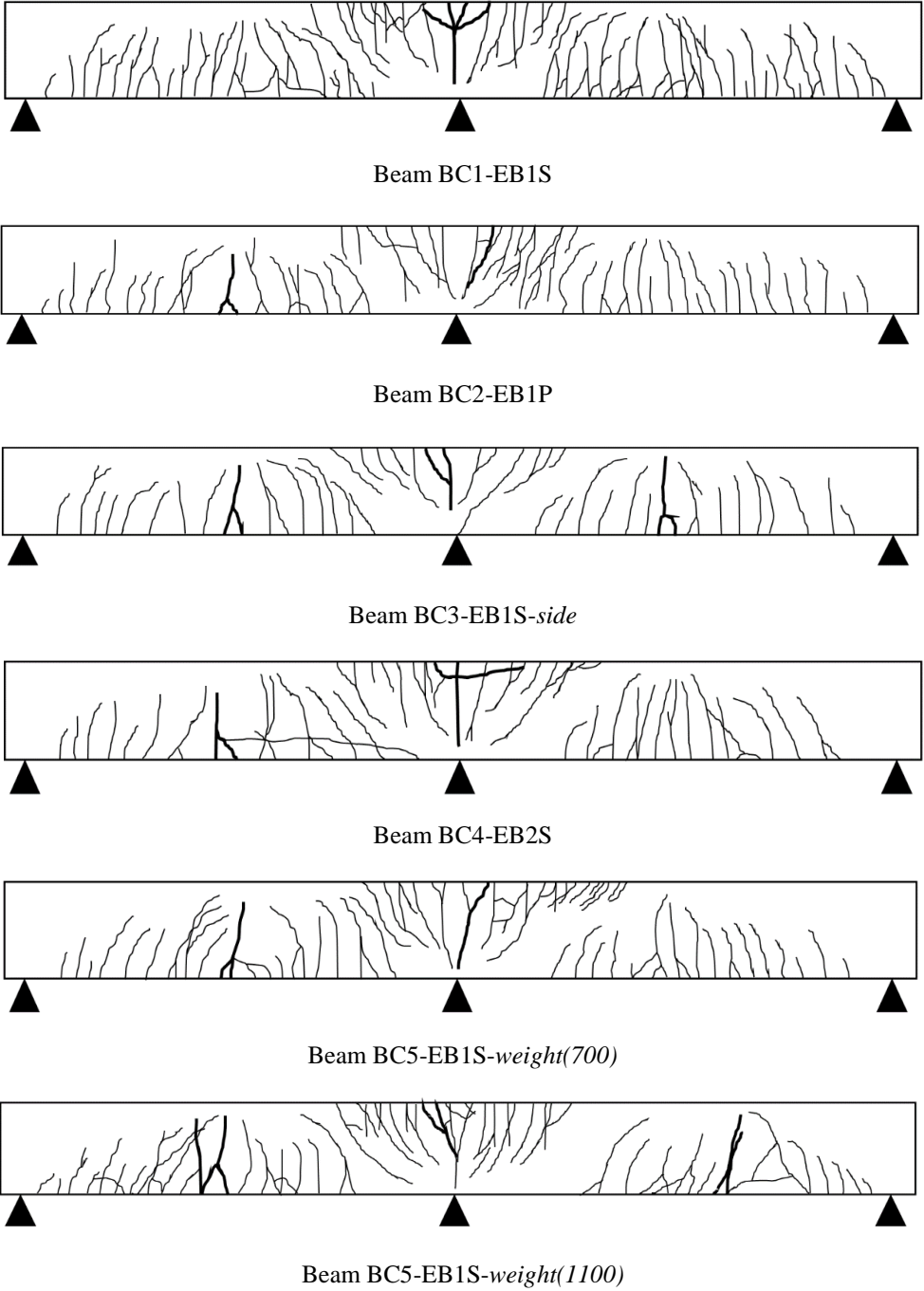


Figure 4-15 : Crack maps of tested beams

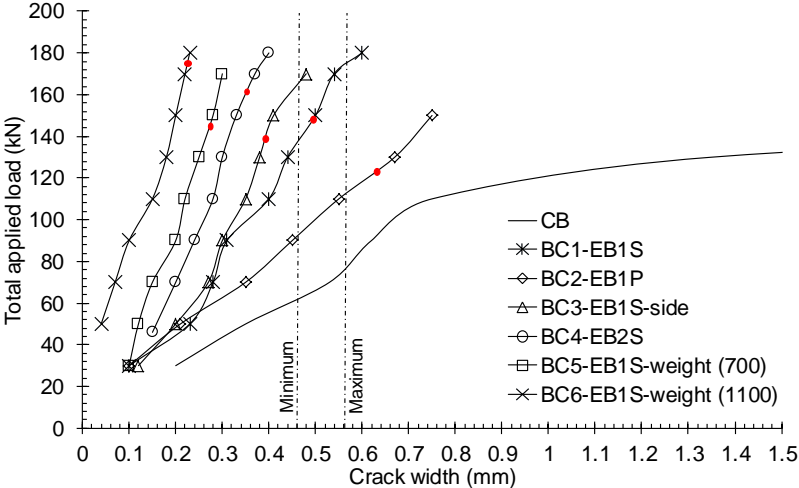


Figure 4-16 : Total applied load vs. the cracks width of control and strengthened beams.

**4.3.4 Strain of steel and CFRP reinforcement**

Figure 4-17 shows the total applied load versus the tensile strain of the bottom steel bars at the midspan (sagging region) and the top steel bars at the intermediate support (hogging region). Besides acting as tensile reinforcements, EB-CFRP composites have also been demonstrated to be useful in reducing the tensile strain of tension steel bars. Under the same level of applied load, and compared to the control beam, the steel strain decreased in both the hogging and sagging regions of the EB beams. The intensity degree of this decrease varies depending on the form, position, and number of CFRP sheets used, as well as the weight of the carbon fibers.

In general, the strain response of tension steel bars is affected by two characteristic points: the concrete cracking load point, which has been discussed in the previous section, and the steel yielding load point. It can be seen in Figure 4-17 that the EB-CFRP composite material delayed the yield of the steel bars. Thus, both the yield and the ultimate load of the strengthened beam increased in comparison to those of the control beam. It was also observed that steel yielding ( $\epsilon_s > 0.003$ ) occurred in all the strengthened beams prior to the debonding failure of the CFRP. Although such yielding was comparable in both the hogging and sagging regions because the amount of reinforcement used was the same, most of the tested beams exhibited their first yielding in the hogging region. Thus, the comparisons provided below are based on the yielding load of tension steel in the hogging region.

- *Influence of the axial stiffness ratio:* The load-strain diagrams show that both forms of CFRP (sheets and plates) allow an increase in the yielding load. This increase was found to be approximately 29.6% and 29.2% for beams BC1-EB1S (171.4 kN) and BC2-EB1P (170.9 kN), respectively. Such similarity in the yielding load values of the aforementioned beams, despite the different forms of CFRP used, is most probably due to the affinity of the axial stiffness ratio, which is nearly 1.13 in BC1-EB1S and 1.16 in BC2-EB1P. Similarly, the yielding loads of beams BC4-EB2S (190 kN), BC5-EB1S-weight (700) (172.2 kN), and BC6-EB1S-weight (1100) (210.5 kN) increased by 43.6%, 30.2%, and 59.1% respectively, over the control beam. The axial stiffness ratio of beams BC4-EB2S, BC5-EB1S-weight (700), and BC6-EB1S-weight (1100) was about 1.26, 1.17, and 1.33, respectively. It was also found that positioning the CFRP sheets on the



side instead of the bottom/top surfaces has a negligible effect. Although the position of the CFRP has changed, the yielding load of BC3-EB1S-side (166.1 kN) was about 97% that of BC1-EB1S. The axial stiffness ratio of beam BC3-EB1S-side was similar to that of beam BC1-EB1S. Figure 4-18 shows the relationship between increasing the axial stiffness ratio and the yielding load of EB-CFRP beams.

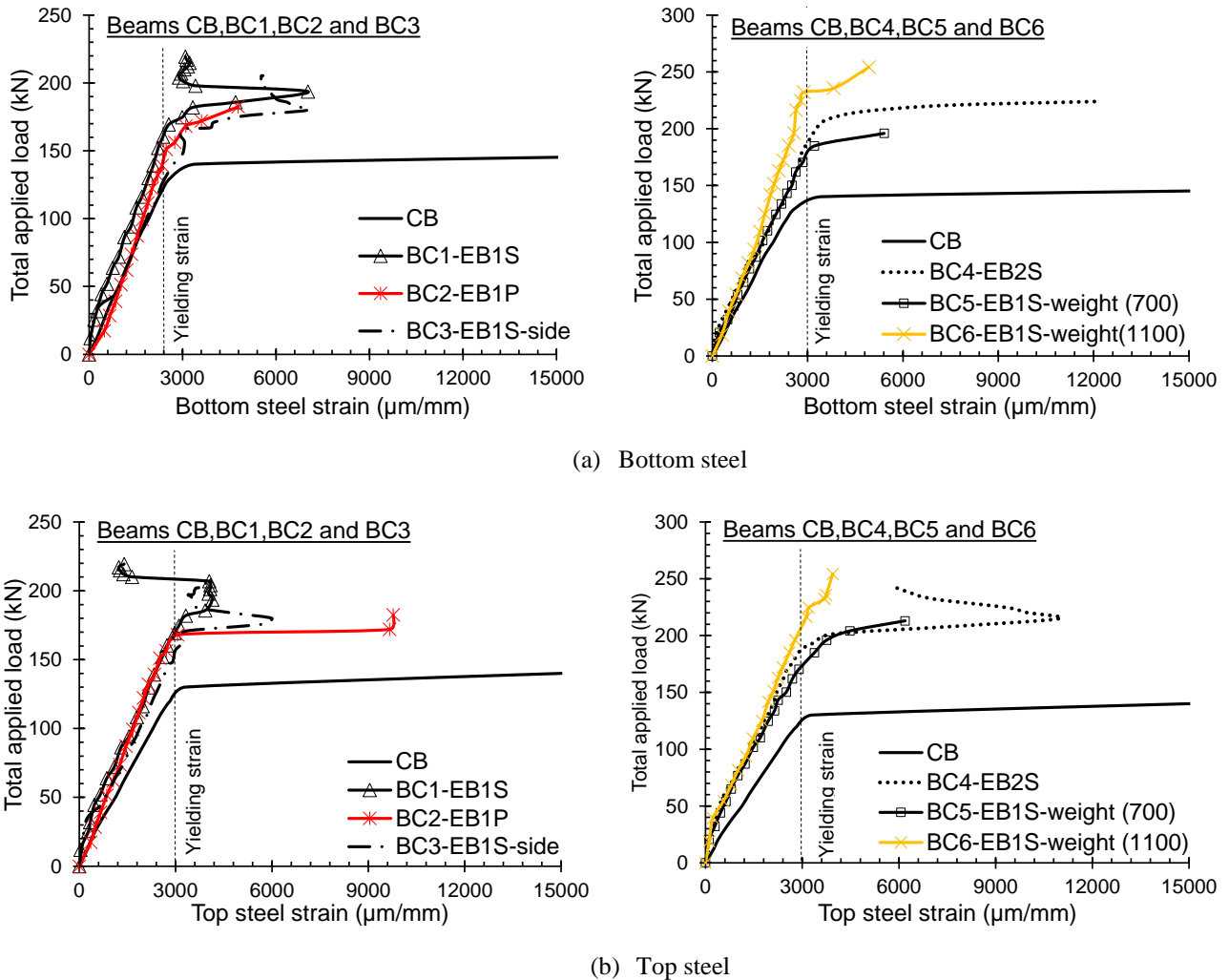


Figure 4-17 : Total applied load versus tensile strain of the steel bars.

Figure 4-19 shows a plot of the total applied load versus tensile strain in the CFRP composites at the midspan and over the intermediate support of the tested beams. The maximum recorded tensile strain values in the CFRP materials obtained from the experimental investigations of beams BC1-EB1S, BC2-EB1P, BC3-EB1S-side, BC4-EB2S, BC5-EB1S-weight (700), and BC-EB1S-weight (1100) were found to be, respectively, 0.0113 (66%), 0.005 (29.4%), 0.0114 (67%), 0.0068 (40.1%), 0.0082 (48%), and 0.0069 (40.4%) at the midspan and 0.0082 (48%), 0.0061 (35.9%), 0.0106 (62%), 0.0075 (44.2%), 0.0085 (49.8%), and 0.0051 (30.2%) at the intermediate support. The values in parentheses represent the percentages of the maximum recorded strain ( $\epsilon_{FRP}^{max}$ ) to the ultimate strain ( $\epsilon_{FRP}^{ult}$ ) of the CFRP. On the basis of the above results, the following points can be made:

- *Influence of the CFRP form:* Using EB-CFRP plates instead of EB-CFRP sheets significantly decreases the maximum tensile strain of CFRP and, hence, decreases the probability that its capacity could be further exploited. Such decrease is due to the early IC debonding failure that was observed in the plated beam in comparison to the sheeted beam, as discussed in Section 3.2.2.
- *Influence of the CFRP sheet position:* Among all the tested beams, the largest maximum strain was achieved by bonding CFRP sheets to the side surfaces of beam BC3-EB1S-side. It should be noted that, in the side-bonded beam, the tensile stress distribution of CFRP varies along the width of the sheets. This variation allows the extreme top carbon fibers in the hogging region and the extreme lower carbon fibers in the sagging region to elongate rapidly before the global debonding failure occurs. This variation between the strains of the top and bottom carbon fibers in beam BC3-EB1S-side is also presented in Figure 4-19c and Figure 4-19d.
- *Influence of the CFRP sheet area:* Increasing the CFRP reinforcement area through the number of CFRP sheet layers (BC4-EB2S) and the weight of the carbon fibers (BC5-EB1S-weight(700) and BC6-EB1S-weight(1100)) was found to have a similar impact on the maximum strain of EB-CFRP sheets ( $\epsilon_{FRP}^{max}$ ). Both process significantly decreased the value of  $\epsilon_{FRP}^{max}$  in the hogging and sagging regions. For example the debonding strain of CFRP sheet in the hogging region decreased from 0.0113 in beam BC1-EB1S to 0.0068, 0.008, and 0.0069 in beams BC4-EB2S, BC5-EB1S-weight (700), and BC5-EB1S-weight (1100), respectively. The relationship between increasing the CFRP reinforcement area and debonding strain is presented in Figure 4-20. This relationship was found to be nonlinear for both hogging and sagging regions.

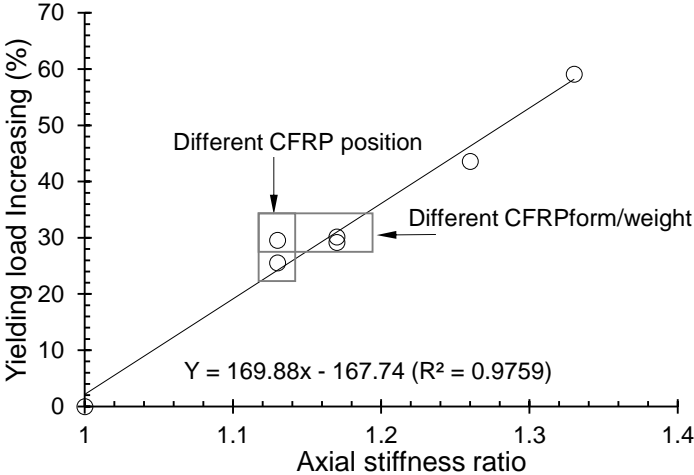


Figure 4-18 : Axial stiffness ratio vs. increasing the yielding load.

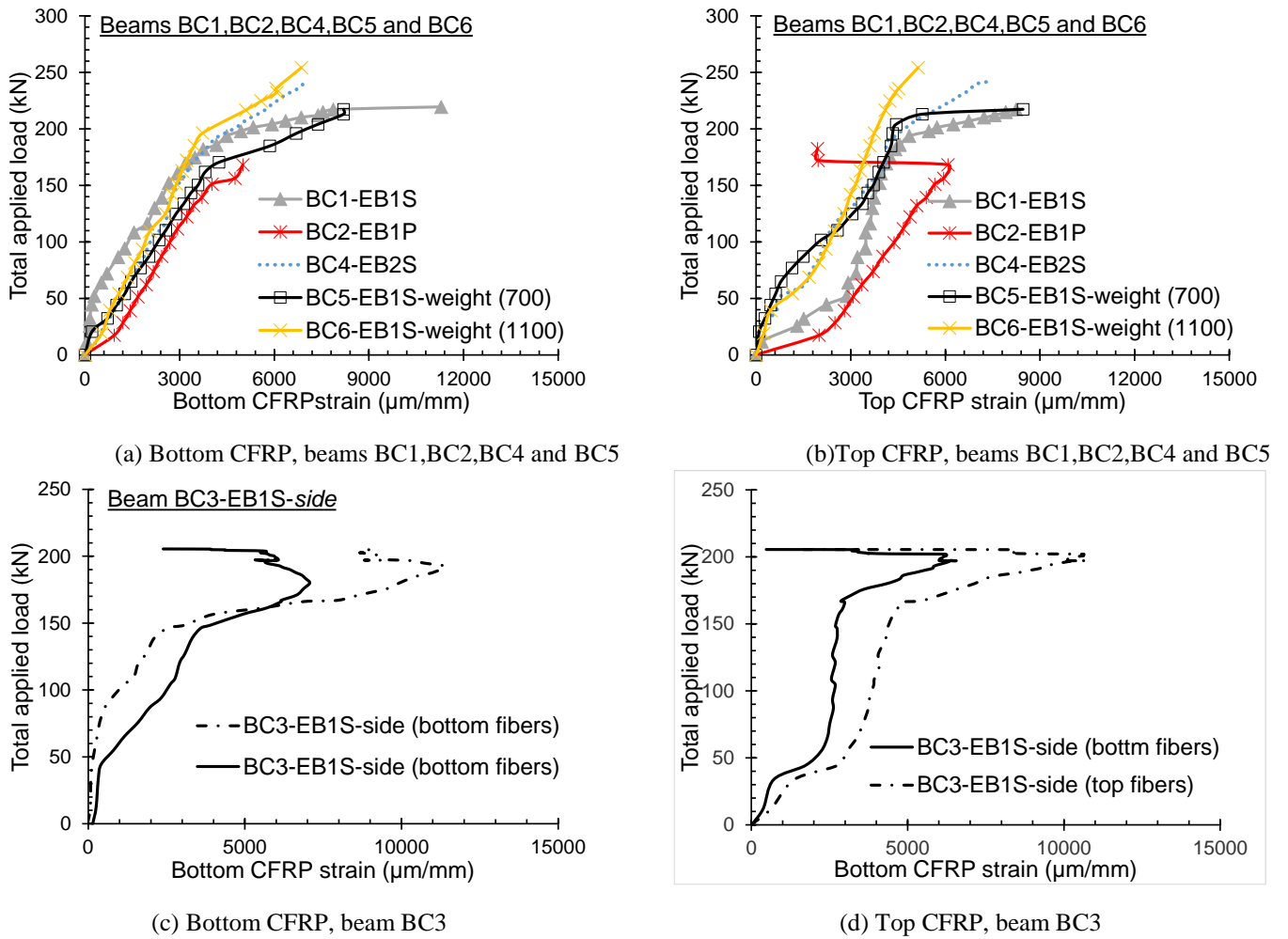


Figure 4-19 : Total applied load versus tensile strain of CFRP reinforcement.

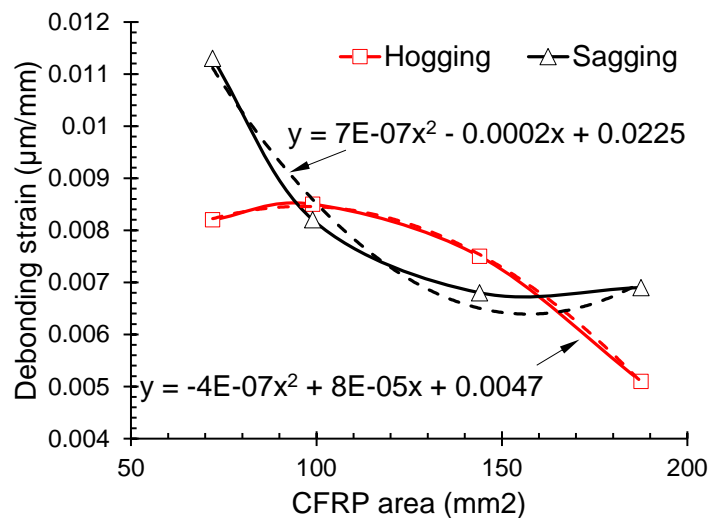


Figure 4-20 : CFRP sheet area vs. debonding strain.

### 4.3.5 Moment redistribution

Although a considerable number of studies have addressed the behavior of statically determinate members, such as SSBs strengthened with FRP composites, few research studies have focused on the behavior of strengthened indeterminate members, such as continuous

beams. Redistribution of the bending moment in ordinary continuous RC beams can be attributed to the structural redundancy and nonlinear behavior of RC. Such redistribution is affected by several factors, such as the quantity, arrangement, and mechanical characteristics of the internal steel; loading arrangement; geometry of the member; and the width and regions of the internal supports. Nonlinear analysis is an accurate approach for calculating the actual internal forces. However, existing building codes [35-37] allow us to take advantage of linear-elastic analysis with moment redistribution (15%–30%) for conventional structural designs. This means that the incorporation of moment redistribution in structural analysis is reasonable and accurate to reduce the differences between the results of linear-elastic analysis and actual internal forces, which emerge as a result of the nonuniform stiffness distribution.

In ordinary indeterminate RC beams, the moment redistribution primarily depends on the amount of tension steel reinforcement ( $\rho_s$ ) in the bending moment regions. At the ultimate state, moment transfer occurs from the hogging region ( $h$ ) to the sagging region ( $s$ ) when  $\rho_s^h/\rho_s^s$  is not greater than 1.0, whereas when  $\rho_s^h/\rho_s^s$  is greater than 1.5 moment transfer occurs from the sagging region to the hogging region. However, when  $\rho_s^h/\rho_s^s$  lies between 1.0 and 1.5 the moment transfer is indistinct.

It should be noted that existing building codes [35-37] often tend to be conservative and do not allow moment redistribution for FRP strengthened structures, regardless of the amount of steel reinforcement at the critical sections. These codes prove that moment redistribution is a phenomenon that is mainly associated with flexural ductility, whereas FRPs are brittle materials. In addition, applying FRPs to strengthen and retrofit RC beams usually leads to nonconventional failure modes, such as IC debonding and peeling-off in the case of externally bonded laminates and pull-out in the case of internally bonded bars. These nonconventional failures may lead to a significant reduction in the beam's ductility state and its degree of moment redistribution ( $\beta$ ). However, despite being very limited in number, previous studies on EB-CFRP strengthened RC beams have indicated that moment redistribution is possible to some extent at the ultimate state, as shown in

Table 4-4. In fact, moment redistribution is not only occurs at the ultimate state but also evolves throughout the whole loading process, even before the formation yielding of the tension steel reinforcement. According to the experimental results obtained from the tests performed in the present research, evolution of moment redistribution also seems to be significantly influenced depending on the strengthening state of the beam, as shown in Figure 4-21.

In general, the degree of moment redistribution ( $\beta$ ) can be quantified using the values of flexural moments at the critical sections of a beam [41], as provided in Eq. 4-1, where  $M_{th}$  is the theoretical bending moment calculated on the basis of the linearly elastic statement and  $M_{exp}$  is the actual bending moment calculated from the experiment after moment redistribution:

$$\beta (\%) = \left( \frac{M^{Th} - M^{Exp}}{M^{Th}} \right) \times 100\% \quad (4-1)$$



Figure 4-22 shows the experimental and elastic bending moments at the critical sections induced by the applied load, and the evolution of the moment ratio. The sagging bending moment ( $M_1$ ) is presented with a positive sign, and the hogging bending moment ( $M_2$ ) is presented with a negative sign. The experimental ( $M_1$ )<sub>exp</sub> and ( $M_2$ )<sub>exp</sub> values were calculated using Eqs. 4-2 and 4-3, respectively, and the elastic ( $M_1$ )<sub>el</sub> and ( $M_2$ )<sub>el</sub> values were calculated using Eqs. 4-4 and 4-5, respectively. Overall, the experimental moments differed from the elastic ones, particularly after the concrete cracking load was reached. For all the tested beams, the elastic moment ratio ( $M_1/M_2$ )<sub>el</sub> remained constant over the loading process, whereas the experimental moment ratio ( $M_1/M_2$ )<sub>exp</sub> varied from one beam to another.

$$M_1^{\text{Exp}} = \frac{(P_u - R_c) \times L}{4} \quad (4-2)$$

$$M_2^{\text{Exp}} = \frac{(P_u - 2R_c) \times L}{4} \quad (4-3)$$

$$M_1^{\text{Th}} = \frac{5P_u L}{64} \quad (4-4)$$

$$M_2^{\text{Th}} = \frac{3P_u L}{32} \quad (4-5)$$

As can be seen in Figure 4-22, the development of the actual moment ratio ( $M_1/M_2$ )<sub>exp</sub> is strongly associated with the strengthening scenario applied. A decrease in ( $M_1/M_2$ )<sub>exp</sub> indicates moment redistribution from the midspan toward the intermediate support, an increase in ( $M_1/M_2$ )<sub>exp</sub> indicates moment redistribution from the intermediate support toward the midspan, and stabilization of ( $M_1/M_2$ )<sub>exp</sub> indicates the stabilization of moment redistribution. It has also been shown that the majority of the moment redistribution, despite being limited, occurred in the stage between the concrete cracking and the first steel yielding. In this stage, the moment clearly transferred from the hogging region to the sagging region in beams BC1-EB1S, BC5-EB1S-weight(700), and BC6-EB1S-weight(1100), whereas it was pendulous about the elastic moment ratio ( $M_1/M_2$ )<sub>el</sub> in beams BC2-EB1P and BC3-EB1S-side. The direction of moment transfer totally changed when the number of CFRP sheets layers was increased. This can be observed in beam BC4-EB2S, in which the moment was transferred from the sagging region to the hogging region. However, after the yielding of the tension steel bars, slight moment redistribution occurred in all the beams, which could be attributed to the fact that a similar amount of steel reinforcement was used in the beam's critical sections.

At the ultimate state, using EB-CFRP composites significantly decreased the moment redistribution degree ( $\beta$ ) of two-span continuous RC beams. The value of  $\beta$  for the control beam was +20.53% at the central support and -12.43% at the midspan. With regard to strengthened beams, beams BC1-EB1S, BC2-EB1P, BC3-EB1S-side, BC4-EB2S, BC5-EB1S-weight(700), and BC6-EB1S-weight(1100) were found to have moment redistribution degrees of, respectively, +13.87%, +2.72%, +1.48%, -17.44%, +9.8%, and +6.1% at the central support, and -8.32%, -1.63%, -0.89%, +10.46%, -5.9%, and -3.7% at the midspan.

Table 4-4 : Moment redistribution, as reported from literature, for continuous beams strengthened with EB-FRP at the ultimate state level.

Reference	Number of spans and dimensions <sup>(1)</sup>	Strengthening scenario	Failure mode	Mid-support $\beta$ (%)	Mid-span $\beta$ (%)
H. Akbarzadeh et al. [7]	Two-span beams 150×170×6000	Control beam	Flexural failure	16.06	-9.62
		EB-One sheet-CFRP in S and H <sup>(3)</sup>	rupture of top CFRP	8.22	-4.92
		EB-Two sheets-CFRP in S and H	IC debonding of FRP sheet and rupture of end strap at hogging region	3.57	-2.13
		EB-Three sheets-CFRP in S and H	IC debonding at hogging region	1.51	-0.71
		EB-Three sheets-GFRP in S and H	IC debonding at hogging region	3.81	-2.34
M. A. Aiello et al. [38]	Two-span beams 150×200×3500	Control beam	Flexural failure	-0.08	0.05
		EB-One sheet-CFRP in S		12.23	-8.82
		EB-One sheet-CFRP in S and H	Detaching of the FRP sheets together with concrete crushing	3.88	-2.78
		EB-Two sheets-CFRP in S		25.75	-18.57
		EB-One sheet-CFRP in H		-16.10	11.57
R. Feng et al. [39]	Two-span beams 150×250×2400	Control beam	Flexural failure	8.98	-5.37
		EB-Two layers of C-FRCM in S and H	Flexural failure and slippage of carbon fabric meshes within cementitious matrix	6.02	-3.63
		EB-Three layers of C-FRCM in S and H	Flexural failure, slippage of carbon fabric meshes within cementitious matrix, and debonding of C-FRCM from concrete substrate	5.45	-3.25
D.J. Oehlers et al. [40]	Two-span beams 375×120×5000	EB-One CFRP plate in H		35	N.A. <sup>(2)</sup>
		EB-One CFRP plate in H	CFRP plate debonding	36	N.A.
		EB-One CFRP plate in H		28	N.A.

(1) Beam dimension: width×depth×total length, all dimensions are in mm, (2) N.A. : data not available, (3) S: sagging region and H: hogging region.

Chapter 4: Efficiency of EB CFRP composites for flexural strengthening of continuous RC beams: A comparative study with NSM CFRP rods

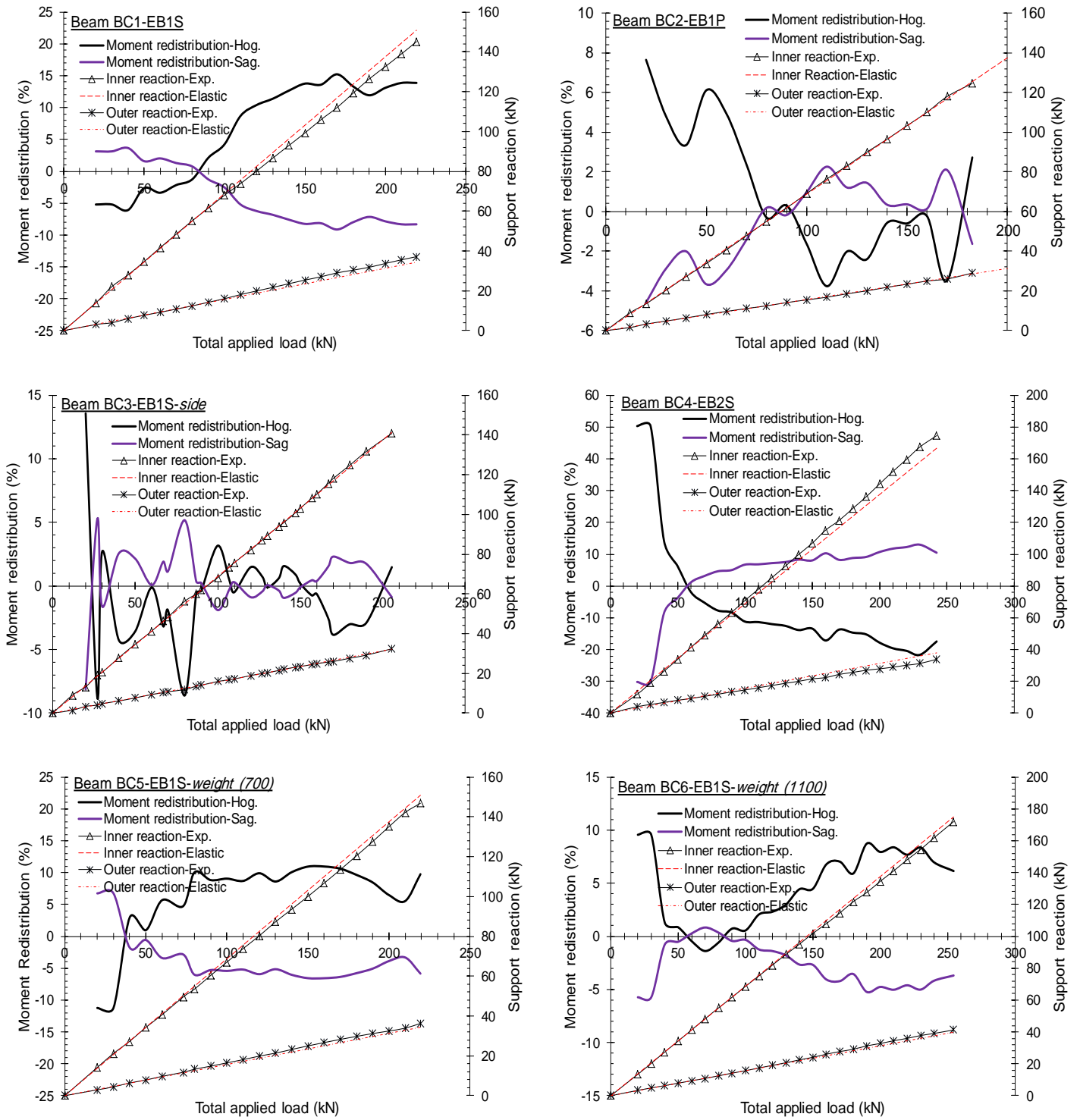
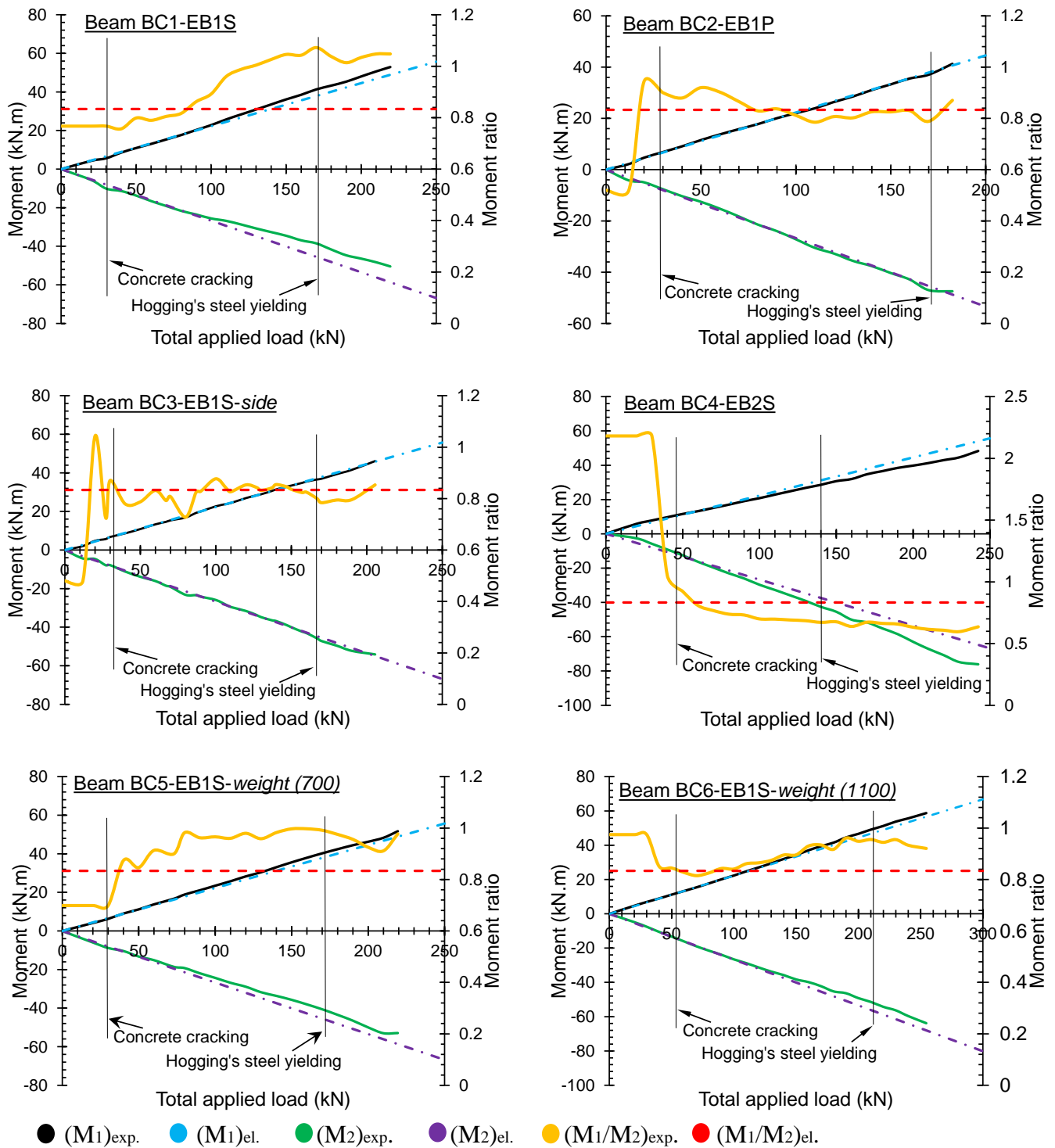


Figure 4-21 : Moment redistribution of tested strengthened beams.



M1: Moment at sagging; and M2: Moment at hogging

Figure 4-22 : Moment ratio of tested strengthened beams.

#### 4.4 Evaluation of the effectiveness of the current guidelines in determining the flexural strength of EB-CFRP continuous beams

In this section, three analytical models for the estimation of the flexural capacity of RC beams strengthened with EB-CFRP sheets/plates are analyzed. The experimental ultimate bending moments of EB-CFRP beams were compared with the design ultimate bending moments

computed using the formula provided in the American ACI 440.2R-08 [30], Italian CNR-DT 200 R1/2013 [33], and technical report of FIB Bulletin 14 [34]. Notably, the compressive strength of concrete cylinders ( $f'_c$ ) is normally used in these guidelines, which is determined in the laboratory in this study. It is important to note that the ultimate compressive strain of concrete ( $\epsilon_{cu}$ ) defined in the aforementioned design guidelines is different. In ACI 440.2R-08 [30],  $\epsilon_{cu}$  is defined as 0.003, whereas it is defined as 0.0035 in CNR-DT 200 R1/2013 [33] and *fib* Bulletin 14 [34]. These three guidelines include the same procedure for calculating the depth of the neutral axis based on the strain compatibility and internal forces equilibrium. However, they feature different assumptions regarding the effective strain of EB-FRP composites, as will be discussed in detail in the following sections. The steel reinforcement used was elasto-plastic with an elastic modulus of 192.85 GPa, and the material behavior of the CFRP reinforcement was linearly elastic until failure, which is defined by the manufacturer and the current design guidelines.

#### 4.4.1 ACI 440.2R-08

According to the ACI 440.2R-08 guideline [30], the tensile strain of the external CFRP composite should be limited to the debonding strain  $\epsilon_{fd}$ , as provided in Eq. 4-6, where;  $f'_c$  is the compressive strength of concrete;  $n$ ,  $E_f$ , and  $t_f$  are the number of layers, modulus of elasticity, and thickness of the CFRP, respectively; and  $\epsilon_{fu} = C_E \epsilon_{fu}^*$  is the design rupture strain, which is calculated by considering reduction for environmental exposure condition. In this study, an environmental reduction factor ( $C_E$ ) of 0.95 is considered.

$$\epsilon_{fd} = 0.41 \sqrt{\frac{f'_c}{nE_f t_f}} \leq 0.9 \epsilon_{fu} \quad (4-6)$$

The effective level of strain in the CFRP ( $\epsilon_{ef}$ ), concrete ( $\epsilon_c$ ), tension steel ( $\epsilon_s$ ), and compression steel ( $\epsilon'_s$ ) can be estimated using the following strain compatibility equations:

$$\epsilon_{ef} = \epsilon_{cu} \left( \frac{d_f - c}{c} \right) \leq \epsilon_{fd} \quad (4-7)$$

$$\epsilon_c = \epsilon_{ef} \left( \frac{c}{d_f - c} \right) \quad (4-8)$$

$$\epsilon_s = \epsilon_{ef} \left( \frac{d - c}{d_f - c} \right) \quad (4-9)$$

$$\epsilon'_s = \epsilon_{ef} \left( \frac{c - d'}{d_f - c} \right) \quad (4-10)$$

where  $c$  is the depth of the neutral axis, which is calculated using the internal force equilibrium:

$$\alpha_1 \beta_1 f'_c b c + A'_s f'_s = A_s f_s + A_f f_{fe} \quad (4-11)$$

where  $\alpha_1$  (Eq. 4-12) and  $\beta_1$  (Eq. 4-13) are the concrete stress block factors, and  $\epsilon'_c$  (Eq. 4-14) is the compressive strain of unconfined concrete. Hence,

$$\alpha_1 = \frac{3 \epsilon'_c (\epsilon_c - \epsilon_c^2)}{3 \beta_1 \epsilon_c'^2} \quad (4-12)$$

$$\beta_1 = \frac{4\varepsilon'_c - \varepsilon_c}{6\varepsilon'_c - 2\varepsilon_c} \quad (4-13)$$

$$\varepsilon'_c = \frac{1.7f'_c}{E_c} \quad (4-14)$$

Following the above indications, the flexural strength of the strengthened section ( $M_n$ ) can be calculated as provided in Eqs. 4-15, 4-19 and 4-17. In these equations,  $M_{ns}$  and  $M_{nf}$  are the steel and CFRP contribution to bending, respectively;  $\phi$  and  $\psi_f$  are the strength reduction factor ( $\phi = 0.9$ ) and additional recommended reduction factor ( $\psi_f = 0.85$ ) on the flexural strength contribution of the CFRP reinforcement, respectively;  $A_s$  and  $A_f$  are the areas of the tension steel and CFRP, respectively; and  $d$  and  $d_f$  are the effective depths of steel and CFRP, respectively. Hence,

$$\phi M_n = \phi [M_{ns} + \psi_f M_{nf}] \quad (4-15)$$

$$M_{ns} = A_s f_s \left( d - \frac{\beta_1 c}{2} \right) \quad (4-16)$$

$$M_{nf} = A_f f_{fe} \left( d_f - \frac{\beta_1 c}{2} \right) \quad (4-17)$$

#### 4.4.2 CNR-DT 200 R1/2013

According to the Italian CNR-DT 200 R1/2013 guideline [33], the tensile strain of the external CFRP composite should be limited to  $\varepsilon_{fd}$ , as provided in Eq. 4-18, where  $n_a$  (0.85) is the environmental conversion factor,  $\gamma_f$  is the material safety factor (1.1 for the ultimate limit state),  $\varepsilon_{fk} = \frac{f_{fk}}{E_f}$  is the CFRP characteristic failure strain, and  $\varepsilon_{fdd}$  is the CFRP IC-induced debonding strain. Hence,

$$\varepsilon_{fd} = \min \left[ \frac{n_a \varepsilon_{fk}}{\gamma_f}, \varepsilon_{fdd} \right] \quad (4-18)$$

The CFRP IC-induced debonding strain can be determined as follows:

$$\varepsilon_{fdd} = \frac{k_q}{\gamma_{f,d}} \sqrt{\frac{2k_b k_{G2}}{t_f E_f FC} \sqrt{f_{cm} \cdot f_{ctm}}} \geq \varepsilon_{sy} - \varepsilon_0 \quad (4-19)$$

where  $k_q$  is a coefficient that considers load distribution and is equal to 1.25 for distributed loads and 1.0 for all other load configurations;  $\gamma_{f,d}$  is a safety factor that depends on the probability associated with debonding failure, which can be chosen by the designer in the range between 1.20 and 1.50; FC is a calibrated factor of confidence related to the level of knowledge of the element to be strengthened;  $k_{G2}$  is a corrective factor calibrated on the experimental results and is equal to 0.10 mm irrespective of the type of reinforcement;  $f_{cm}$  and  $f_{ctm}$  are the concrete mean compressive and tensile strength, respectively;  $\varepsilon_{sy}$  is the design yield strain of the steel reinforcement;  $\varepsilon_0$  is the maximum tensile strain present before the FRP is applied; and  $k_b$  (Eq. 4-20) is the geometrical corrective factor, which is a function of the ratio between the CFRP and the concrete width ( $b_f/b$ ):

$$k_b = \sqrt{\frac{2-b_f/b}{1+b_f/b}} \geq 1 \text{ for } b_f/b \geq 0.25 \quad (4-20)$$

For a bond length ( $l_b$ ) shorter than the design optimal bond length ( $l_{ed}$ ), the debonding strain ( $\varepsilon_{fdd}$ ) should be reduced to the plate-end debonding strain as follows:

$$\varepsilon_{fdd} = \frac{k_q}{\gamma_{f,d}} \sqrt{\frac{2k_b k_{G2}}{t_f E_{fFC}} \sqrt{f_{cm} \cdot f_{ctm}} \cdot \frac{l_b}{l_{ed}} \left(2 - \frac{l_b}{l_{ed}}\right)} \geq \varepsilon_{sy} - \varepsilon_0 \quad (4-21)$$

where

$$l_{ed} = \min\left[\frac{1}{\gamma_{Rd}} \sqrt{\frac{\pi^2 t_f E_f S_u^2 FC}{8k_b k_{G2} \sqrt{f_{cm} \cdot f_{ctm}}}}, 200\text{mm}\right] \quad (4-22)$$

In which  $S_u$  is the FRP-concrete interfacial debonding slip and  $\gamma_{Rd}$  is the partial factor for resistance models (assuming  $\gamma_{Rd} = 1$  in this study).

However, the CNR-DT 200 R1/2013 guideline classifies the failure mode of the strengthened section into two categories: (i) failure due to concrete crushing if  $\mu_f > \mu_{f1-2}$  and (ii) failure due to rupture of the FRP if  $\mu_f < \mu_{f1-2}$ , in which  $\mu_f$  and  $\mu_{f1-2}$  are defined in Eq. 4-23 and Eq. 4-24, respectively. In the case of failure due to concrete crushing, the effective strain in the CFRP ( $\varepsilon_f$ ), concrete ( $\varepsilon_c$ ), tension steel ( $\varepsilon_{s1}$ ), and compression steel ( $\varepsilon_{s2}$ ) can be obtained from Eq. 4-25. In the case of failure due to rupture of the FRP, the effective strain in the materials can be obtained from Eq. 4-26.

$$\mu_f = \frac{b_f(n_f t_f) f_{dd,2}}{f_{cd} b d} \quad (4-23)$$

$$\mu_{f1-2} = \frac{0.8 \varepsilon_{cu} h/d}{\varepsilon_{cu} + \varepsilon_{fd} + \varepsilon_0} - \mu_s (1 - u) \quad (4-24)$$

$$\left\{ \begin{array}{l} \text{CFRP} \\ \text{Concrete} \\ \text{Tension steel} \\ \text{Compression steel} \end{array} \right. \quad \left\{ \begin{array}{l} \varepsilon_f = \frac{\varepsilon_{cu}}{x} (h - x) - \varepsilon_0 \leq \varepsilon_{fd} \\ \varepsilon_c = \varepsilon_{cu} \\ \varepsilon_{s1} = \varepsilon_{cu} \frac{d-x}{x} \\ \varepsilon_{s2} = \varepsilon_{cu} \frac{x-d_2}{x} \end{array} \right. \quad (4-25)$$

$$\left\{ \begin{array}{l} \text{CFRP} \\ \text{Concrete} \\ \text{Tension steel} \\ \text{Compression steel} \end{array} \right. \quad \left\{ \begin{array}{l} \varepsilon_f = \varepsilon_{fd} \\ \varepsilon_c = (\varepsilon_{fd} + \varepsilon_0) \frac{x}{h-x} \leq \varepsilon_{cu} \\ \varepsilon_{s1} = (\varepsilon_{fd} + \varepsilon_0) \frac{d-x}{h-x} \\ \varepsilon_{s2} = (\varepsilon_{fd} + \varepsilon_0) \frac{x-d_2}{h-x} \end{array} \right. \quad (4-26)$$

Following the above indications, the flexural strength of the strengthened section ( $M_{Rd}$ ) can be calculated as follows:

$$M_{Rd} = \frac{1}{\gamma_{Rd}} [\psi b x f_{cd} (d - \lambda x) + A_{s2} \sigma_{s2} (d - d_2) + A_f \sigma_f d_1] \quad (4-27)$$



where  $\psi$  and  $\lambda$  are nondimensional coefficients representing the intensity and position of the compressive concrete resultant, respectively;  $f_{cd}$  is the design concrete compressive strength;  $d$ ,  $d_1$  and  $d_2$  are the effective depths of the tension steel, CFRP, and compression steel, respectively;  $\sigma_{s2}$  is the stress in the compression steel;  $\sigma_f$  is the stress in the CFRP;  $A_{s2}$  and  $A_f$  are the areas of the compression steel and CFRP, respectively; and  $x$  is the depth of the neutral axis, calculated as in the following equation:

$$0 = \psi b x f_{cd} + A_{s2} \sigma_{s2} - A_{s1} \sigma_{s1} - A_f \sigma_f \quad (4-28)$$

#### 4.4.3 *fib* Bulletin 14

Although the technical report of *fib* Bulletin 14 [34] provides a formula (Eq. 4-29) for limiting stress in the FRP composite in the service limit state, it does not provide a specific formula for reducing the strain of the external CFRP composite during analysis in the ultimate limit state. The only check provided in the ultimate limit state so far is the straining of the FRP ( $\epsilon_f$ ) not exceeding the ultimate strain ( $\epsilon_{fud}$ ) when a conventional failure occurs. The design bending moment of the strengthened cross section (Eq. 4-30) is calculated on the basis of the general principles of the RC design [36]. The neutral axis depth ( $x$ ) is calculated from the strain compatibility and internal force equilibrium, and the design moment is obtained from the moment equilibrium:

$$\sigma_{FRP} = E_f \left( \epsilon_c \frac{h - X_e}{X_e} - \epsilon_0 \right) \leq \eta f_{fk} \quad (4-29)$$

where  $X_e$  is the neutral axis depth;  $\eta$  is the FRP stress limitation coefficient, which depends on the type of FRP and should be obtained through experiments; the suggested  $\eta$  value for the CFRP is 0.8; and  $f_{fk}$  is the characteristic value of the FRP tensile strength:

$$M_{Rd} = A_{s1} f_{yd} (d - \delta_G x) + A_f E_f \epsilon_f (h - \delta_G x) + A_{s2} E_s \epsilon_{s2} (\delta_G x - d_2) \quad (4-30)$$

where  $\delta_G = 0.4$  is the coefficient of the rectangular stress centroid for concrete in compression and  $x$  is the depth of the neutral axis, which is calculated as follows:

$$0.85 \psi f_{cd} b x + A_{s2} E_s \epsilon_{s2} = A_{s1} f_{yd} + A_f E_f \epsilon_f \quad (4-31)$$

In Eq. 4-31,  $\psi = 0.8$  is the coefficient of the rectangular stress area for concrete in compression.

It is worth noting that, in the case of failure due to the FRP reinforcements, FIB Bulletin 14 [34] provides modifications for the values of  $\delta_G$  and  $\psi$  as follows:

$$\psi = \begin{cases} 100 \epsilon_c \left( 0.5 - \frac{1000}{12} \epsilon_c \right) & \text{for } \epsilon_c \leq 0.002 \\ 1 - \frac{2}{3000 \epsilon_c} & \text{for } 0.002 \leq \epsilon_c \leq 0.0035 \end{cases} \quad (4-32)$$

$$\delta_G = \begin{cases} \frac{8 - 1000 \epsilon_c}{4(6 - 1000 \epsilon_c)} & \text{for } \epsilon_c \leq 0.002 \\ \frac{1000 \epsilon_c (3000 \epsilon_c - 4) + 2}{2000 \epsilon_c (3000 \epsilon_c - 2)} & \text{for } 0.002 \leq \epsilon_c \leq 0.0035 \end{cases} \quad (4-33)$$

#### 4.4.4 Comparison of the ultimate moment obtained from tests and current design codes

The experimental ultimate bending moments of the EB-CFRP beams were compared with the design ultimate bending moments obtained from the American ACI 440.2R-08 [30], Italian CNR-DT 200 R1/2013 [33], and technical report of FIB Bulletin 14 [34]. Comparisons regarding are listed in Table 4-5. It is worth noting that the design formulas provided in these codes do not include the mechanical properties of adhesive resin materials, however, they generally provide an acceptable prediction of the beam's flexural strength. The main observation pertained to the prediction accuracy for the flexural strength of multi-layer CFRP sheet beams, which was low and did not reflect the actual value. However, the mean values of the design-to-experimental bending moment ratios ( $M_{ACI}/M_{Exp}$ ,  $M_{CNR}/M_{Exp}$ , and  $M_{FIB}/M_{Exp}$ ) were found to be, respectively, 0.89, 0.88, and 1.06 in the hogging region and 1.01, 0.97, and 1.21 in the sagging region. Therefore, it can be concluded that the American ACI 440.2R-08 [30] and Italian CNR-DT 200 R1/2013 [33] are relatively more conservative and appropriate than the technical report of FIB Bulletin 14 [34] in terms of predicting the flexural strength of RC continuous beams strengthened with EB-CFRP.

#### 4.5 Comparison between the EB and NSM for strengthening continuous RC beams.

For the sake of comparison, two additional beams, namely BC1-NSM and BC2-SNSM, were strengthened using the NSM technique and statically tested. The procedure followed in the NSM technique has already been described [9]. The experimental results of the two beams mentioned above were compared with the experimental results of beams BC1-EB1S and BC3-EB1S-*side* from Section 2. Beams BC1-NSM and BC2-SNSM were strengthened with 2 $\emptyset$ 6 CFRP rods in both the hogging and sagging regions. The only difference between them was the location of the CFRP bars. In beam BC2-SNSM, the CFRP bars were inserted in the vertical sides adjacent to the tension steel rebars instead of the bottom/top sides, as shown in Figure 4-23. The dimensions, steel reinforcement ratio, and test setup, including the load and support conditions of the NSM beams, were all comparable to those employed in the experimental investigation of the EB beams, as shown in Figure 4-1. In addition, the mechanical properties of the adhesive epoxy-resin (Epx SC980) used to bond the CFRP bars with concrete were similar to those reported in Table 4-3.

Table 4-6 presents the strengthening details of the NSM beams. Their axial stiffness ratio was found to be approximately 1.16, which is slightly larger than that recorded for EB beams (i.e. 1.13; see Table 4-1), although the area of the CFRP bars used in BC1-NSM and BC2-SNSM (2 $\emptyset$ 6 = 56.5 mm<sup>2</sup>) was smaller than that of the sheet used in BC1-EB1S and BC3-EB1S-*side* (one sheet = 72 mm<sup>2</sup>).

Table 4-5 : Comparison of the ultimate bending moment obtained from the tests and current design codes.

Specimen	Experimental ultimate bending moment, $M_{exp}$ (kN.m)		ACI 440.2R-08 [30]		CNR-DT 200 R1/2013 [33]		FIB Bulletin 14 [34]	
	Hogging ( $h$ )	Sagging ( $s$ )	$M_{ACI}$ (kN.m)	$M_{ACI}/M_{Exp}$	$M_{CNR}$ (kN.m)	$M_{CNR}/M_{Exp}$	$M_{FIB}$ (kN.m)	$M_{FIB}/M_{Exp}$
CB	36	42.5	----	----	----	----	----	----
BC1-EB1S	50.5	52.9	48.87	0.97( $h$ ) 0.92( $s$ )	48.90	0.97( $h$ ) 0.92( $s$ )	53.9	1.07( $h$ ) 1.02( $s$ )
BC2-EB1P	47.4	41.3	41.49	0.88( $h$ ) 1.00( $s$ )	40.10	0.85( $h$ ) 0.97( $s$ )	57.26	1.21( $h$ ) 1.39( $s$ )
BC3-EB1S-side	54.1	46.2	46.14	0.85( $h$ ) 1.00( $s$ )	47.54	0.87( $h$ ) 1.03( $s$ )	50.94	0.94( $h$ ) 1.10( $s$ )
BC4-EB2S	76.1	48.3	55.64	0.73( $h$ ) 1.15( $s$ )	51.90	0.68( $h$ ) 1.07( $s$ )	66.16	0.87( $h$ ) 1.37( $s$ )
BC5-EB1S-weight(700)	52.9	51.7	51.75	0.98( $h$ ) 1.00( $s$ )	51.45	0.97( $h$ ) 0.99( $s$ )	59.06	1.12( $h$ ) 1.14( $s$ )
BC6-EB1S-weight(1100)	63.82	58.76	58.88	0.92( $h$ ) 1.00( $s$ )	58.74	0.92( $h$ ) 1.00( $s$ )	71.84	1.13( $h$ ) 1.22( $s$ )
Mean				0.89( $h$ ) 1.01( $s$ )		0.88( $h$ ) 0.97( $s$ )		1.06( $h$ ) 1.21( $s$ )

Table 4-6 : Details of the NSM-CFRP bar beams.

Beam	Hogging region strengthening			Sagging region strengthening			$A_s$ (mm <sup>2</sup> )	$A_f$ (mm <sup>2</sup> )	$E_f * A_f$ (kN)	$1 + \frac{E_f * A_f}{E_s * A_s}$
	No.	Length	SL/BL	No.	Length	SL/BL				
BC1-NSM	2Ø6	2.0	0.70	2Ø6	2.3	0.65	307.88	56.5	9322.5	1.16
BC2-SNSM	2Ø6	2.0	0.70	2Ø6	2.3	0.65	307.88	56.5	9322.5	1.16

4.5.1 Overall performance

Table 4-7 presents a comparison between the experimental results of the NSM beams and those of the EB beams in terms of the load-carrying capacity ( $P_u$ ), attained central reaction at the ultimate load level ( $R_c$ ), ultimate bending moment in the hogging ( $M_h^{Exp}$ ) and sagging ( $M_s^{Exp}$ ) regions, moment redistribution ratio ( $\beta$ ), ductility index ( $\mu$ ), and energy absorption capacity ( $E_{ab}$ ). The ductility index ( $\mu$ ) is defined as the ratio of deflection at the ultimate load to that at which the steel starts yielding. The energy absorption capacity ( $E_{ab}$ ) is calculated from the area under the load-deflection curve up to the ultimate load.

In general, despite the smaller CFRP reinforcement area, continuous RC beams internally strengthened with CFRP rods exhibited a better flexural performance than that of beams strengthened externally with CFRP sheets. The same was also true regarding the ultimate strength capacity, moment redistribution capability, ductility state, and energy absorption capacity. This overall improvement is most likely attributed to the fact that the NSM-CFRP rods were located inside the strengthened members, providing an advanced level of strengthening that is less prone to premature failure and has high bonding efficiency. Indeed, according to the test results, the NSM technique showed a higher capability than that of the EB technique to delay the debonding failure. This can be clearly seen in Figure 4-24 and Figure 4-25, which present the variations in the longitudinal tensile strain of the CFRP under several load levels. It can also be observed that the debonding strain in beam BC1-NSM was 51.5% greater than that in beam BC1-EB1S and, similarly, 17.6% greater in beam BC2-SNSM than in beam BC3-EB1S-side.

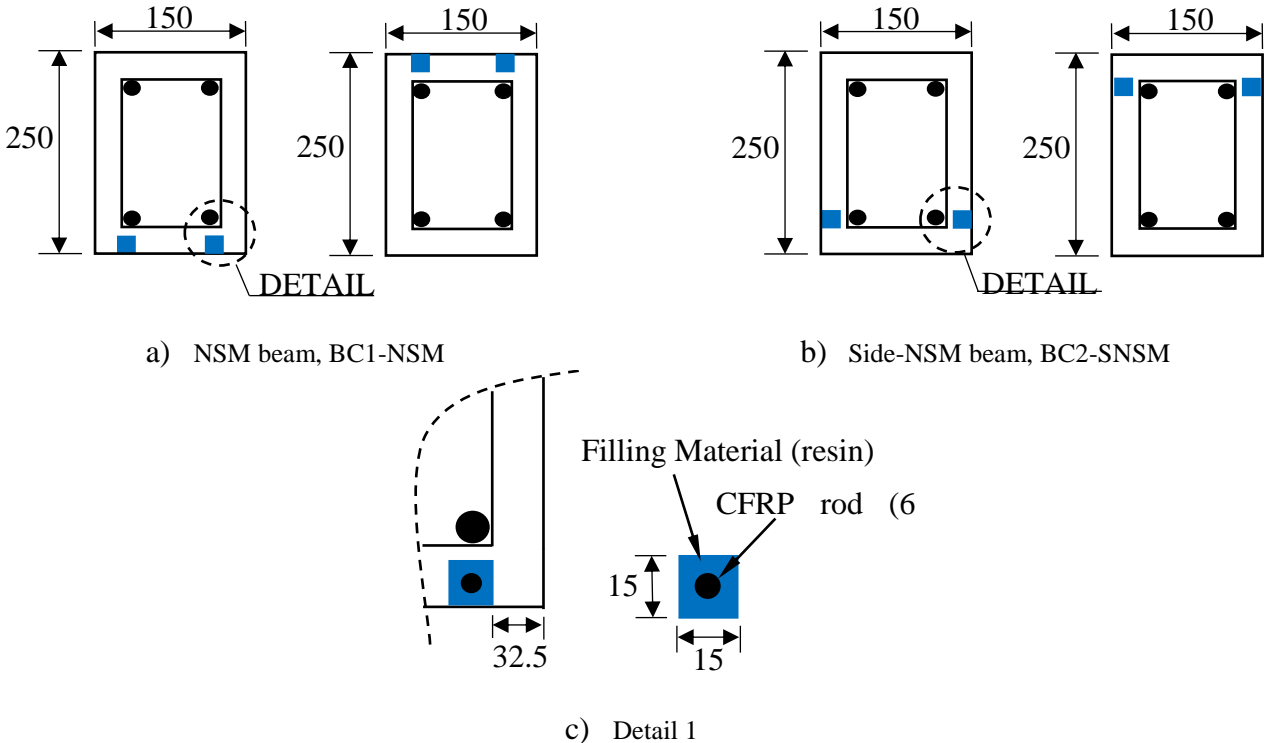


Figure 4-23 : Cross-section and groove dimensions details of NSM beams (All dimensions are in mm).

### 4.5.2 Failure mode and cracks maps

As stated in Section 3.2, the failure that occurred in the EB beams was primarily debonding of the CFRP sheets and plates at the critical sections as a result of the IC followed by either CCD or CFRP rupture. Table 4-8 presents the failure modes and crack maps of the NSM beams. The typical failure mode was yielding of the tension steel followed by debonding of the CFRP bars. No delamination of the concrete cover or rupture of the CFRP bars was observed. Notably, the debonding failure of beam BC1-NSM was brittle as a consequence of the sudden pulling-out of the CFRP bars in the hogging region close to the central support, accompanied by minor concrete crushing at the applied load points. The debonding failure of beam BC2-SNSM was characterized by the cracking of the epoxy-resin cover and the fracture in the concrete at the hogging and sagging regions, with high-intensity concrete crushing at the applied load points and minor concrete crushing at the central support. It was also found that, in each beam, one end of the CFRP bars moved from its initial position to the central support, indicating that the debonding failure primarily occurred at the resin-CFRP interface, not as a result of the IC. This finding confirms that the NSM-CFRP bars in continuous RC beams are less sensitive to debonding phenomena due to the IC, which is similar to the results observed in SSBs [24].

The number of cracks at the failure stage was also found to be lower in the EB beams than that reported in the NSM beams, especially in the hogging region. Compared to the control beam, the number of cracks in beam BC1-NSM was higher by 200% (189% for BC1-EB1S) and 62.5% (125% for beam BC1-EB1S) in the hogging and sagging regions, respectively, whereas the number of cracks in beam BC2-SNSM was higher by 250% (63% for beam BC3-EB1S-side) in the hogging region and 193.8% (19% for BC3-EB1S-side) in the sagging region.

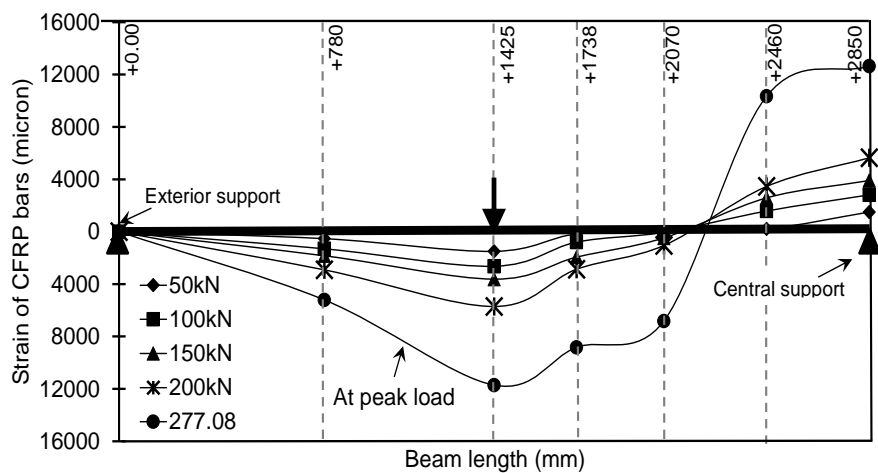
### 4.5.3 Yield and ultimate strength capacity

Although the axial stiffness ratios of beams BC1-NSM, BC2-SNSM, BC1-EB1S, and BC3-EB1S-side were very close, the amount of CFRP reinforcement used to strengthen the EB beams (BC1-EB1S, BC3-EB1S-side) was nearly 1.27 times that used to strengthen the NSM beams (BC1-NSM, BC2-SNSM). According to Figure 4-26, the tested beams, regardless of the strengthening technique used, displayed an almost identical response in the elastic stage (i.e. before the concrete cracking). In the postcracking and postyielding stages, however, the flexural stiffness, yielding load, and ultimate load of the NSM beams were considerably higher than those of the EB beams. The tension steel in the hogging region of beams BC1-NSM and BC2-SNSM yielded at a load of 195.1kN (13.8% increase over BC1-EB1S) and 180.8 kN (8.9% increase over BC3-EB1S-side), respectively. Similarly, the ultimate strength capacity of beams BC1-NSM and BC2-SNSM was about 277.1 kN (26.3% increase over BC1-EB1S) and 250.1 kN (21.8% increase over BC3-EB1S-side), respectively. These results indicate that improving the flexural behavior of continuous RC beams is more dependent on the strengthening technique used than on the CFRP reinforcement amount or axial stiffness ratio applied. This was also true regarding beam BC4-EB2S (see Figure 4-17), in which the area of the CFRP sheets (two layers) was nearly 2.5 times that used to strengthen beam BC1-NSM (2Ø6). Moreover, the yielding and ultimate capacity of the latter beam (BC1-NSM) were still greater by about 2.7% and 14.3%, respectively. Therefore, it is confirmed that the NSM technique is more efficient than the EB technique.

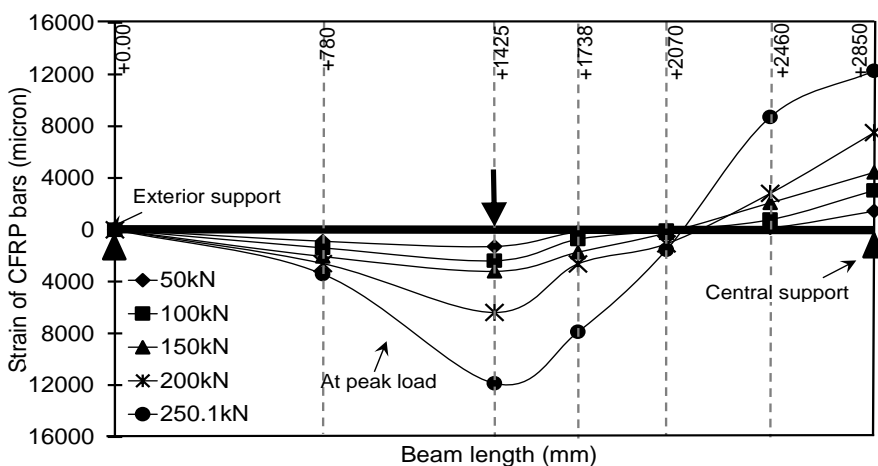
In general, positioning the CFRP reinforcements on the vertical sides instead of the bottom/top sides decreases the effective arm depth of the tension reinforcements, thereby decreasing the yield and ultimate strength of the beam. In this study, the reduction in the ultimate strength due to changing the position of the CFRP was marginally affected by the strengthening technique used. The percentage drops of the ultimate strength for beams strengthened with EB sheets and NSM-CFRP rods were 6.4% and 9.7%, respectively. In SSBs, however, this percentage drop was 16.1% in the EB-CFRP beams [10] and 12.9% in the NSM-CFRP beams [11].

#### 4.5.4 Moment redistribution

As discussed previously in section 3.5, strengthening continuous RC beams with EB-CFRP sheets significantly decreases the moment redistribution degree at the ultimate state and can even change the direction of redistribution depending on the strengthening state. However, by comparing the moment redistribution values of beams BC1-NSM and BC2-SNSM with those of the RC beam strengthened with EB-CFRP sheets (BC1-EB1S, BC3-EB1S-side), it can be concluded that applying the NSM technique allows a higher moment redistribution value at the ultimate state, as shown in Table 4-7. Further research studies are strongly recommended in this direction.

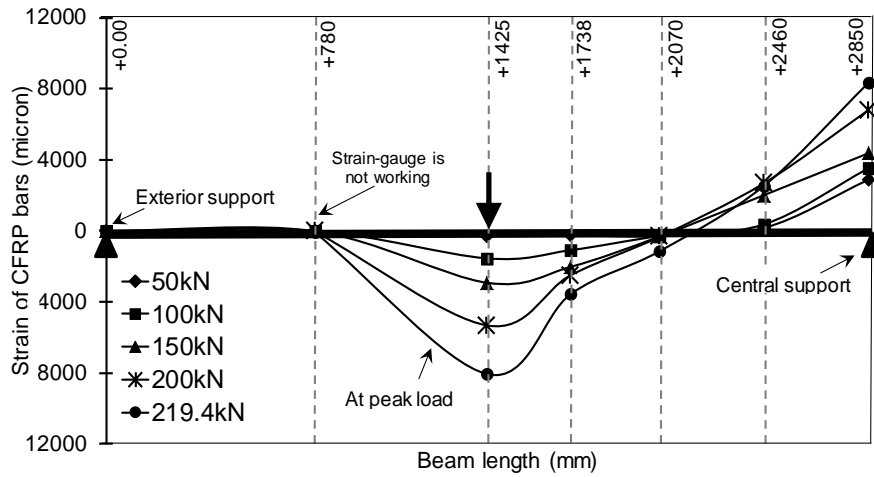


(a) BC1-NSM

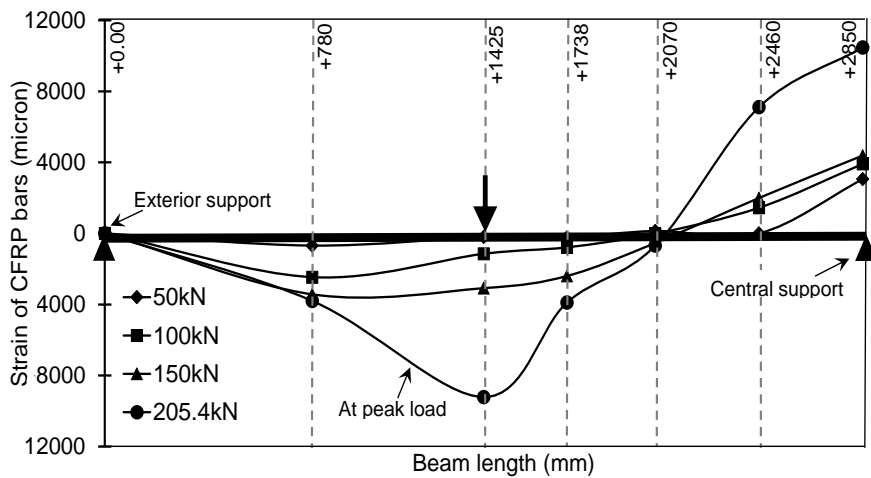


(b) BC2-SNSM

Figure 4-24 : Variation in longitudinal strain of NSM-CFRP bars at different loads.



(a) BC1-EB1S



(b) BC3-EB1S-side

Figure 4-25 : Variation in longitudinal strain of EB-CFRP bars at different loads.

## 4.6 Conclusion

In this study, a total of nine beams were experimentally tested (i) to primarily investigate the effectiveness of the EB technique in improving the flexural performance of two-span RC beams in terms of important influential factors, such as the position, form, and reinforcement ratio of the CFRP, as well as the weight of carbon fibers; (ii) to evaluate the effectiveness of the current guidelines in determining the flexural strength of continuous RC beams strengthened externally with CFRP; and (iii) to assess and compare the efficiency of the EB technique in strengthening continuous beams to that of the NSM technique.

Regarding the effectiveness of the EB technique in improving the flexural performance of two-span RC beams, the following conclusions can be drawn:

- 1) Regardless of the strengthening scenario applied, all the strengthened beams displayed an improvement in their flexural strength in comparison to the unstrengthened control beam. The increase in the percentage of the yield and ultimate load as a result of the CFRP composites ranged from 25.5% to 59.1% and from 7.6% to 49.8%, respectively.



- 2) Increasing the carbon fiber weight per unit area was found to be effective in improving the strength capacity of the beam and it may be used as an alternative to multiple sheet layers, but this efficiency was conditional upon the total axial stiffness ratio of the beam and the proper adhesive resin used. The failure load of beam BC5-EB1S (one sheet, weight: 700 g/m<sup>2</sup>, axial stiffness: 1.17, Epx TFC 350) was found to be 99.2% of the total failure load of beam BC1-EB1S (one sheet, weight: 350 g/m<sup>2</sup>, axial stiffness =1.13, Epx TFC 350), whereas the failure load of beam BC6-EB1S (one sheet, weight: 1100 g/m<sup>2</sup>, axial stiffness =1.33, Epx TFC 1000) was found to be 116% of the failure load of beam BC1-EB1S.
- 3) Bonding the CFRP sheet on the side surfaces may be a feasible alternative to bonding on the bottom/top surfaces. Compared to beam BC1-EB1S, the decreases observed in the yield and ultimate load of beam BC3-EB1S-*side* were only 3.1% and 6.4%, respectively.
- 4) Moment redistribution analysis showed that the majority of moment redistribution occurred in the stage between the concrete cracking and the first steel yielding for all the tested beams, while slight moment redistribution occurred during later stage.

Regarding the evaluation of the effectiveness of the current guidelines in determining the flexural strength capacity of continuous RC beams strengthened externally with CFRP, the following conclusion can be drawn:

The current design guidelines provide an acceptable prediction regarding the ultimate strength of beams strengthened with one layer of CFRP composites, however, they show a low accuracy in predicting the ultimate strength for beams strengthened with multiple CFRP layers.

Regarding the comparison between the two strengthening techniques, NSM and EB, the following conclusions can be drawn:

- 1) The NSM technique allows the CFRP tensile strength to be better exploited than the EB technique. The debonding strain in beam BC1-NSM was found to be 51.5% greater than that in beam BC1-EBIS and was also 17.6% greater in beam BC2-SNSM than in beam BC3-EBIS-*side*.
- 2) The flexural stiffness, yielding load, ultimate load, ductility state, and energy absorption capacity of the NSM beams were found to be considerably higher than those of the EB beams, confirming the higher efficiency of the NSM technique in comparison to the EB technique.
- 3) The NSM-CFRP bars in continuous RC beams were found to be less sensitive to debonding phenomena caused by the IC, which is not the case in EB-CFRP. The failure of the EB beams was characterized by debonding of the CFRP composites at the critical sections as a result of the IC followed by either CCD or CFRP rupture.
- 4) The NSM technique allows a higher moment redistribution value at the ultimate state than that achieved with the EB technique. Beams BC1-NSM and BC2-SNSM were found to exhibit moment redistribution degree of +19.59% and +11.49% in the hogging region and -11.83% and -6.92% in the sagging region, respectively, whereas their counterpart EB beams exhibited values of +13.87% and +1.48% in the hogging region and -8.32% and -0.89% in the sagging region.

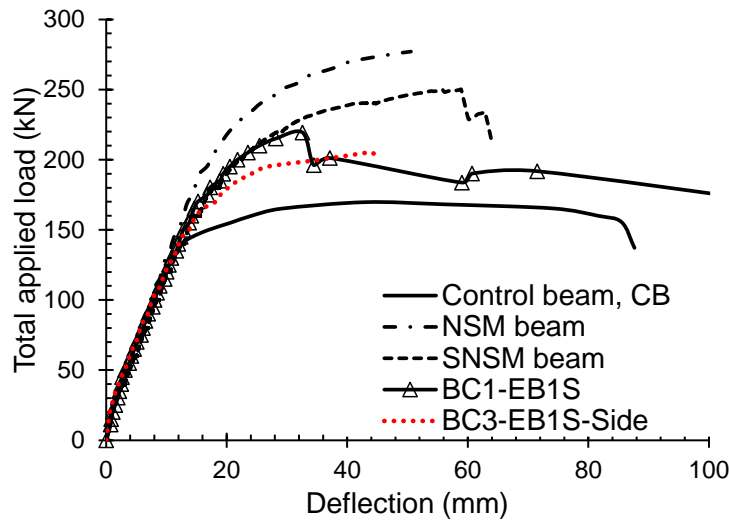





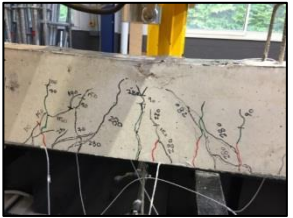



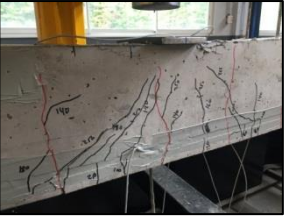
Figure 4-26 : Load deflection curves of NSM beams and EB beams.

Table 4-7 : Comparison between the test results of the NSM/SNSM beams and EB beams.

Beam	Ultimate load ( $P_u$ )	Central support reaction <sup>[1]</sup> , $R_c$	Flexural moment at hogging ( $M_h$ )			Flexural moment at sagging ( $M_s$ )			$\mu$ <sup>[7]</sup>	$E_{ab}$ <sup>[8]</sup>
			$M_h^{Exp}$ <sup>[2]</sup>	$M_h^{Th}$ <sup>[3]</sup>	$\beta(\%)$ <sup>[6]</sup>	$M_s^{Exp}$ <sup>[4]</sup>	$M_s^{Th}$ <sup>[5]</sup>	$\beta(\%)$ <sup>[6]</sup>		
CB	169.7	110.1	36	45.3	20.53	42.5	37.8	-12.43	4.8	8082.8
BC1-NSM	277.1	180.3	59.5	74	19.59	69	61.7	-11.83	3.3	10356.6
BC2-SNSM	250.1	166.6	59.3	67	11.49	59.4	55.6	-6.92	3.6	11242.1
BC1-EB1S	219.4	145.1	50.5	58.6	13.87	52.9	48.9	-8.32	2.2	6044.3
BC3-EB1S-side	205.5	140.7	54.1	54.9	1.48	46.2	45.8	-0.89	2.8	6994.7

(1) Central reaction measured by attached load cell at ultimate load  $P_u$ . (Both in kN); (2) Experimental ultimate negative moment calculated by:  $M_h^{Exp} = \frac{(P_u - 2R_c) \times L}{4}$ , where L is the beam length. (kN.m); (3) Theoretical ultimate negative moment calculated by:  $M_h^{Th} = \frac{3P_u L}{32}$ . (kN.m); (4) Experimental ultimate positive moment calculated by:  $M_s^{Exp} = \frac{(P_u - R_c) \times L}{4}$ . (kN.m); (5) Theoretical ultimate positive moment calculated by:  $M_s^{Th} = \frac{5P_u L}{64}$ . (kN.m); (6) Moment redistribution calculated by:  $\beta(\%) = \left( \frac{M_h^{Th} - M_h^{Exp}}{M_h^{Th}} \right) \times 100\%$ . ; (7) Ductility index.; (8) Energy absorption capacity. (kN.mm).

Table 4-8 : Crack maps and failure mode of the NSM beams .

Beam	Cracks map	Failure mode		
BC1-NSM				
		Central support	Left span	Right span
Debonding: Pull out of the CFRP bars in the hogging region				
BC2-SNSM				
		Central support	Left span	Right span
Debonding: Cracking of the epoxy-resin cover and fracture in the concrete in the hogging and sagging regions				

## 4.7 References

1. Goertzen WK, Kessler MR. Creep behavior of carbon fiber/epoxy matrix composites. *Materials Science and Engineering A* 421 (2006) 217–225.
2. Nayak AN, Kumaria A, Swain RB. Strengthening of RC beams using externally bonded fibre reinforced polymer composites. *Structures* 2018;14:137–52.
3. Al-Mahmoud F, Caste A I, François R, Tourneur C. Strengthening of RC members with near surface mounted CFRP rods. *Composite Structures* 2009; 91:138-147
4. Al-Mahmoud F, Castel A, François R, Tourneur C. Effect of surface preconditioning on bond of carbon fiber reinforced polymer rods to concrete. *Cem Concr Compos* 2007;29(9):677–89.
5. Ceroni F, Pecce M, Bilotta A, Nigro E. Bond behavior of FRP NSM systems in concrete elements . Ceroni et al./Composites: Part B 43 (2012) 99–109.
6. Ashour AF, El-Refaie SA, Garrity SW. Flexural strengthening of RC continuous beams using CFRP laminates. *Cem Concr Compos* 2004;26:765–75.
7. Akbarzadeh H, Maghsoudi AA. Experimental and analytical investigation of reinforced high strength concrete continuous beams strengthened with fiber reinforced polymer. *Mater Des* 2010;31:1130–47.
8. Ali H, Assih J, Li A. Flexural capacity of continuous reinforced concrete beams strengthened or repaired by CFRP/GFRP sheets. *International Journal of Adhesion and Adhesives* 104 (2021) 102759.
9. Abdallah M, Al Mahmoud F, Khelil A, Mercier J, Almassri B. Assessment of the flexural behavior of continuous RC beams strengthened with NSM-FRP bars, experimental and analytical study, *Composite Structures*, 242 (2020) 112127.
10. Salama ASD, Hawileh RA, Abdalla JA. Performance of externally strengthened RC beams with side-bonded CFRP sheets. *Composite Structures* 212 (2019) 281–290
11. Abdallah M, Al Mahmoud F, Boissière R, Khelil A, Mercier J. Experimental study on strengthening of RC beams with Side Near Surface Mounted technique-CFRP bars. *Composite Structures* 234 (2020) 111716.
12. Capozucca R, Nilde Cerri M. Static and dynamic behaviour of RC beam model strengthened by CFRP-sheets. *Construction and Building Materials* 16 2002 91 Ž . 99.
13. Zhou CY, Yu YN, Xie EL. Strengthening RC beams using externally bonded CFRP sheets with end selflocking. *Composite Structures* 241 (2020) 112070
14. Ababneh AN, Al-Rousan RZ, Ghaith IMN. Experimental study on anchoring of FRP-strengthened concrete beams. *Structures* 23 (2020) 26–33.
15. Sharaky IA, Baena M, Barris C, Sallam HEM, Torres L. Effect of axial stiffness of NSM FRP reinforcement and concrete cover confinement on flexural behaviour of strengthened RC beams: Experimental and numerical study. *Engineering Structures* 173 (2018), 987–1001.
16. Le-Trung K, Lee K, Lee J, Lee DH, Woo S. Experimental study of RC beam–column joints strengthened using CFRP composites. *Composites: Part B* 41 (2010) 76–85

17. Jawdhari A, Peiris A, Harika I. Experimental study on RC beams strengthened with CFRP rod panels. *Engineering Structures* 173 (2018) 693–705
18. Obaidat YT, Abu-Farsakh GAFR, Ashteyat AM. Retrofitting of partially damaged reinforced concrete beam-column joints using various plate-configurations of CFRP under cyclic loading. *Construction and Building Materials* 198 (2019) 313–322
19. Akhlaghi A, Mostofinejad D. Experimental and analytical assessment of different anchorage systems used for CFRP flexurally retrofitted exterior RC beam-column connections. *Structures* 28 (2020) 881–893.
20. Lignola GP, Prota A, Manfredi G, Cosenza E. Experimental performance of RC hollow columns confined with CFRP. *J Compos Construct* 2007;11(1). 1090-0268.
21. Shaikh FUA, Alishahi R. Behaviour of CFRP wrapped RC square columns under eccentric compressive loading. *Structures* 20 (2019) 309–323
22. Saljoughian A, Mostofinejad D. Axial-flexural interaction in square RC columns confined by intermittent CFRP wraps. *Composites Part B* 89 (2016) 85-95.
23. Akter Hosen Md, Jumaat MZ, Saiful Islam ABM. Side Near Surface Mounted (SNSM) technique for flexural enhancement of RC beams. *Materials & Design* 2015; 83 : 587–597.
24. Bilotta A, Ceroni F, Nigro E, Pecce M. Efficiency of CFRP NSM strips and EBR plates for flexural strengthening of RC beams and loading pattern influence. *Composite Structures* 124 (2015) 163–175.
25. Al-Mahmoud F, Castel A, François R, Tourneur C. RC beams strengthened with NSM CFRP rods and modeling of peeling-off failure. *Compos Struct* 2010;92(8):1920–30.
26. Pham H, Al-Mahaidi R. Prediction models for debonding failure loads of carbon fiber reinforced polymer retrofitted reinforced concrete beams. *J Compos Construct, ASCE* 2006;10(1):48–59.
27. Xiong GJ, Jiang X, Liu JW, Chen L. A way for preventing tension delamination of concrete cover in midspan of FRP strengthened beams. *Construct Build Mater* 2007;21:402–8.
28. Zaki MA, Rasheed HA, Roukerd RR, Raheem M. Performance of reinforced concrete T beams strengthened with flexural CFRP sheets and secured using CFRP splay anchors. *Engineering Structures* 210 (2020) 110304.
29. Obaidat YT, Barham WS, Aljarah AH. New anchorage technique for NSM-CFRP flexural strengthened RC beam using steel clamped end plate. *Construction and Building Materials* 263 (2020) 120246.
30. ACI Committee 440. Guide For The Design And Construction Of Externally Bonded FRP Systems For Strengthening Concrete Structures. American Concrete Institute, 2017, Farmington Hills, MI., USA.
31. Li L, Zheng W, Wang Y. Review of moment redistribution in statically indeterminate RC members. *Engineering Structures* 196 (2019) 109306.
32. Scott RH, Whittle RT. Moment redistribution effects in beams. *Mag Concr Res* 2005;57:9–20.

33. CNR-DT 200 R1/2013, Guide for the design and construction of externally bonded FRP systems for strengthening existing structures, Rome, Italy: National Research Council; 2013.
34. FIB Bulletin 14. Externally Bonded FRP Reinforcement for RC Structures. International Federation for Structural Concrete, Zürich, Switzerland, 2001.
35. ACI. Building code requirements for structural concrete and commentary. American Concrete Institute, ACI 318-14, Farmington Hills, MI., September 2014.
36. BS EN 1992-1-1:2004. Eurocode 2: Design of concrete structures - Part 1-1: General rules and rules for buildings. London, UK: British Standards Institution; 2004.
37. AS 3600-2009. Concrete structures. Sydney, Australia: Australia Standards; 2009.
38. Aiello MA, Valente L, Rizzo A. Moment Redistribution In Continuous Reinforced Concrete Beams Strengthened With Carbon-Fiber-Reinforced Polymer Laminates. *Mechanics of Composite Materials*, Vol. 43, No. 5, 2007.
39. Feng R, Liu Y, Zhu JH, Xing F. Flexural behaviour of C-FRCM strengthened corroded RC continuous beams. *Composite Structures* 245 (2020) 112200.
40. Oehlers DJ, Ju G, Liu IST, Seracino R. Moment redistribution in continuous plated RC flexural members. Part 1: neutral axis depth approach and tests. *Engineering Structures* 26 (2004) 2197–2207.
41. Cohn M. Continuity in prestressed concrete partial prestressing from theory to practice, vol I, Survey Reports, NATO ASI Series Boston, Mass: Martinus Nijhoff Publishers. 1986. p. 189–256.

### III. GENERAL CONCLUSION AND FUTURE WORK

This thesis primarily aims to study the global flexural response of RC beams strengthened with FRP reinforcements. Overall, the thesis consists of three main parts: an experimental, analytical and numerical part.

In the experimental part, the NSM, side-NSM, EB, and side-EB techniques were employed for strengthening 21 full-scale RC beams. Different types and forms of the FRP reinforcements were used. The carbon and glass FRP bars were utilized in the beams internally strengthened by means of the NSM and side-NSM techniques, while the carbon plates and sheets were used in the beams externally strengthened by means of the EB and side-EB techniques.

In the analytical part, a simplified linear model was initially introduced for predicting the load-deflection response of SSBs strengthened with side-NSM-CFRP bars. This analytical model was based on the recommendations of the American Concrete Institute ACI 318-08. Later, a more accurate nonlinear analysis of the RC beam cross-section was developed to construct and compare the theoretical moment-curvature curves of NSM-FRP continuous beams with the experimental curves, furthermore, to predict the beams' ultimate load capacities. This analytical model employed the nonlinearity behavior of concrete and steel materials. An additional analytical study, presented at the end of this thesis, was conducted to evaluate the effectiveness of the current design codes (ACI 440.2R-08, CNR-DT 200 R1/2013 and *fib* Bulletin 14) for determining the flexural strength of continuous beams externally strengthened with CFRP sheets or plates.

In the numerical part, the ABAQUS computer program was used for creating an efficient three-dimensional model that can simulate and predict the behavior of continuous RC beams internally strengthened with CFRP bars (NSM or side-NSM). Afterward, the proposed FE models were used to extend the thesis by implementing a parametric study that depends on a beam's steel reinforcement ratio and arrangement of the CFRP bars.

However, the first objective of this thesis (see Chapter 1) was to investigate the possibility of strengthening RC beams on their sides using the side-NSM technique. The side-NSM technique was proposed and examined in order to overcome the limitations and operational obstacles of the conventional NSM technique. To achieve this, five SSBs were strengthened in bending with CFRP bars using the side-NSM technique and were tested in four-point loadings tests up to failure. The side-NSM beams were designed to evaluate the effects of the CFRP length, CFRP position and type of filling material on their flexural performance. The test results showed that the side-NSM technique helped to improve the global flexural performance of beams, whatever strengthening scenario was used. Nevertheless, placing the CFRP bars on the same level as the steel bars and using resin as a filling material was the best strengthening scenario. The ratio of the strengthening length (SL) to the beam length (BL) was found to have a significant impact on the failure mode of the side-NSM beams. The beams with SL/BL less than 0.6 showed a premature failure mode due to the insufficient CFRP length. The efficiency of the side-NSM technique for strengthening RC beams was compared with that of the NSM technique (from the literature). The comparison study revealed that the proposed side-NSM strengthening system can be used as an alternative to the NSM system, and it can in some cases help to avoid the



nonconventional failure modes (pull-out of CFRP rods or an early debonding failure). Furthermore, the side-NSM-CFRP beams showed higher ductility behavior compared to the NSM-CFRP beams.

The second objective of this thesis (see Chapter 2) was to use the NSM-FRP bars for strengthening continuous two-span RC beams. For this purpose, six large-scale beams were fabricated and tested: one control beam and five others were internally strengthened using the NSM technique in the positive (hogging) and negative (sagging) bending moment regions with FRP bars. The global flexural performance of the strengthened beams was studied according to the type, ratio and length of the FRP bars as well as the filling material characteristics (resin or mortar). The experimental results showed that the NSM-FRP bars technique is able to improve the flexural behavior of continuous RC beams. Indeed, the improvement in the load-carrying capacity of tested beams due to the FRP bars ranged from 25.7% to 63.3%. Additionally, the NSM-FRP bars reduced the tensile strain of steel bars and the compressive strain of concrete in the strengthened beams compared to the strains in the control beam under the same applied load. It was also found that, using the NSM-FRP bars increases the number of the cracks in the hogging and sagging regions of the continuous beams, whereas the average crack spacing and crack width were significantly decreased. The reported debonding strain ( $\epsilon_d$ ) of the FRP bars was found to range from 46% to 100% of the ultimate strain ( $\epsilon_{ult}$ ). However, terminating the FRP bars before the inflection point caused the failure mode of a beam to change from debonding to premature peeling-off of the concrete cover, which caused an about 11% decrease in the load-carrying capacity and a 45% drop in the ductility as compared to those observed in the beam employed FRP bars with sufficient development length beyond the inflection point. Furthermore, using the conventional mortar instead of epoxy-resin to bond the FRP bars with concrete was found to form less bonding strength at the concrete-filling material interface, which in turn decreased the load-carrying capacity and ductility of a beam by about 18% and 42%, respectively. The amount of moment redistribution in NSM-FRP bars continuous beams was found to be dependent on the quantity and length of the FRP bars as well as on the characteristic of the filling material. The moment redistribution capacity of tested NSM beams was compared with the moment redistribution capacity of externally bonded beams from the literature. Overall, the comparison study proved that applying the NSM-FRP technique allows more moment redistribution value at the ultimate load than the conventional EB-FRP technique.

The third objective of this thesis (see Chapter 3) was to introduce the side-NSM technique for strengthening continuous RC beams with CFRP bars and, furthermore, to study the influence of the steel reinforcement ratio in the negative bending moment as well as the CFRP strengthening arrangement on the flexural behavior of continuous beams strengthened internally using the NSM and side-NSM techniques. For this end, comprehensive experimental and numerical studies were conducted. For the experimental part, an additional two continuous beams were fabricated and tested up to failure, whereas for the numerical part, the ABAQUS computer program was utilized to three-dimensionally model and simulate the nonlinear behavior of 21 continuous beams. Three combinations of bond model and the behavior of CFRP bars, namely the PBM, modified PBM with a reduction in the tensile strength of CFRP, and the CZM, were considered. The three dimensional FE analysis developed with the CZM was able to capture the main aspects observed from the experiments such as the load-deflection response,

failure mode and cracks patterns. However, the experimental and FE results proved that the side-NSM-CFRP bars system is a convenient alternative to the conventional NSM system for strengthening continuous beams. For all the adopted strengthening configurations, the increase of the load-carrying capacity ( $\lambda$ ) of beams strengthened with NSM-CFRP bars varied between 18% and 64%, whereas an increase in  $\lambda$  between 23% and 61%, was registered for beams strengthened with side-NSM-CFRP bars. In both techniques, the highest increase of  $\lambda$  was achieved when the strengthening configuration composed CFRP bars in both hogging and sagging regions. Nevertheless, the side-NSM technique was relatively more efficient than the bottom/top NSM technique when the CFRP bars were applied only in either the hogging region or the sagging region. The results also showed that the side-NSM-CFRP bars considerably increase the number of cracks in the bending regions of beams more than do the NSM-CFRP bars. It was also found that the side-NSM-CFRP bars had almost the same effectiveness, debonding strain and bonding strength with concrete as the NSM-CFRP bars did. The arrangement of the CFRP and the amount of steel reinforcement were found to have significant effects on the moment redistribution capacity of continuous RC beams, and they can even change the direction of redistribution. In such cases, increasing the steel ratio in the hogging region ( $\rho_s^H$ ) was found to decrease the moment redistribution of beams regardless of the strengthening technique used. However, for beams reinforced with the same  $\rho_s^H$ , strengthening only the sagging regions was found to increase the moment redistribution.

Finally, the fourth objective of this thesis (see Chapter 4) was to contribute to fill in the gaps in the literature regarding strengthening continuous RC beams with EB-CFRP. In addition, to assess the efficiency of the EB and side-EB techniques to strengthen continuous beams in comparison with the NSM and side-NSM techniques. For this purpose, an additional six large-scale continuous beams were externally strengthened with carbon sheets or plates and tested in bending up to failure. The flexural performance of the strengthened beams was studied according to the CFRP reinforcement position, the CFRP form, the CFRP layer number, and the weight of the carbon fibers. The tested beams were failed by the debonding of the CFRP composites at the critical sections as a result of the intermediate crack followed by either concrete cover delamination or rupture of the CFRP. The axial stiffness ratio of the strengthened beams was found to be the key factor affecting the first crack and yielding load. On the other hand, the bonding area and resin type were found to influence the ultimate load of the beam when compared on the basis of the CFRP form and weight of the carbon fibers, respectively. Increasing the carbon fiber weight per unit area and using a modified soft adhesive resin can be used as an alternative to the multiple sheet layers. The highest improvement in the load-deflection response was achieved in the beam employing one layer of 1100 g/m<sup>2</sup> CFRP sheet, whereas the lowest improvement was reported in the beam strengthened with CFRP plates. However, bonding the CFRP sheet on the side surfaces of the beam proved again to be a feasible alternative to bonding on the bottom/top surfaces without significant reduction in the load-carrying capacity (about 6%). The experimental results also showed that the majority of the moment redistribution in continuous beams strengthened externally with CFRP occurs in the stage between the concrete cracking and the first steel yielding, and slight moment redistribution occurs after that. Furthermore, the debonding strain of CFRP reinforcement ranged between 29% and 67% of the ultimate strain. Regarding the comparison between the

efficiency of internal (NSM and side-NSM) and external (EB and side-EB) techniques for strengthening continuous beams, it was found that the flexural stiffness, yielding load, ultimate load, ductility state, energy absorption capacity, bonding strength between CFRP and concrete, and the moment redistribution of the beams strengthened internally with CFRP bars were considerably higher than those of the beams strengthened externally with CFRP sheets.

#### **Future work**

This thesis has been mainly focused on initially flexural strengthening of continuous RC beams with FRP reinforcements. Unfortunately, strengthening or repairing of pre-cracked continuous RC beams with FRPs was not studied in this thesis and has been left for future work due to the unexpected stop that occurred due to the COVID-19 pandemic.

Nevertheless, this section attempts to provide an introduction regarding repairing of pre-cracked continuous RC beams. For this purpose, an additional beam called BC1-RE has been fabricated and tested to examine the potential use of the NSM-CFRP technique to repair pre-cracked two-span continuous RC beams. The beam dimensions and its flexural and shear steel reinforcements were all similar to those used for the beams in Chapter 2. The beam BC1-RE was loaded into two phases. In the first phase, the beam was loaded to 70% of its ultimate load, and then the applied loads were totally removed for the strengthening purpose. The NSM technique was employed to strengthen BC1-RE. The CFRP bars were applied in the hogging and sagging regions of the beam. The SL to the BL ratio as well as the mechanical properties of the CFRP and resin were kept similar to those used in Chapter 2. In the second loading phase, the repaired beam BC1-RE was loaded again from zero to failure.

Obviously, the experimental load-deflection result (Figure III-1) shows the possibility of using NSM-FRP for repairing pre-cracked continuous beams despite the nonconventional pull-out failure mode (Figure III-2). In addition, Table III-1 shows that repairing of pre-cracked RC beams with FRP bars could be beneficial for reducing the crack width. These results open different perspectives and encourage carrying out future studies regarding using FRP reinforcements for repairing pre-cracked indeterminate structures. Particularly, to investigate the influence of the type and form of the FRP reinforcements and the impact of different techniques used.

In addition to the above discussion, there are other possible extensions of the present research, and they could be classified as follows:

- 1) In the present work, FRP reinforcements were only used for strengthening purposes. As we found, the brittle behavior of FRP materials is their main disadvantage, as this can restrict the ductility and energy absorption capacity of a strengthened RC beam. However, shape-memory alloy (SMA) is a new smart material that is capable of improving the ductility and energy absorption capacity of strengthened RC members due to its super elastic response. Therefore, it would be very interesting to use a hybrid technique of both FRP and SMA to solve the ductility issue of strengthened indeterminate beams.
- 2) The present research does not consider the dynamic behavior, long term and environmental effects, and pre-stressed FRPs and concrete. These topics are still

### III. General conclusion & future work

essentially required to confirm and validate the use of FRP reinforcements for improving the performance of indeterminate RC structures.

- 3) Prevention of the nonconventional failure modes in the strengthened FRP continuous RC beams would be inevitable for future work.

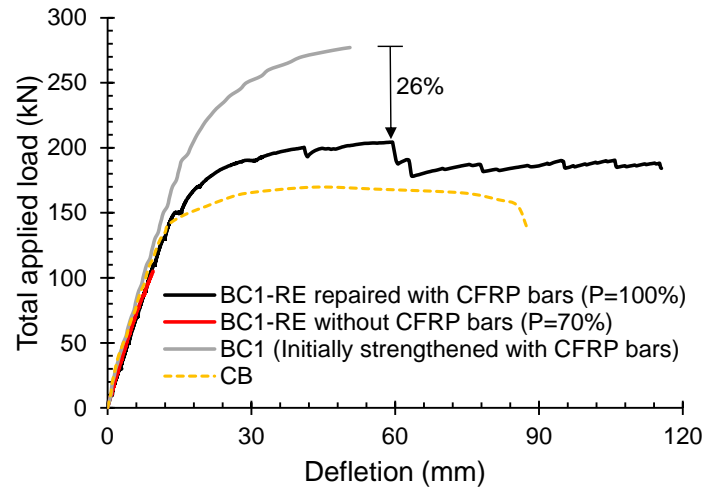


Figure III-1: Load-deflection curve of repaired beam

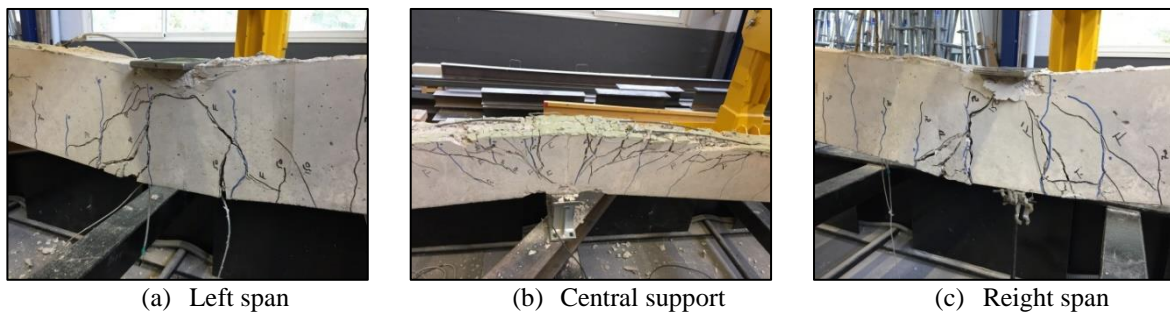


Figure III-2: FRP pull-out failure mode of repaired beam (BC1-RE)

Table III-1: Crack width

BC1-RE without CFRP bars (P=70% Pu), 1 <sup>st</sup> loading stage		BC1-RE with CFRP bars (P=100% Pu)-2 <sup>nd</sup> loading stage.	
Load	Crack width	Load	Crack width
0	0	0	0.16
30	0.20	30	0.20
50	0.35	50	0.28
70	0.53	70	0.33
90	0.62	90	0.40
110	0.75	110	0.47
130	1.35	130	0.52
150	3.10	150	0.60



## IV. SCIENTIFIC PRODUCTION

### **Papers in international Journals:**

Abdallah M, Al Mahmoud F, Boissière R, Khelil A, Mercier J. Experimental study on strengthening of RC beams with Side Near Surface Mounted technique-CFRP bars. *Composite Structures* 234 (2020) 111716.

Abdallah M, Al Mahmoud F, Khelil A, Mercier J, Almassri B. Assessment of the flexural behavior of continuous RC beams strengthened with NSM-FRP bars, experimental and analytical study. *Composite Structures* 242 (2020) 112127.

Abdallah M, Al Mahmoud F, Tabet-Derraz MI, Khelil A, Mercier J, Experimental and numerical investigation on the effectiveness of NSM and side-NSM CFRP bars for strengthening continuous two-span RC beams, *Journal of Building Engineering*, 41 (2021) 102723.

Abdallah M, Al Mahmoud F, Khelil A, Mercier J. Efficiency of EB CFRP composites for flexural strengthening of continuous RC beams: A comparative study with NSM CFRP rods. *Structures*, 34 (2021) 1567-1588.

### **Papers in international conferences:**

Abdallah M, Al Mahmoud F, Boissière R, Khelil A, Mercier J. Strengthening of RC Beams with SNSM-CFRP Rods. 3<sup>rd</sup> International Conference on International Conference on Recent Advances in Nonlinear Design, Resilience and Rehabilitation of Structures, CoRASS 2019, 16<sup>th</sup> -18<sup>th</sup> October. Coimbra, Portugal.

Al-Mahmoud F, Boissiere R, Abdallah M, Khelil A, Mercier J. Renforcement des poutres en beton arme par insertion de joncs de carbone sur les cotes. 20th Edition des Journees scientifiques du Regroupement Francophone pour la Recherche et la Formation sur le Beton (RF)2B, Bruxelles Belgique, 03-05 July 2019.

### **Presentations in international conferences:**

Abdallah M. Strengthening of RC Beams with SNSM-CFRP Rods. 3<sup>rd</sup> International Conference on International Conference on Recent Advances in Nonlinear Design, Resilience and Rehabilitation of Structures, CoRASS 2019, 16<sup>th</sup>-18<sup>th</sup> October. Coimbra, Portugal.

Abdallah M. Finite Element Study of Strengthening RC Beams with Side Near Surface Mounted (SNSM) Technique. The 14th Virtual Congress WCCM & ECCOMAS 2020, organized in virtual format from January 11<sup>th</sup> to 15<sup>th</sup>, 2021.



## V. REFERENCES

Note: *All the references used in each chapter are listed here in an alphabetical order*

- ABAQUS version 6.13, 2013. Computer software, Assault Systems, Waltham. MA.
- ABAQUS, 2013, ABAQUS Analysis User's Manual Version 6.13, Assault Systems.
- Ababneh AN, Al-Rousan RZ, Ghaith IMN. Experimental study on anchoring of FRP-strengthened concrete beams. *Structures* 23 (2020) 26–33.
- Abdallah M, Al Mahmoud F, Boissière R, Khelil A, Mercier J. Experimental study on strengthening of RC beams with Side Near Surface Mounted technique-CFRP bars. *Composite Structures* 234 (2020) 111716. <https://doi.org/10.1016/j.compstruct.2019.111716>.
- Abdallah M, Al Mahmoud F, Khelil A, Mercier J, Almassri B. Assessment of the flexural behavior of continuous RC beams strengthened with NSM-FRP bars, experimental and analytical study, *Composite Structures*, 242 (2020) 112127.
- Abouali S, Shahverdia M, Ghassemieh M, Motavallia M. Nonlinear simulation of reinforced concrete beams retrofitted by nearsurface mounted iron-based shape memory alloys, *Engineering Structures*, 187(2019), 133–148.
- ACI. Building code requirements for structural concrete and commentary. American Concrete Institute, ACI 318-14, Farmington Hills, MI., September 2014.
- ACI Committee 440. Guide For The Design And Construction Of Externally Bonded FRP Systems For Strengthening Concrete Structures. American Concrete Institute, 2017, Farmington Hills, MI., USA.
- ACI. Guide for the design and construction of externally bonded FRP systems for strengthening concrete structures. Farmington Hills: American Concrete Institute, ACI 440.2R-08; 2008.
- ACI. Building code requirements for reinforced concrete. American Concrete Institute, ACI 318, Farmington Hills, Michigan; 2008.
- Aiello MA, Valente L, Rizzo A. Moment Redistribution In Continuous Reinforced Concrete Beams Strengthened With Carbon-Fiber-Reinforced Polymer Laminates. *Mechanics of Composite Materials*, Vol. 43, No. 5, 2007.
- Akbarzadeh H, Maghsoudi AA. Experimental and analytical investigation of reinforced high strength concrete continuous beams strengthened with fiber reinforced polymer. *Mater Des* 2010;31:1130–47.
- Akhlaghi A, Mostofinejad D. Experimental and analytical assessment of different anchorage systems used for CFRP flexurally retrofitted exterior RC beam-column connections. *Structures* 28 (2020) 881–893.
- Akiel MS, El-Maaddawy T, El Refai A. Serviceability and moment redistribution of continuous concrete members reinforced with hybrid steel-BFRP bars. *Constr Build Mater* 2018;175:672–81.
- Akter Hosen Md, Jumaat MZ, Saiful Islam ABM. Side Near Surface Mounted (SNSM) technique for flexural enhancement of RC beams. *Materials & Design* 2015; 83 : 587–597.



- Akter Hosen Md, Jumaat MZ, Alsubari B, Ramli Sulong NH, Ibrahim Z, Johnson Alengaram U, Hashim H. Effect of bonding materials on the flexural improvement in RC beams strengthened with SNSM technique using GFRP bars. *Journal of Building Engineering* 32 (2020) 101777.
- Algaard W, Lyle J, Izzat C. Perforation of composite floor. 5th European LS-DYNA Users Conference, 2005, Birmingham, UK, May
- Alfarah B, López-Almansa F, Oller S. New methodology for calculating damage variables evolution in plastic damage model for RC structures, *Engineering Structures*. 132 (2017), 70–86.
- Ali H, Assih J, Li A. Flexural capacity of continuous reinforced concrete beams strengthened or repaired by CFRP/GFRP sheets. *International Journal of Adhesion and Adhesives* 104 (2021) 102759.
- Al-Mahmoud F, Caste A I, François R, Tourneur C. Strengthening of RC members with near surface mounted CFRP rods. *Composite Structures* 2009; 91:138-147
- Al-Mahmoud F, Castel A, François R, Tourneur C. Effect of surface preconditioning on bond of carbon fiber reinforced polymer rods to concrete. *Cem Concr Compos* 2007;29(9):677–89.
- Al-Mahmoud F, Castel A, François R. Failure modes and failure mechanisms of RC members strengthened by NSM CFRP composites – analysis of pull-out failure mode. *Compos B* 2012;43:1893–901.
- Al-Mahmoud F, Castel A, François R, Tourneur C. Anchorage and tension-stiffening effect between near-surface-mounted CFRP rods and concrete. *Cem Concr Compos* 2011;33:346–52.
- Al-Mahmoud F, Castel A, François R, Tourneur C. RC beams strengthened with NSM CFRP rods and modeling of peeling-off failure. *Compos Struct* 2010;92(8):1920–30.
- Almassri B, Al Mahmoud F, Francois R. Behaviour of corroded reinforced concrete beams repaired with NSM CFRP rods, experimental and finite element study. *Composites Part B*, 92
- Almassri B, Kreit A, Al Mahmoud F, François R. Mechanical behaviour of corroded RC beams strengthened by NSM CFRP rods. *Compos B* 2014;64:97–107.
- Almassri B, Al Mahmoud F, Francois R. Behaviour of corroded reinforced concrete beams repaired with NSM CFRP rods, experimental and finite element study. *Compos B Eng* 2016;92:477–88.
- Al-Obaidi S, Saeed Y M., Rad FN, Flexural strengthening of reinforced concrete beams with NSM-CFRP bars using mechanical interlocking *Journal of Building Engineering*, 31 (2020) 101422.
- Arduini M, Di Tommaso A, Nanni A. Brittle Failure in FRP plate and sheet bonded beams. *ACI Struct J* 1997;94(4):363–70.
- Arruda MRT, Firmo JP, Correia JR, Tiago C. Numerical modelling of the bond between concrete and CFRP laminates at elevated temperatures, *Engineering Structures*, 110 (2016), 233-243.
- Ashour AF, El-Refaie SA, Garrity SW. Flexural strengthening of RC continuous beams using CFRP laminates. *Cem Concr Compos* 2004;26:765–75.

- AS 3600-2009. Concrete structures. Sydney, Australia: Australia Standards; 2009.
- Ayesha Siddika, Abdullah Al Mamun Md, Rayed Alyousef, Mugahed Amran YH. Strengthening of reinforced concrete beams by using fiber-reinforcedpolymer composites: A review. *Journal of Building Engineering* 25 (2019) 100798.
- Barros JA, Ferreira D R, Fortes AS, Dias SJ. Assessing the effectiveness of embedding CFRP laminates in the near surface for structural strengthening. *Constr. Build Mater* 2006; 20(7):478–91.
- Bezerra LM, Cavalcante OO, Chater L, Bonilla J. V-shaped shear connector for composite steel-concrete beam, *Journal of Constructional Steel Research*, 150(2018), 162-174.
- Bilotta A, Ceroni F, Nigro E, Pecce M. Efficiency of CFRP NSM strips and EBR plates for flexural strengthening of RC beams and loading pattern influence. *Composite Structures* 124 (2015) 163–175.
- Branson DE. Instantaneous and time-dependent deflections of simple and continuous reinforced concrete beams. HPR Report No. 7, Part 1, Alabama Highway Department, Bureau of Public Roads, Alabama. 1965.
- BS EN 1992-1-1:2004. Eurocode 2: Design of concrete structures - Part 1–1: General rules and rules for buildings. London, UK: British Standards Institution; 2004.
- Capozucca R, Nilde Cerri M. Static and dynamic behaviour of RC beam model strengthened by CFRP-sheets. *Construction and Building Materials* 16 2002 91 Ž . 99.
- Capozucca R. Analysis of bond-slip effects in RC beams strengthened with NSM CFRP rods, *Composite Structures*, 102(2013), 110–123.
- Ceroni F, Pecce M, Bilotta A, Nigro E. Bond behavior of FRP NSM systems in concrete elements . *Ceroni et al./Composites: Part B* 43 (2012) 99–109.
- Chai, Y. H., Priestley, M. J. N., and Seible, F. (1991), Seismic retrofit of circular bridge columns for enhanced flexural performance, *ACI Structural Journal*, Vol. 88, No. 5, pp. 572–584.
- Chen G, Teng J, Chen J. Finite-element modeling of intermediate crack debonding in FRP-plated RC beams. *Journal of Composites for Construction*, 15(2011), 339–53.
- CNR-DT 200 R1/2013, Guide for the design and construction of externally bonded FRP systems for strengthening existing structures, Rome, Italy: National Research Council; 2013.
- Cohn M. Continuity in prestressed concrete partial prestressing from theory to practice, vol I, Survey Reports, NATO ASI Series Boston, Mass: Martinus Nijhoff Publishers. 1986. p. 189–256.
- Dalfré G. M. and Barros J. A.O. Flexural Strengthening of RC Continuous Slab Strips Using NSM CFRP Laminates. *Advances in Structural Engineering* Vol. 14 No. 6 2011.
- De Lorenzis L, Teng JG. Near-surface mounted FRP reinforcement: an emerging technique for strengthening structures. *Composites Part B-Engineering* 2007; 38(2):119-143.
- De Lorenzis L, Nanni A. Characterization of FRP rods as near surface mounted reinforcement. *J Compos Constr*, ASCE 2001;5(2):114–21.

- De Lorenzis L, Micelli F, La Tegola A. Passive and active near surface mounted FRP rods for flexural strengthening of RC beams. Proceeding of ICCI 02, San Francisco, 10-12 June 2002.
- De Lorenzis L, Nanni A. Bond between near-surface mounted fiber-reinforced polymer rods and concrete in structural strengthening. *ACI Struct J* 2002;99(2):123–32.
- De Lorenzis L, Nanni A, La Tegola A. Flexural and shear strengthening of reinforced concrete structures with near surface mounted FRP rods. Proceeding of the 4<sup>th</sup> international Conference on Advanced Composites Materials in Bridges and Structures. (ACMBS) Ottawa. 2000. p. 521–8.
- De Lorenzis L. Strengthening of RC structures with near surface mounted FRP rods PhD Thesis Italy: University of Lecce; 2002.
- De Lorenzis L, Rizzo A, La Tegola A. A modified pull-out test for bond of near surface mounted FRP rods in concrete. *Compos B Eng* 2002;33(8):589–603.
- De Lorenzis L.; Lundgren K; Rizzo A. Anchorage Length of Near-Surface-Mounted FRP Bars for Concrete Strengthening—Experimental Investigation and Numerical Modeling, *ACI Structural Journal*, 101 (2004), 269-278
- Dias SJE, Barros JAO, Janwaen W. Behavior of RC beams flexurally strengthened with NSM CFRP laminates, *Composite Structures*, 201(2018), 363-376.
- Eberline DK, Klaiber FW, Dunker K (1988), Bridge Strengthening with Epoxy-Bonded Steel Plates, *Transportation Research Record* 1180, pp.7–11.
- Feng R, Liu Y, Zhu JH, Xing F. Flexural behaviour of C-FRCM strengthened corroded RC continuous beams. *Composite Structures* 245 (2020) 112200.
- Ferracuti B, Savoia M, Mazzotti C. A numerical model for FRP–concrete delamination. *Composites Part B: Engineering*, 37(2006), 356-364.
- FIB Bulletin 14. Externally Bonded FRP Reinforcement for RC Structures. International Federation for Structural Concrete, Zürich, Switzerland, 2001.
- Goertzen WK, Kessler MR. Creep behavior of carbon fiber/epoxy matrix composites. *Materials Science and Engineering A* 421 (2006) 217–225.
- Goldberg JE, Richard RM. Analysis of nonlinear structures. *ASCE J Struct Div – Proc Am Soc Civ Eng* 1963;89:333–51.
- Gopalaratnam VS, Gettu R. On the characterization of flexural toughness in fiber reinforced concretes. *Cement Concr Compos* 1995;17(3):239–54.
- Hanoon AN, Jaafar MS, Hejazi F, Abdul Aziz FNA. Energy absorption evaluation of reinforced concrete beams under various loading rates based on particle swarm optimization technique. *Eng Optim* 2017;49(9):1483–501.
- Haddad RH, Yaghmour EM. Side NSM CFRP strips with different profiles for strengthening reinforced concrete beams. *Journal of Building Engineering* 32 (2020) 101772.

- Hassan T, Rizkalla S. Investigation of bond in concrete structures strengthened with near surface mounted carbon fiber reinforced polymer strips. *J Compos Constr.*, 2003; 7(3):248–57
- Hassan T, Rizkalla S. Bond mechanism of near-surface-mounted fiber reinforced polymer bars for flexural strengthening of concrete structures. *ACI Struct J* 2004;101(6):830–9.
- Hawileh RA. Nonlinear finite element modeling of RC beams strengthened with NSM FRP rods, *Construction and Building Materials*, 27(2012), 461–471.
- Hollaway LC, Teng JG. *Strengthening and rehabilitation of civil infrastructures using FRP composites*. Cambridge, U.K.: Woodhead; 2008.
- Jawdhari A, Peiris A, Harika I. Experimental study on RC beams strengthened with CFRP rod panels. *Engineering Structures* 173 (2018) 693–705
- Khalifa AM. Flexural performance of RC beams strengthened with near surface mounted CFRP strips. *Alexandria Eng J* 2016;55:1497–505.
- Kreit A, Al-Mahmoud F, Castel A, François R. Repairing corroded RC beam with near surface mounted CFRP rods. *Mater Struct* 2011;44(7):1205–17.
- Lam L, Teng JG. Strength models for fiber-reinforced plastic-confined concrete. *J Struct Eng* 2002;128(5).
- Le-Trung K, Lee K, Lee J, Lee DH, Woo S. Experimental study of RC beam–column joints strengthened using CFRP composites. *Composites: Part B* 41 (2010) 76–85
- Lee J, Fenves GL, Plastic-damage model for cyclic loading of concrete structures, *Journal of Engineering Mechanics*, 124 (1998), 892–900.
- Li LJ, Guo YC, Liu F, Bungey JH. An experimental and numerical study of the effects of thickness and length of CFRP on performance of repaired reinforced concrete beams. *Constr Build Mater* 2006;20(10):901–9.
- Li L, Zheng W, Wang Y. Review of moment redistribution in statically indeterminate RC members. *Engineering Structures* 196 (2019) 109306.
- Lignola GP, Prota A, Manfredi G, Cosenza E. Experimental performance of RC hollow columns confined with CFRP. *J Compos Construct* 2007;11(1). 1090-0268.
- Lou T, Lopes SMR, Lopes AV. Effect of relative stiffness on moment redistribution in reinforced high-strength concrete beams. *Mag Concr Res* 2017;69:716–27.
- Lubliner J, Oliver J, Oller S, Oñate E. A plastic-damage model for concrete, *Int. J. Solids Structures*. 25(1989), 229–326.
- Maghsoudi AA, Akbarzadeh H. Flexural ductility of HSC members. *Struct Eng Mech* 2006;24(2).
- Mahmoud MH, Afefy HM, Kassem NM, Fawzy TM. Strengthening of defected beam–column joints using CFRP. *Journal of Advanced Research* (2014) 5,67-77
- Mahroug MEM, Ashour AF, Lam D. Tests of continuous concrete slabs reinforced with carbon fibre reinforced polymer bars. *Compos B Eng* 2014;66:348–57.

- Meier U. Strengthening of structures using carbon fibre/epoxycomposites. *Construct Build Mater* 1995;9(6):341 – 51.
- Mukhopadhyaya P, Swamy RN, Lynsdale C. Optimizing structural response of beams strengthened with GFRP plates. *J Compos Construct, ASCE* 1998;2(2):87–95.
- Nadim Hassoun M, Al-Manaseer A. *Structural concrete: theory and design*. John Wiley & Sons; 2012.
- Nayak AN, Kumaria A, Swain RB. Strengthening of RC beams using externally bonded fibre reinforced polymer composites. *Structures* 2018;14:137–52.
- Ninoslav Pešić, Kypros Pilakoutas. Concrete beams with externally bonded flexural FRP-reinforcement: analytical investigation of debonding failure. *Composites: Part B* 34 (2003) 327–338.
- Nguyen HT, Kim SE. Finite element modeling of push-out tests for large stud shear connectors, *Journal of Constructional Steel Research*, 65(2009), 1909-1920.
- Obaidat YT, Abu-Farsakh GAFR, Ashteyat AM. Retrofitting of partially damaged reinforced concrete beam-column joints using various plate-configurations of CFRP under cyclic loading. *Construction and Building Materials* 198 (2019) 313–322
- Obaidat YT, Heyden S, Dahlblom O. The effect of CFRP and CFRP/concrete interface models when modeling retrofitted RC beams with FEM. *Composite Structures*, 92(2010), 1391–1398.
- Obaidat YT, Barham WS, Aljarah AH. New anchorage technique for NSM-CFRP flexural strengthened RC beam using steel clamped end plate. *Construction and Building Materials* 263 (2020) 120246.
- Oehlers DJ, Ju G, Liu IST, Seracino R. Moment redistribution in continuous plated RC flexural members. Part 1: neutral axis depth approach and tests. *Engineering Structures* 26 (2004) 2197–2207.
- Omran HY, El-Hacha R. Nonlinear 3D finite element modeling of RC beams strengthened with prestressed NSM-CFRP strips, *Construction and Building Materials*, 31(2012), 74–85.
- Onal Mustafa M. Strengthening reinforced concrete beams with CFRP and GFRP. *Adv Mater Sci Eng* 2014:1–8.
- Pham H, Al-Mahaidi R. Prediction models for debonding failure loads of carbon fiber reinforced polymer retrofitted reinforced concrete beams. *J Compos Construct, ASCE* 2006;10(1):48–59.
- Radfar S, Foret G, Saeedi N, Sab K. Simulation of concrete cover separation failure in FRP plated RC beams. *Constr Build Mater* 2012;37:791–800.
- Reda RM, Sharaky IA, Ghanem M, Seleem MH, Sallam HEM. Flexural behavior of RC beams strengthened by NSM GFRP Bars having different end conditions. *Compos Struct* 2016;147:131–42.
- Rezazadeh M, Costa I, Barros J. Influence of prestress level on NSM CFRP laminates for the flexural strengthening of RC beams, *Composite Structures*, 116(2014), 489-500.

- Richard RM, Abbott BJ. Versatile elastic-plastic stress-strain formula. *ASCE J Eng Mech Div – Proc Am Soc Civ Eng* 1975;101:511–5.
- Rosenboom O, Rizkalla S. Behavior of prestressed concrete strengthened with various CFRP systems subjected to fatigue loading. *J Compos Constr* 2006;10(6):492–502.
- Sabaua C, Popescu C, Sas G, Schmidt JW, Blanksvärd Th, Täljsten B. Strengthening of RC beams using bottom and side NSM reinforcement. *Compos B* 2018;149:82–91.
- Salama ASD, Hawileh RA, Abdalla JA. Performance of externally strengthened RC beams with side-bonded CFRP sheets. *Composite Structures* 212 (2019) 281–290
- Saljoughian A, Mostofinejad D. Axial-flexural interaction in square RC columns confined by intermittent CFRP wraps. *Composites Part B* 89 (2016) 85-95.
- Scott BD, Park R, Priestley MJN. Stress-strain behavior of concrete confined by overlapping hoops at low and high strain rates. *J Am Concr Inst* 1982;79:13–27.
- Scott RH, Whittle RT. Moment redistribution effects in beams. *Mag Concr Res* 2005;57:9–20.
- Sebastian WM, Vincent J, Starkey S. Experimental characterisation of load responses to failure of a RC frame and a NSM CFRP RC frame. *Constr Build Mater* 2013;49:962–73.
- Seracino R, Saifulnaz MMR, Oehlers DJ. Generic debonding resistance of EB and NSM plate-to-concrete joints, *Journal of Composites for Construction*, 11(2007), 62–70.
- Shaikh FUA, Alishahi R. Behaviour of CFRP wrapped RC square columns under eccentric compressive loading. *Structures* 20 (2019) 309–323
- Sharaky IA, Baena M, Barris C, Sallam HEM, Torres L. Effect of axial stiffness of NSM FRP reinforcement and concrete cover confinement on flexural behaviour of strengthened RC beams: Experimental and numerical study. *Engineering Structures* 173 (2018), 987–1001.
- Sharaky IA, Torres L, Comas J, Barris C. Flexural response of reinforced concrete (RC) beams strengthened with near surface mounted (NSM) fiber reinforced polymer (FRP) bars. *Compos Struct* 2014;109:8–22.
- Sharaky IA, Torres L, Sallam HEM. Experimental and analytical investigation into the flexural performance of RC beams with partially and fully bonded NSM FRP bars/strips. *Compos Struct* 2015;122:113–26.
- Simão PD, Barros H, Ferreira CC, Marques T. Closed-form moment-curvature relations for reinforced concrete cross sections under bending moment and axial force. *Eng Struct* 2016;129:67–80.
- Shomali A, Mostofinejad D, Esfahani MR. Experimental and numerical investigation of shear performance of RC beams strengthened with FRP using grooving method. *Journal of Building Engineering* 31 (2020) 101409
- Song L, Yu Zh. Fatigue performance of corroded reinforced concrete beams strengthened with CFRP sheets. *Construction and Building Materials* 90 (2015) 99–109
- Tahnat YBA., Dwaikat MMS, Samaaneh MA. Effect of using CFRP wraps on the strength and ductility behaviors of exterior reinforced concrete joint. *Composite Structures*, 201 (2018), 721–739.

- Teng JG, Chen JF, Smith ST, Lam L. FRP strengthened RC structures. New York: Wiley; 2002.
- Visintin P, Mohamad Ali MS, Xie T, Sturm AB. Experimental investigation of moment redistribution in ultra-high performance fibre reinforced concrete beams. *Constr Build Mater* 2018;166:433–44.
- Wahalathantri BL, Thambiratnam DP, Chan THT, Fawzia S. A material model for flexural crack simulation in reinforced concrete elements using ABAQUS. First International conference on engineering, designing and developing the built environment for sustainable wellbeing, 2011, Brisbane, Australia, April.
- Xiong GJ, Jiang X, Liu JW, Chen L. A way for preventing tension delamination of concrete cover in midspan of FRP strengthened beams. *Construct Build Mater* 2007;21:402–8.
- Yanga Y, Fahmy Mohamed FM, Cui J, Pan Zh, Shi J. Nonlinear behavior analysis of flexural strengthening of RC beams with NSM FRP laminates. *Structures* 2019;20:374–84.
- Zaki MA, Rasheed HA, Roukerd RR, Raheem M. Performance of reinforced concrete T beams strengthened with flexural CFRP sheets and secured using CFRP splay anchors. *Engineering Structures* 210 (2020) 110304.
- Zhang SS, Yu T, Chen GM. Reinforced concrete beams strengthened in flexure with near-surface mounted (NSM) CFRP strips: current status and research needs. *Compos B* 2017;131:30–42.
- Zhou CY, Yu YN, Xie EL. Strengthening RC beams using externally bonded CFRP sheets with end selflocking. *Composite Structures* 241 (2020) 112070